Lowering the Fuel Requirement During Active Regeneration of Soot

Thesis submitted in accordance with the requirement of Cardiff University for the degree of Doctor of Philosophy

Anna Cooper

October 2021

Abstract

This thesis focuses on finding a single catalyst for the simultaneous removal of NOx and soot from a diesel car exhaust. Finding a single catalyst which can operate at low temperatures would remove the need to inject fuel to regenerate the soot filter. It has been shown that a Ag/CeO_2-ZrO_2-Al_2O_3 (CZA) catalyst was found to have the ability to simultaneously reduce NOx and oxidise soot and utilise *in situ* formed N_2O to oxidise soot at low temperatures. This project develops the work by investigating ways to improve the NOx reduction and soot oxidation ability of the catalyst.

Initially, the effect of preparation method on 2%Ag-20%K/CZA was carried out. Potassium was added to the catalyst, as it is a well-known enhancer of soot oxidation. Several preparation methods were carried out including wet impregnation, incipient wetness and chemical vapour impregnation (CVI) at four different temperatures. It was found that the wet impregnation technique was the superior preparation technique, however, the presence of potassium appeared to enhance soot oxidation but hinder the reduction of NOx. The wet impregnation catalyst showed the ability to utilise the *in situ* formed N_2O to oxidise soot at low temperatures, but to a lesser extent than that observed over Ag/CZA.

The effect of potassium weight loading was investigated, with the aim of determining whether a lower weight loading of potassium was sufficient to enhance soot oxidation, but not hinder the reduction of NOx. This was found not to be the case with an increase in potassium weight loading resulting in greater high temperature soot oxidation, but altering the potassium weight loading had little effect on the reduction of NOx. *In situ* XRD studies were carried out to investigate the nature of potassium under reaction conditions which suggested that the potassium becomes mobile under reaction conditions.

A variety of Cu/CZA catalysts were studied for their ability to simultaneously remove NOx and soot. Copper zeolites are frequently used to reduce NOx from diesel exhausts. Under the preparation conditions used, the copper was present in the form of Cu^{2+} rather than the active Cu^0 form, resulting in poor activity. The introduction of a range of secondary metals into Ag/CZA and Ag-K/CZA catalysts were investigated. The secondary metals were chosen based on their ability to either reduce NOx or oxidise soot under diesel exhaust conditions. As with the addition of potassium to the catalyst, the introduction of a secondary metal hindered the reduction of NOx. However, several metals such as Rh and Pt, were shown to enhance high temperature soot oxidation under reaction conditions.

Acknowledgments

I would like to acknowledge Jaguar Land Rover and the EPSRC for providing funding through an icase award. I would like to thank my supervisor, Stuart Taylor for his guidance, knowledge and support throughout my PhD especially for the times when everything seemed to be going wrong. I would also like to thank Stan Golunski and Cat Davies for always being happy to give insight and advice on my work.

There are several people who contributed towards my thesis including, Dave Morgan for XPS, Tom Davies for SEM and TEM, James Hayward for *in situ* XRD, and Greg Shaw and Nia Richards for providing invaluable support when the equipment broke.

The advantage of having been a part of the catalysis CDT and the CCI was the opportunity to meet and work alongside so many different people which helped make the PhD entertaining. Particularly, Liam and Kieran who make up 'Team Stu' and together we have survived completing PhDs despite COVID-19.

I would like to thank my family and friends for their support during my PhD and for listening to my stresses through the years. I would also like to thank my community and friends at St. Michaels and All Angels who have always been happy to listen. Finally, I would like to thank my partner Owen who I would not have met without doing my PhD. He has provided calm advice and support during stressful times even when isolating together.

List of Publications

1. C. Davies, K. Thompson, A. Cooper, S. Golunski, S.H. Taylor, M. Bogarra Macias, O. Doustdar, A. Tsolakis, Simultaneous removal of NOx and soot particulate from diesel exhaust by *in situ* catalytic generation and utilisation of N_2O, Appl. Catal. B Environ., 2018, **239**, 10–15.

2. A. Cooper, T.E. Davies, D.J. Morgan, S. Golunski, S.H. Taylor, Influence of the Preparation Method of Ag-K/CeO_2-ZrO_2-Al_2O_3 Catalysts on Their Structure and Activity for the Simultaneous Removal of Soot and NOx, Catalysts, 2020, **10**, 294.

Table of Contents

Abstract i

Acknowledgments ii

List of Publications iii

1. Introduction ***1***

1.1 Air Pollution **1**

1.1.1 Nitrogen Oxides 2

1.1.1.1 NOx Formation 2

1.1.1.2 Thermal NOx Formation 2

1.1.1.2.1 Fuel NOx Formation 4

1.1.1.2.2 Prompt NOx Formation 4

1.1.1.3 NOx Toxicological Effects 5

1.1.2 Diesel Particulate Matter 6

1.1.2.1 Soot Formation 7

1.1.2.2 Health and Environmental Impacts of Particulate Matter 8

1.1.2.3 Polycyclic Aromatic Hydrocarbons 9

1.1.3 Other Pollutants 12

1.1.3.1 N_2O 13

1.1.4 Difference Sources of Pollution 13

1.2 Automotive Aftertreatment **14**

1.2.1 NOx Abatement Technology 16

1.2.1.1.1 Catalysts for Selective Catalytic Reduction 18

1.2.1.1.2 Zeolites 18

1.2.1.1.3 Copper Based Zeolites 19

1.2.1.1.4 Silver Catalysts 20

1.2.2 Diesel Particulate Filters 20

1.2.2.1 Catalysts 21

1.2.2.1.1 Ceria redox catalysts for soot oxidation 22

1.2.2.1.2 Transition and rare earth metal promotors 23

1.2.2.1.3 Alkali metal promotors 24

1.2.2.1.4 Silver Catalysts for Soot Oxidation 25

1.2.3 The Simultaneous Removal of NOx and PM 26

1.2.4 Current Problems and the Future of Aftertreatment Technology 28

1.2.4.1 Cold Start 28

1.2.4.2 Effect of Catalyst Aging 29

1.2.4.3 Future Regulations 30

1.3 Project Aims 30

1.4 References 32

2 Experimental 37

2.1 Introduction 37

2.2 Materials Used 37

2.3 Catalyst Preparation 37

2.3.1 CeO_2-ZrO_2-Al_2O_3 Support Preparation Method 37

2.3.2 Catalyst Preparation 38

2.3.2.1 Chemical Vapour Impregnation 38

2.3.2.1.1 Ag-K/CeO_2-ZrO_2-Al_2O_3 39

2.3.2.1.2 Cu/CeO_2-ZrO_2-Al_2O_3 39

2.3.2.2 Incipient Wetness 39

2.3.2.3 Wet Impregnation 40

2.3.2.3.1 K/CeO_2-ZrO_2-Al_2O_3 40

2.3.2.3.2 Ag-K/CeO_2-ZrO_2-Al_2O_3 40

2.3.2.3.3 Cu-Ag/CeO_2-ZrO_2-Al_2O_3 40

2.3.2.4 Sol Immobilisation 41

2.4 Catalyst Testing 41

2.4.1 The SCR Reactor 41

2.4.1.1 On-line Process Analysis Using Fourier Transform Infrared (FTIR) Spectroscopy 42

2.4.1.1.1 Experimental 43

2.4.2 Catalyst Characterisation 44

2.4.3 Physisorption, Specific Surface Area and B.E.T. Theory 44

2.4.3.1 Experimental 46

2.4.4 Powder X-Ray Diffraction 46

2.4.4.1 Experimental 48

2.4.4.1.1 Powder XRD 48

2.4.4.1.2 *In situ* XRD 48

2.4.5 Raman Spectroscopy 49

2.4.5.1 Experimental 50

2.4.6 X – Ray Photoelectron Spectroscopy 51

2.4.6.1 Experimental 52

2.4.7 Electron Microscopy 52

2.4.7.1 Scanning Electron Microscopy (SEM) 53

2.4.7.1.1 Experimental 54
2.4.7.2 Transmission Electron Microscopy (TEM) 54
2.4.7.2.1 Experimental 55
2.5 References 56
3. The Influence of Preparation Method of Ag-K/CeO_2-ZrO_2-Al_2O_3 Catalysts on Their Structure and Activity for Simultaneous Removal of Soot and NOx..... 61
3.1 Introduction 61
3.2 CeO_2-ZrO_2-Al_2O_3 (CZA) Support 62
3.3 Catalysts Prepared *via* Chemical Vapour Impregnation 63
3.3.1 Reaction Data 63
3.3.1.1 CVI60 65
3.3.1.2 CVI70 66
3.3.1.3 CVI80 67
3.3.1.4 CVI90 69
3.3.2 Characterisation of the Catalysts Prepared *via* Chemical Vapour Impregnation 69
3.3.3 Conclusions 76
3.4 Catalysts Prepared via Incipient Wetness and Wet Impregnation 76
3.4.1 Incipient Wetness 76
3.4.2 Wet Impregnation 77
3.4.3 Characterisation Data 79
3.4.4 Conclusions 82
3.5 Discussion 82
3.6 Conclusions and Future Work 85
3.7 References 87
4 Investigation into the Ideal Weight Loading of Potassium in Ag-K/CeO_2-ZrO_2-Al_2O_3 Catalysts for the Simultaneous Removal of NOx and Soot from Diesel Exhausts 87
4.1 Introduction 87
4.2 Results 87
4.2.1 Catalyst Performance Data 87
4.2.1.1 2%Ag-20%K/CZA 88
4.2.1.2 2%Ag-15%K/CZA 89

4.2.1.3 2%Ag-10%K/CZA 90
4.2.1.4 2%Ag-5%K/CZA 91
4.2.1.5 2%Ag-2%K/CZA 92
4.2.1.6 Discussion 93
4.2.2 Characterisation Data 94
4.2.2.1 CO_2 Trace Investigation 95
4.2.2.2 X-ray Diffraction 98
4.2.2.3 Raman Spectroscopy 99
4.2.2.4 BET Analysis 101
4.2.2.5 XPS Analysis 101
4.2.2.6 Microscopy 104
4.2.2.7 *In situ* XRD 107
4.2.2.8 Discussion 111
4.3 Conclusions and Future Work 111
4.4 References 113
5 Copper-Silver Catalysts for the Simultaneous Removal of NOx and Soot 116
5.1 Introduction 116
5.2 Results 117
5.2.1 Catalyst performance 117
5.2.1.1 The Effect of Potassium Addition to Copper 117
5.2.1.2 The Effect of Changing Calcination Temperature 119
5.2.1.3 Sol immobilisation 122
5.2.1.4 Effect of Order of Catalyst Precursors 123
5.2.1.5 Catalysts Prepared *via* CVI 124
5.2.1.6 Silver vs Palladium 126
5.2.1.7 Comparison of the Catalysts 128
5.2.2 Characterisation 129
5.2.2.1 X-ray Diffraction Data 129
5.2.2.2 BET Analysis 132
5.2.2.3 Raman Spectroscopy 132
5.2.2.4 XPS Analysis 134
5.2.2.5 SEM-EDX Analysis 137
5.3 Conclusions 138
5.4 Future Work 139

5.5 References 141

6. A Study into Silver Bimetallic Catalysts for the Simultaneous Removal of NOx and Soot from a Diesel Exhaust 142

6.1 Introduction 142

6.2 Results 143

6.2.1 Catalyst Performance Data 143

6.2.1.1 Co based Catalysts 144

6.2.1.2 Mn based Catalysts 144

6.2.1.3 Ba based Catalysts 146

6.2.1.4 La based Catalysts 147

6.2.1.5 Sr based Catalysts 148

6.2.1.6 Ni based Catalysts 150

6.2.1.7 Fe based Catalysts 151

6.2.1.8 Pt based Catalysts 152

6.2.1.9 Pd based Catalysts 153

6.2.1.10 Rh based Catalysts 154

6.2.2 Discussion 155

6.2.3 Characterisation Data 159

6.2.3.1 X-ray Diffraction 159

6.2.3.2 Raman Spectroscopy 164

6.2.3.3 BET Analysis 166

6.2.3.4 TEM and XPS Analysis 167

6.3 Discussion 170

6.3.1 Co Catalysts 170

6.3.2 Mn Catalysts 170

6.3.3 Ba Catalysts 171

6.3.4 La Catalysts 172

6.3.5 Sr Catalysts 172

6.3.6 Ni Catalysts 172

6.3.7 Fe Catalysts 173

6.3.8 PGM Catalysts 174

6.4 Conclusions and Future Work 174

6.5 References 177

7 Conclusions and Future Work 180

7.1 Conclusions 180

7.2 Future Work 181

7.3 References 183

1. Introduction

1.1 Air Pollution

The European Environment Agency (EEA) states that air pollution is the; *'biggest environmental health threat in Europe.'*[1] Air pollution is a broad term, which can be defined as, '*the presence in or introduction into the air of a substance which has harmful or poisonous effects.*'[2] The World Health Organisation (WHO) estimates that air pollution kills over 7 million people each year,[3] with the majority of deaths being due to the inhalation of air pollution leading to strokes, heart disease, pulmonary disease, lung cancer and respiratory infections.[3]

Air pollution originates from a wide range of sources, including: the burning of fossil fuels for transport, electricity generation, households and industry; industrial and chemical processes; waste treatment; natural sources, which includes volcanic eruptions, forest fires, sea-salt spray and windblown dust.[4]

In December 1952, the city of London was covered in a fog so dense that visibly was reduced to only a few meters. This fog was a consequence of high levels of air pollution combined with extreme weather conditions.[5] It is estimated that over 10,000 people died as a result of the fog, most of these people being the elderly, young or those with pre-existing respiratory conditions.[6] In the aftermath of the disaster, the 1956 Clean Air Act was introduced.[7] This was one of the first pieces of legislation in the UK to limit the amount of pollution being released into the atmosphere.

Since 1956, further and more stringent legislation has been introduced including the Kyoto and Gothenburg protocols. For automotive legislation, the EURO limits are the guidelines which OEMs (original engine manufacturers) must adhere to in Europe. The Euro limits were first introduced in 1993 and are updated approximately every four years.[8]

The most recent EURO limit (EURO 6), applies to all new cars made from 2015 onwards. The emissions covered by the standard are CO, nitrogen oxides (NOx), hydrocarbons (HCs), and particulate matter (PM). The EURO limits for diesel and gasoline passenger vehicles are shown in Table 1.1. The EURO 6 standard includes a significant reduction in the permitted NOx emission from diesel engines, a 67% reduction compared to the previous standard.[9,10] Future legislation will only become more stringent. It is also speculated that the next set of EURO limits will regulate currently unregulated pollutants such as N_2O and CH_4.[11,12]

In order to ensure OEMs are meeting the requirements, vehicles must pass laboratory testing and be tested on the road, *i.e.* Real Driving Emissions (RDE). The first RDE was established in March 2016, the second in April 2016 and the third in July 2017.[13] The RDE test must last between 90 and 120 minutes and is carried out using a portable emissions monitoring system (PEMS). The route has to consist of urban (<60 km h^{-1}), rural (60 – 90 km h^{-1}) and motorway (>90 km h^{-1}) roads with each segment lasting for at least 16 km.[10]

Table 1.1: EURO 6 Limits, data from dieselnet[10]

Pollutant	Positive Ignition (Gasoline)	Compression Ignition (Diesel)
CO / g^{-1} km	1.0	0.50
HC / g^{-1}km	0.10	-
HC + NOx / g^{-1}km	-	0.17
NOx / g^{-1}km	0.06	0.08
PM / g^{-1}km	0.005	0.005
PN / $\#^{-1}$km	6.0×10^{11}	6.0×10^{11}

This thesis focuses on control of NOx and PM emissions hence the following sections of the introduction will focus on the formation, toxicological effects and abatement strategies for these pollutants.

1.1.1 Nitrogen Oxides

During fuel combustion nitrogen combines with oxygen atoms to form nitric oxide (NO). NO further reacts with oxygen to form nitrogen dioxide (NO_2). Under standard ambient conditions NO is not thought to be harmful to human health but NO_2 is. NO and NO_2 are referred together as NOx. NOx reacts to form smog and acid rain in addition to being involved in the formation of PM and ground level ozone, both of which are hazardous to human health.

1.1.1.1 NOx Formation

NOx in a diesel engine can be formed by three main routes: thermal NOx, fuel NOx and Prompt NOx.

1.1.1.2 Thermal NOx Formation

Thermal NOx is formed when nitrogen reacts with excess oxygen at high temperatures (greater than 1800 K) during combustion. The thermal NOx route occurs most readily at high gas temperatures as the thermodynamic equilibrium favours NO formation through the dissociation

of nitrogen and oxygen. Nitrogen's triple bond requires high temperatures to be homolytically broken into its constituent radicals.[14]

The majority of NO_2 formed during combustion decomposes rapidly into NO, which then can dissociate into N_2 and O_2, however, this occurs at a very slow rate.[14].As a consequence, the majority of NOx emitted is NO. The Zeldovich mechanism describes the main reactions for the formation of thermal NOx.

NO in the flame zone is converted to NO_2:

$$\mathbf{^1/_2}\,\boldsymbol{O_{2(g)}} + \boldsymbol{N_{2(g)}} \rightarrow \boldsymbol{NO_{(g)}} + \mathbf{^1/_2}\,\boldsymbol{N_{2(g)}} \qquad \textbf{Equation 1.1}$$

$$\mathbf{^1/_2}\,\boldsymbol{N_{2(g)}} + \boldsymbol{O_{2(g)}} \rightarrow \boldsymbol{NO_{(g)}} + \mathbf{^1/_2}\,\boldsymbol{O_{2(g)}} \qquad \textbf{Equation 1.2}$$

At near stoichiometric and fuel mixtures:

$$\mathbf{^1/_2}\,\boldsymbol{N_{2(g)}} + \boldsymbol{OH_{(g)}} \rightarrow \boldsymbol{NO_{(g)}} + \mathbf{^1/_2}\,\boldsymbol{H_{2(g)}} \qquad \textbf{Equation 1.3}$$

NO produced in Equation 1.1 and Equation 1.3 is converted to NO_2:

$$\boldsymbol{NO_{(g)}} + \boldsymbol{HO_{2(g)}} \rightarrow \boldsymbol{NO_{2(g)}} + \boldsymbol{OH_{(g)}} \qquad \textbf{Equation 1.4}$$

NO_2 is converted to NO:

$$\boldsymbol{NO_{2(g)}} + \mathbf{^1/_2}\,\boldsymbol{O_{2(g)}} \rightarrow \boldsymbol{NO_{(g)}} + \boldsymbol{O_{2(g)}} \qquad \textbf{Equation 1.5}$$

Thermal NO formation rate is slow below 1800 K. Thermal NO formed through Equation 1.1 and Equation 1.2 are formed in the combustion exhaust gases. In 1988, Heywood stated the relationship of NO formation rate with oxygen concentration, nitrogen concentration and temperature.[15]

Thermal NOx Formation Rate Equation

$$\frac{d[NO]}{dt} = \frac{6 \times 10^6}{\sqrt{T}} \times e^{\frac{-69090}{T}} \times [N_2]_e \times \sqrt{[O_2]_e} \qquad \textbf{Equation 1.6}$$

Equation 1.6 shows that NO formation increases exponentially with temperature. Other key factor in thermal NOx formation is the residence time *i.e.* the longer the duration of the high temperature the greater the NOx formation.

1.1.1.2.1 Fuel NOx Formation

Nitrogen containing fuels (e.g. diesel) forms fuel NOx as a consequence of oxidation of ionized nitrogen contained in the fuel.[16] The extent of fuel NOx formation is dependent on the initial concentration of nitrogen bound species in the fuel. As fuel is heated, fuel-bound nitrogen containing compounds are released in the gas phase.

These compounds decompose thermally in the reaction and their radicals (e.g. HCN, NH_3, N, CN and NH) are formed and consequently are converted to NOx. These radicals compete between an oxidation and reductive reaction. Houser *et al.* found that HCN is the main product if nitrogen is in the form of aromatic in the fuel, however, if it is present as aliphatic amines, ammonia is the major product.[17]

1.1.1.2.2 Prompt NOx Formation

When nitrogen in the air combines with fuel in fuel-rich conditions prompt NOx is formed. This happens to some degree during all combustion. The abundance of prompt NOx is controversial in the literature, due to fuel intrinsically containing nitrogen.[16]

The prompt NOx formation mechanism was first identified by Fenimore.[18] Prompt NOx forms in low temperature, fuel-rich conditions and with short residence times. Combustion systems, surface burners and gas turbines have these conditions.[19]

The accepted route for prompt NOx formation is:

$$CH_{(g)} + N_{2(g)} \rightarrow HCN_{(g)} + {}^{1}/_{2}\, N_{2(g)} \qquad \textbf{Equation 1.7}$$

$${}^{1}/_{2}\, N_{2(g)} + O_{2(g)} \rightarrow NO_{(g)} + {}^{1}/_{2}\, O_{2(g)} \qquad \textbf{Equation 1.8}$$

$$HCN_{(g)} + OH_{(g)} \rightarrow CN_{(g)} + H_2O_{(g)} \qquad \textbf{Equation 1.9}$$

$$CN_{(g)} + O_{2(g)} \rightarrow NO_{(g)} + CO_{(g)} \qquad \textbf{Equation 1.10}$$

Several species from fuel fragmentation have been suggested as the source of prompt NOx, but the main contribution is from CH (Equation 1.7) and CH_2 *via*:

$$\boldsymbol{CH_{2(g)} + N_{2(g)} \rightarrow HCN_{(g)} + NH_{(g)}} \qquad \textbf{Equation 1.11}$$

The products can form ammines and cyano compounds, which consequently react and form NO. Prompt NOx formation is proportional to the number of carbon atoms per unit volume. The quantity of HCN formed increases with increase of hydrocarbon radicals, this increases the equivalence ratio. As the equivalence ratio increases NOx production also increases, until a lack of oxygen causes the production to decrease.

Equation 1.7 is the key reaction. Studies have shown that comparison of probability density distributions for the location of the NOx compared to the CH peak have close correspondence.[20] This indicates that the majority of prompt NOx is formed by the CH reaction. Assuming that Equation 1.7 controls the formation rate:

$$\frac{\boldsymbol{d[NO]}}{\boldsymbol{dt}} = \boldsymbol{k_0[CH][N_2]} \qquad \textbf{Equation 1.12: Prompt NOx formation reaction rate}$$

1.1.1.3 NOx Toxicological Effects

NO_2 has an adverse effect on human health. When inhaled, it reacts with moisture in the respiratory tract forming nitric acid. At low concentrations this is restricted to the upper respiratory tract whilst at higher concentrations the reaction reaches the lower respiratory tract. Once inhaled NO_2 may remain in the lung or be transported to other regions of the body in the bloodstream. In the bloodstream NO_2 can react with haemoglobin to form methemoglobin (MetHb). MetHb is an ineffective oxygen carrier hence this can increase the risk in people who have hypoxia associated with pulmonary and cardiac disease. Furthermore, after exposure to NO_2 increased levels of nitrates in the blood and urine have been reported, hence suggesting that NO_2 reacts to form nitrates.[21]

NOx also has a negative impact on the environment. NO_2 reacts in the atmosphere to form tropospheric ozone (O_3) and acid rain. The EPA (US Environmental Protection Agency) has established the National Ambient Air Quality Standards (NAAQS) for NO_2 and tropospheric ozone.[21]

NO_2 forms ozone and nitric oxide in the presence of air and UV light. Radicals in the atmosphere, formed by UV reacting with volatile organic compounds (VOCs), react with NO. This

recycles NO back to NO_2. Consequently, each NO_2 molecule can produce ozone multiple times. These reactions continue until the VOCs are reduced to short un-photo reactive chains.[22]

Acid deposition is due to airborne acidic compounds, primarily sulphates and nitrates. Acid deposition can occur through rain, snow, fog or transfer of particles or gases. According to the clean air act, acid deposition and NOx "represent a threat to natural resources, ecosystems, visibility, materials, and public health".[21]

1.1.2 Diesel Particulate Matter

Diesel particulates are defined by the EPA as 'all compounds collected on a pre-conditioned filter in diluted diesel exhaust gases at a maximum temperature of 325 K'.[23]

Diesel particulates are made up of a soot nuclei (carbon), inorganic material, adsorbed hydrocarbons (also known as SOF *i.e.* soluble organic fraction), SOx (sulphur oxides) and water. The majority of sulphur in the fuel is oxidised to SO_2, however, further oxidation can take place resulting in the formation of SO_3, which consequently forms sulphuric acid.[24] Figure 1.1b shows a schematic of the composition of diesel particulate.

In addition to compounds restricted by emission standards, there are many other harmful compounds which are present in exhaust gases. The most significant ones are listed in Table 1.2. Polycyclic aromatic hydrocarbons (PAHs) are present both in the gas phase and adsorbed onto soot particles, comprise of a number of compounds from lubricant oil, diesel fuel, and the HC degradation and formation process which take place throughout combustion.[25] PAHs have negative effects on human health and several PAHs found in diesel exhaust gas have been found to be carcinogenic.[25] PAH emissions have been reported to increase with an increase in aromatic content in fuel.[26] PAHs will be further discussed in Section 1.1.2.3.

Table 1.2: Typical diesel and gasoline exhaust gas compositions for unregulated harmful compounds. In mg mile^{-1} for 4-5 cylinder Volkswagen passenger cars. Adapted from[23]

Compound	Diesel	Gasoline
Aldehydes	0	60
Ammonia	2	4
Cyanide	1	10
Benzene	6	80
Toluene	2	240
PAHs	0.3	0.2

1.1.2.1 Soot Formation

Diesel particulates are comprised of 'nuclei' and 'accumulation' mode particles.[23] Frequently, the nuclei particles are referred to as nanoparticles which are defined as particles less than 50 nm in diameter. The accumulation mode particles are defined as particles between 50 nm and 1000 nm in diameter.[27,28] The accumulation particles are formed *via* agglomeration of carbon particles with adsorbed gases, such as condensed hydrocarbons. In the early stages of soot formation primary particles are formed through two different mechanisms, surface growth and collision coagulation. After the formation of the initial primary particles, collisions take place resulting in formation of clusters and hence the final soot agglomerate.[29]

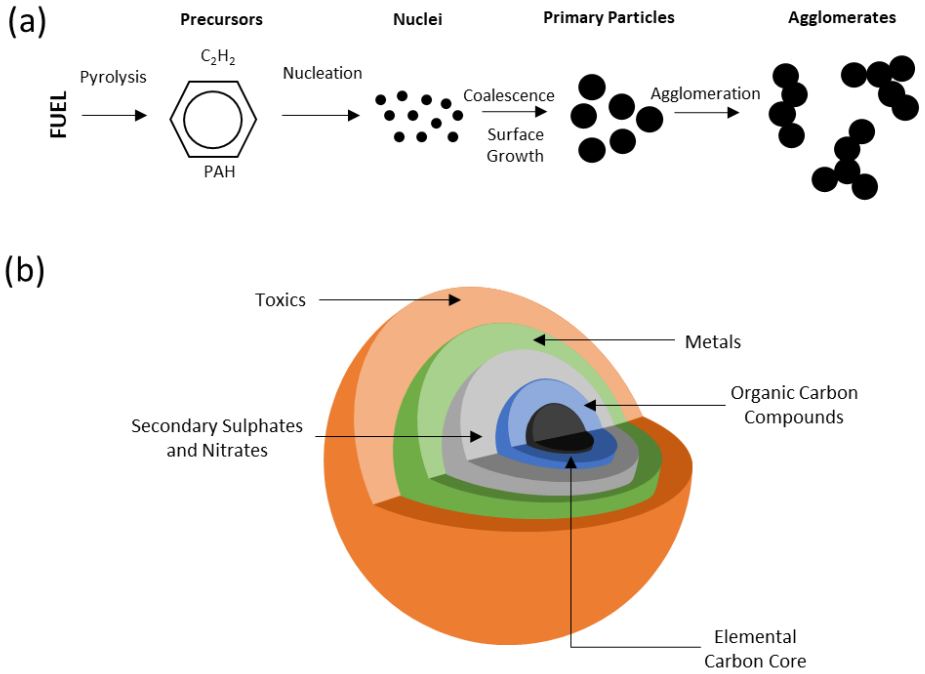

Figure 1.1: (a) Soot formation schematic replicated from[36] (b) Soot structure schematic replicated from [37]

Soot formation in vehicles takes place in the high temperature fuel rich zone, where fuel HCs are oxidised under stoichiometric oxygen conditions, consequently oxidation is limited by oxygen concentration.[30] This reaction area is referred to as the *diffusion flame*, as oxygen transport takes place *via* diffusion through the flame front. Combustion in diesel engines also takes place in the 'premixed flame', where there is a premixed amount of fuel and air. Temperatures are higher in the premixed flame.

Soot particulate formation takes place over six steps: pyrolysis, nucleation, coalescence, surface growth, agglomeration, and oxidation. The first five steps are depicted Figure 1.1a, whilst

the final step (oxidation) converts hydrocarbons into CO, CO_2 and H_2O at any point throughout the process.

The first step in the process, pyrolysis, is where gas phase molecules form soot precursor molecules *via* free radical mechanisms. Pyrolysis can take place in oxygen-free areas (pure pyrolysis) or in oxygen-containing areas.[23] The formation of soot precursor molecules depends on the competition between the rate of pure fuel pyrolysis and oxidation of the precursor by OH. Both of these rates increase with temperature, however, the rate of pyrolysis increases at a slower pace.[31] Pyrolysis produces unsaturated HCs, PAHs, and polyactylenes. If sufficient O species are present acetylene can be oxidised into inert products.[32]

The nucleation step involves the oxidation of the soot precursor molecules at high temperatures in the presence of ions and radicals of HCs, resulting in growth of the soot nuclei.

The majority of soot formation is due to surface growth processes.[28] The surface growth process involves the attachment of gas phase species, e.g. acetylene and PAHs, to the surface of particles. This increases the particles' mass, but not the number of overall soot particles. Heavy HCs can be chemically or physically adsorbed onto the primary particles. Smaller particles have greater surface growth rates than larger particles as they have more reactive radical sites.[33]

Coalescence (also known as coagulation) and agglomeration are the steps where particles combine. During coalescence two particles collide and join together to form one larger spherical particle. Whilst agglomeration is when particles stick together to form a 'chain' of particles.[34]

The sixth step, oxidation, takes place throughout the soot formation process. The oxidation of small particles is a two-step process. Initially, oxygen is absorbed onto the surface of the particle and then it desorbs to attach to a fuel component.[35] Under fuel rich and stoichiometric conditions OH dominates soot oxidation, whilst under lean conditions it is oxidised by OH and O_2.[36]

1.1.2.2 Health and Environmental Impacts of Particulate Matter

Diesel particulate matter is comprised of various species, many of which are known for their harmful effect on human health. Adverse health effects linked to PM include death as result of respiratory and cardiovascular disease, heightened symptoms in asthmatic people as well as some species in PM being carcinogenic.[39]

In 2002, an assessment by the United States Environmental Protection Agency, investigating the health effect of particulate inhalation, established that short term exposure to PM can lead to

irritation of respiratory tract, whilst long term exposure increases the risk of lung cancer in addition to other chronic lung damage.[40]

The World Health Organisation (WHO) have determined that fine particles are "strongly associated with mortality and other endpoints such as hospitalization for cardio-pulmonary disease". However, there is not a specific size threshold in which no negative health effects arise. WHO further states that organic compounds from PM, in particular PAHs, "exert pro-inflammatory as well as adjuvant effects".[41] In 2005 it was estimated that approximately 3 % of cardiopulmonary and 5 % of lung cancer deaths globally are a result of PM. In Europe, these percentages are 1-3 % and 2-5 % respectively.[42] In 2010, ambient air pollution was the cause of 3.1 million deaths.[43] Exposure to $PM_{2.5}$, on average, reduces life expectancy by 8.6 months.[44] Where $PM_{2.5}$ refers to PM less than 2.5 nm in size.

Reports from both the US EPA and WHO bring attention to the carcinogenic and mutagenic characteristics of PAHs.

In addition to adverse effects on human health, diesel PM has undesirable effects on the environment. PM contributes to the greenhouse effect and to global warming as it effects cloud formation. Deposition of PM on vegetation can be related to reduction in light required for photosynthesis, as well as an increase in leaf temperature as a consequence to changes in surface optical properties.[45]

1.1.2.3 Polycyclic Aromatic Hydrocarbons

Polycyclic aromatic hydrocarbons (PAHs), which are also known as polynuclear aromatic hydrocarbons (PNAs), are a class of aromatic compounds which have two or more fused aromatic rings.[46] PAHs typically have between two (naphthalene) and seven (coronene) rings.[47] PAHs are organic species which only contain carbon and nitrogen. Polycyclic aromatic compounds (PACs) are closely related to PAHs, but an atom of sulphur, nitrogen or oxygen replace a carbon in the aromatic ring.[48] PAHs frequently have aliphatic hydrocarbons attached to the rings, hence these are referred to as 'branched' or 'alkylated' PAHs. Hundreds of PAH compounds in nature have been identified,[49] some of the commonly known PAHs are shown in Figure 1.2.

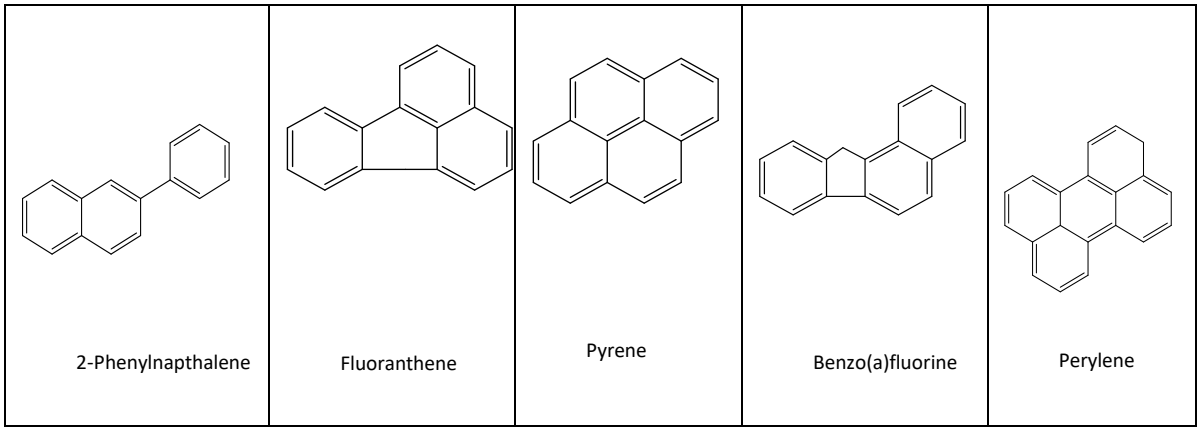

Figure 1.2: Five examples of common polycyclic aromatic hydrocarbons

PAHs are formed by both natural and anthropogenic processes, and they are present in high concentrations in the environment. Storm water runoff, wastewater, atmospheric transport and petroleum sources (drilling, refining, spills, combustion and transport) are all ways in which PAHs spread across the environment. PAHs are most highly concentrated in urban areas, as a consequence of vehicles and urbanisation, the exception to this is areas of recent forest fires.[50]

PAHs are formed in four different ways:

1. Fast, low temperature (<70 °C) transformation of organic matter.
2. Slow, moderate temperature (100 – 300 °C) formation of fossil fuel.
3. Fast, high temperature (>500 °C) incomplete combustion of organic biomass (pyrolysis), which takes place naturally (*i.e.* forest fires) and anthropogenically (*i.e.* fossil fuel combustion).
4. Biosynthesis by plants and animals.[46]

Oil seepages and erosion of petroliferous shales are natural sources of petrogenic PAHs.[51] Other natural sources are from the incomplete combustion of wood and biomass during forest and grass fires.[52] The majority of the anthropogenic PAHs are due to high temperature combustion of automotive, shipping and power plant fuels.[53]

Many PAHs are toxic, mutagenic and/or carcinogenic. They are lipid soluble compounds and therefore can easily be absorbed from the gastrointestinal tract of mammals.[54] There are at least 17 PAHs which are thought to have significantly harmful effects on human health. The International Agency for Research on Cancer classifies PAHs as possibly (Group 2A), or probably (Group 2B) carcinogenic to humans[44]. In addition to being carcinogenic, some PAHs are mutagens

and teratogens and hence are serious threat to human health. Kim *et al.* state that the most significant effect from inhalation of PAHs is the increased risk of lung cancer.[55] A review by J. Jacob has shown that PAHs with four or more rings contribute between 70 – 90 % of PAHs with carcinogenic potential.[56] Using chromatographically fractioned Soxhlet extracts of PM Durant *et al.* were able to observe that PAHs with MWs of 302 contribute 30 % of total PAH mutagenic activity.[57]

The toxic equivalency factor (TEF) is used to describe the cancer potency of a PAH relative to Table 1.3: TEF: Toxic equivalency factors for selected PAHs. I: inadequate evidence; L: limited evidence; S: sufficient evidence; 2A: probably carcinogenic to humans; 2B: possibly carcinogenic to humans; 3: not classifiable; -: negative; +: positive; +/-: questionable; (): limited number of studies. a Evaluated by IARC[58,59] and b WHO.[60] c Data from reference[61]WHO: World Health Organisation. Table replicated from[30]

Compound	MW	IARC[a]		WHO[b]	TEF[c]
		Animal	Human		
Phenanthrene	178	I	3	(+/-)	0.0005
Anthracene	178	I	3	-	0.0005
Fluoranthene	202	I	3	(+)	0.05
Pyrene	202	I	3	(+/-)	0.001
Benzo(ghi)fluoranthene	226	I	3	(-)	
Benzo(c)phenanthrene	228	I	3	(+/-)	
Cyclopenta(c,d)pyrene	226	I	3	+	
Benzo(a)athrancene	228	S	2A	+	0.005
Chrysene	228	I	3	+	0.03
Benzo(b)fluoranthene	252	S	2B	+	0.075
Benzo(k)fluoranthene	252	S	2B	+	0.075
Benzo(e)pyrene	252	I	3		
Benzo(a)pyrene	252	S	2A	+	1
Perylene	252	I	3	(-)	
Indeno(1,2,3-cd)pyrene	276	S	2B	+	0.1
Dibenz(a,h)anthracene	278	S	2A	+	
Benzo(ghi)perylene	276	I	3	-	0.02
Dibenzo(a,l)pyrene	302	S	2B	+	
Coronene	300	I	3	(+/-)	
Dibenzo(a,i)pyrene	302	S	2B	+	
Dibenzo(a,h)pyrene	302	S	2B	+	

The toxic equivalency factor (TEF) is used to describe the cancer potency of a PAH relative to the potency of benzo(a)pyrene. Benzo(a)pyrene's TEF is set at 1, hence PAHs with values higher than 1 have carcinogenic potencies greater than benzo(a)pyrene and values lower than 1 have potencies less than benzo(a)pyrene.[62]

Table 1.3 shows the TEF values for some of the commonly found PAHs in nature.

1.1.3 Other Pollutants

The key pollutants monitored by the EURO limits are not the only harmful pollutants emitted from vehicles which need to be reduced. SOx (sulphur oxides) are emitted when sulphur containing fuels are burnt. SOx results in the formation of sulphuric acid, which has negative impacts on aquatic ecosystems and damages woodland.[63]

Greenhouse gases (GHS) such as methane, CO_2 and N_2O are also emitted from vehicles. Carbon dioxide is the principle GHG, and despite not being directly harmful to human health, it contributes to global warming. Methane is a colourless gas with a global warming potential of more than 20 times that of CO_2 and it can remain in the atmosphere for over 12 years. N_2O can be a by-product

from the abatement of NOx from diesel cars. N_2O has a global warming potential of over 300 times that of CO_2 and can remain in the environment for over 100 years.[64]

The reduction of GHG emissions is directly related to the 12 principles of green chemistry.[65] Green chemistry is the design and use of chemical products/processes which reduce or remove completely hazardous substances. The 12 principles are:

i. Prevent Waste
ii. Atom Economy
iii. Less Hazardous Synthesis
iv. Design Benign Chemicals
v. Benign Solvents and Auxiliaries
vi. Design for Energy Efficiency
vii. Use of Renewable Feedstocks
viii. Reduce Derivatives
ix. Catalysis (vs. Stoichiometric)

x. Design for Degradation

xi. Real-Time Analysis for Pollution Prevention

xii. Inherently Benign Chemistry for Accident Prevention

The main principles being applied to the reduction of GHGs are less hazardous synthesis, energy efficiency, the use of renewable feedstocks and real-time analysis for pollution prevention.

1.1.3.1 N_2O

Ravishankara *et al.* described N_2O as the single most ozone depleting substance. If the amount of N_2O released into the atmosphere were reduced it would greatly enhance the recovery of the ozone layer. Contributions of ozone depleting substances can be compared by using the ozone depletion potential (ODP). An ODP uses the amount of stratospheric ozone destroyed by a unit mass of a substance compared to the amount that would be destroyed by a unit mass of chlorofluorocarbon 11 (CFC-11).[66]

Despite N_2O being a known ozone depleting substance it does not face the same restrictions as other ODS (ozone depleting substances), such as CFCs. Ravishankara *et al.* found that in 2019 of all ODSs the N_2O anthropogenic ODP-weighted emissions were largest and it is expected to remain that way for the rest of the 21st century. The majority of anthropogenic N_2O emissions are from the use of fertilizers, fossil fuel combustion and biomass burning.[66] For diesel vehicles N_2O is an undesired by-product from selective catalytic reduction (SCR) and other abetment technology.[67] The industry is yet to find a solution for the formation of N_2O as a by-product.

1.1.4 Difference Sources of Pollution

There are several different sources, static and non-static, which contribute to air pollution. Where static sources include static engines used for energy generation and non-static sources includes transportation.[68] Different vehicles contribute differing amounts of pollution depending on the engine type (diesel or gasoline) and the type of vehicle (heavy duty or passenger vehicle).

Diesel and petrol vehicles emit different amounts of pollutants due to the differences in the engines. Gasoline vehicles operate using spark-plug ignition whilst diesel vehicles use a compression based system. Spark-plug ignition works by the spark-plug delivering an electric current to the combustion chamber of the engine which ignites the mixture of air and fuel.[69] Whilst compression ignition engines work by compressing air in the compression chamber which subsequently increases the temperature. The air temperature is so high that when atomised diesel fuel is injected into the chamber it combusts.[70]

Diesel vehicles produce less CO_2 emissions than gasoline vehicles, however, diesel vehicles form greater amounts of NOx and particulate matter. Furthermore, diesel vehicles can emit ammonia as a result of excess ammonia being used in its aftertreatment system (Section 1.2.1), this is known as an ammonia slip.[71] The different engine types is why diesel and gasoline vehicles have different emission limits as shown in Section 1.1.

Heavy (e.g. trucks) and light duty vehicles also produce different amounts of pollutants. Heavy duty vehicles operate at higher temperatures resulting in different catalysts being required in their aftertreatment systems compared to light duty vehicles. The difference in emission standards is shown in Table 1.4.

Biofuels are becoming a more common type of vehicle fuel, this results in different emission issues. The consequence of biofuels is that a greater amount of methane is emitted.[11] Methane is currently unregulated but will become regulated upon the introduction of the EURO VII limits. As discussed previously (Section 1.1.3), methane is a greenhouse gas which has negative consequences for the environment.

Table 1.4: Euro VI limits for diesel heavy duty and light duty vehicles. Data obtained from Dieselnet

Pollutant	Heavy Duty[72]	Light Duty[10]
CO / g^{-1} km	1.5	0.50
HC / g^{-1}km	0.13	-
HC + NOx / g^{-1}km	-	0.17
NOx / g^{-1}km	0.40	0.08
PM / g^{-1}km	0.001	0.005
PN / $\#^{-1}$km	8.0×10^{11}	6.0×10^{11}

1.2 Automotive Aftertreatment

In order to meet the ever changing emission legislation, the automotive industry has developed, and continues to develop, advanced technology to reduce emissions. One of the key factors in emission abatement is the air to fuel ratio.

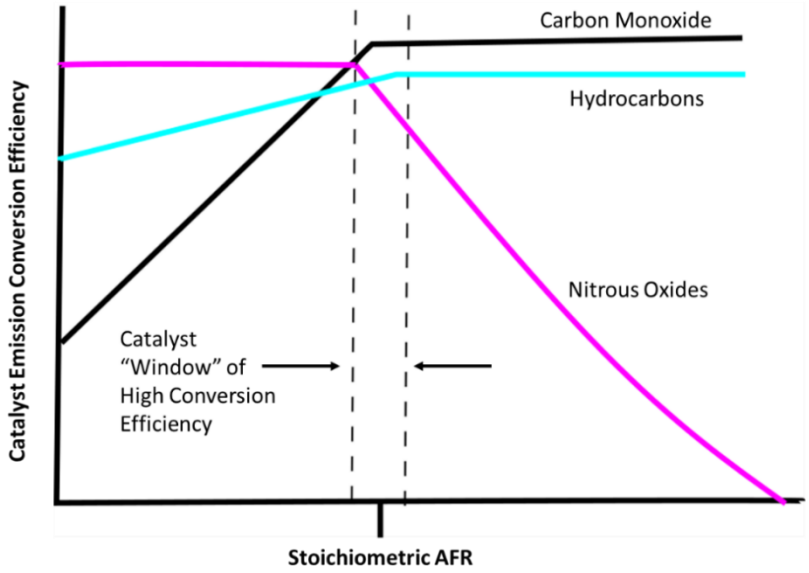

Figure 1.3: The catalyst emission conversion efficiency for carbon moxide, hydrocarbons and nitrous oxides against the air to fuel ratio (AFR) shows where the window for high conversion is in terms of AFR. Replicated from[73]

The three-way catalytic (TWC) converter was first introduced in the 1980s in spark – ignited gasoline engines. The TWC converter operates using the selective catalytic reduction of NOx by CO and HC. This works in gasoline engines as they have a stoichiometric air to fuel ratio.[74] Modern gasoline engines have an oxygen sensor so that the air: fuel can be maintained, as in the presence of excess oxygen the catalyst becomes ineffective at reducing NOx. Figure 1.3 shows the air to fuel ratio against the catalyst conversion efficiency for NOx, HCs and CO.

The stoichiometric operation of diesel engines has also been investigated, however this proved too costly.[75] Diesel engines run under lean conditions, *i.e.* in excess oxygen, (air: fuel ratios between 18: 1 and 21: 1) and hence the TWC technology cannot be used for diesel vehicles. It is kinetically difficult to remove NOx in the presence of oxygen, consequently so far no catalyst has been developed for this application in diesel vehicles. Instead, other technology has been developed for use in diesel cars. Diesel cars typically use a diesel oxidation catalysts (DOC) to remove the majority of CO and HCs, SCR to remove NOx, and a diesel particulate filter (DPF) to trap and oxidise particulate matter. Diesel aftertreatment also includes an ammonia slip catalyst (ASC) to remove any excess ammonia from the SCR system. The DPF requires an injection of fuel at high temperatures to regenerate the filter (*via* combustion of the trapped soot).

In summary, gasoline vehicles only require a single aftertreatment system, the three-way catalytic converter, whilst diesel vehicles require a series of aftertreatment technology (DOC, SCR, DPF and ASC) to remove emissions. There is research into combining the diesel aftertreatment components, but it is complex due to the engine running lean. The combination of the DPF and SCR systems is an area of particular interest as a single catalyst operating at lower temperatures

would remove the need of a fuel injection. This would improve the fuel economy of the vehicle as well enabling abatement to take place at lower temperatures.

A major problem in automotive abatement for both diesel and gasoline engines is cold start. Automotive catalysts operate within certain temperature ranges which are typically high (usually > 300 °C). This leads to problems when a vehicle is first turned on and if it is only being used for short journeys resulting in the required temperatures not being reached. Consequently, full abatement does not take place and the majority of harmful emission from vehicles takes place during the cold start.[76,77] Therefore, this is a major area of automotive research with focus on finding a solution to cold start emissions. Various solutions are being investigated including the use of electric heated catalysts and adsorbers for cold starts (Section 1.2.4) in addition to finding catalysts which operate at lower temperature ranges.[78,79]

1.2.1 NOx Abatement Technology

A selection of different NOx abatement technologies have been developed over the years. Including; Exhaust Gas Recirculation (EGR), a technique which replaces air intake with recycled exhaust gas, which reduces the amount of nitrogen available to be oxidised to NOx; Lean NOx traps; NOx absorbers and Selective Catalytic Reduction (SCR).

The most commonly used NOx abatement technology for diesel passenger vehicles is NH_3 - SCR. SCR technology was first developed in Japan in the 1970s for use in thermal power plants, the technology became more popular in Europe in the 1980s.Urea – SCR technology has been used in mobile diesel engines since the mid-2000s. NH_3- SCR was chosen by several OEMs to meet the EURO V (2008) NOx limits for heavy duty vehicles, whilst the United States introduced it in 2010 to meet the US EPA NOx limit.

For passenger vehicles, SCR technology was introduced in Europe in certain models in 2008 to help meet EURO V limits, with the majority of diesel passenger cars having SCR technology to meet EURO VI limitations. In the United States diesel passenger cars were introduced to SCR technology between 2012 – 2015 to meet emission standards.

Commercial SCR catalysts are typically coated onto honeycomb monoliths or plates.[80] The catalysts are made up of a carrier metal oxide which then supports the active components.

NH_3 - SCR uses NH_3 to selectively catalytically reduce NOx to H_2O and N_2. Due to the toxicity of NH_3 a -liquid known as AdBlue is used to provide NH_3 for the SCR reaction. AdBlue is made up of 67.5% deionised water and 32.5% high-purity urea.[81] AdBlue is stored in a tank separate from the diesel fuel and when injected into the hot exhaust pipe upstream of the SCR catalyst it

reacts to form NH_3 (as shown in Equation 1.13). It is essential that the injection of urea into the exhaust is precise, as too little results in incomplete conversion of NO and too much results in undesirable NH_3 being released (ammonia slip). Thus, SCR systems have highly complex control systems, which continually adjust the quantity of urea injected to match the operation of the vehicle. The control system also has to take into account the storage capacity of the SCR catalyst, as NH_3 is stored at low temperatures and released at high temperature.

$$\boldsymbol{CO(NH_2)_{2(g)} + H_2O_{(g)} \rightarrow 2NH_{3(g)} + CO_{2(g)}} \quad \textbf{Equation 1.13}$$

$$\boldsymbol{4NO_{(g)} + 4NH_{3(g)} + O_{2(g)} \rightarrow 4N_{2(g)} + 6H_2O_{(g)}} \quad \textbf{Equation 1.14}$$

$$\boldsymbol{6NO_{2(g)} + 8NH_{3(g)} \rightarrow 7N_{2(g)} + 12H_2O_{(g)}} \quad \textbf{Equation 1.15}$$

$$\boldsymbol{6NO_{(g)} + 4NH_{3(g)} \rightarrow 5N_{2(g)} + 6H_2O_{(g)}} \quad \textbf{Equation 1.16}$$

$$\boldsymbol{2NO_{2(g)} + 4NH_{3(g)} + O_{2(g)} \rightarrow 3N_{2(g)} + 6H_2O_{(g)}} \quad \textbf{Equation 1.17}$$

$$\boldsymbol{NO_{(g)} + NO_{2(g)} + 2NH_{3(g)} \rightarrow 2N_{2(g)} + 3H_2O_{(g)}} \quad \textbf{\textit{Equation 1.18}}$$

NH_3 reacts with NOx in various conditions as shown in Equation 1.14 - Equation 1.18. Equation 1.14 is the most significant SCR reaction and is known as the 'standard SCR reaction'.[73] The standard SCR reaction uses stoichiometric amounts of NO and NH_3. It takes place quickly on the catalyst in the temperature range of 250 °C – 450 °C in excess of oxygen. Equation 1.16 does not consume oxygen and takes place slowly. Approximately, 5 % of NOx reactions involves NO_2 and consequently Equation 1.15 and Equation 1.18 are less significant. The presence of NO_2 accelerates NOx conversion for Equation 1.18. It has been observed that when NO and NO_2 are present in equimolar quantities the rate of reaction is much faster than that of the standard SCR reaction.[82,83]

One of the key advantages of SCR systems is that they can operate over a wide temperature range with many systems achieving 90 % NOx conversion under steady state conditions. However, the SCR catalyst can be poisoned by sulphur, phosphorous and other species found in automotive fuel, this can lead to deactivation of the catalyst. Thermal deactivation of the catalyst is possible if exposed to extreme temperatures for long periods of time. Some of the undesirable reactions which may occur are:

$$4NH_{3(g)} + 5O_{2(g)} \rightarrow 4NO_{(g)} + 6H_2O_{(g)}$$ **Equation 1.19**

$$4NH_{3(g)} + 3O_{2(g)} \rightarrow 2N_{2(g)} + 6H_2O_{(g)}$$ **Equation 1.20**

$$2NH_{3(g)} + 3O_{2(g)} \rightarrow N_2O_{(g)} + 3H_2O_{(g)}$$ **Equation 1.21**

$$SO_{2(g)} + {}^{1}/_{2}\, O_{2(g)} \rightarrow SO_{3(g)}$$ **Equation 1.22**

Equation 1.21 shows how N_2O may be formed as a consequence of NOx reduction *via* SCR, as mentioned in Section 1.1.3.1 has an extremely negative impact on the ozone layer.

1.2.1.1.1 Catalysts for Selective Catalytic Reduction

Different catalysts are required for heavy duty and passenger vehicles, due to the different temperature windows at which the vehicles operate at. Heavy duty vehicles operate, higher temperatures, and hence the catalysts have to active and not sinter at these high temperatures. A wide range of catalysts are used and are being researched for use in passenger diesel vehicles, and includes zeolites, silver, precious group metals and base metal oxides.

1.2.1.1.2 Zeolites

Zeolites are popular catalysts for SCR, with research on Pd, Co, Fe and Cu zeolites catalysts having been completed. Zeolite based catalysts are active and selective over a wide temperature range, as well as being thermally stable, however, they do have high NH_3 storage.

An early review on the catalytic oxidation of NH_3 compared the catalytic ability of several transition metals on a Y type zeolite for NH_3 oxidation.[84] The transition metals studied were Mn^{2+}, Fe^{3+}, Co^{2+}, Ni^{2+}, Cu^{2+}, Cr^{3+} and Ag^{+}. Activity for NH_3 oxidation was found to follow the order:

CuY > CrY > AgY > CoY > FeY > NiY = MnY

The main reaction product in all cases was molecular nitrogen, however, N_2O was formed over the AgY and CrY catalysts.[85]

Li and Armor studied ZSM-5 modified with Pd, Rh and Pt for NH_3 selective catalytic oxidation.[86] The Pd modified zeolite was found to have the highest activity and selectivity towards N_2 at low temperatures, this is confirmed by other literature.[87,88] For both Y and ZSM-5 type catalysts the location and loading of the noble metal has significant impact on the catalytic performance of the catalyst. PdY has been found to be an active catalyst, with the catalytic activity increasing with the increase of Pd loading. The activity of the catalyst was due to the presence of palladium oxide species.

A comparative study of NH_3-SCR over Cu and Fe zeolites showed that the Cu system had greater NH_3 storage capacity (ASC) and higher activity for NH_3-SCR. At low temperatures an inhibiting effect of NH_3 was observed over the Fe-zeolite. Formation of N_2O was observed over the Cu system. N_2O still formed over the Cu catalyst when NO_2 was absent from the gas stream. Whilst the Fe-catalyst only formed N_2O when the gas mixture contained an excess of NO_2.[89] Kamasamudram also compared the activity of Fe- and Cu- based zeolites, as well as vanadium based catalysts. In this work it was also found that a Cu-zeolite had greater ASC than the Fe based zeolite.[90]

1.2.1.1.3 Copper Based Zeolites

Copper based zeolites for SCR are a particularly active area of research. Cu-zeolites are active for SCR at low temperatures (< 350 °C). Copper exchanged into chabazite (CHA) is a successful SCR catalyst for diesel passenger vehicles. The key types of chabazite for SCR are SSZ-13 and SAPO-34. These zeolites are known to be active, selective and hydrothermally stable catalysts for NH_3-SCR.

Experiments utilizing X-ray absorption fine structure (XAFS) and XRD characterisation Deka *et al.*[91] and Fickel *et al.*[92] found that one type of copper site is present on the Cu-SSZ-13 catalysts. The Cu site is located in the zeolite cage coordinated to three oxygen atoms of the six-membered ring. Mononuclear Cu^{2+} species were discovered to be the active sites for Cu-SSZ-13 and Cu-SAPO. However, this contradicts the work completed by Kwak *et al.* who postulated that there were two Cu sites; the first being coordinated in the six membered ring and the second being in the cages of the CHA structure.[93]

Ma *et al.* investigated the differences between Cu-SAPO and Cu-SSZ. Hydrothermal treatment of the catalysts had an impact on the microstructures of the zeolite supports, redox

ability, selectivity and catalytic activities for NH_3-SCR. After aging, Cu-SAPO displayed similar activity to that prior to ageing, whilst Cu-SSZ showed lower conversion rates and selectivity towards N_2 post ageing. It was found that both catalysts had a decrease in surface area and pore volumes after undergoing ageing.[94] Nui *et al.* also investigated the hydrothermal stability of Cu-SAPO catalysts. After XRD, H_2-TPD, NH_3-TPD and XPS analysis it was concluded that the activity and hydrothermal stability of the catalyst is due to the framework, Cu species distribution and the pore properties. After hydrothermal aging at 800 °C for 16 h, Cu-SAPO displayed > 90% NOx conversion in the temperature range 224 – 400 °C.[95] This shows that Cu-SAPO has potential for use in commercial aftertreatment systems.

The Cu-CHA catalyst is still an active area of research especially into the hydrothermal stability of the catalyst. Utilizing *in situ* spectroscopic techniques, further understanding on the redox cycle of the Cu species. It is theorised that oxygen is the sole oxidant for the re-oxidation of Cu^+ to Cu^{2+}. Furthermore, a high density of Cu in the zeolite enhances NH_3-SCR activity by promoting the oxidation of Cu^+.[96] Through TPD testing the ammonia storage capacity of the catalyst determined that the higher the Cu and the SiO_2/Al_2O_3 loading the larger the ammonia storage capacity of the catalyst.[97]

1.2.1.1.4 Silver Catalysts

Ag-Al_2O_3 is a highly active catalyst for HC-SCR (*i.e.* where hydrocarbons are used as the reductant as opposed to NH_3). Ag-Al_2O_3 is limited to low temperatures (150 – 300 °C), which is a consequence of C-containing compounds and nitrate species depositing on the catalyst. Studies have shown that incorporating H_2 into the exhaust stream aids the prevention of catalyst poisoning and improves the catalyst's activity at low temperatures.[98–101]

Ag-Al_2O_3 has also been shown to be active for NH_3-SCR, however, H_2 is required in the exhaust stream. The presence of H_2 enhances the NOx reduction over a range of temperatures.[102–105]

1.2.2 Diesel Particulate Filters

Diesel particulate filters (DPFs) are compulsory in all diesel cars, since the introduction of the EURO 5 limits in 2009.[106] Figure 1.4 shows a schematic of a DPF. DPFs are ceramic (typically coredrite) filters with alternatingly blocked channels. The channel walls are coated with a soot combustion catalyst. As the exhaust gas flows through the filter the particulate matter is trapped in the filter. In the majority of passenger vehicles, an injection of fuel at high temperature combusts the soot and the filter is regenerated. This is known as active regeneration and is highly effective (> 90 %),[107] however, it does have a negative impact on the fuel economy of the vehicle.

An alternative regeneration technique is known as passive regeneration. Passive regeneration does not require an injection of fuel to regenerate the filter, instead it relies on NO_2 in the exhaust gas to oxidise the soot.[108] In principle this is a highly efficient way of removing soot and maintaining good fuel economy. However, it does depend on the exhaust gas being at a higher enough temperature for the NO_2 to oxidise the soot. This is a difficult parameter to control. Hence, passive regeneration is not commonly used, and when it is it is more frequently used in heavy duty vehicles, as they operate at higher temperatures then passenger vehicles.

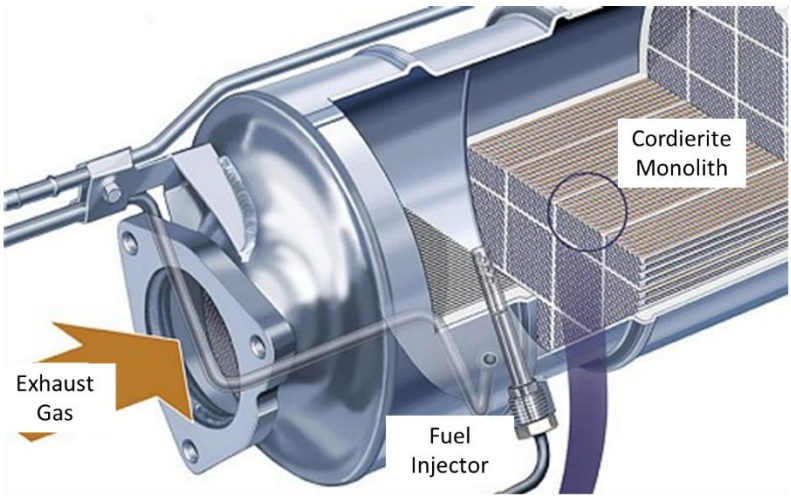

Figure 1.4: Schematic of a diesel particulate filter from the Telegraph[98]

1.2.2.1 Catalysts

It is widely acknowledged that soot in a DPF can be oxidised in a variety of different ways: non-catalytically and catalytically by NO_2 and O_2. Catalysts are used to lower the temperature and fuel requirement needed for regeneration of DPFs by facilitating soot oxidation.

In order to test the oxidation ability of soot catalysts they have to be in contact with soot. There are two main types of contact which can be achieved, tight and loose contact.

Tight contact is achieved by grinding the catalyst and soot together, either using a pestle and mortar or mechanically in a ball mill. This establishes close contact between the catalyst and soot resulting in high levels of soot oxidation.

Whilst loose contact is where the soot and catalyst is mixed with a spatula or shaken until homogenous. Loose contact achieves less contact with the catalyst and hence less oxidation is observed compared to tight contact. However, loose contact is more comparable to conditions in DPFs, hence, to make research studies applicable to real exhaust after treatment loose contact should be used.

Soot oxidation catalysts commonly have a platinum group metal (PGM) as the active component due to their high activity and durability. PGM catalysts however are expensive, resulting in research into non-PGM catalysts for soot oxidation. Ceria based catalysts are incredibly popular for soot oxidation catalysts, due to their redox ability and capability to deliver oxygen from the lattice to the soot particles.

1.2.2.1.1 Ceria redox catalysts for soot oxidation

Cerium can exhibit both the +3 (Ce_2O_3) and +4 (CeO_2) oxidation states and from thermodynamic data it has been concluded that cerium metal is not stable in the presence of oxygen. Cerium's high lattice ion mobility, the ability to readily switch between $Ce^{3+}$and Ce^{4+} and Ce^{4+}'s high oxidising power results in ceria exhibiting good catalytic properties.[110] As a consequence of ceria's high redox and lability of lattice oxygen it is most suitable for total oxidation reactions, such as the oxidation of soot.[111] Ceria's oxidation ability can be improved by the addition of dopants, or the incorporation of elements into ceria's lattice. Doped-ceria catalysts for soot oxidation for diesel vehicles are highly popular due to their oxygen storage capacity (OSC).

Pure ceria is not suitable for industrial applications. It has low OSC, as well as experiencing substantial loss of surface area as a consequence of thermal sintering and deactivation of the Ce^{4+} and Ce^{3+}.[112,113]The presence of a foreign ion in the ceria lattice can improve OSC, thermal deactivation and catalytic activity.[112,114]

A soot oxidation catalyst must be able to withstand the harsh conditions in an exhaust. Deactivation of automotive after treatment catalysts is generally due to thermal deactivation, or by poisoning.[115] The temperature inside a DPF can reach as high as 1100 °C because of the exothermic soot combustion process.[116] Whilst poisoning of the catalyst occurs from fuel-derived sulphur and lubricant-derived phosphorous. The deactivation of ceria in exhausts has hindered its use in the automotive industry. Hence, it is essential to assess the thermal stability and chemical durability of modified ceria catalysts.

Ceria-based soot oxidation catalysts with different components have different activities, this is due to their structural properties and the catalytic mechanisms of the catalysts. Bueno-López *et al.* determined that there are two ceria-catalysed soot oxidation mechanisms. The active oxygen-assisted mechanism and the NO_2-assisted mechanism.[117]

Ceria promotes the formation of reactive oxygen species, which then oxidise soot in the active oxygen-assisted mechanism. Whilst for the NO_2-assisted mechanism, ceria aids NO

oxidation which forms NO_2, which consequently oxidises soot. Active oxygen species have a lower stability than NO_2, due to this the active oxygen mechanism works best with soot and catalyst in tight contact with each other, whilst the NO_2-assisted mechanism works in both tight and loose conditions.[117] The mechanisms are described in further detail in Figure 1.5

Modified ceria catalysts can be divided into several subcategories: ceria-containing mixed metal oxides, transition metal promoters and alkali metal promoters.

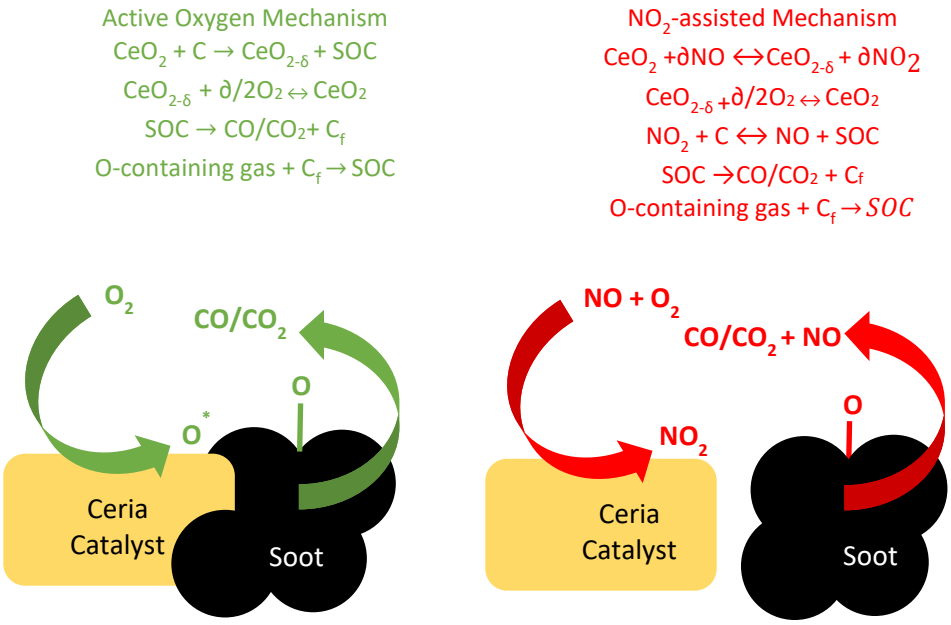

Figure 1.5: Schematic for the active oxygen and NO_2-assisted mechanism where SOC is the surface oxygen-carbon complexes and C_f is the free carbon sites. Replicated from[105]

1.2.2.1.2 Transition and rare earth metal promotors

The valence states of some transition metals (Co, Mn, Cu, Fe and Cr) are changeable to a certain degree, hence they have good redox abilities and therefore can be active components for soot oxidation catalysts.[118,119] Transition metals are much cheaper than PGMs and hence hold appeal to the automotive industry.

Transition metal promoted ceria oxidation catalysts can experience deactivation due to sulphur poisoning. To combat this addition additives can be added into the catalyst such as Cs_2O, K_2O, BaO, ZrO_2 or Al_2O_3.[110,120,121] The alkali species mixed with the transition metal catalyst aids with improving the catalytic activity as well as the durability of the catalyst. Whilst, modification with inert oxides (such as Al_2O_3, ZrO_2, SiO_2 and V_2O_5) increases the thermal stability of the catalyst, but has a negative effect on the catalytic activity.[122,123]

Mukherjee *et al.*[112] investigated a range of dopants for ceria soot oxidation catalysts, the dopant ions had a range of ionic radii. Of the studied dopants (Fe, Zr, Hf, Pr, La and Mn) ceria-Mn was found to have superior catalytic activity for CO and soot oxidation. This is believed to be due to CeO_2-Mn having a low binding energy to surface oxygen, this promoted CO oxidation. Furthermore, CeO_2-Mn had the highest concentration of oxygen vacancies, which enhanced the redox properties of the catalyst.

Reddy *et al.*[124] found that a CuO-CoO/CZ bimetallic catalyst showed excellent catalytic activity, as well as having extremely high product selectivity (CO_2 > 99%). The stability and activity of the catalyst is partially due to it's oxygen vacancies and it's specific surface area.

1.2.2.1.3 Alkali metal promotors

Unlike the rare-earth and transition metals, which contribute to the redox ability of the catalyst, alkali metal promoters contribute very little to the redox ability.[125,126] The alkali metals have good NOx storage abilities and increase the catalyst/soot contact, consequently improving the oxidation of soot.[127]

Aneggi *et al.*[125] investigated ceria doped with different alkali metals for their ability to oxidise soot, and found that K- and Cs-modified CeO_2 was the most active catalyst for soot oxidation. Olong *et al.*[128] found that a weight loading of 20 % Cs was the optimum loading. CaO and MgO have been shown to be active for NOx-assisted soot combustion.[128]

The K precursor has a major impact on the reactivity of K/CeO_2 catalysts. Zhang *et al.*[129] found that the soot oxidation activity followed an order of:

$KF/CeO_2 = KCl/CeO_2 > KBr/CeO_2 > KI/CeO_2$

Aneggi *et al.*[125] also reached the conclusion that KCl resulted in a poor K/CeO_2 oxidation catalyst, when compared to K_2CO_3 and KOH. Whilst researching $BaKCo/CeO_2$ catalysts for soot oxidation Peralta *et al.*[130] found that KNO_3 was more active than K_2CO_3, however, K_2CO_3 produced a more thermally stable catalyst. In 2017, Rinkenburger *et al.*[131] investigated the catalytic effect of potassium compounds in soot oxidation and found that activity of the potassium salt depends on the anions following the order:

$K_2CO_3 \approx KOH > KHCO_3 > KNO_3 > K_2SO_4 \approx KCl$

This is in agreement with other literature, and hence, KNO_3, K_2CO_3 and KOH have all been found to be suitable precursors for K/CeO_2.

Modifying ceria catalysts with alkali metals does not enhance the redox or the OSC ability of the ceria. Instead, the alkali metal aids soot oxidation in three different ways.

It is acknowledged that alkali (Na, K and Cs) species (oxides, peroxides, hydroxide, nitrates, carbonate and chloride) with a volatile nature increase the catalyst-soot contact and hence improve catalytic activity.[132,133] This promotional effect is not observed for alkali-earth metals, e.g. Ba, Mg and Ca, due to their poor mobility on the surface of the catalyst.[133]

Secondly, K species can enhance soot oxidation through a carbonates-assisted mechanism. The carbonates-assisted mechanism was first suggested by Querini *et al.,*[132] when investigating CoK/MgO catalysts for soot oxidation. It was found that K favoured soot oxidation by forming carbonate species from the soot. Later, this theory was expanded to include catalysts formed of Co and K supported on MgO, La_2O_3 and CeO_2.[133,134] They theorised that superoxides and peroxides over the CeO_2 catalyst could react with the soot, resulting in formation of K_2CO_3, which consequently decomposes to produce CO_2. This theory was supported by Aneggi *et al.,*[125] who further suggested that the carbonates-assisted mechanism could also be applicable to soot oxidation over alkali metals-modified ceria. Pisarello *et al.* discovered that CO_2 did not interact with BaO or MgO in soot oxidation catalysts and hence the carbonates-assisted mechanism does not apply to all alkali-earth metals.[135]

Alkali and alkali-earth metals have good NOx storage ability in the presence of NOx.[136,137] It has been found that NOx storage ability of alkali metals improves soot oxidation over transition metals-ceria catalysts. Ito *et al.* found that the temperature of soot combustion could be lowered using a MnOx-CeO_2 catalyst. MnOx-CeO_2 also formed surface nitrates which oxidise soot.[138]

1.2.2.1.4 Silver Catalysts for Soot Oxidation

Platinum group metals on a ceria support have been investigated thoroughly for use as soot oxidation catalysts. However, due to the high cost of PGMs they cannot be used economically for real life applications. Pt, Pd and Au catalysts are used with loadings of 2 – 10 w.t. %.[139] One more affordable alternative is Ag. Ag-ceria catalysts have been proven to be active soot[140,141] and CO[142] oxidation catalysts. Ag-CeO_2 can have charge transfer between the Ag and CeO_2 and the Ag enhances CeO_2 redox properties, which is caused by the interaction between Ag^+/Ag^0 and the Ce^{3+}/Ce^{4+} pairs.[143]

Grabchenko *et al.*[139] investigated the role of metal-support interaction for CO and soot oxidation over 10% Ag/CeO_2 catalysts, which were prepared by different techniques. The catalysts were prepared *via* incipient impregnation, co-precipitation and impregnation of pre-reduced

CeO_2. It was determined that there was a clear correlation between the catalytic activity and metal support interaction in Ag/CeO_2 catalysts. With the catalysts' MSI (metal support interactions) enhancement having the following order:

Ag/ CeO_2 (imp) < $Ag\text{-}CeO_2$ (co-DP) ≤ Ag/CeO_2 (red-imp)

This enhancement was thought to be due to increased oxygen vacancies. Sadlivskaya *et al.*[144] conducted a similar investigation into Ag/CeO_2, preparing the catalysts by co-precipitation and wet impregnation. It was also concluded that the preparation technique had an impact on the catalyst's structure and activity. The catalyst prepared *via* co-precipitation exhibited greater activity for soot oxidation, as a result of superior interaction between the CeO_2 and Ag particles.

Ag for soot oxidation has been investigated using ceria, zirconia and alumina as supports. An Ag/Ag_2O mixture is observed for all three supports however the ceria support stabilises Ag in the oxidised state, whilst with ZrO_2 and Al_2O_3 metallic Ag is formed. Aneggi *et al.* suggest that the addition of Ag to ceria has little impact on soot oxidation as ceria is already an active catalyst for soot oxidation.[140]

$AgSO_4/Al_2O_3$ has been shown to be an active catalyst for soot oxidation, as well as being resistant to sulphur poisoning.[145] High temperature XRD experiments imply that some of the Ag_2SO_4 on the Al_2O_3 support melts at high temperatures and forms contact between Ag_2SO_4 and soot, resulting in a high oxidation rate of soot. Kikugawa *et al.*[145] has found that Ag_2SO_4 displays superior activity for soot oxidation than Ag/CeO_2 and Ag/Al_2O_3. Gao *et al.*[146] also found that a sulphation pre-treatment resulted in higher catalytic activity than Ag/Al_2O_3 without pre-treatment.

1.2.3 The Simultaneous Removal of NOx and PM

As explained in Section 1.2 diesel cars currently have three separate aftertreatment systems for the removal of Nox, PM, CO and HCs. However, it would be advantageous if the systems could be combined. Due to the excess of oxygen in the diesel exhaust stream the two more difficult systems to combined are the DPF and SCR. Despite the challenges associated with combining these systems, it is an active area of automotive aftertreatment research with the perfect solution yet to be found.

The main solution being investigated is to coat the DPF with an SCR catalyst (known as SCRF), allowing PM to be trapped and Nox to be reduced as the exhaust gas flows through the filter. The catalyst coated on the DPF monolith (an alternatingly blocked channelled monolith) must be suitable for both the reduction of Nox and the oxidation of soot. A key difficulty in this scenario is the active regeneration of the DPF. In the majority of diesel passenger vehicles the DPF is actively

regenerated at high temperatures (as described in Section 1.2.2), these high temperatures can result in deactivation and sintering of the SCR catalyst. Hence, a thermally stable catalyst needs to be found if this approach is to be used commercially. SCRFs are thought to be key in meeting the future EURO VII regulations hence extensive research is being performed to find the ideal catalyst for the system. BASF have commercialised a SCRF using a zeolite catalyst which has been shown to be able to withstand active regeneration of the filter and performs to a similar level of the separate SCR and DPF systems.[147]

An early publication on this topic investigated the use of perovskite-related oxides for the simultaneous removal of Nox and particulate matter from a diesel exhaust. It was found that perovskite-type and Cu-based K_2NiF_4-type oxides were superior catalysts than transition metals and Pt/Al_2O_3 for the simultaneous removal of Nox and soot. It was found that introducing K into the catalyst had a promotional effect on soot oxidation. Furthermore, Teraoka *et al.* suggested that NO_2 participated in the reaction. [148]

Co, K and/or Ba supported on MgO, La_2O_3 and CeO_2 were investigated for their ability to oxidise soot. With K/La_2O_3 and K/CeO_2 showing the best activity for soot oxidation, this is believed to be due to the redox ability of the catalysts. However, $Co,K/LaO_3$ and $Co,K/CeO_2$ catalysts had the ability to simultaneously remove soot and HNO_3. When K and La were on the soot surface higher combustion rates were observed. Ba was introduced to the catalysts with the belief that it would promote the interaction of soot with NO_2, however, the formation of stable nitrates inhibited the soot oxidation.[135] Soot has been shown to negatively impact Nox storage over a $PtBa/Al_2O_3$ catalyst. When the stored Nox is released, the NO_2 actively oxidises the soot.[149]

Fe-Ce-Zr oxides have also been investigated for the simultaneous removal of Nox and soot from diesel exhausts. Cheng *et al.* found that using this catalyst NO was reduced by >90 % and soot was fully combusted in a temperature range of 265 – 420 °C. The presence of Zr and Fe reduced the soot combustion temperature and Fe enhanced Nox reduction and soot oxidation at intermediate temperatures.[150]

A commercial V_2O_5/TiO_2 SCR catalyst was tested for its ability to also oxidise soot. At low temperatures the presence of soot did not have an overall effect on the catalyst's ability to reduce Nox. However, at temperatures higher than 400 °C Nox conversion was inhibited by the presence of soot. An addition of 2% Ca to the V_2O_5 catalyst resulted in deactivation of the SCR catalyst.[151]

Davies *et al.* found that a Ag/CZA (CeO_2-ZrO_2-Al_2O_3) soot combustion catalyst had the ability to simultaneously remove Nox and soot *via* the generation of *in situ* N_2O.[152] As previously discussed N_2O is extremely harmful to the environment and it is frequently a by-product of the non-selective reduction of Nox. Ag/CZA has the ability to utilise this N_2O to oxidise soot at low temperatures. At higher temperatures, where N_2O is no longer formed, oxidation of soot takes place in a series of steps:

- non-catalytic oxidation by NO_2
- catalytic oxidation by O_2
- non-catalytic oxidation by O_2

This work shows that it is possible to advantageously utilise the *in situ* generated N_2O to combust soot at low temperatures. Engine testing showed promising results for the use of the catalyst in a real exhaust treatment system. The advantage of a catalyst which combusts soot at low temperature is that active generation would no longer be required to regenerate the filter and hence there would no longer be a negative impact on the fuel economy of the vehicle.

1.2.4 Current Problems and the Future of Aftertreatment Technology

1.2.4.1 Cold Start

As discussed previously in Section 1.2 cold start is a major issue in automotive abatement. The combination of low temperatures and a temperature sink over the DOC results in more than 50 % of NOx emissions taking place in the first 350 seconds of a journey due to the low SCR temperature.[153] Up to 80% of HC and CO emissions occur during the cold start period.[154] Hence, developing technology to combat cold start is essential. There are various different technologies being developed including retarded fuel ignition timing, lean air:fuel ratio operation, modification of catalysts, adsorbers for cold start and electrically heated catalysts (EHC).[154]

EHC is a popular solution to problems caused by cold start as it provides thermal energy directly to the catalytic systems from either the vehicle's battery or from an onboard generator as and when required. The increasing number of hybrid vehicles also makes the use of EHC a promising solution. There are several advantages of EHC over the other suggested sold start solutions, these are:

1. Thermal energy providing directly on the aftertreatment system.[155]
2. High level of control over the heating.[156]
3. Lower loadings of precious metals required for the catalysts.[157]

The use of EHC has been found to reduce emissions in diesel and gasoline vehicles.[158–161] The EHC is placed upstream of the DOC this increases the catalyst's ability to remove emissions from the exhaust. The use of an EHC increases the DOC's outlet temperature which consequently is advantageous for SCR heating and the regeneration of the DPF.[154]

One of the other popular solutions to cold start is the use of adsorbers. Absorbers aid cold start emissions by adsorbing the pollutants formed during the cold start and releasing them at higher temperatures when the aftertreatment systems can work effectively. Some NOx adsorbers usually used for the removal of NOx from diesel vehicles have been found to be effective adsorbers for cold start emissions. NOx adsorbers are comprised of an active metal, typically platinum, and a storage component, BaO, both of which are supported on a high surface area support, Al_2O_3. The BaO stores NOx whilst the engine is running lean. When the BaO is saturated, the system is regenerated by a brief period where the engine operates in a fuel rich atmosphere. During the fuel rich period the stored NOx is catalytically reduced to N_2 and released. The technology is now being utilised to combat cold start emissions. However, the catalysts have to be altered to adsorb the NOx at lower temperatures. Honda has found that a Pt/ZSM-5 catalyst has the ability to adsorb both HCs and NOx during cold start.[162] Ceria based catalysts have also been found to be promising due to the vacancies which can form in ceria's cubic fluorite phase.[163] The doping of rare-earth metals has also been found to enhance the storage of NOx at low temperatures.[164,165]Chen *et al.* has investigated combining the NOx adsorber and DOC systems. The catalysts investigated were $Pt/CeO_2/Al_2O_3$ and $Pd/CeO_2/Al_2O_3$. The Pd based catalyst was found to be superior at storing NOx at low temperatures however the presence of adsorbed NOx on both catalysts had a negative impact on the light-off of CO and HCs.[166]

1.2.4.2 Effect of Catalyst Aging

Another major problem in automotive catalysis is the effect of aging on the catalysts. The catalysts have to be able to withstand high temperatures for long period of times hence the catalysts have to be hydrothermally stable. Long periods of exposure to high temperatures can result in the catalyst sintering *i.e.* the nanoparticles merging to become larger particles. This reduces the surface area of the catalyst and reduces the active sites available for catalysis. Sintering poses as significant threat for SCRF catalysts which still require active regeneration of the filter.

As a consequence of the effect of sintering on catalytic performance, research into catalysts which remain stable at high temperatures and research into catalysts which work effectively at

low temperatures (*i.e.* no need for a high temperature regeneration) is prominent. Catalysts used in automotive abatement undergo accelerated aging testing to ensure they remain active for a long period of time under *real-life* conditions.[167] An example of improving a catalysts hydrothermal stability is incorporating zirconia into a ceria-based support. Zirconia is known to be resistant to sintering.[168] Zeolites have also been found to be hydrothermally stable hence they are commonly used as catalysts in automotive abatement.[169–171]

1.2.4.3 Future Regulations

The next set of EURO limits (EURO VII) are yet to be formally announced this is expected to take place at some point in 2022 with the new regulations coming into force in 2025. Despite not having a formal announcement yet there have been indications about what the EURO VII limits will include. It is expected the new set of regulations will move towards vehicles with zero emissions as well as more stringent emission allowances for internal combustion engine vehicles. Some of the expected regulations are:

1. EURO VII regulations are expected to focus on real driving time emission tests.
2. Currently, there are separate emission limits for gasoline and diesel vehicles this expected to change in the new set of legislation.
3. More stringent emission limits which will require vehicles to be able to combat cold start emissions.
4. Currently unregulated pollutants (*e.g.* NH_3, N_2O, CH_4 and ultra-fine particles smaller than 23 nm) will become regulated.
5. The introduction of real-world emission monitoring over the entire lifetime of a vehicle.[172,173]

These new regulations require the continuing research into automotive aftertreatment technology.

1.3 Project Aims

This PhD project has focused on investigating catalysts for the simultaneous removal of NOx and soot from a simulated diesel exhaust. Automotive abetment is still a key area of essential research with continuous research required to meet government emission legislation. Ag/CZA has been previously found to be active for the reaction. This thesis has attempted to improve upon this catalyst for the simultaneous reduction of NOx and oxidation of soot. The aim of this work was to contribute towards finding a catalyst which could operate at low temperatures which would have a three-fold advantage: improving the stability of the catalyst, increasing the lifetime

of the catalyst and removing the need to ignite fuel to regenerate the soot filter. This project also had the objective of finding a PGM free catalyst for this purpose.

The overall aim of improving Ag/CZA for the simultaneous reaction was investigated by first introducing potassium, a well-known, soot oxidation enhancer into the catalyst as well as investigating the ideal preparation method of the catalyst. The ideal potassium weight loading was also studied.

In addition to the addition of potassium to the catalyst, various secondary metals were introduced into the catalyst. The aim of introducing a second metal was for synergistic effects to take place enhancing the NOX reduction capabilities of the catalyst. Alongside reaction testing, characterisation of the catalysts was carried out to enable deeper understanding of the catalysts.

1.4 References

1 E. E. Agency, Citizen science projects on air quality produce useful information and raise public awareness, https://www.eea.europa.eu/highlights/citizen-science-on-air-quality, (accessed 8 April 2020).

2 F. . M. R. Sweeney, *Ecology, Environment and Pollution*, ED-Tech Press, Essex, 2019.

3 C. Bauters and G. Bauters, Air pollution, https://www.who.int/health-topics/air-pollution#tab=tab_1, (accessed 8 April 2020).

4 European Energy Agency, Air pollution, http://www.eea.europa.eu/themes/air/intro, (accessed 8 April 2020).

5 The Met Office, The Great Smog of 1952, https://www.metoffice.gov.uk/weather/learn-about/weather/case-studies/great-smog, (accessed 8 April 2020).

6 Livingstone Ken, *50 years on*, London, 2002.

7 Clean Air Act 1956, https://www.legislation.gov.uk/ukpga/Eliz2/4-5/52/section/23/enacted, (accessed 11 October 2021).

8 Emission Standards: Europe: Cars and Light Trucks, https://dieselnet.com/standards/eu/ld.php, (accessed 8 April 2020).

9 The European Commission Online, http://ec.europa.eu/environment/air/transport/road.htm, (accessed 28 August 2019).

10 Dieselnet, https://www.dieselnet.com/standards/eu/ld.php, (accessed 28 August 2019).

11 News — Emissions Analytics, https://www.emissionsanalytics.com/news, (accessed 4 September 2021).

12 Euro 7 Emissions Standards Update - Diesel Progress, https://www.dieselprogress.com/news/euro-7-emissions-standards-update/5035371.article, (accessed 4 September 2021).

13 *COMMISSION REGULATION (EU) 2016/ 646 - of 20 April 2016 - amending Regulation (EC) No 692 / 2008 as regards emissions from light passenger and commercial vehicles (Euro 6)*, .

14 G. S. Hebbar, *NOx FROM DIESEL ENGINE EMISSION AND CONTROL STRATEGIES-A REVIEW*,

Gurumoorthy S Hebbar, 2014.

15 H. J. B, *Internal Combustion Engine Fundamentals*, McGraw-Hill, New York, 1988.

16 *Nitrogen Oxides (NOx), Why and How They Are Controlled*, 1999.

17 T. J. Houser, M. E. McCarville and T. Biftu, *Int. J. Chem. Kinet.*, 1980, **12**, 555–568.

18 C. P. Fenimore, *FORMATION OF NITRIC OXIDE IN PREMIXED HYDROCARBON FLAMES*, .

19 and R. M. F. J. Barnes, J. H. Bromly, T. J. Edwards, *J. Inst. Energy*, 988, **155**, 184–188.

20 and J. K. R. W. Schefer, M. Namazian, *Combust. Res. Facil. News*.

21 EPA, *Air Quality Criteria for Oxides of Nitrogen*, Washington, D.C., 1993.

22 EPA, *Nitrogen Oxides: Impacts on Public Health and the Environment*, .

23 J. P. A. Neeft, M. Makkee and J. A. Moulijn, *Diesel particulate emission control*, 1996, vol. 47.

24 D. B. Kittelson, *ENGINES AND NANOPARTICLES: A REVIEW*, 1998, vol. 29.

25 P. T. Williams, K. D. Bartle and G. E. Andrews, *Fuel*, 1986, **65**, 1150–1158.

26 C. R. Clark, T. R. Henderson, R. E. Royer, A. L. Brooks, R. O. McClellan, W. F. Marshall and T. M. Naman, *Fundam. Appl. Toxicol.*, 1982, **2**, 38–43.

27 P. T. J. Scheepers and R. P. Bos, *Int. Arch. Occup. Environ. Health*, 1992, **64**, 163–177.

28 J. Lahaye and F. Ehrburger-Dolle, *Carbon N. Y.*, 1994, **32**, 1319–1324.

29 T. E. Jensen and R. A. Hites, *Anal. Chem.*, 1983, **55**, 594–599.

30 A. Christensen, Stockholm University, 2003.

31 D. R. Tree and K. I. Svensson, *Prog. Energy Combust. Sci.*, 2007, 33, 272–309.

32 O. I. Smith, *Prog. Energy Combust. Sci.*, 1981, **7**, 275–291.

33 B. S. Hayne, *Fossil Fuel Combustion: A Source Book*, Wiley, New York, 1991.

34 M. Frenklach, *Phys. Chem. Chem. Phys.*, 2002, **4**, 2028–2037.

35 I. Glassman, *Combustion*, Elsevier, 3rd edn., 1996.

36 A. F. Bartok, W., Sarofim, Ed., *Fossil Fuel Combustion*, Wiley, New York, 1991.

37 I. M. Kennedy, *Prog. Energy Combust. Sci.*, 1997, **23**, 95–132.

38 B. S. Haynes and H. G. Wagner, *Prog. Energy Combust. Sci.*, 1981, **7**, 229–273.

39 Dieselnet - Health Effects of Diesel Particulates, https://www.dieselnet.com/tech/health_pm.php, (accessed 22 September 2019).

40 *Health assessment document for diesel engine exhaust*, 2002, vol. 67.

41 WHO, *Health Aspects of Air Pollution with Particulate Matter, Ozone and Nitrogen Dioxide Report on a WHO Working Group OZONE-adverse effects NITROGEN DIOXIDE-adverse effects AIR POLLUTANTS, ENVIRONMENTAL-adverse effects META-ANALYSIS AIR-standards GUIDELINES*, 2003.

42 F. Inc, A. J. Cohen, H. Ross Anderson, B. Ostra, K. Dev Pandey, M. Krzyzanowski, N. Künzli, K. Gutschmidt, A. Pope, I. Romieu, J. M. Samet, K. Smith, B. Ostro, M. Kryzanowski and N. Kuenxli, *J. Toxicol. Environ. Heal. Part A*, 2005, **68**, 1–7.

43 et al. Lim, S. S., Vos, T., *A comparative risk assessment of burden of disease and injury attributable to 67 risk factors and risk factor clusters in 21 regions, 1990-2010: A systematic analysis for the Global Burden of Disease Study 2010*, 2012, vol. 380.

44 W. Health Organization and R. Office for Europe, *HealtH effects of particulate matter*, 2013.

45 K. Mohapatra and S. K. Biswal, *Effect of particulate matter (PM) on plants, climate and human health*, 2014, vol. 2.

46 P. D. Boehm, *Environ. Forensics*, 1964, 313–337.

47 L. C. Sander and S. A. Wise, *Polycyclic aromatic hydrocarbon structure index*, 1997, vol. Special pu.

48 C. Achten and J. T. Andersson, *Polycycl. Aromat. Compd.*, 2015, **35**, 177–186.

49 C. Poole, *Gas Chromatography* , Elsevier, Oxford, 2012.

50 J. P. Meador, *Encycl. Ecol.*, 2008, 2881–2891.

51 A. E. Bence, K. A. Kvenvolden and M. C. Kennicutt, *Org. Geochem.*, 1996, **24**, 7–42.

52 R. E. Laflamme and R. A. Hites, *Geochim. Cosmochim. Acta*, 1978, **42**, 289–303.

53 F. W. Karasek, *Handbook of polycyclic aromatic hydrocarbons*, New York, 1985, vol. 320.

54 H. I. Abdel-Shafy and M. S. M. Mansour, *Egypt. J. Pet.*, 2016, **25**, 107–123.

55 K.-H. Kim, S. A. Jahan, E. Kabir and R. J. C. Brown, , DOI:10.1016/j.envint.2013.07.019.

56 J. Jacob, *Polycycl. Aromat. Compd.*, 2008, **28**, 242–272.

57 W. G. T. J. L. Durant, A. L. Lafleur, E. F. Plummer, K. Taghizadeh, W. F. Busby, *Environ. Sci. Technol.*, 1998, **32**, 1894–1906.

58 International Agency for Research on Cancer., *Polynuclear aromatic compounds, Part 1, Chemical, environmental and experimental data.*, International Agency for Research on Cancer, 1983, vol. 32.

59 IARC Working Group on the Evaluation of Carcinogenic Risks to Humans. and International Agency for Research on Cancer., *Overall evaluations of carcinogenicity : an updating of IARC monographs, volumes 1 to 42.*, International Agency for Research on Cancer, 1987.

60 World Health Organization., International Program on Chemical Safety. and Inter-Organization Programme for the Sound Management of Chemicals., *Selected non-heterocyclic polycyclic aromatic hydrocarbons.*, World Health Organization, 1998.

61 J. C. Larsen, *Chemical Carcinogens, in Air Pollution and Health*, Cambridge, 1998.

62 G.-C. Fang, K.-F. Chang, C. Lu and H. Bai, , DOI:10.1191/0748233702th151oa.

63 *DIESEL ENGINES EXHAUSTS: MYTHS AND REALITIES*, .

64 N. Resources Canada, *Learn the facts: Emissions from your vehicle*, .

65 12 Principles of Green Chemistry - American Chemical Society, https://www.acs.org/content/acs/en/greenchemistry/principles/12-principles-of-green-chemistry.html, (accessed 17 April 2020).

66 A. R. Ravishankara, J. S. Daniel and R. W. Portmann, *Science (80-.).*, 2009, **326**, 123–125.

67 M. Jabłońska and R. Palkovits, *Catal. Sci. Technol.*, 2016, **6**, 7671–7687.

68 Air pollution sources — European Environment Agency, https://www.eea.europa.eu/themes/air/air-pollution-sources-1, (accessed 21 January 2022).

69 Y. Peng, F. Zhang, C. Xu, Q. Xiao, Y. Zhong and W. Zhu, *J. Chem. Eng. Data*, 2009, **54**, 3079–3081.

70 P. Breeze, *Pist. Engine-Based Power Plants*, 2018, 47–57.

71 Ammonia Slip Catalyst l Umicore Automotive Catalysts | Umicore, https://ac.umicore.com/en/technologies/ammonia-slip-catalyst/, (accessed 21 January 2022).

72 Emission Standards: Europe: Heavy-Duty Truck and Bus Engines, https://dieselnet.com/standards/eu/hd.php#stds, (accessed 21 January 2022).

73 L. Xie, F. Liu, K. Liu, X. Shi and H. He, *Cite this Catal. Sci. Technol*, 2014, **4**, 1104.

74 P. G. Eastwood, *Critical Topics in Exhaust Gas Aftertreatment*, Research Studies Press, Baldock, UK, 2000.

75 X. Tauzia and A. Maiboom, *Appl. Energy*, 2013, **105**, 116–124.

76 B. Puértolas, M. Navlani-García, T. García, M. V. Navarro, D. Lozano-Castelló and D. Cazorla-Amorós, *J. Hazard. Mater.*, 2014, **279**, 527–536.

77 M. Weilenmann, J. Y. Favez and R. Alvarez, *Atmos. Environ.*, 2009, **43**, 2419–2429.

78 S. Jones, Y. Ji, A. Bueno-Lopez, Y. Song and M. Crocker, *Emiss. Control Sci. Technol. 2016 31*, 2016, **3**, 59–72.

79 J. Ning and F. Yan, *IFAC-PapersOnLine*, 2016, **49**, 14–19.

80 L. Lietti, I. Nova and P. Forzatti, *Selective catalytic reduction (SCR) of NO by NH 3 over TiO 2-supported V 2 O 5-WO 3 and V 2 O 5-MoO 3 catalysts*, 2000, vol. 11.

81 AdBlue® : a solution for a better air quality, https://changeforblue.com/en/adblue/, (accessed 24 January 2022).

82 M. Koebel, G. Madia, F. Raimondi and A. Wokaun, *J. Catal.*, 2002, **209**, 159–165.

83 A. Grossale, I. Nova, E. Tronconi, D. Chatterjee and M. Weibel, *J. Catal.*, 2008, **256**, 312–322.

84 N. I. Il'chenko, *Russ. Chem. Rev.*, 1976, **45**, 1119–1134.

85 M. Al'tshuller, O.V., Ya. Kushnerev, *Probl. Kinet. Katal.*, 1973, **15**, 56.

86 Y. Li and J. N. Armor, *Appl. Catal. B Environ.*, 1997, **13**, 131–139.

87 M. Jabłońska, A. Król, E. Kukulska-Zajac, K. Tarach, L. Chmielarz and K. Góra-Marek, *J. Catal.*, 2014, **316**, 36–46.

88 R. Q. Long and R. T. Yang, *Chem. Commun.*, 2000, 1651–1652.

89 M. Colombo, I. Nova and E. Tronconi, *Catal. Today*, 2010, **151**, 223–230.

90 K. Kamasamudram, N. W. Currier, X. Chen and A. Yezerets, in *Catalysis Today*, Elsevier, 2010, vol. 151, pp. 212–222.

91 U. Deka, A. Juhin, E. A. Eilertsen, H. Emerich, M. A. Green, S. T. Korhonen, B. M. Weckhuysen and A. M. Beale, *J. Phys. Chem. C*, 2012, **116**, 4809–4818.

92 D. W. Fickel and R. F. Lobo, *J. Phys. Chem. C*, 2010, **114**, 1633–1640.

93 J. Hun Kwak, H. Zhu, J. H. Lee, C. H. F. Peden and J. Szanyi, *Chem. Commun.*, 2012, **48**, 4758–4760.

94 L. Ma, Y. Cheng, G. Cavataio, R. W. McCabe, L. Fu and J. Li, *Chem. Eng. J.*, 2013, **225**, 323–330.

95 C. Niu, X. Shi, F. Liu, K. Liu, L. Xie, Y. You and H. He, *Chem. Eng. J.*, 2016, **294**, 254–263.

96 C. Liu, H. Kubota, T. Amada, K. Kon, T. Toyao, Z. Maeno, K. Ueda, J. Ohyama, A. Satsuma, T. Tanigawa, N. Tsunoji, T. Sano and K. Shimizu, *ChemCatChem*, 2020, cctc.202000024.

97 R. Villamaina, S. Liu, I. Nova, E. Tronconi, M. P. Ruggeri, J. Collier, A. York and D. Thompsett, *ACS Catal.*, 2019, **9**, 8916–8927.

98 K. Arve, H. Backman, F. Klingstedt, K. Eränen and D. Y. Murzin, *Appl. Catal. B Environ.*, 2007, **70**, 65–72.

99 K. Theinnoi, S. Sitshebo, V. Houel, R. R. Rajaram and A. Tsolakis, *Energy and Fuels*, 2008, **22**, 4109–4114.

100 H. Kannisto, H. H. Ingelsten and M. Skoglundh, in *Topics in Catalysis*, 2009, vol. 52, pp. 1817–1820.

101 J. P. Breen and R. Burch, *Top. Catal.*, 2006, **39**, 53–58.

102 W. Wang, J. M. Herreros, A. Tsolakis and A. P. E. York, *Chem. Eng. J.*, 2015, **270**, 582–589.

103 S. Tamm, S. Fogel, P. Gabrielsson, M. Skoglundh and L. Olsson, *Appl. Catal. B Environ.*, 2013, **136**–**137**, 168–176.

104 L. Ström, P. A. Carlsson, M. Skoglundh and H. Härelind, *Catalysts*, 2018, **8**, 38.

105 K. I. Shimizu and A. Satsuma, *J. Phys. Chem. C*, 2007, **111**, 2259–2264.

106 Emission Standards: Europe: Cars and Light Trucks, https://dieselnet.com/standards/eu/ld.php, (accessed 17 April 2020).

107 Diesel Particulate Filters, https://dieselnet.com/tech/dpf.php, (accessed 17 April 2020).

108 Continuously regenerating trap ((C)CRT®) systems | Johnson Matthey, https://matthey.com/en/products-and-services/emission-control-technologies/stationary-emissions-control/continuously-regenerating-trap-c-crt-systems, (accessed 17 April 2020).

109 DPFs: The Facts, https://www.telegraph.co.uk/motoring/10573720/DPF-removal-the-facts.html.

110 S. LIU, X. WU, D. WENG and R. RAN, *J. Rare Earths*, 2015, **33**, 567–590.

111 A. Trovarelli, , DOI:10.1080/01614949608006464.

112 D. Mukherjee, B. G. Rao and B. M. Reddy, *Appl. Catal. B Environ.*, 2016, **197**, 105–115.

113 J. Kašpar, P. Fornasiero and M. Graziani, *Catal. Today*, 1999, **50**, 285–298.

114 X. Tang, Y. Li, X. Huang, Y. Xu, H. Zhu, J. Wang and W. Shen, *Appl. Catal. B Environ.*, 2006, **62**, 265–273.

115 A. K. Neyestanaki, F. Klingstedt, T. Salmi and D. Y. Murzin, *Fuel*, 2004, **83**, 395–408.

116 A. Bueno-López, *Appl. Catal. B Environ.*, 2014, **146**, 1–11.

117 A. Bueno-López, *Appl. Catal. B Environ.*, 2014, **146**, 1–11.

118 X. Li, S. Wei, Z. Zhang, Y. Zhang, Z. Wang, Q. Su and X. Gao, *Catal. Today*, 2011, **175**, 112–116.

119 H. Muroyama, S. Hano, T. Matsui and K. Eguchi, *Catal. Today*, 2010, **153**, 133–135.

120 X. Wu, F. Lin, L. Wang, D. Weng and Z. Zhou, *J. Environ. Sci.*, 2011, 1205–1210.

121 K. Ito, K. Kishikawa, A. Watajima, K. Ikeue and M. Machida, *Catal. Commun.*, 2007, **8**, 2176–2180.

122 K. N. Rao, P. Venkataswamy and B. M. Reddy, *Ind. Eng. Chem. Res*, 2011, **50**, 11960–11969.

123 E. Aneggi, C. de Leitenburg, G. Dolcetti and A. Trovarelli, *Catal. Today*, 2006, **114**, 40–47.

124 B. M. Reddy and K. N. Rao, *Catal. Commun.*, 2009, **10**, 1350–1353.

125 E. Aneggi, C. de Leitenburg, G. Dolcetti and A. Trovarelli, *Catal. Today*, 2008, **136**, 3–10.

126 F. Lin, X. Wu and D. Weng, *Catal. Today*, 2011, **175**, 124–132.

127 A. L. Kustov and M. Makkee, *Appl. Catal. B Environ.*, 2009, **88**, 263–271.

128 N. E. Olong, K. Stöwe and W. F. Maier, *Appl. Catal. B Environ.*, 2007, **74**, 19–25.

129 Z. Zhang, Z. Mou, P. Yu, Y. Zhang and X. Ni, *Catal. Commun.*, 2007, **8**, 1621–1624.

130 M. A. Peralta, M. S. Zanuttini and C. A. Querini, *Appl. Catal. B Environ.*, 2011, **110**, 90–98.

131 A. Rinkenburger, T. Toriyama, K. Yasuda and R. Niessner, *ChemCatChem*, 2017, **9**, 3513–3525.

132 C. . Querini, L. . Cornaglia, M. . Ulla and E. . Miró, *Appl. Catal. B Environ.*, 1999, **20**, 165–177.

133 L. Castoldi, R. Matarrese, L. Lietti and P. Forzatti, *Appl. Catal. B Environ.*, 2009, **90**, 278–285.

134 M. S. Gross, M. A. Ulla and C. A. Querini, *Appl. Catal. A Gen.*, 2009, **360**, 81–88.

135 M. . Pisarello, V. Milt, M. . Peralta, C. . Querini and E. . Miró, *Catal. Today*, 2002, **75**, 465–470.

136 A. L. Kustov and M. Makkee, *Appl. Catal. B Environ.*, 2009, **88**, 263–271.

137 X. Wu, Z. Zhou, D. Weng and F. Lin, *Catal. Commun.*, 2010, **11**, 749–752.

138 K. Ito, K. Kishikawa, A. Watajima, K. Ikeue and M. Machida, *Catal. Commun.*, 2007, **8**, 2176–2180.

139 M. V. Grabchenko, G. V. Mamontov, V. I. Zaikovskii, V. La Parola, L. F. Liotta and O. V. Vodyankina, *Appl. Catal. B Environ.*, 2020, **260**, 118148.

140 E. Aneggi, J. Llorca, C. de Leitenburg, G. Dolcetti and A. Trovarelli, *Appl. Catal. B Environ.*, 2009, **91**, 489–498.

141 K. Shimizu, H. Kawachi and A. Satsuma, *Appl. Catal. B Environ.*, 2010, **96**, 169–175.

142 Z. Qu, F. Yu, X. Zhang, Y. Wang and J. Gao, *Chem. Eng. J.*, 2013, **229**, 522–532.

143 M. V. Grabchenko, N. N. Mikheeva, G. V. Mamontov, M. A. Salaev, L. F. Liotta and O. V. Vodyankina, *Catalysts*, 2018, **8**, 285.

144 M. V. Sadlivskaya, N. N. Mikheeva, V. I. Zaikovskii and G. V. Mamontov, *Kinet. Catal.*, 2019,

60, 432–438.

145 M. Kikugawa, K. Yamazaki, A. Kato, T. Uyama, N. Takahashi and H. Shinjoh, *Appl. Catal. A Gen.*, 2019, **576**, 32–38.

146 Y. Gao, X. Wu, S. Liu, M. Ogura, M. Liu and D. Weng, *Catal. Sci. Technol.*, 2017, **7**, 3524–3530.

147 SCR on Filter NOx and PM control on one substrate SCR on Filter controls NOx (nitrogen oxides) and PM (particulate matter or soot) emissions from diesel engines, on a single substrate. Clean Air Technology Technology, www.catalysts.basf.com, (accessed 24 January 2022).

148 Y. Teraoka, K. Nakano, W. Shangguan and S. Kagawa, *Catal. Today*, 1996, **27**, 107–113.

149 L. Castoldi, N. Artioli, R. Matarrese, L. Lietti and P. Forzatti, *Catal. Today*, 2010, **157**, 384–389.

150 Y. Cheng, W. Song, J. Liu, H. Zheng, Z. Zhao, C. Xu, Y. Wei and E. J. M. Hensen, *ACS Catal.*, 2017, **7**, 3883–3892.

151 J. Schobing, V. Tschamber, J. F. Brilhac, A. Auclaire and Y. Hohl, *Comptes Rendus Chim.*, 2018, **21**, 221–231.

152 C. Davies, K. Thompson, A. Cooper, S. Golunski, S. H. Taylor, M. Bogarra Macias, O. Doustdar and A. Tsolakis, *Appl. Catal. B Environ.*, 2018, **239**, 10–15.

153 C. H. Kim, M. Paratore, E. Gonze, C. Solbrig and S. Smith, *SAE Tech. Pap.*, , DOI:10.4271/2012-01-1092.

154 M. R. Hamedi, O. Doustdar, A. Tsolakis and J. Hartland, *Energy*, 2021, **230**, 120819.

155 D. Culbertson, M. Khair, S. Zhang, J. Tan and J. Spooler, *SAE Int. J. Engines*, 2015, **8**, 1187–1195.

156 W. Maus, R. Brück, R. Konieczny and A. Scheeder, *MTZ Worldw. 2010 715*, 2010, **71**, 34–39.

157 U. Pfahl, A. Schatz and R. Konieczny, *SAE Tech. Pap.*, , DOI:10.4271/2012-01-1090.

158 L. S. Socha and D. F. Thompson, *SAE Tech. Pap.*, , DOI:10.4271/920093.

159 T. Zobel, C. Schürch, K. Boulouchos and C. Onder, *Energies 2020, Vol. 13, Page 1862*, 2020, **13**, 1862.

160 J. Gao, G. Tian and A. Sorniotti, *Energy Sci. Eng.*, 2019, **7**, 2383–2397.

161 F. Payri, J. Benajes, J. V. Pastor and S. Molina, *SAE Tech. Pap.*, , DOI:10.4271/2002-01-0502.

162 Y. Murata, T. Morita, K. Wada and H. Ohno, *SAE Int. J. Fuels Lubr.*, 2015, **8**, 454–459.

163 E. Mamontov, T. Egami, R. Brezny, M. Koranne and S. Tyagi, *J. Phys. Chem. B*, 2000, **104**, 11110–11116.

164 J. Wang, Y. Ji, U. Graham, C. C. S. de Oliveira and M. Crocker, *Chinese J. Catal.*, 2011, **32**, 736–745.

165 X. Wang, Z. Chen, Y. Wang and R. Wang, *ChemCatChem*, 2014, **6**, 237–244.

166 P. Boutikos, A. Žák and P. Kočí, *Chem. Eng. Sci.*, 2019, **209**, 115201.

167 Catalyst Aging Services | Southwest Research Institute, https://www.swri.org/industry/emissions/catalyst-aging-services, (accessed 26 January 2022).

168 L. Nossova, G. Caravaggio, M. Couillard and S. Ntais, *Appl. Catal. B Environ.*, 2018, **225**, 538–549.

169 F. Gao and J. Szanyi, *Appl. Catal. A Gen.*, 2018, **560**, 185–194.

170 M. Cheng, B. Jiang, S. Yao, J. Han, S. Zhao, X. Tang, J. Zhang and T. Wang, *J. Phys. Chem. C*, 2018, **122**, 455–464.

171 J. García-Martínez, M. Johnson, J. Valla, K. Li and J. Y. Ying, *Catal. Sci. Technol.*, 2012, **2**, 987–994.

172 Upcoming Euro 7 Emission Regulations to Drive Europe's Zero-Emission Mobility Goal, https://dieselinformation.aecc.eu/upcoming-euro-7-emission-regulations-to-drive-europes-zero-emission-mobility-goal/, (accessed 26 January 2022).

173 Emissions standards in the EU – Beyond Euro 6, https://ricardo.com/emleg/emissions-legislation-database/emission-standards-in-the-eu-beyond-euro-6, (accessed 26 January 2022).

2 Experimental

2.1 Introduction

This chapter discusses the experimental techniques used throughout this project. This includes the preparation methods and experimental techniques used for the preparation, testing and characterisation of various catalysts.

A variety of catalyst preparation methods were used, including chemical vapour impregnation (CVI), wet impregnation, incipient wetness and sol immobilisation to deposit active species onto the catalyst support. Characterisation was carried out using X - ray Diffraction (XRD), Surface Area Analysis (B.E.T.), Raman Spectroscopy, X - ray Photoelectron Spectroscopy (XPS) and Electron Microscopy.

Catalysts were tested for their ability to catalyse the selective catalytic reduction of NOx (SCR) and their ability to catalyse the simultaneous removal of NOx and soot from a simulated diesel exhaust. The reactions were carried out using a micro reactor connected to a Fourier Transform Infrared Spectrometer (FTIR).

2.2 Materials Used

A range of catalysts were prepared during this project detailed in the methods below. All the chemical precursors used in the preparations of the catalysts and supports are listed in Appendix 1. A list of all of the catalysts prepared are also listed in Appendix 1.

Throughout this project a soot substitute which has previously found to be a substitute for diesel soot was used.[1] The soot mimic used was Cabot Black Pearls 2000 and the same batch was used throughout the project. A soot mimic overcompensates for soot oxidation as it contains a greater percentage of carbon than diesel soot does (Section 1.1.2.1). Consequently, this means that if a catalyst has the ability to oxidise the soot mimic it certainly has the ability to oxidise diesel soot.

2.3 Catalyst Preparation

The catalytic support was prepared *via* co-precipitation using an autotitrator and the catalysts were prepared by a variety of methods.

2.3.1 CeO_2-ZrO_2-Al_2O_3 Support Preparation Method

A Metrohm 902 Titrando system was used for addition of nitrate precursor solution and the carbonate precipitating agent. A basic schematic of the autotitrator set-up is shown in Figure 2.1. 0.25 M solutions of ammonium cerium(IV) nitrate, zirconium (IV) oxynitrate and aluminium

nitrate nonahydrate were used as the precursor solutions. These solutions were mixed into a single 200 ml solution. To achieve Ce:Zr:Al in the desired molar ratio of 7:3:10 the precursor solution required 100 ml, 50 ml and 100 ml of the 0.25 M solutions of ammonium cerium (IV) nitrate, zirconium (IV) oxynitrate and aluminium nitrate nonahydrate respectively. A 1 M solution of sodium carbonate was used as the precipitating agent.

The vessel was heated to 80°C and 20 ml of nitrate solution was added under continuous mechanical stirring, the precipitating agent was added until pH 9 was obtained. The nitrate solution was then added at a rate of 3 ml min^{-1} for 50 minutes, whilst the sodium carbonate solution was added at a rate to maintain a pH of 9. Once addition of the nitrate solution was complete, the solution was aged for 1 h under constant stirring. The resulting precipitate was filtered and washed (2 L hot deionised water). The support was then dried for 16 h at 110°C. The dried support was then ground into a fine powder in a pestle and mortar and calcined under flowing air for 5 h at 500 °C with a ramp rate (r.r.) of 10°C min^{-1}.

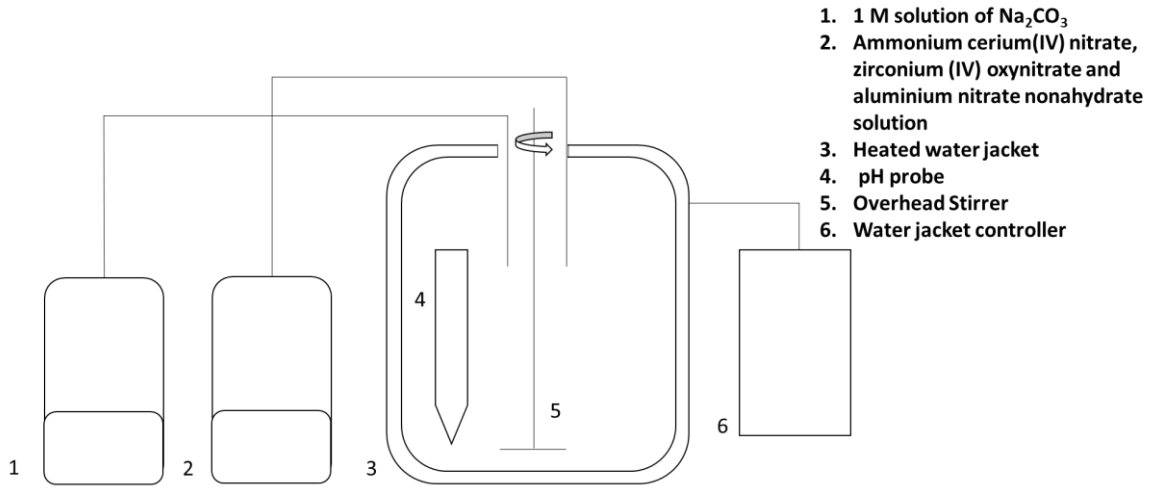

Figure 2.1: Basic Schematic of Autotitrator Set-up

2.3.2 Catalyst Preparation

The catalysts were prepared by four different techniques, chemical vapour impregnation; incipient wetness; sol immobilisation and wet impregnation, which are detailed below.

2.3.2.1 Chemical Vapour Impregnation

Figure 2.2 shows a basic schematic of the set up for the CVI preparation technique.

2.3.2.1.1 Ag-K/CeO_2-ZrO_2-Al_2O_3

For a 2%Ag weight loading, $C_{13}H_{13}AgF_8O_2$ (0.51 g) was shaken with 20%K/CZA, previously prepared as stated in Section 2.3.2.3.1, (0.98 g) then placed in a Schlenck flask. Which was placed in an oil bath of the desired temperature (60, 70, 80 or 90°C) and connected to the vacuum. A liquid nitrogen cold trap was used to condense all vapours. The catalyst was magnetically stirred whilst being heated for 1 h. The catalyst was then calcined at 500°C under flowing air for 5 h at a ramp rate of 10°Cmin^{-1} in a fume cupboard.

2.3.2.1.2 Cu/CeO_2-ZrO_2-Al_2O_3

For the Cu based catalysts prepared *via* CVI, Copper(II) Acetylacetonate (0.083 g for 2w.t.%) was used as the Cu precursor and $C_{13}H_{13}AgF_8O_2$ (0.51 g for 2w.t.%) as the silver precursor. The precursors were shaken together then mixed with the CZA support then placed in a Schlenk flask. The Schlenk flask was placed in an oil bath which was at 140°C and connected to the vacuum. A liquid nitrogen cold trap was used to condense all vapours. The catalyst was magnetically stirred whilst being heated for 1 h. The catalyst was then calcined at 500 °C under flowing air for 5 h at a ramp rate of 10 °C min^{-1} in a fume cupboard.

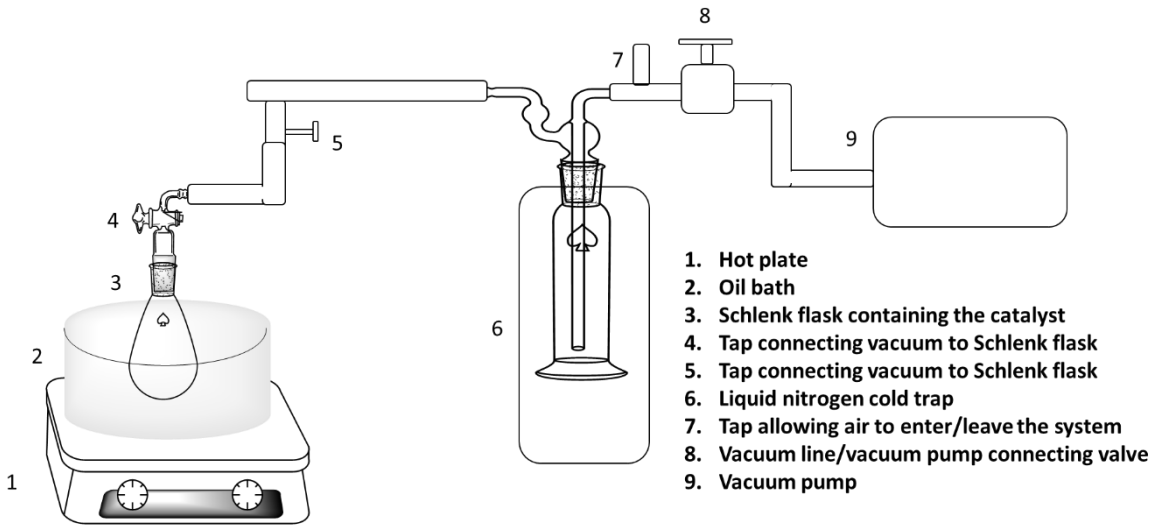

Figure 2.2: Schematic of CVI preparation set-up

2.3.2.2 Incipient Wetness

To prepare 2%Ag –20%K/CZA, $AgNO_3$ (0.0315 g) and K_2CO_3 (0.345 g) were dissolved in minimal water and then the CZA (0.88 g) support was added. H_2O was added dropwise whilst stirring until the support reached its maximum water capacity. The catalyst was then dried at 110°C for 16 h, ground into a fine powder and then calcined at 500°C under flowing air for 5 h at a

ramp rate of 10°Cmin^{-1}. The quantities used were adjusted depending on the weight loading required.

2.3.2.3 Wet Impregnation

2.3.2.3.1 K/CeO_2-ZrO_2-Al_2O_3

The 20%K/CZA used in the wet impregnation preparations was prepared by first dissolving K_2CO_3 (0.345 g) in distilled water (5 ml) whilst being heated to 80°C in an oil bath. Once all the K_2CO_3 had dissolved and the temperature had reached 80°C, CZA (0.88 g) was added and the solution was stirred at 80°C until the water had evaporated/ adsorbed and a grey paste formed. The paste was then dried (110°C, 16 h) and calcined (500°C under flowing air, 5 h, r.r. 10°C min^{-1}). The quantities used were adjusted depending on the weight loading required.

2.3.2.3.2 Ag-K/CeO_2-ZrO_2-Al_2O_3

To prepare 2%Ag–20%K/CZA, $AgNO_3$ (0.0315 g) and K_2CO_3 (0.345 g) were impregnated onto the CZA support (0.88 g), heated in vessel immersed in an oil bath to 80°C under constant magnetic stirring, until a 'toothpaste like' consistency was achieved. The catalyst was then dried at 110°C for 16 h, ground into a fine powder and then calcined at 500°C under flowing air for 5 h at a ramp rate of 10°C min^{-1}. The same method was used for the other catalysts prepared *via* wet impregnation with the quantities and precursors being adjusted depending on the weight loading and desired catalyst.

2.3.2.3.3 Cu-Ag/CeO_2-ZrO_2-Al_2O_3

For 2%Cu-2%Ag/CZA, $CuNO_3.(H_2O)_3$ (0.152 g) and $AgNO_3$ (0.0628 g) were dissolved in distilled water (5 ml) and heated to 80°C using an oil bath under constant magnetic stirring. The CZA support (1.96 g) was then added to the solution. The temperature was maintained at 80°C until a 'toothpaste-like' consistency was achieved. The paste was dried for 16h at 110°C and then calcined (flowing air, 5 h, r.r. 10°C min^{-1}, 500°C). The quantities of precursors were adjusted depending on the required weight loading. For copper catalysts containing potassium, K_2CO_3 was used as the precursor.

For the 2%Cu-2%Ag/CZA (a) catalyst the precursors were added in a stepwise fashion *i.e.* the two precursors were dissolved and heated to 80°C separately before being added to the CZA support. Whilst, for 2%Cu-2%Ag/CZA (b) the precursors were dissolved and heated together as in the previous paragraph.

2.3.2.4 Sol Immobilisation

A 2%Cu-2%Ag/CZA was prepared *via* sol immobilisation. This method involved dissolving $AgNO_3$ in distilled water (6 mM) and adding 0.2w.t.% PVA (20 ml, 0.002 g). The solution was then diluted to 400 ml and $NaBH_4$ (25 mM) was added. The solution was mechanically stirred for 30 minutes then $Cu(NO_3)_2$ (6 mM), PVA (polyvinyl alcohol) (0.2%) and $NaBH_4$ (25 mM) was added. Next, the CZA support (0.96 g) and PDDA (polydiallyldimethylammonium chloride)(0.08 w.t.%) was added. The resultant solution was then mechanically stirred at room temperature for 2 h, then filtered and washed with de-ionised water. Finally, it was dried (16 h, 110°C) and calcined (500°C, 5 h, r.r. 10°C min^{-1}, under flowing air).

2.4 Catalyst Testing

A reactor which will be referred to as the SCR Reactor throughout this thesis, was used to test catalysts for their ability to catalyse the SCR reaction and for the simultaneous removal of NOx and soot.

2.4.1 The SCR Reactor

The activity of the catalysts for the selective catalytic reduction of NO by NH_3 was analysed using a micro-reactor connected to an FTIR (Gasmat). A schematic for the reactor is shown in Figure 2.3. A half inch wide steel tube was packed with 0.25 g of catalyst, secured in place with quartz wool. The reactor tube was fixed to the gas inlet using a Swagelok system and placed inside the furnace. The catalyst temperature was monitored using a thermocouple projecting into the centre of the catalyst bed. The reactor lines were wrapped in heating tapes which were set to 120°C. The lines were initially flushed with N_2 for approximately 30 minutes to ensure there were no contaminates in the lines (e.g. CO_2 and H_2O). Then a background scan was ran. Initially bypassing the catalyst, a reactant gas mixture comprising of 500 ppm NO, 500 ppm NH_3, 8% (by volume) O_2 and N_2 as the balance gas was introduced into the reactor. The flows of the four gases to achieve these concentrations were set at: 30 ml min^{-1} (NO), 18 ml min^{-1} (NH_3), 13 ml min^{-1} (O_2) and 120 ml min^{-1} (N_2), with an overall gas flow of 200 ml min^{-1} being maintained throughout the experiments. The GHSV for the experiments was 40,000 h^{-1}, where the catalyst volume was 0.22 cm^3. Typically for automotive experiments H_2O and CO_2 would also be present in the exhaust stream however these gases were deliberately excluded from these experiments as the formation of CO_2 and H_2O were used to track oxidation of carbon black. Once the gas flows had stabilised, a by-pass reading was taken to ensure constant gas concentration at the start of each test. The furnace was heated to 125°C, after this temperature was obtained the gas flows were switched from by-pass to flow through the reactor tube. The furnace temperature was then periodically

increased in 25°C increments up to 550°C. Before taking measurements, the temperature and gas concentrations were allowed to stabilise.

For monitoring the catalyst's performance to simultaneously remove NOx and soot, the same set up as above was used except carbon black was mixed with the catalyst using a spatula until homogenous, in a 10:1 ratio by mass, to achieve loose contact. Previous work has shown carbon black to be a suitable substitute for real diesel soot.[1] Throughout the remaining of the thesis the carbon black will be referred to as soot.

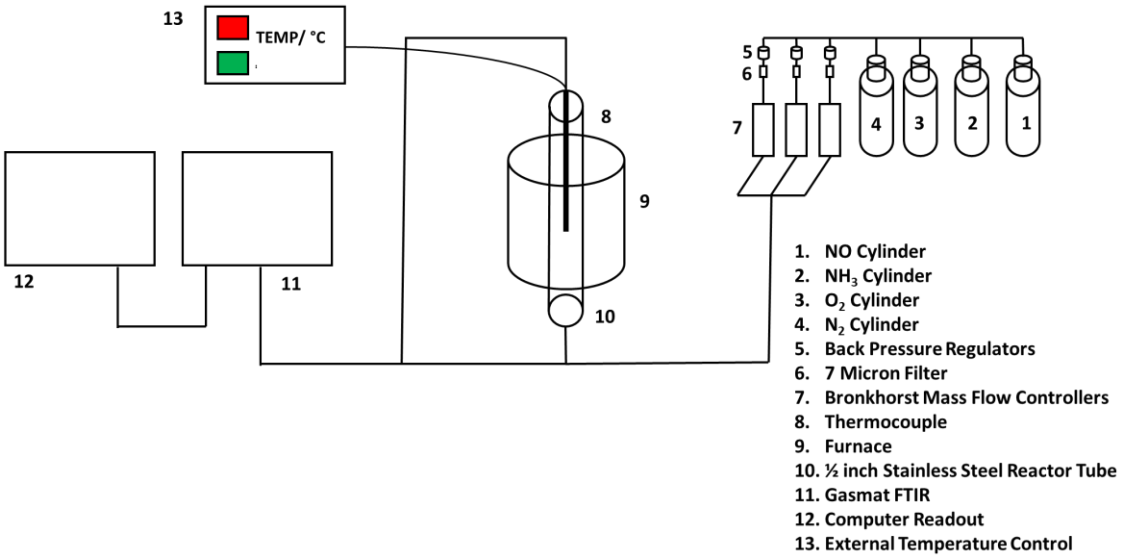

Figure 2.3: SCR reactor schematic

2.4.1.1 On-line Process Analysis Using Fourier Transform Infrared (FTIR) Spectroscopy

Infrared Spectroscopy is a versatile technique which can be used to identify chemical species present in gas, liquid and solid samples. It can provide both quantitative and qualitative information as well as being a fast technique.

When covalent bonds in molecules absorb electromagnetic radiation in the IR region (2.5 – 25 µm) it causes them to bend or vibrate. Different bonds absorb infrared light at certain wavelengths, hence the wavelength at which a molecule absorbs radiation can be used to identify the species present. Every molecule has a characteristic spectrum which is referred to as its *fingerprint*. A molecule can be identified by comparing its absorption peak to a standard bank of fingerprint regions.

Table 2.1: The vibrational modes for SO_2

Symmetric Streach IR active (1151 cm^{-1})	Asymmetric Streach IR active (1362 cm^{-1})	Scissoring (symmetric bend) IR active (518 cm^{-1})
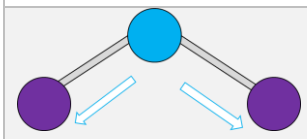	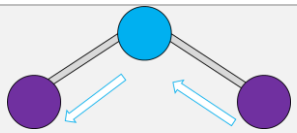	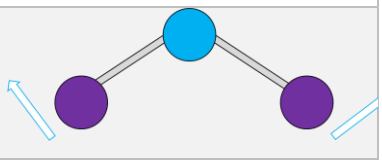

A non-linear molecule, with N atoms, has 3N – 5 vibrational modes whilst a linear molecule has 3N – 6 vibrational modes. Table 2.1 shows an example of the vibrational modes for a non-linear molecule. For a molecule to be IR active it must undergo a change in dipole moment when vibrating. Hence, molecules such as O_2 and N_2 are not IR active.

Fourier transform IR spectroscopy uses a polychomatic light source and an interferometer to measure multiple wavenumbers simultaneously. Consequently, the signal-to-noise ratio is increased and the sampling time needed is reduced.[2]

2.4.1.1.1 Experimental

In this work a Gasmet FTIR equipped with a 0.4 L sample cell was used to analyse the simulated exhaust gas, after having passed over a catalyst for the SCR and combined SCR and soot oxidation reactions. A flow rate of 200 $mlmin^{-1}$ was used for all of the experiments as the FTIR sample cell was 0.4 L in volume it took approximately 2 minutes to fill the cell. The FTIR readings were always allowed to stabilise before taking a reading to ensure that the correct concentrations were recorded. As discussed in the previous section, N_2 is not IR active and hence could not be directly measured. Where N_2 is presented in reaction data it was calculated as a nitrogen balance. The concentrations of CO, CO_2, H_2O, NH_3, NO, NO_2 and N_2O were measured, with their concentrations being determined by the Calcmet software using a set of calibration files for each species. The reference range used to detect and monitor each gas is shown in Table 2.2. The gas concentrations were plotted against temperature using Origin17.

Table 2.2: The ranges used by the Calcmet software to detect and calculate the concentrations of each compound

Compound	Reference Ranges / cm^{-1}
CO	2000-2150
CO_2	2270-2450
H_2O	1350-1600 and 3800-4050
NH_3	895-1400 and 2450-3450
NO	1850-2000
NO_2	1500-1700
N_2O	2100-2255 and 2500-2650

2.4.2 Catalyst Characterisation

The following sections introduce the characterisation techniques which were used throughout the project. The theory and experimental details are discussed for each technique.

2.4.3 Physisorption, Specific Surface Area and B.E.T. Theory

Physisorption is the reversible adsorption of a gas onto a surface due to the intermolecular force between the adsorbates and adsorbents. The force is van der Waals force, which is a weak interaction, hence the rate of adsorption and desorption is fast. Multiple layers can be adsorbed forming a multilayer. Physisorption is used to determine the specific surface area, porosity and pore size distribution of a substance. Typically, this is achieved by dosing the sample with gas (typically N_2), generally at the boiling temperature of the probe gas, at a series of pressures. The data is collected and displayed as an isotherm where the volume of gas is plotted as a function of the changing pressure. The different adsorption isotherms are shown in Figure 2.4.

Type I depicts monolayer adsorption, type II shows the gradual formation of a monolayer followed by the formation of multilayers as a consequence of increased pressure. Type IV shows monolayer formation followed by the filling of micropores. The dots in Figure 2.4 indicates the point at which a monolayer has formed.

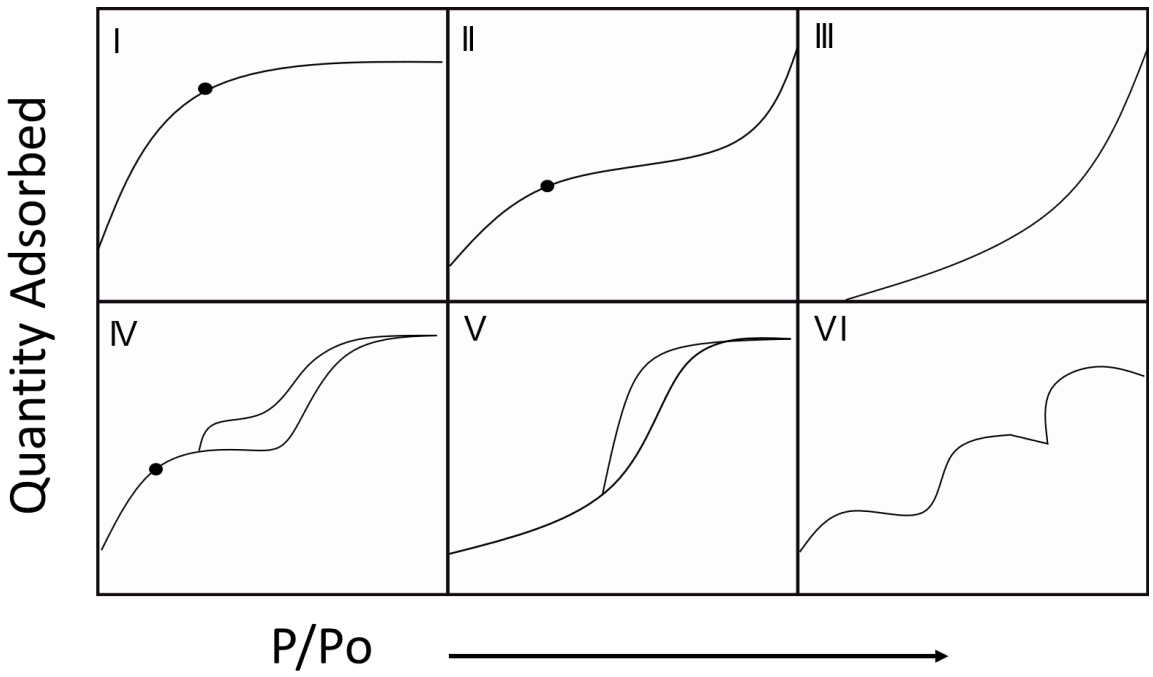

.

Figure 2.4: Nitrogen adsorption isotherm types, where the dot represents the point at which a monolayer has formed, adapted from reference[3]

Brunnaer, Emmett and Teller (BET) theory can be used to calculate the surface area of a substance from it's isotherm. BET acknowledges the formation of multilayers and can calculate the number of molecules needed to form a monolayer.

$$\frac{P}{V(Po-P)} = \frac{1}{Vm-C} + \frac{(C-1)}{Vm-C}\frac{P}{Po}$$

Equation 2.1: BET equation. Where P is the equilibrium pressure, Po is the saturation pressure, V is the volume adsorbed, Vm is the monolayer volume and C is a constant.

In order for the BET equation to be used, a linear region of the isotherm is needed, therefore at least 5 points are measured from $\frac{P}{Po} = \ 0.05 - 0.035.$ A plot of $\frac{P}{V(Po-P)}$ against $\frac{P}{Po}$ gives a straight line with the intercept being equal to $\frac{1}{VmC}$ and has a gradient of $\frac{(C-1)}{VmC}$. The surface area can then be calculated using Equation 2.1. The specific surface area ($m^2\ g^{-1}$) can be calculated (Equation 2.2) by dividing the surface area (m^2) by the samples mass for comparison between different samples.[4]

$$S = \frac{Vm}{22414} N_A \sigma$$

Equation 2.2: Equation used to calculate surface area using BET theory. Where S is the surface area, N_A is Avogadro's constant and σ is the cross-sectional area of N_2 (0.162 nm^2).

2.4.3.1 Experimental

The characterisation was carried out on a Quantachome Quadrabsorb. A sample mass, equivalent to approximately 10 m^2, was degassed for 16 hours at 120 °C, before N_2 physisorption was performed at 77 K. The specific surface area was calculated using BET theory with 20 adsorption points measured in the linear region 0.05-0.35 p/p0. This technique was used to find the surface area of the catalysts studied to be able to relate the SA to the catalytic performance. Typically, higher the surface area the better the catalyst.

2.4.4 Powder X-Ray Diffraction

Powder X–ray diffraction (XRD) is a non-destructive technique primarily used for phase identification of crystalline materials. XRD can also provide information on crystallite sizes. X–ray powder diffraction patterns have peaks as functions of 2θ. Diffraction occurs when x–rays are scattered from an object and constructively and destructively interfere with each other. In 1912, M. von Laue was the first person to note that x–rays diffract from a periodic arrangement of atoms in a crystal, corresponding to how visible light diffracts though a grating. Building on this, Bragg was able to determine that x–ray diffraction from a crystal could be described by Equation 2.3, which is known as the Bragg law.[5]

$$n\lambda = 2d_{hkl}\, sin\theta$$

Equation 2.3: The Bragg Equation

Constructive interference is achieved when x–rays are in phase with each other. For a certain d – spacing a corresponding angle of incident radiation (θ) results in constructive interference as shown in Figure 2.5. XRD requires the sample to have long range order to produce constructive interference *i.e.* a repeating unit cell. Consequently, amorphous samples produce no diffraction data. The diffraction from a crystal can be described in terms of reflection from a set of lattice planes

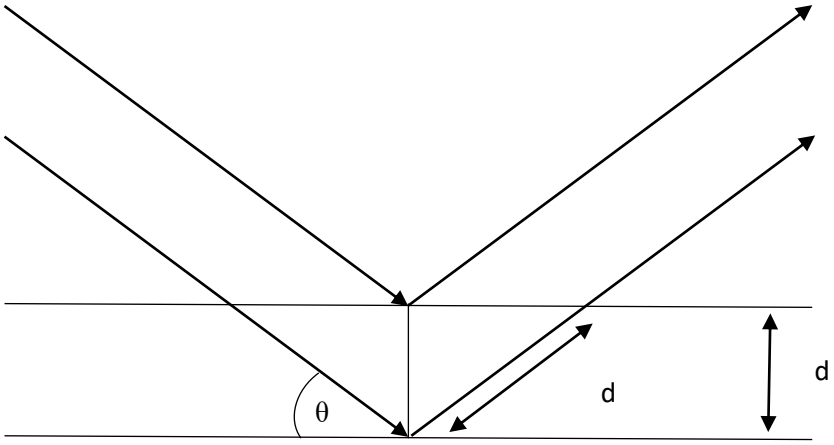

Figure 2.5: X-ray diffraction pattern according to Bragg's Law. When 2dsinθ is equal to an integer of the wavelength, constructive interference occurs. Where n is an integer, λ is the wavelength of the x – ray, d is the periodic spacing between planes and θ is the angle of incident radiation

A mono-chromatic X-ray source bombards the sample and the sample is scanned though a range of 2θ angle. All the possible diffraction directions of the lattice are obtained due to the random orientation of the powdered material. Diffraction occurs when waves interact with each other. Destructive interference occurs when the X-rays are out of phase with one another and cancel each other out. Constructive interference occurs when the waves are in phase with each other. The detector can determine the X-ray intensity with respect to 2θ. Sample identification is achieved *via* comparison of a sample with standard reference patterns.[6] Conversion of the diffraction peaks to d – spacings allows identification of a material as each material has its own unique set of d – spacings.[7] The crystal structure of the sample determines the position and intensity of the diffraction peaks in the XRD pattern. The interatomic distances in a compound determine the positions of the diffraction peaks and the atom type and position determines the intensities of the diffraction peaks.

The Scherrer equation can be used to calculate average crystallite size, see Equation 2.4. The Scherrer equation is based on the requirement of crystallinity for XRD diffractograms to be produced. Narrow and sharp reflections are a result of large crystallite sizes. Despite this, for particles which are < 100 nm in size line broadening takes place as a consequence of incomplete destructive interference.

$$\tau = \frac{K\lambda}{B cos\theta}$$

Equation 2.4: The Scherrer Equation Where τ is the mean crystallite size, 2θ is the scattering angle in radians, λ is the X–ray wavelength, K is a constant (typically between 0.89 – 0.94) and B is the line broadening at FWHM (full width half maximum) after the subtraction of instrumental line broadening[8]

The data obtained from the XRD analysis may also be used to calculate the volume of a cubic unit cell. This is achieved by first calculating the lattice parameter of the cell (Equation 2.5) and then as the structure is cubic the lattice parameter (a) may be cubed to find the unit cell volume (Equation 2.6).

$$a = d\sqrt{h^2 + k^2 + l^2}$$

Equation 2.5: Equation to calculate the lattice parameter of a cubic structure where a is the lattice parameter, d is the lattice spacing and h, k and l are the miller indices.

$$Unit\ cell\ volume = a^3$$

Equation 2.6: Equation for calculation of unit cell volume

2.4.4.1 Experimental

2.4.4.1.1 Powder XRD

Powder XRD analysis was performed on a (θ-θ) PANalytical Xpert Pro powder diffractometer with a Cu X-ray source operating at 40 keV and 40 mA, with Kα1 X-rays selected using a Ge (111) single crystal monochromator. Analysis was performed using a back filled sample holder. Phases were identified by matching experimental patterns to the ICDD database. PANalytical HighScore Plus was used for the analysis of the data and patterns. Crystallite sizes were estimated by using the Scherrer equation (Equation 2.4). Using the XRD data unit cell volumes were calculated for the Cu based catalysts (Equation 2.5 and Equation 2.6). Powder XRD was used to identify the species present in the catalysts as well as being used to calculate crystallite sizes and unit cell volumes. Smaller crystallites sizes are related to better activity and the volume unit cell can be used to understand whether external species have been incorporated into the ceria lattice.

2.4.4.1.2 *In situ* XRD

In situ powder x-ray diffraction was carried out by Dr James Hayward on a PANalytical X'pert Pro diffractometer with a Cu X-ray source operating at 40 keV and 40 mA, with Kα1 X-rays selected using a Ge (111) single crystal monochromator. The *in situ* sample holder was a XRK reaction cell manufactured by ANTON PAAR. In this cell, the gas flow was forced through the sample. The gas flow (air) was fixed at 20 ml min^{-1}.The following *in situ* XRD profile was performed:

1. Set air flow to 20 $mlmin^{-1}$.
2. Heat to 50°C, run initial scan of sample from 10 – 70°.
3. Maintain temperature at 50°C, wait for 10 min, run two scans between 35 – 45°.
4. Heat to 100°C, wait 10 min, run two scans from 35 – 45°.
5. Heat in 50 °C intervals at 10 °C min^{-1} and wait 10 min, perform 2 scans from 35 - 45° at each temperature up to 600°C.
6. Cool to 50°C, run final scan from 10 – 70°

PANalytical HighScore Plus was used for the analysis of the data and patterns.

In situ XRD was used to examine any changes in the catalyst during reaction conditions.

2.4.5 Raman Spectroscopy

Raman spectroscopy is a non-destructive technique, which uses inelastic light scattering to provide information on the vibrational motions of molecules.[9] Raman spectroscopy provides a fingerprint which can be used to identify samples.

Vibrational Raman uses inelastic scattering of monochomatic light from a laser to provide chemical and structural information. When a particle is irradiated at a specific frequency the radiation is scattered with the photons having a shift in energy (higher or lower), depending on the vibrational state of the molecule.[10] A schematic of this is shown in Figure 2.6.

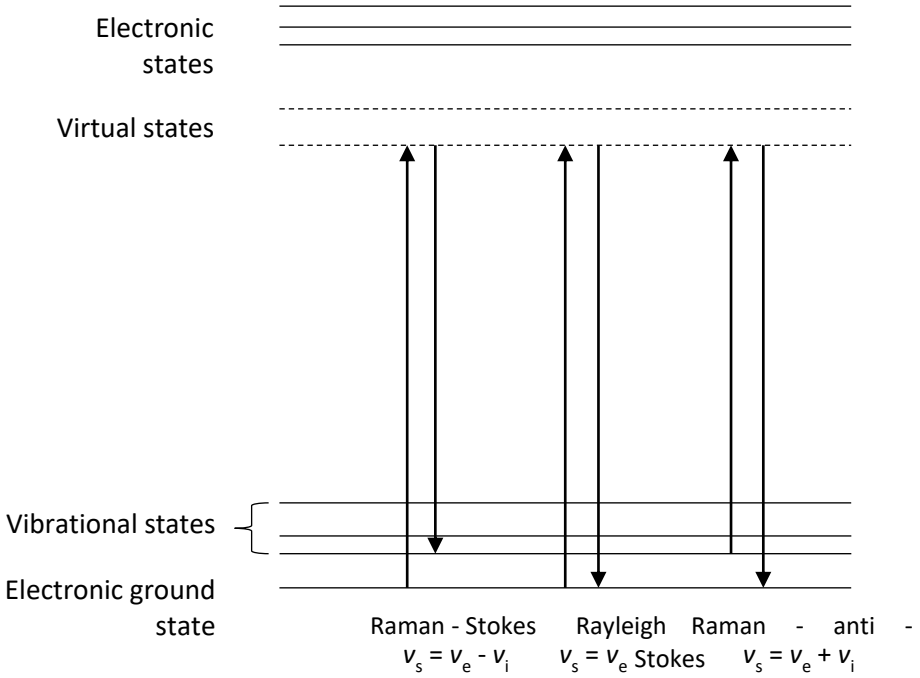

Figure 2.6: Where v_e = excitation frequency and v_s = scattering frequency and v_i = vibrational frequency. The molecule is excited to a virtual state then returns to the ground state and light is emitted. If the frequency of the light does not change then this is Rayleigh scattering. If the frequency is less than that of the incident light its Raman – Stokes scattering. Raman – anti – Stokes scattering is where scattered light has higher energy than the incident light.

Raman Spectroscopy is complementary to infrared (IR) absorption spectroscopy as both techniques analyse vibrations, and hence provide similar information, however there are some differences. To be Raman active there has to be a change in polarisability of the molecule during the vibration whilst for IR the molecule must have a change in dipole moment during the vibration.[11] Hence, molecules such as O_2 and N_2 are not IR active. Molecules with greater polarizability will exhibit more intense Raman scattering. Raman spectroscopy can provide information on crystal structure, polymorph forms and phase transitions.[11]

2.4.5.1 Experimental

Raman spectroscopy was carried out using a Renishaw inVia confocal Raman microscope equipped with an argon ion visible green laser. The laser wavelength used was 514 nm and spectra were collected in reflective mode using a highly sensitive charge couple device detector. Laser power was set at 5 %, with exposure time at 5 s and accumulations of 10 s for each spectra. CVI catalysts were dark in colour and therefore it was difficult to obtain a Raman spectrum from the pure catalysts hence they were diluted with KBr to enable suitable spectra to be obtained. In this project, Raman was mainly used to calculate the ceria defects in the catalysts.

2.4.6 X – Ray Photoelectron Spectroscopy

X-ray photoelectron spectroscopy (XPS) is a useful non-destructive surface technique, which can be used to provide information on oxidation states and the surface composition of a sample. XPS may also be used for more complex studies to investigate depth-profiling of samples, as well as the dispersion of nanoparticles.

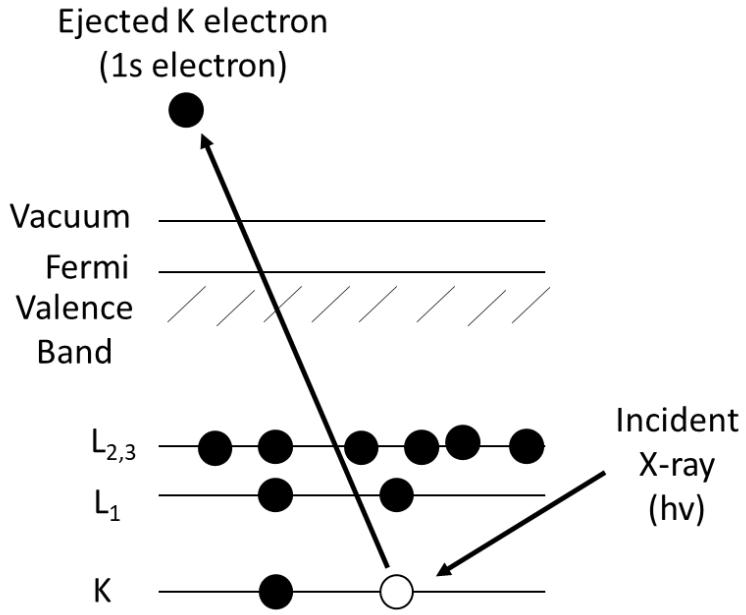

Figure 2.7: A schematic of the photoemission process involved in XPS analysis. Where the circles represent electrons and the lines energy levels within the material being analysed. The schematic is recreated from reference[13]

XPS works on the principle of Einstein's photoelectric effect. When a molecule/atom absorbs an X-ray photon an electron is ejected. Figure 2.7 shows a schematic of the photoemission process involved in XPS analysis. The kinetic energy (KE) of the electron depends on two things: the binding energy of the electron (BE), the energy needed to remove the electron from the surface, and the photon energy (h*v*). The photoemission equation is shown in Equation 2.7**.** The elemental composition of the surface can be determined by measuring the kinetic energy of the emitted electron. The binding energy of the electron and the oxidation states of the elements can also be established[12]. The BE of the electron is influenced by various factors:

- The element from which it is emitted
- The orbital that it is emitted from
- The chemical environment of the atom which it was emitted from

$$\mathrm{Ek} = \mathrm{hv} - \mathrm{E_b} - \varphi$$

Equation 2.7: The photoemission equation. Where Ek is the kinetic energy, H is planks constant (6.626×10^{-34}Js), v is the frequency of the photon, E_b is the binding energy and φ is the work function.

2.4.6.1 Experimental

XPS was carried out by Dr David Morgan using a Kratos Axis Ultra DLD photoelectron spectrometer utilising monochromatic AlKα radiation, operating at an energy of 120 W (10 x 12 kV). Data was analysed using CasaXPS and modified Wagner sensitivity factors as supplied by the instrument manufacturer after subtraction of a Shirly background. All spectra were calibrated to the C(1s) line taken to be 284.8 eV. The atomic percentage was calculated by CasaXPS. The program used Equation 2.8 to calculate the atomic percentage from the XPS spectra. From the atomic percentage the weight loading of elements could be calculated (Equation 2.9).

$$C_x = \frac{I_x/S_x}{\Sigma I_i/S_i}$$

Equation 2.8: Equation used to calculate atomic percentage of elements in a compound from XPS analysis. Where C_x is the fraction of element x, I_x is the peak area of element x, S_x is relative sensitivity of photoelectron peak x and Σ is the sum over all elements

$$W.t.\%x = \frac{(C_x)(At.Wt.x)}{\Sigma(C_i)(At.Wt.i)}$$

Equation 2.9: Equation used to calculate weight percent of element x from the atomic percentage. Where C_x is the atomic percent of element x, At. Wt. x is the atomic weight percent of x, and Σ is the sum over all the of the elements in the compound

XPS was used to calculate the elemental surface concentrations and the oxidation states of the elements.

2.4.7 Electron Microscopy

Electron microscopy uses a high energy electron beam to produce a variety of signals when incident on a sample. Electron microscopy operates on a similar principle to optical microscopes, but as the wavelength of electrons is much smaller than that of visible light much greater resolution can be achieved. The signals can be used to provide images of the sample which allows morphology, crystal structure and chemical composition to be determined. When an electron beam comes into contact with a sample the electrons' kinetic energy is dispersed as a variety of signals as shown in Figure 2.8. The secondary electrons (SE) and Backscattered electrons (BSE) are used in scanning electron microscopy (SEM). Characteristic X-rays are also generated. Excited electrons collide with the electrons in the sample, exciting the samples electrons. When the excited electrons return to lower energy levels an X-ray which is characteristic of the element is

emitted. This allows the elemental composition of a sample to be estimated. Transmitted and diffracted electrons are used for Transmission Electron microscopy (TEM).[14] Other microscopy techniques which utilise signals are Electron Energy Loss Spectroscopy (EELS) and X-ray Dispersive Spectroscopy (X-EDS).

Limitations of electron microscopy include the sample size and damage to the sample from the electron beam. The sample area shown in the microscopy images are small and therefore it can be difficult to ensure the section imaged is representative of the whole sample. When measuring particle size > 100 particles should be measured from different areas of the sample surface. The electron beam is extremely powerful and hence the sample may be damaged.

2.4.7.1 Scanning Electron Microscopy (SEM)

SEM uses an energy beam which scans across the sample surface, detecting either secondary or backscattered electrons. SEM can be used to determine the composition of the sample, morphology and topology, up to a depth of 3 – 10 nm. The secondary electrons have relatively low energies (≈ 5 – 50 eV) and are generated from close to the surface of the sample. SE are produced when the incident electron excites an electron in the sample and loses some of its energy. If the excited electron has sufficient energy, it moves towards the surface of the sample and excites the surface. Whilst BSE are produced when electrons from the beam are scattered by atoms in the sample without loss of energy. Figure 2.9 and Figure 2.8 show schematics of an SEM and a schematic explaining signal generation for SEM.

When detecting secondary electrons, the intensity is related to surface orientation consequently the surfaces facing the electron beam appear brighter than those facing away. However, when using the backscattered detector, the contrast is due to atomic mass. The heavier an atom is, the more likely it is to backscatter electrons resulting in heavier elements appearing brighter. Hence, an image generated using BSE can also provide information about the sample's composition.[15]

Energy dispersive x-ray spectroscopy (EDX) is frequently used in conjunction with SEM and TEM. EDX uses the x-rays emitted from the sampled to characterise the elemental composition of the sample. The EDX x-ray detector measures the number of x-rays emitted and their energy. A spectra of the energy against the number of x-rays with that energy is produced which allows qualitative and quantitative determination of the element present in a sample to be determined as well as an estimation of the amount of each element present in the sample.[16]

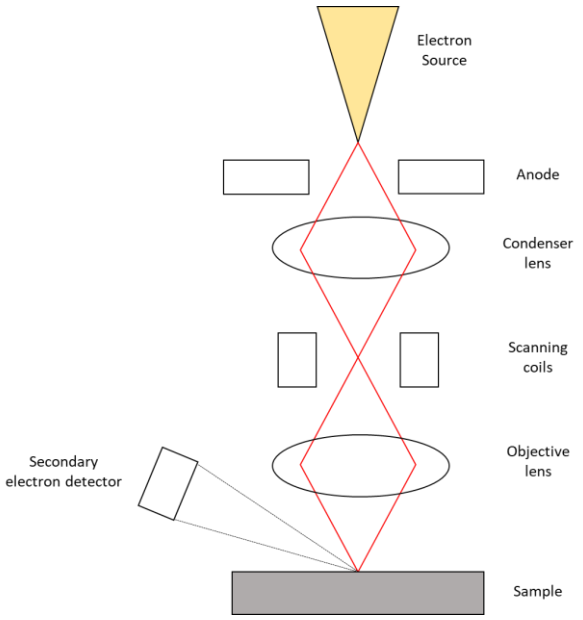

Figure 2.9: A basic schematic of a scanning electron microscope

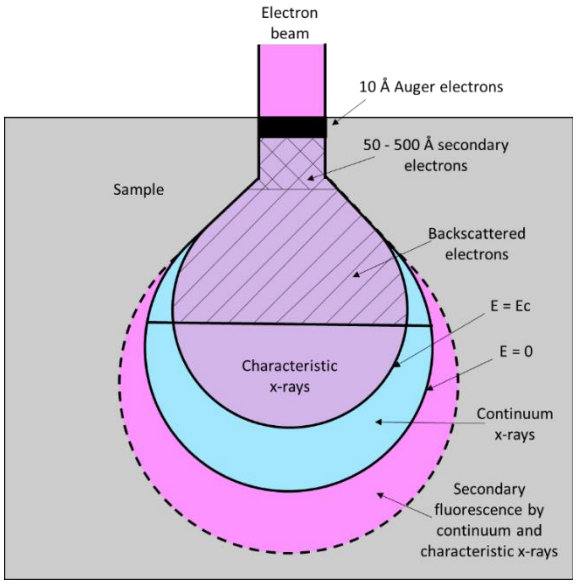

Figure 2.8: Schematic of signal generation for scanning electron microscopy

2.4.7.1.1 Experimental

SEM-EDX was carried out by Dr Thomas Davies at the University of Cardiff.

Scanning Electron microscopy was performed on a Tescan MAIA3 field emission gun scanning electron microscope) fitted with an Oxford Instruments X-ray MaxN 80 detector. The catalysts were loaded onto a carbon tape. To help prevent charging of the samples due to presence of insulating components the catalysts were sputter coated with Ag/Pd. SEM was used to observe the morphology of the catalysts and determine whether there was contact between the active metal and potassium.

2.4.7.2 Transmission Electron Microscopy (TEM)

Transmission electron microscopy uses a high energy beam of electrons to study features on a sample. Figure 2.10 shows the basic set-up of a TEM.

TEM detects both transmitted and diffracted electrons. The condenser lens focuses the electron beam into a small coherent beam. The beam then hits the sample and parts of it are transmitted which is then focused by the objective lens, forming an image on a charged couple device (CCD) camera. The image formed from transmitted is known as a bright-field image. The lighter regions of the image is due to more electrons being transmitted whilst the darker sections are where less electrons were transmitted though the sample. The intensity of the bright-field image depends on the mass distribution of the atoms and the density and thickness of the

sample. By utilising the diffracted electron beams, which are at a different angle to that of the transmitted beam, the dark field image can be obtained.[14]

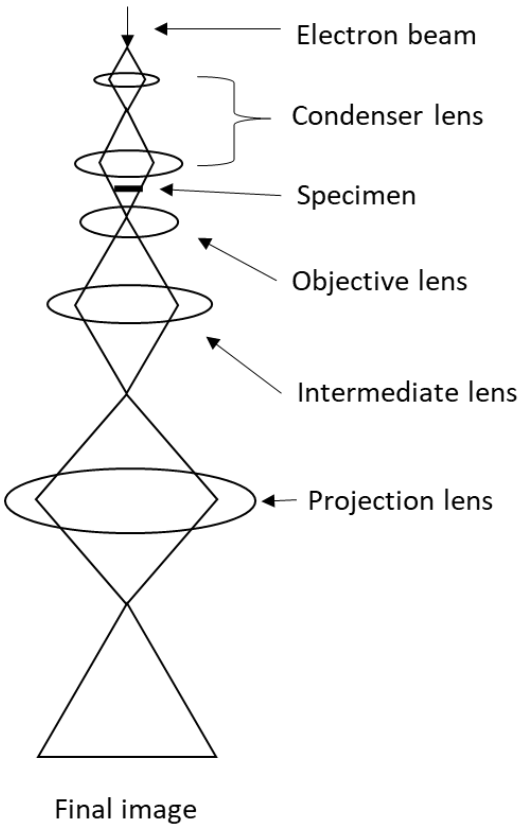

Figure 2.10: A basic schematic of a transmission electron microscope

2.4.7.2.1 Experimental

Transmission electron microscopy (TEM) was performed by Dr Thomas Davies at Cardiff University on a Jeol JEM 2100 LaB6 microscope operating at 200 kV. Samples were deposited on holey carbon-coated copper grids. TEM allowed the morphology of the catalysts to be studied and was used to determine if there was contact between the active metal and potassium.

2.5 References

1 C. Davies, K. Thompson, A. Cooper, S. Golunski, S. H. Taylor, M. Bogarra Macias, O. Doustdar and A. Tsolakis, *Appl. Catal. B Environ.*, 2018, **239**, 10–15.

2 B. C. Smith, *Fundamentals of Fourier transform infrared spectroscopy*, CRC Press, 2nd edn., 2011.

3 J. Cortés, *Adv. Colloid Interface Sci.*, 1985, **22**, 151–176.

4 J. Atkins, Peter de Paula, *Elements of Physical Chemistry*, Oxford University Press, 5th edn., 2009.

5 S. T. Misture and R. L. Snyder, *Encyclopedia of Materials: Science and Technology*, Pergamon, 2001.

6 J. P. G. and K. N. Trueblood, *Crystal Structure Analysis: A Primer*, Oxford University Press, 2010.

7 S. B. D. and B. C. Gilbert, *Foundations of Spectroscopy,* Oxford University Press, Incorporated, 2000.

8 J. R. H. Ross, *Catalyst Characterization*, Elsevier, 2019.

9 C. C. van den Akker, M. Schleeger, M. Bonn and G. H. Koenderink, in *Bio-nanoimaging*, Elsevier, 2014, pp. 333–343.

10 Edward Lau, in *Separation Science and Technology*, Elsevier, 2001, vol. 3, pp. 173–233.

11 R. Lewandowska, in *Encyclopedia of Materials: Science and Technology*, Elsevier, 2010, pp. 1–6.

12 P. Van der Heide, *X-ray photoelectron spectroscopy : an introduction to principles and practices*, Wiley-Blackwell, 2012.

13 Thermo Scientific XPS: What is XPS, https://xpssimplified.com/whatisxps.php, (accessed 18 August 2021).

14 J. W. Niemantsverdriet, *Spectroscopy in Catalysis*, VCH, Weinheim, 1993.

15 K. Akhtar, S. A. Khan, S. B. Khan and A. M. Asiri, *Handbook of Materials Characterization*, Springer, Cham, 2018.

16 EDX Analysis - SEM - EDS Analysis - Accelerating Microscopy,

https://www.thermofisher.com/blog/microscopy/edx-analysis-with-sem-how-does-it-work/, (accessed 14 July 2021).

Appendix 1

Precursor chemicals used in catalyst and catalyst support preparation

Chemical	Source and Purity
Ammonium Cerium Nitrate $(NH_4)_2Ce(NO_3)_6$	ACROS Organics, 99%
Aluminium Nitrate Nonahydrate $Al(NO_3)_3.9H_2O$	Sigma Aldrich, 99.997%
Zirconyl Oxynitrate Hydrate $ZrO(NO_3)_2.xH_2O$	Sigma Aldrich, 99.99%
Silver Nitrate $AgNO_3$	Sigma Aldrich, 99.9999%
Potassium Carbonate K_2CO_3	Fisher Scientific, 99%
Sodium Carbonate $NaCO_3$	Fisher Scientific, 99.5%
(1,5 – cyclooctadiene)(hexafluoroacetylacetonato)silver(I) $C_{13}H_{13}AgF_6O_2$	Sigma Aldrich, 99 %
Barium acetate $C_4H_6BaO_4$	Sigma Aldrich, 99 %
Dinitrodiammine platinum $Pt(NH_3)_2(NO_2)_2$	Johnson Matthey
Alumina Al_2O_3	Fisher Scientific
Barium sulphate $BaSO_4$	Sigma Aldrich, 99.99 %
Copper(II) Nitrate Trihydrate $Cu(NO_3).3H_2O$	Merk,
Copper(II) Acetylacetonate $Cu(C_5H_7O_2)_2$	Sigma Aldrich, 99.99 %
Manganese(II) nitrate tetra hydrate $Mn(NO_3)_2.4H_2O$	Sigma Aldrich, 99.99 %
Lanthanum(III) Nitrate Hexahydrate $La(NO_3)_3.6H_2O$	Sigma Aldrich, 99.99 %

Cobalt(II) Nitrate Hexahydrate **$Co(NO_3)_2.6H_2O$**	Sigma Aldrich, 99.99 %
Platinum Chloride **$PtCl_2$**	Sigma Aldrich, 99.99 %
Palladium Chloride **$PdCl_2$**	Sigma Aldrich, 99.99 %
Nickel(II) Oxide **NiO**	Sigma Aldrich, 99.99 %
Iron Nitrate **$Fe(NO_3)_3$**	Sigma Aldrich, 99.99 %
Strontium Nitrate **$Sr(NO_3)$**	ACROS Organics, 99+%

List of Samples Prepared where CVI is chemical vapour impregnation, IW is incipient wetness, IMP is wet impregnation and CZA is CeO_2-ZrO_2-Al_2O_3

Sample	Preparation Method and Conditions
2%Ag-20%K/CZA	CVI at 60°C, calcined 500°C, 5 h, 10°Cmin^{-1}, flowing air
2%Ag-20%K/CZA	CVI at 70°C, calcined 500°C, 5 h, 10°Cmin^{-1}, flowing air
2%Ag-20%K/CZA	CVI at 80°C, calcined 500°C, 5 h, 10°Cmin^{-1}, flowing air
2%Ag-20%K/CZA	CVI at 90°C, calcined 500°C, 5 h, 10°Cmin^{-1}, flowing air
2%Ag-20%K/CZA	Incipient Wetness, calcined 500°C, 5 h, 10°Cmin^{-1}, flowing air
2%Ag-20%K/CZA	Wet Impregnation, calcined 500°C, 5 h, 10°Cmin^{-1}, flowing air
2%Ag-15%K/CZA	Wet Impregnation, calcined 500°C, 5 h, 10°Cmin^{-1}, flowing air
2%Ag-10%K/CZA	Wet Impregnation, calcined 500°C, 5 h, 10°Cmin^{-1}, flowing air
2%Ag-5%K/CZA	Wet Impregnation, calcined 500°C, 5 h, 10°Cmin^{-1},

	flowing air
2%Ag-2%K/CZA	Wet Impregnation, calcined 500°C, 5 h, 10°Cmin^{-1}, flowing air
2%Cu/CZA	Wet Impregnation, calcined 500°C, 5 h, 10°Cmin^{-1}, flowing air
2%Cu-2%K/CZA	Wet Impregnation, calcined 500°C, 5 h, 10°Cmin^{-1}, flowing air
2%Cu-2%Ag/CZA 400°C	Wet Impregnation, calcined 400°C, 5 h, 10°Cmin^{-1}, flowing air
2%Cu-2%Ag/CZA 450°C	Wet Impregnation, calcined 450°C, 5 h, 10°Cmin^{-1}, flowing air
2%Cu-2%Ag/CZA 500°C	Wet Impregnation, calcined 500°C, 5 h, 10°Cmin^{-1}, flowing air
2%Cu-2%Ag/CZA Sol Immobilisation	Sol Immobilisation, calcined 500°C, 5 h, 10°Cmin^{-1}, flowing air
2%Cu-2%Ag/CZA (a)	Wet Impregnation where the precursors were added in a step-wise fashion, calcined 500°C, 5 h, 10°Cmin^{-1}, flowing air
2%Cu-2%Ag/CZA (b)	Wet Impregnation where the precursors were added at the same time, calcined 500°C, 5 h, 10°Cmin^{-1}, flowing air
2%Cu-2%Ag/CZA CVI	CVI at 140°C, calcined 500°C, 5 h, 10°Cmin^{-1}, flowing air
1%Cu-1%Ag/CZA CVI	CVI at 140°C, calcined 500°C, 5 h, 10°Cmin^{-1}, flowing air
1%Cu-1%Ag/CZA	Wet Impregnation, calcined 500°C, 5 h, 10°Cmin^{-1}, flowing air
1%Cu-1%Pd /CZA	Wet Impregnation, calcined 500°C, 5 h, 10°Cmin^{-1}, flowing air
1%Ag-1%Co/CZA	Wet Impregnation, calcined 500°C, 5 h, 10°Cmin^{-1}, flowing air
1%Ag-1%Mn/CZA	Wet Impregnation, calcined 500°C, 5 h, 10°Cmin^{-1}, flowing air
1%Ag-1%La/CZA	Wet Impregnation, calcined 500°C, 5 h, 10°Cmin^{-1},

	flowing air
1%Ag-1%Ba/CZA	Wet Impregnation, calcined 500°C, 5 h, 10°Cmin^{-1}, flowing air
1%Ag-1%Ni/CZA	Wet Impregnation, calcined 500°C, 5 h, 10°Cmin^{-1}, flowing air
1%Ag-1%Sr/CZA	Wet Impregnation, calcined 500°C, 5 h, 10°Cmin^{-1}, flowing air
1%Ag-1%Fe/CZA	Wet Impregnation, calcined 500°C, 5 h, 10°Cmin^{-1}, flowing air
1%Ag-1%Pt/CZA	Wet Impregnation, calcined 500°C, 5 h, 10°Cmin^{-1}, flowing air
1%Ag-1%Pd/CZA	Wet Impregnation, calcined 500°C, 5 h, 10°Cmin^{-1}, flowing air
1%Ag-1%Co-1%K/CZA	Wet Impregnation, calcined 500°C, 5 h, 10°Cmin^{-1}, flowing air
1%Ag-1%Mn-1%K/CZA	Wet Impregnation, calcined 500°C, 5 h, 10°Cmin^{-1}, flowing air
1%Ag-1%La-1%K/CZA	Wet Impregnation, calcined 500°C, 5 h, 10°Cmin^{-1}, flowing air
1%Ag-1%Ba-1%K/CZA	Wet Impregnation, calcined 500°C, 5 h, 10°Cmin^{-1}, flowing air
1%Ag-1%Ni-1%K/CZA	Wet Impregnation, calcined 500°C, 5 h, 10°Cmin^{-1}, flowing air
1%Ag-1%Sr-1%K/CZA	Wet Impregnation, calcined 500°C, 5 h, 10°Cmin^{-1}, flowing air
1%Ag-1%Fe-1%K/CZA	Wet Impregnation, calcined 500°C, 5 h, 10°Cmin^{-1}, flowing air
1%Ag-1%Pt-1%K/CZA	Wet Impregnation, calcined 500°C, 5 h, 10°Cmin^{-1}, flowing air
1%Ag-1%Pd-1%K/CZA	Wet Impregnation, calcined 500°C, 5 h, 10°Cmin^{-1}, flowing air

3. The Influence of Preparation Method of Ag-K/CeO_2-ZrO_2-Al_2O_3 Catalysts on Their Structure and Activity for Simultaneous Removal of Soot and NOx

3.1 Introduction

Previous work has shown that Ag/CZA is a suitable catalyst for the simultaneous removal of NOx and diesel particulates utilising in situ generated N_2O from diesel exhausts.[1] The *in situ* generated N_2O has the ability to oxidise diesel soot at low temperatures (< 300°C) over the Ag/CZA catalyst. An Ag-K/CZA has also been shown to be active for diesel soot oxidation.[2] However, the suitability of Ag-K/CZA for the simultaneous removal of NOx and PM has not previously been investigated. Potassium is a known enhancer of soot oxidation[3] and hence has the potential to enhance and lower the temperature required for soot oxidation during the simultaneous reaction. Therefore, various preparation methods (wet impregnation, incipient wetness and chemical vapour impregnation at four different temperatures) for preparing Ag-K/CZA were investigated for the simultaneous reaction.

Chemical vapour impregnation is becoming a commonly used preparation technique for a large variety of catalysts[4–7] however there is little literature on CVI for silver catalysts. The main example in literature used silver acetylacetonate ($C_5H_7AgO_2$) as the silver precursor using a temperature of 60°C.[8] However, due to the toxic nature of silver acetylacetonate in this work (1,5 – Cyclooctadiene)(Hexafluoroacetylacetonato)Silver(I) was used as an alternative. As there were no reaction conditions for this precursor four different low temperatures were initially investigated. It was found that the temperature of the chemical vapour impregnation preparation had a significant impact on the catalyst's reactivity, with the preparation at 80°C resulting in the most suitable catalyst for the reaction.

In previous work, a Ag/CZA catalyst was prepared by wet impregnation hence for comparison the same technique was used in this work. Additionally, incipient wetness was used to compare various preparation methods. With wet impregnation and incipient wetness, the active metal (silver) and potassium was impregnated into the support whilst for CVI the silver was deposited on the surface of K/CZA.

The six catalysts were prepared as described in Section 2.3.2. Each catalyst was tested for its ability to catalyse the SCR reaction and its ability to simultaneously remove NOx and soot at low temperatures as described in Section 2.4. Catalytic testing was carried out using a simulated exhaust gas which deliberately excluded the major combustion products (CO_2 and H_2O) as these

gases could mask small changes in the composition of the gas stream. This allowed the desorption of CO_2 from the catalyst (in the absence of soot) and its formation during the oxidation of soot to be effectively monitored. It is of particular interest that the catalyst's preparation method and preparation temperature determined whether it had the ability to utilise *in situ* generated N_2O to oxidise soot.

3.2 CeO_2-ZrO_2-Al_2O_3 (CZA) Support

Due to equipment limitations the CZA support used throughout this project could only be prepared in batches of 3 g in an autotitrator as described in 2.3.1. Hence, it was imperative to establish whether the different batches produced were similar if not identical to each other. As any major differences between the batches could impact the activity and morphology of the different catalysts being studied. Figure 3.1 shows the X-ray diffraction pattern for three different batches of the CZA support used during this work. Figure 3.1 shows that each sample has four key reflections at 28.8, 33.4, 47.9 and 57.1 ° which are due to CeO_2.

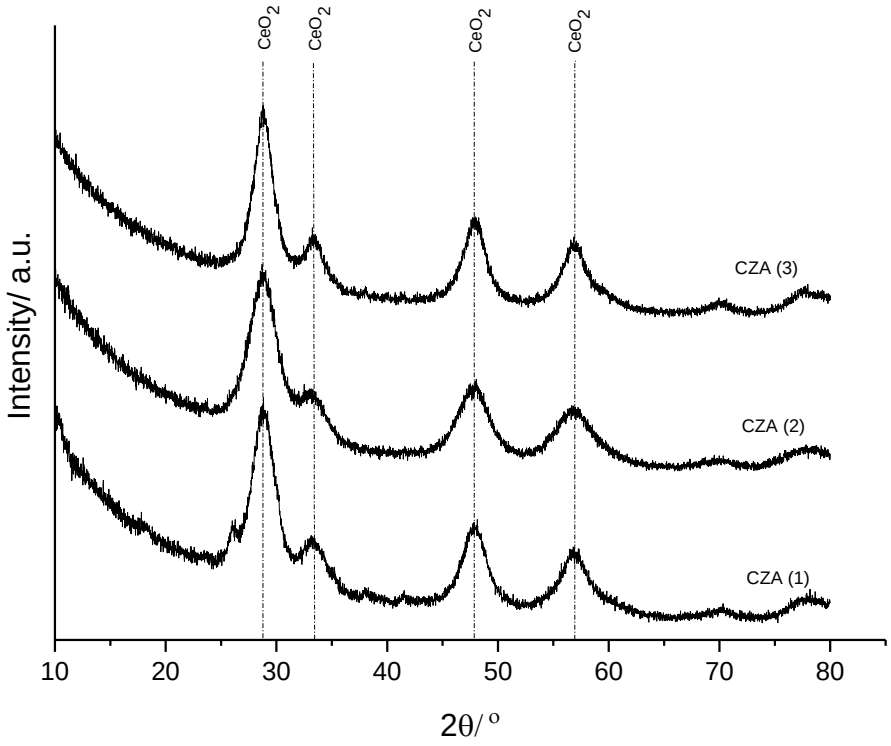

Figure 3.1: XRD pattern for three different batches of the CZA support

The CeO_2 crystallite sizes were calculated from the XRD data using the Scherer equation, Table 3.1. The three XRD patterns are almost identical and the calculated crystallite sizes are similar indicating that making the support in batches is reproducible.

Table 3.1: CeO_2 crystallite sizes for different batches of CZA calculated from XRD data

Sample	2θ [°]	Crystallite size [Å]
CZA 1	28.8	35
	33.4	40
	47.8	36
	57.0	26
CZA 2	28.8	27
	33.2	40
	47.8	30
	56.9	21
CZA 3	28.8	40
	33.4	42
	47.8	35
	57.0	26

3.3 Catalysts Prepared *via* Chemical Vapour Impregnation

As discussed in Section 2.3.2.1.1. 2wt.%Ag-20wt.%K/CZA was prepared *via* chemical vapour impregnation (CVI) at four different temperatures: 60°C, 70°C, 80°C and 90°C. The catalysts will be referred to as CVI60, CVI70, CVI80 and CVI90. Each of the catalysts was tested for their ability to catalyse the SCR reaction and to catalyse the simultaneous removal of NOx and soot as described in Section 2.4. Of the four catalysts only the catalyst prepared at 80°C showed the potential to simultaneously remove NOx and oxidise soot. However, the other catalysts, to varying degrees, could oxidise soot but not reduce NOx.

3.3.1 Reaction Data

Figure 3.2 shows the SCR reaction data and Figure 3.3 shows the SCR + soot reaction data for each of the four CVI catalysts.

For each catalyst the conditions were kept the same (500 ppm NO, 500 ppm NH_3, 8 % O_2 and N_2 as the balance gas with a flow rate of 200 ml min^{-1} being maintained throughout the experiments). It is obvious that the temperature in which CVI preparation method was performed at had a significant influence on the activity towards soot oxidation and NOx reduction.

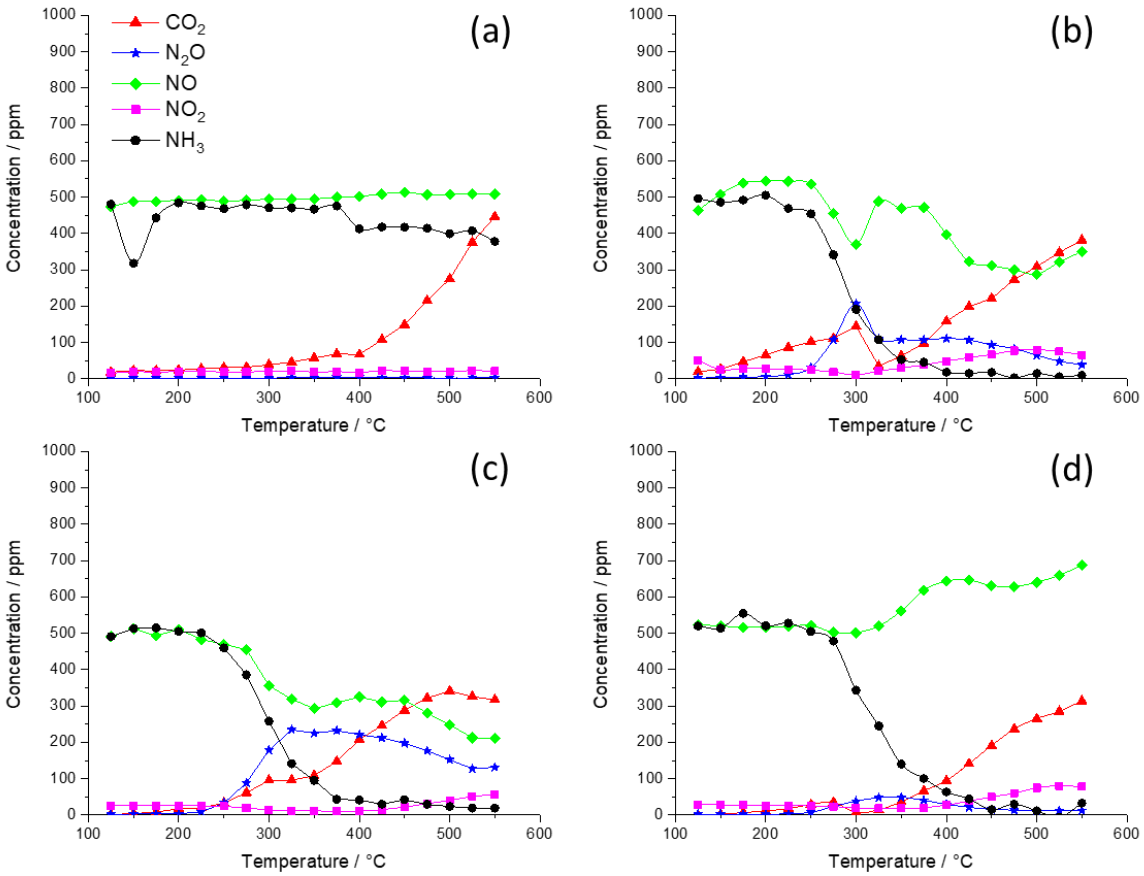

Figure 3.2: Reaction data for SCR reaction where (a) CVI60, (b) CVI70, (c) CVI80 and (d) CVI90. The simulated exhaust gas consisted of 500 ppm NO, 500 ppm NH_3, 8% O_2, with a balance of N_2. The total flow rate was 200 $mlmin^{-1}$. The temperature was increased in 25°C intervals from 125 to 550°C, the gas concentrations were allowed to stabilise before readings were taken at each temperature. 0.25 g of catalyst was used.

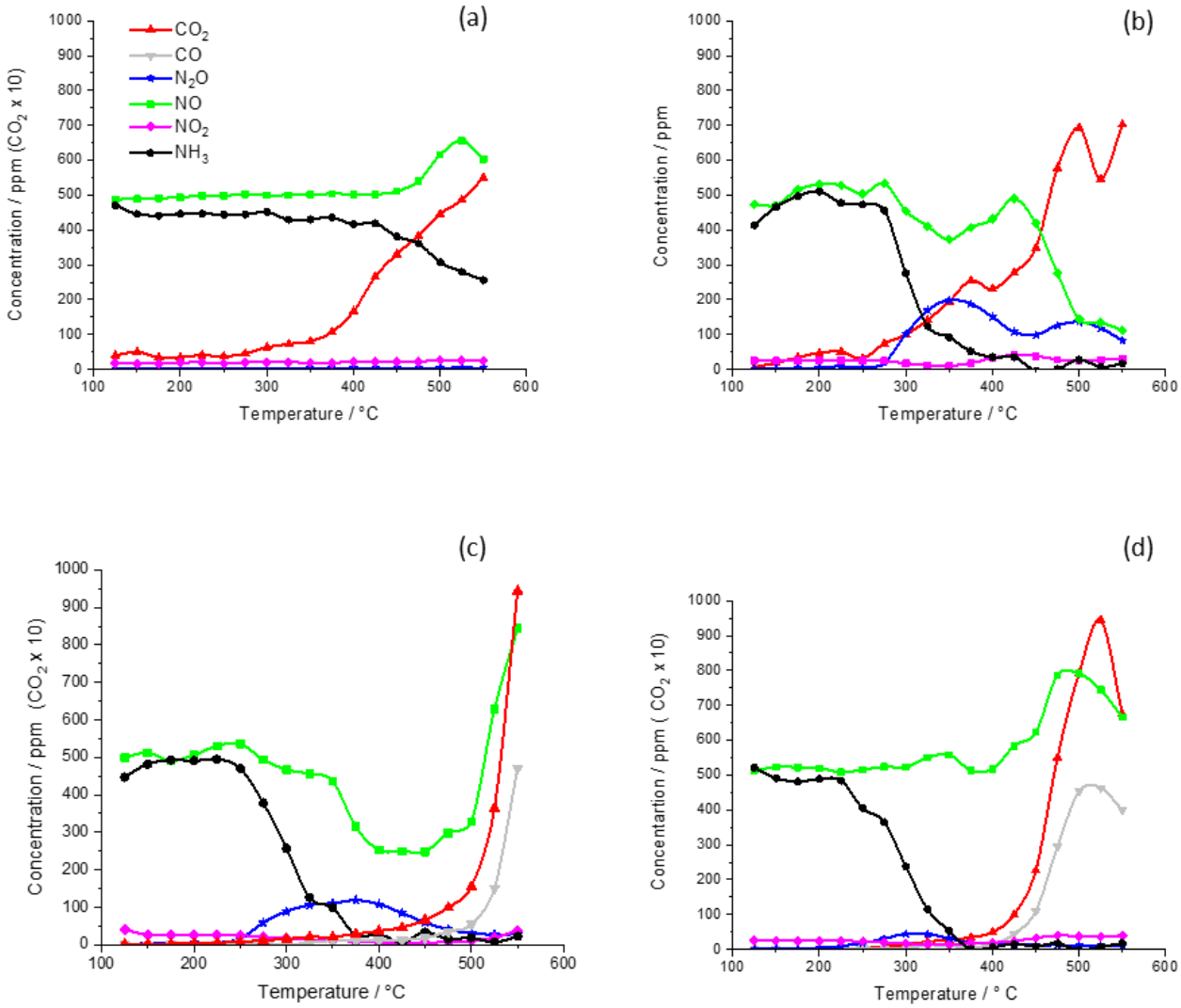

Figure 3.3: Reaction data for SCR + soot reaction where (a) CVI60, (b) CVI70, (c) CVI80 and (d) CVI90. The simulated exhaust gas consisted of 500 ppm NO, 500 ppm NH_3, 8% O_2, with a balance of N_2. The total flow rate was 200 $mlmin^{-1}$. The temperature was increased in 25°C intervals from 125 to 550°C, the gas concentrations were allowed to stabilise before readings were taken at each temperature. 0.25 g catalyst was mixed in a 10:1 ratio by mass with soot.

3.3.1.1 CVI60

Figure 3.2a shows the reaction data for the SCR reaction and Figure 3.3a shows the reaction data for the SCR + soot reaction. When Figure 3.2a and Figure 3.3a are compared, the CO_2 traces are very similar. This implies that the CO_2 observed for the combination testing is not due to soot oxidation but rather due to the decomposition of surface carbonate or hydrogencarbonate species. Figure 3.3a shows that the concentration in NO remains at 500 ppm until 475°C where it increases in concentration to 656 ppm. This rise in NO concentration is parallel to the decrease in NH_3 concentration, hence demonstrating that the rise in NO concentration at high temperatures is due to oxidation of NH_3 forming NO (Equation 3.1).

$$2NH_3 + 4O_2 \rightarrow 2NO + 6H_2O$$

Equation 3.1: High temperature oxidation of NH_3

$$4NH_3 + 4NO + O_2 \rightarrow 4N_2 + 6H_2O$$

Equation 3.2: The equation for the selective catalytic reduction of NO by NH_3

$$2NH_3 + 2NO + 1\,{}^{1}/_{2}\,O_2 \rightarrow 2N_2O + 3H_2O$$

Equation 3.3: The non-selective catalytic reduction of NO resulting in the formation of N_2O

As with Figure 3.2a, Figure 3.3a shows negligible quantities of NO_2 and N_2O demonstrating that neither the SCR (Equation 3.2) nor the non-selective SCR (Equation 3.3) reaction takes place over this catalyst. This CVI60 catalyst is both a poor soot oxidation catalyst and a poor NOx reduction catalyst.

3.3.1.2 CVI70

Figure 3.2b shows the reaction data for the catalyst prepared *via* CVI at 70°C. A CO_2 trace is observed which is due to adsorbed hydrogencarbonates and carbonates desorbing from the catalytic surface. N_2O begins to form and 225°C, peaking at 300°C. The N_2O trace is almost a mirror image of the inverted NO peak. This is indicative that the non-selective SCR reaction (Equation 3.3) was taking place as for every mole of NO consumed, 1 mole of N_2O was formed. At temperatures higher that 400°C the dominate reaction is no longer the non-selective SCR reaction hence the N_2O concentration decreased. Instead, oxidation of NO and NH_3 into NO and NO_2 (Equation 3.1) is the dominate reaction which explains the rise in concentration of NO and NO_2 at high temperatures.

Figure 3.3b shows the reaction data when soot has been mixed with the catalyst to form loose contact. A decrease in concentration for NO and NH_3 took place however the gases' reduction in concentration was not simultaneous. This is due to the CZA support storing NH_3 at low temperatures. The adsorbed NH_3 on the CZA surface undergoes the selective SCR reaction at higher temperatures *via* a Langmuir-Hinshelwood mechanism.[9] At 275°C N_2O is first observed and peaking at 350°C. This N_2O was formed *via* the non-selective SCR reaction which can be deuced by the inverted NO peak mirroring the N_2O peak. The total amount of N_2O formed in the presence and absence of soot are very similar which indicates that N_2O is not being utilised to oxidise soot at low temperatures. N_2O is first observed at higher temperatures compared to the reaction in the absence of soot this is due to the soot storing N_2O at low temperatures. Between 125°C and

400°C the quantity of CO_2 produced over CVI70 in the presence and absence of soot is very similar and this is due to hydrogencarbonates and carbonates desorbing from the catalyst as the temperature is increased. At higher temperatures (> 400°C) in the presence of soot a greater quantity of CO_2 is observed and this is due to the non-catalytic oxidation of C by O_2.

CVI70 is not a suitable catalyst for the simultaneous removal of NOx and soot as NO is not reduced to 0 ppm and soot is not oxidised at low temperatures *i.e.* within the ideal temperature range of 175 to 400°C.

3.3.1.3 CVI80

Out of the Ag-K/CZA catalysts prepared *via* CVI, CVI80 demonstrated the most promising reactivity for simultaneous removal of NOx and soot particulate from a diesel exhaust. Figure 3.2c shows that in the absence of soot CVI80 catalyses the non-selective SCR reaction with the N_2O peak (onset at 225°C) mirroring the inverted peak of NO. A CO_2 trace is observed in the absence of soot, this is due to the desorption of hydrogencarbonate and carbonate species from the catalyst surface. The NH_3 concentration decreases with increase in temperature reaching almost 0 ppm by 450°C.

Figure 3.3c shows the reaction data for the combination testing for CVI80, where at 225°C N_2O is first observed with a maximum peak concentration (approx. 150 ppm) at 375°C. Compared to Figure 3.2c the maximum concentration is almost 100 ppm less. Figure 3.4 shows that in the presence of soot CO_2 is first observed at 175°C, at 375°C the CO_2 concentration is 286 ppm compared to 147 ppm at the same temperature in the absence of soot this is an increase of 139 ppm. The oxidation of soot by N_2O takes place over the temperature range 175 – 400°C. The rise in CO_2 concentration and the decrease in N_2O concentration when the two sets of data are compared shows that the in situ generated N_2O is being utilised to oxidise soot at low temperatures. At lower temperatures (175 – 250°C) the reduction in N_2O concentration exceeds that of the increase in CO_2 concentration this is due to N_2O being stored by the soot at low temperatures. The ideal diesel exhaust temperature window is between 175 – 400°C, hence it is ideal for reactions to take place within this temperature range. Figure 3.4 demonstrates the catalyst's ability to reduce NOx over the desired temperature range improves in the presence of soot. Furthermore, it clearly shows that CO_2 is being produced at low temperatures. The NH_3 concentration reaches 0 ppm at 400°C in presence of soot. Despite CVI80 being an active catalyst for NOx reduction the NO concentration does not reach 0 ppm. At higher temperatures (> 400°C) A large amount of CO_2 is observed, this is due to catalytic and non-catalytic oxidation by O_2 taking

place. Furthermore, above 500°C a significant ppm of CO was observed, due to the non-catalytic oxidation of C by O_2 as shown by Equation 3.4.

$$C + \frac{1}{2}O_2 \rightarrow CO$$

Equation 3.4: Oxidation of soot to form carbon monoxide

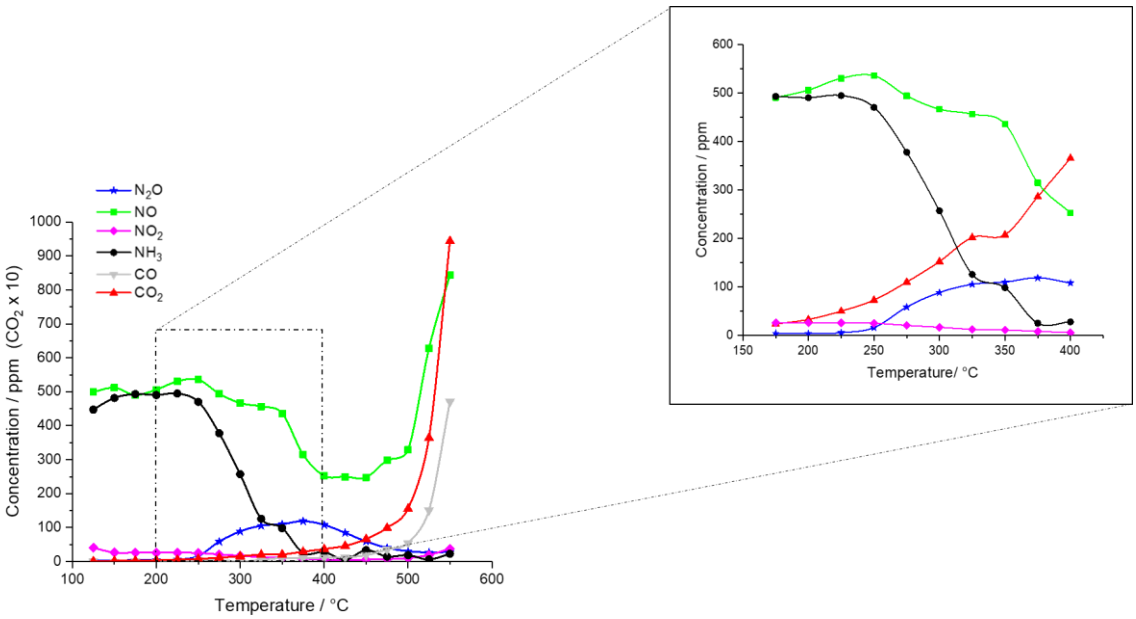

Figure 3.4: SCR + CB reaction data for CVI80 with focus on temperatures between 175 - 400 °C. The simulated exhaust gas consisted of 500 ppm NO, 500 ppm NH_3, 8% O_2, with a balance of N_2. The total flow rate was 200 mlmin^{-1}. The temperature was increased in 25°C intervals from 125 to 550 °C, the gas concentrations were allowed to stabilise before readings were taken at each temperature. 0.25 g catalyst was mixed in a 10:1 ratio by mass with soot.

CVI80 is active for the selective SCR reaction, in the presence of soot, between 175 – 450°C. CVI80 is also shown to be active for soot oxidation especially at higher temperatures due to the catalytic oxidation by oxygen. The reaction data shows that the preparation of 2 wt.% Ag - 20 wt.% K / CZA by CVI80 produces a catalyst which is active for the simultaneous removal of NOx and soot from a diesel exhaust as well as having the ability to utilise *in situ* generated N_2O to oxidise soot at low temperatures.

3.3.1.4 CVI90

The final catalyst to be prepared *via* CVI, CVI90, again showed different reactivity compared to the previous catalysts. Figure 3.2d shows that in the absence of soot CVI90 neither undergoes the selective nor the non-selective SCR reaction (Equation 3.2 and Equation 3.3). The NO concentration remains at approximately 500 ppm until 325°C where it begins to rise in concentration. The increase in NO concentration is due to oxidation of NH_3. A small quantity of N_2O is observed peaking at 350°C. As with the previous CVI catalysts a CO_2 trace is observed due to desorption of hydrogencarbonate and carbonate species from the catalyst surface.

Figure 3.3d shows that in the presence of soot that there is no decrease in concentration of NO only a rise at high temperatures, due to the oxidation of NH_3. An almost identical amount of N_2O is observed in the presence of soot compared to in the absence of soot implying that N_2O has no role in oxidising soot over this catalyst. However, CVI90 is shown to be a good soot oxidation catalyst with CO_2 onset at 375°C and peaking with a concentration greater than 9500 ppm at 500°C. The decrease in CO_2 observed after 500°C shows that almost full combustion of soot was achieved at 500°C. The high concentrations of CO_2 observed over CVI90 is due to catalytic and non-catalytic oxidation by O_2. However, CVI90 is not a suitable preparation technique for preparing a catalyst for the simultaneous removal of NOx and soot from a diesel exhaust.

3.3.2 Characterisation of the Catalysts Prepared *via* Chemical Vapour Impregnation

To understand the differences in reactivity between the CVI catalysts prepared at different temperatures a variety of different characterisation techniques were carried out on each catalyst. The characterisation techniques were carried out as described in Section 2.5.

Table 3.2 contains data on Ag and CeO_2 crystallite sizes which were calculated using the Scherrer equation and XRD data, and the surface areas of the catalysts which was obtained *via* BET analysis.

Table 3.2: Crystallite size calculated from XRD data, CeO_2 defect ratio calculated from Raman data and surface area from BET analysis for each CVI catalyst studied

Sample	Ag Crystallite Size [Å]	CeO_2 Crystallite Size [Å]	CeO_2 Defect Ratio	Catalyst Surface Area [$m^2 g^{-1}$]
CVI60	590	180	-	3.8
CVI70	520	160	0.61	9.2
CVI80	400	330	0.74	11.8
CVI90	>1000	>1000	0.82	8.4

Figure 3.5 shows the XRD patterns for the four CVI catalysts as well as the pattern for the CZA support. The reflections at 2θ = 38° and 44° are due to metallic Ag crystallites. From the XRD pattern it can be determined that the Ag species are not in the form of AgO, this consistent with literature on similar catalysts.[10–14] CVI80 has a significantly lower intensity Ag peak than the other three CVI catalysts. Using the Scherrer equation the Ag crystallite sizes were calculated (Table 3.2). CVI80 had the smallest Ag crystallite size (400 Å) of the four catalysts. The four catalysts and the CZA support have the typical ceria peaks due to ceria's fluoride cubic phase, this is in agreement with the Raman data (Figure 3.6). The ceria peaks are slightly shifted compared to pure ceria[15] this is a consequence of the incorporation of ZrO_2 and Al_2O_3 into the ceria lattice. The catalysts also display small reflections at 31.1° and 38.8° which is due to K_2CO_3 hence showing that some of K is present in the form of the carbonate in ambient conditions. This could explain why CO_2 is observed in the absence of soot in the reaction data.

Table 3.2 also shows the CeO_2 defect ratios which were calculated using the CeO_2 peak and ceria's defect peak from the Raman data, Figure 3.6. The CeO_2 peak is centred between 451 – 469 cm^{-1} this is due to ceria's F_{2g} Raman mode. The peaks which are present between 500 – 600 cm^{-1} are due to defect-induced mode of CeO_2's fluorite phase[16]. The F_{2g} distortion ratio was calculated for CVI70, CVI80 and CVI90 however it could not be calculated for CVI60 due to its lack of a ceria distortion peak. The defect ratio increases as the CVI preparation temperature increases, the changes in the ratios show that the formation of bulk oxygen vacancies ($V_{o\text{-}b}$)[12] are influenced by the preparation temperature of the catalysts. A band was observed between 1052-1064 cm^{-1} for CVI60, CVI70 and CVI90 which is due to carbonate from the Na_2CO_3 used as the precipitant in the CZA support preparation method. The presence of Na in the sample is further supported by XPS

and SEM-EDX analysis. The Raman spectra show that the catalysts have a band between 141 – 158 cm^{-1} which is due to Ag lattice vibrational modes (*i.e*. phonons)[17,18].

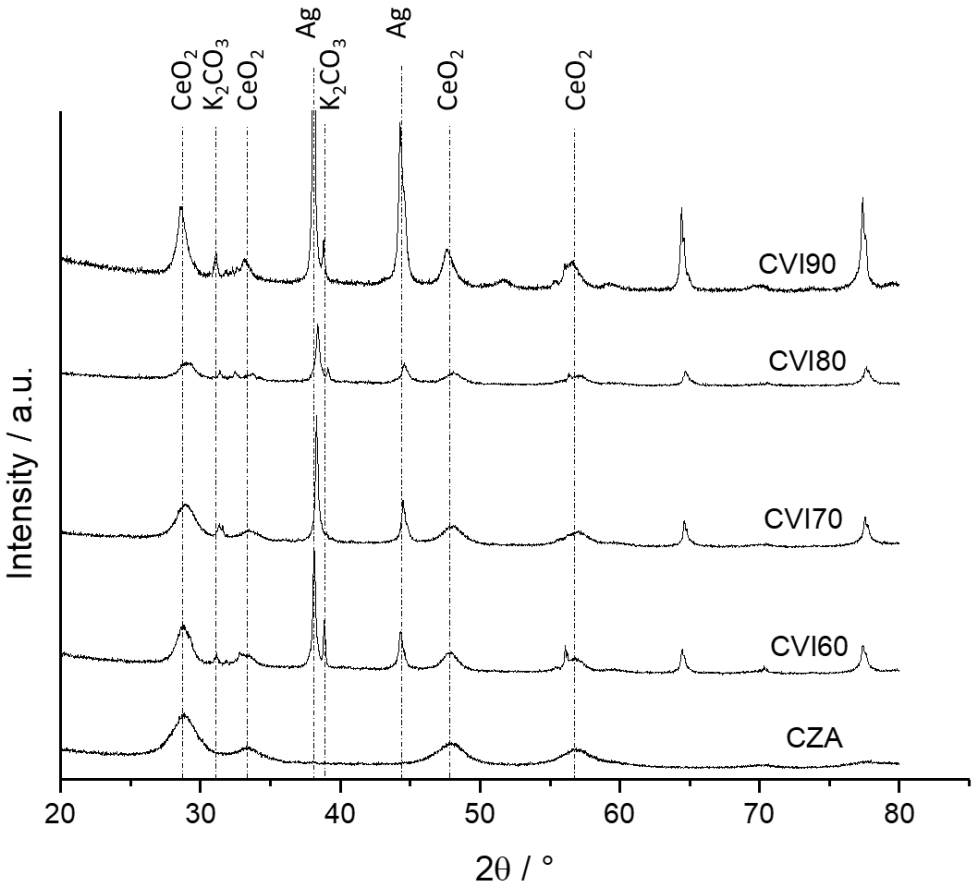

Figure 3.5: XRD pattern for the four CVI catalysts and for the CZA support

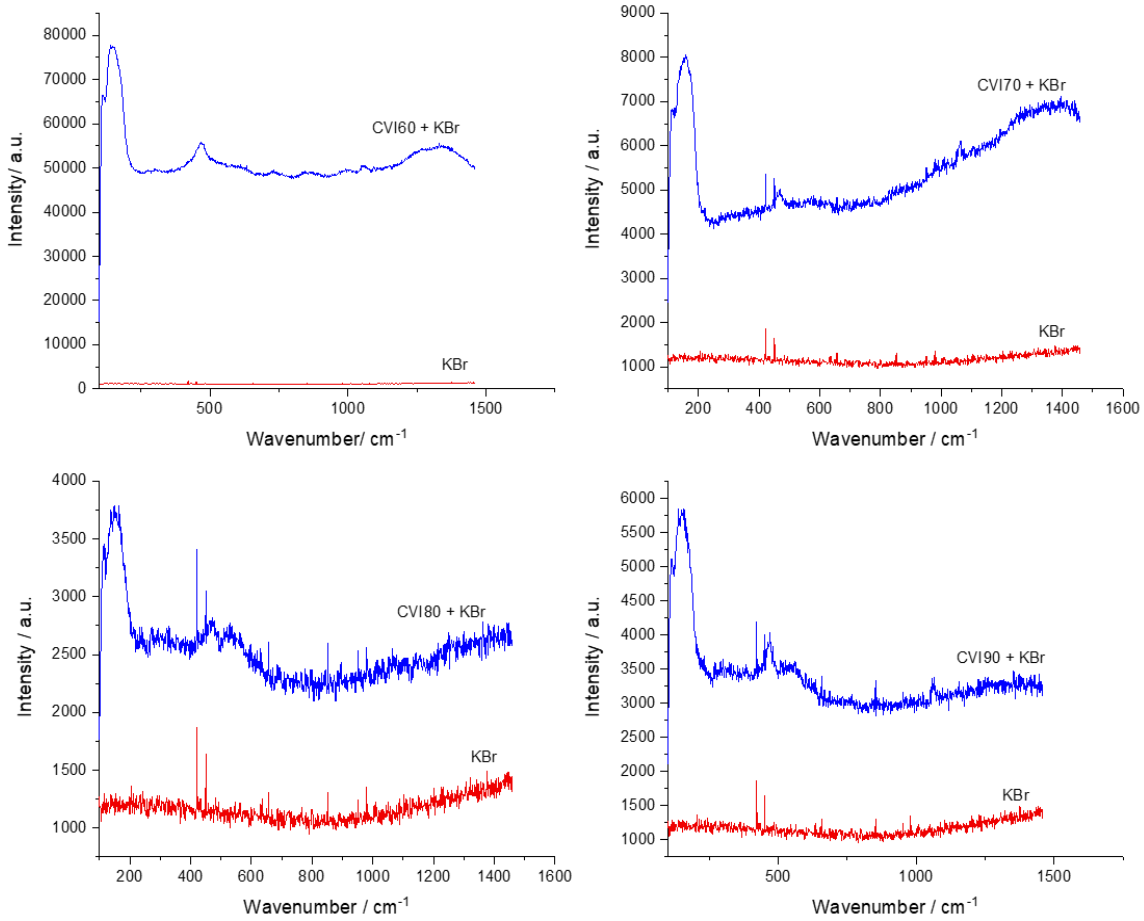

Figure 3.6: Raman spectra for the four CVI catalysts studied. Each spectrum features a catalyst + KBr spectrum and a KBr spectrum as for the samples to be analysed they had to be diluted with KBr.

The atomic elemental % from XPS analysis is shown in Table 3.3. The table shows that 7.2, 5.9, 3.8, 3.4 % of Na is present in CVI60, CVI70, CVI80 and CVI 90 respectively. The percentage of Na present in the catalyst decreases with increase of preparation temperature. However, when the CZA support is prepared it is washed with 2 L of hot de-ionised water which should remove any remaining Na[19] which has not occurred. The XPS analysis also confirms that there is a high amount of carbonate present in the catalysts however the quantity varies between the catalysts as shown by the C(1s) peak at *ca.* 289.5 eV in all spectra (24.6, 22.4, 29.5, 47.4 % for CVI60, CVI70, CVI80 and CVI90 respectively). The percentage of surface Ag varies with the preparation method with CVI60 and CVI70 having 2.3 % and 2.4 %, respectively, whilst CVI80 and CVI90 has considerably lower percentages (0.7 % and 0.3 %). The percentage of K also varies with preparation method although there is no clear pattern: CVI60 11.6 %, CVI70 14.2 %, CVI80 11.5 % and CVI90 7.2 %. Another significant factor which the XPS analysis highlighted is the high percentage of F present in the CVI catalysts. The F is due to the (1,5–

Cyclooctadiene)(Hexafluoroacetylacetonato)Silver(I) precursor used in the CVI preparation method. The percentage of F present in the catalysts decreases as the preparation temperature increases: CVI60 20.1 % F, CVI70 17.0 % F, CVI80 9.1 % F and CVI90 5.1 %. This suggests that the higher the preparation temperature the less F on the surface of the catalyst even though all of the catalysts were dried overnight (16 h, 110°C) and calcined under the same conditions (5 h, 500°C, 10°C min^{-1} in flowing air).

Table 3.3: Atomic % of elements from XPS analysis for each catalyst prepared *via* CVI

Catalyst	Na	Ce	F	O	Ag	K	C	Zr	Al
CVI60	7.2	1.1	20.1	29.5	2.3	11.6	24.6	0.4	3.4
CVI70	5.9	1.1	17.0	31.8	2.4	14.2	22.4	0.3	5.0
CVI80	3.8	0.8	9.1	37.6	0.7	11.5	29.5	0.2	6.7
CVI90	3.4	0.6	5.1	32.0	0.3	7.2	47.4	0.1	4.6

SEM-EDX analysis also highlighted elemental differences between the CVI catalysts. One key feature was that this analysis also showed that as the preparation temperature rose there was less F present in the catalyst, this is also confirmed by the XPS analysis. SEM-EDX showed that CVI60 had significantly less K present on the surface compared to the other catalysts this observation differs from the information provided from XPS analysis. This could be due to section of the catalyst studied by each technique. Figure 3.7 – 3.10 show the elemental data obtained from SEM-EDX.

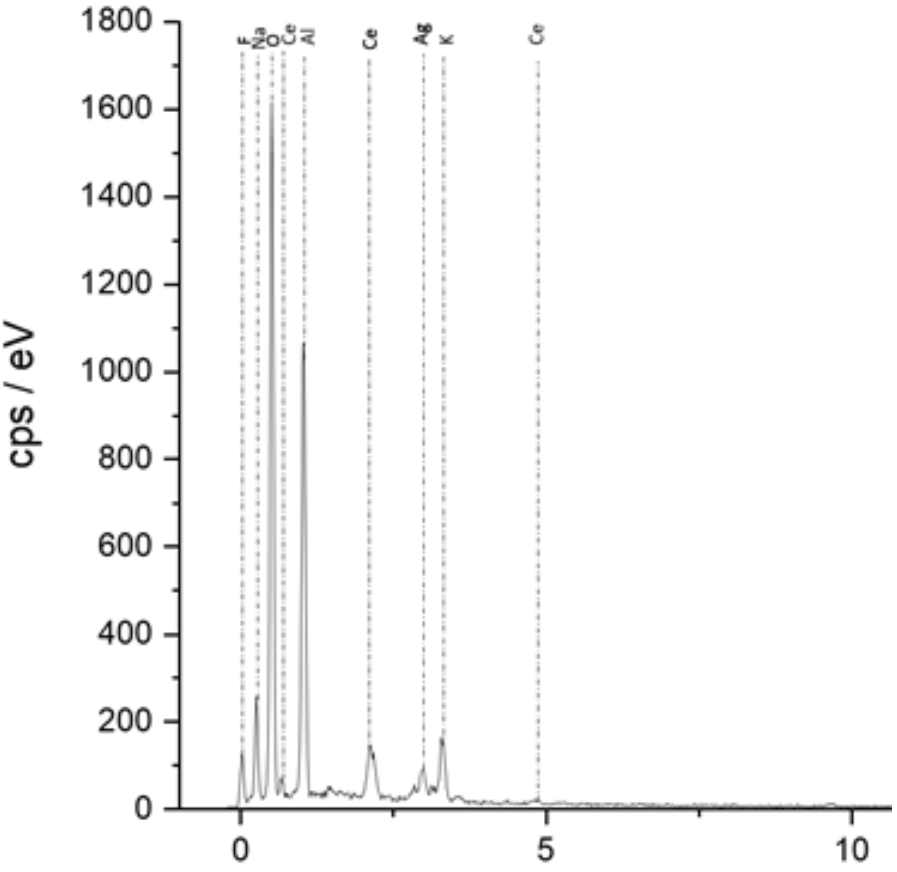

Figure 3.8: Elemental data for CVI60 obtained from SEM-EDX

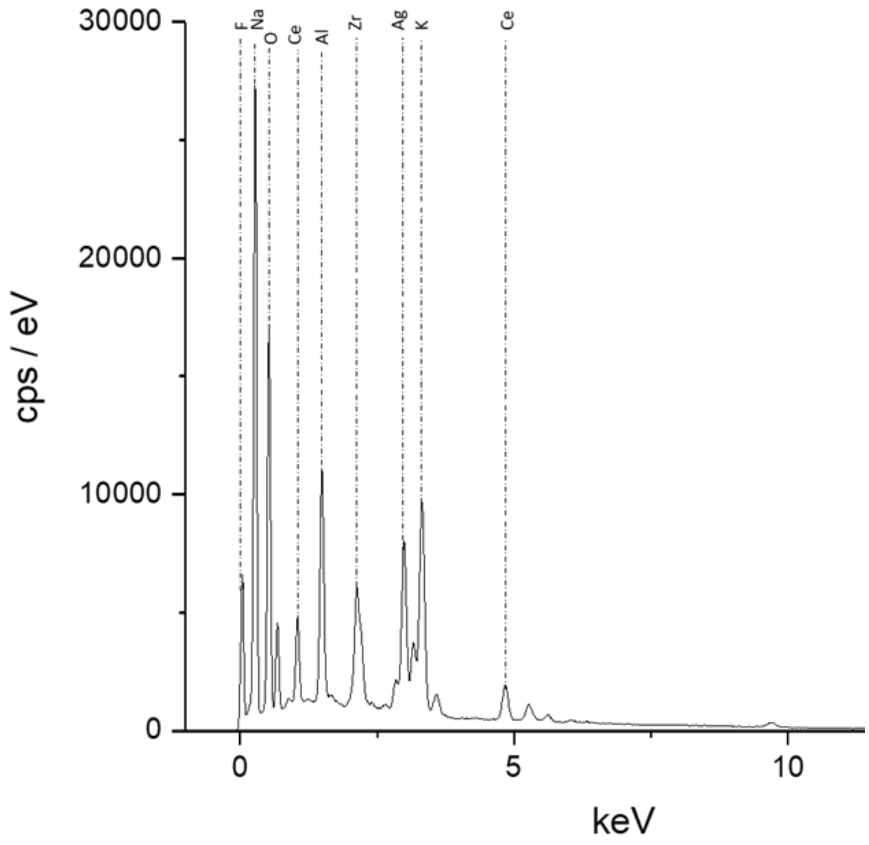

Figure 3.7: Elemental data for CVI70 obtained from SEM-EDX

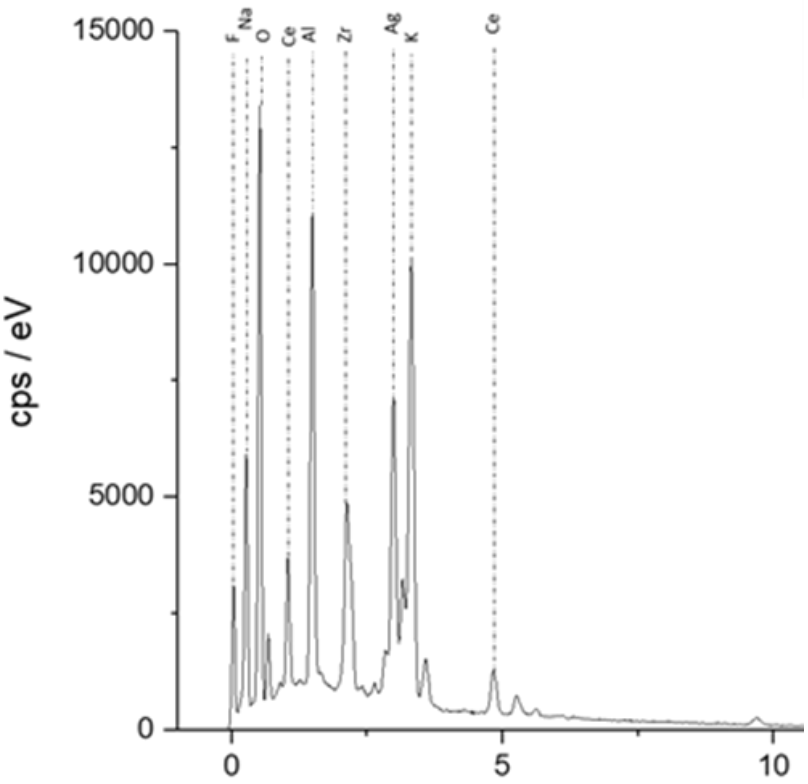

Figure 3.9: Elemental data for CVI80 obtained from SEM-EDX

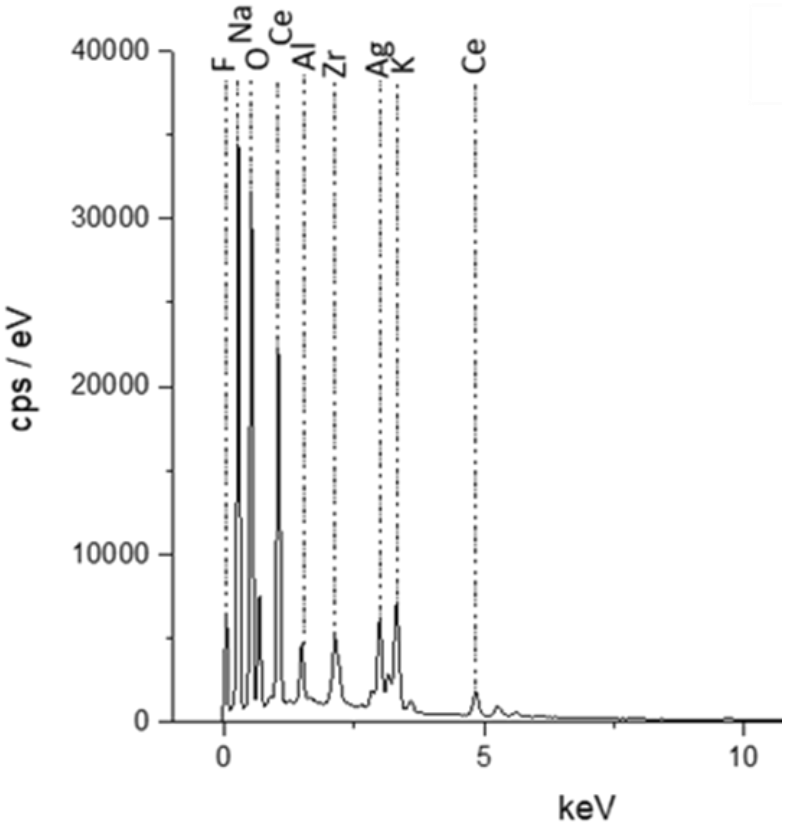

Figure 3.10: Elemental data for CVI90 obtained from SEM-EDX

3.3.3 Conclusions

The key conclusion from this section is that the temperature at which CVI is carried out has an impact on the catalysts' ability to simultaneously remove NOx and soot. The catalyst prepared at 80°C showed promising activity for the desired reactions whilst the catalysts prepared at other temperatures did not. CVI80 also was able to utilise *in situ* generated N_2O to oxidise soot at low temperatures it was also active for the selective SCR reaction between 125 – 400°C.

CVI60 was in particular a poor catalyst. Despite being inactive for Nox reduction CVI90 was shown to be a good soot oxidation catalyst especially at temperatures above 350°C.

Despite characterisation on all four catalysts there is little explanation for the differences in reactivity. From the XRD and B.E.T. data CVI80 has the smallest Ag crystallite size and the highest surface area which results in higher dispersion of Ag across the catalytic surface explaining the catalyst's activity towards SCR and soot oxidation. A key area which may influence the reactivity is the contact between Ag and K in the sample and the mobility of K. Contact between Ag and K was not easily determined *via* SEM due to the high weight loading of K and high percentage of Na and F present in the samples.

3.4 Catalysts Prepared via Incipient Wetness and Wet Impregnation

The 2wt.%Ag-20wt.%K/CZA catalysts prepared via wet impregnation termed IMP, and incipient wetness termed IW, were also tested for their ability to catalyse the SCR reaction and the simultaneous removal of NOx and soot.

3.4.1 Incipient Wetness

The catalyst made *via* incipient wetness displayed promising reactivity in the absence of soot. Figure 3.11 shows the SCR and SCR + soot reaction data for the IW catalyst.

The NH_3 concentration reached 0 ppm at 325°C and like with CVI80, a peak of N_2O mirrored the inverted peak of NO showing that the non-selective SCR reaction was taking place. Figure 3.11a includes a calculated N_2 balance. From the ratios of nitrogen containing species it can be concluded that the non-selective reaction is taking place but a second reaction is also occurring. This second reaction is the oxidation of NH_3 to N_2. As the reactivity in the absence of soot was similar to that of CVI80, it showed potential as a simultaneous catalyst. However, when soot was introduced into the system a very different reactivity was observed. Firstly, the IW catalyst showed that it does have the ability to utilise *in situ* generated N_2O to oxidise soot at low temperatures (225 - 400°C) as shown by the difference in concentrations of CO_2 and N_2O in the absence and presence of soot. The CO_2 trace in the presence of soot is significantly lower in

concentration compared to the other catalysts studied. Furthermore, the NO concentration does not decrease with rise in temperature in fact the concentration rises after 300°C. In both the presence and absence of soot NO_2 is observed this is due to the oxidation of NH_3 and NO being the dominant reactions at temperatures > 400°C.

Despite the ability of the catalyst prepared *via* IW to utilise *in situ* generated N_2O to oxidise soot at low temperatures it is not a suitable preparation method for a catalyst for the simultaneous removal of NOx and soot due to its poor SCR and soot oxidation activity.

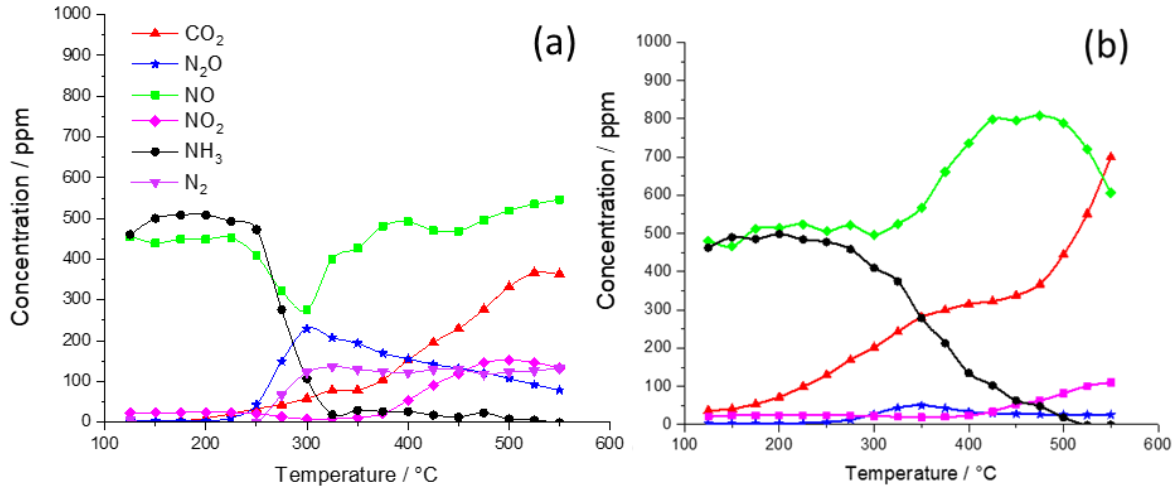

Figure 3.11: Reaction data for incipient wetness prepared catalyst where (a) SCR reaction data and (b) SCR + CB reaction data. The simulated exhaust gas consisted of 500 ppm NO, 500 ppm NH_3, 8% O_2, with a balance of N_2. The total flow rate was 200 mlmin^{-1}. The temperature was increased in 25°C intervals from 125 to 550°C, the gas concentrations were allowed to stabilise before readings were taken at each temperature. For (a) 0.25 g of catalyst was used and (b) 0.25 g catalyst was mixed in a 10:1 ratio by mass with soot.

3.4.2 Wet Impregnation

The catalyst prepared *via* wet impregnation in the absence of soot Figure 3.12a, like the previous catalysts discussed, has a CO_2 trace due to the desorption of hydrogencarbonate and carbonate species, however, for IMP there is a significant peak in the CO_2 concentration at 300°C. Consequently, this results in the dilution of NO, NH_3 and N_2O and hence around 300°C these gases' concentrations fluctuate slightly. The catalyst displays good SCR reactivity with the NH_3 concentration reaching 0 ppm by 400°C and NO reaching 0 ppm by 450°C. The non-selective SCR reaction also takes place over the catalyst at temperatures above 175°C with the peak N_2O concentration at 250°C.

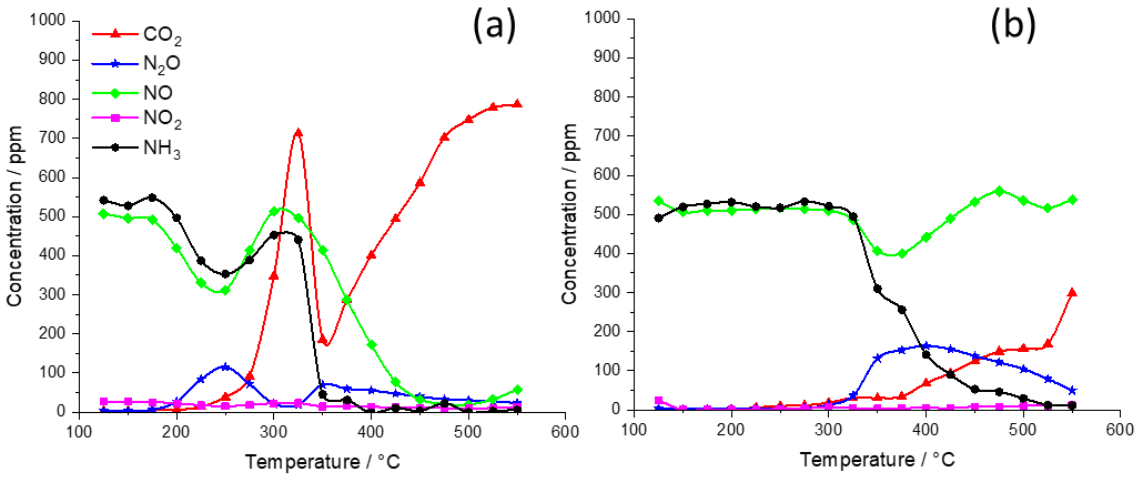

Figure 3.12: Reaction data for the catalyst prepared *via* wet impregnation prepared catalyst where (a) SCR reaction data and (b) SCR + CB reaction data. The simulated exhaust gas consisted of 500 ppm NO, 500 ppm NH_3, 8% O_2, with a balance of N_2. The total flow rate was 200 $mlmin^{-1}$. The temperature was increased in 25°C intervals from 125 to 550°C, the gas concentrations were allowed to stabilise before readings were taken at each temperature. For (a) 0.25 g of catalyst was used and (b) 0.25 g catalyst was mixed in a 10:1 ratio by mass with soot.

Figure 3.12b shows that in the presence of soot IMP has the ability to utilise *in situ* generated N_2O to oxidise soot at low temperatures (175 – 300°C). This is apparent due to the respective decrease and increase in concentration of N_2O and CO_2 compared to that in the absence of soot. However, at temperatures > 300°C N_2O is observed peaking at 400°C. The initial increase in N_2O concentration corresponds to the inverted peak of NO which hence shows that the non-selective SCR reaction is taking place at these temperatures. In the presence of soot, NO no longer undergoes the selective SCR reaction. The C is oxidised to CO_2 in a 'stepwise fashion' (Figure 3.12b) with each step due to oxidation by a different oxidant:

- catalytic oxidation by N_2O
- non-catalytic oxidation by NO
- catalytic oxidation by O_2
- non-catalytic oxidation by O_2

The reaction can be compared to previous work by Davies *et al.*[1] (Figure 3.13) who initially found that Ag/CZA was a potential catalyst for the simultaneous removal of NOx and soot from a diesel exhaust.

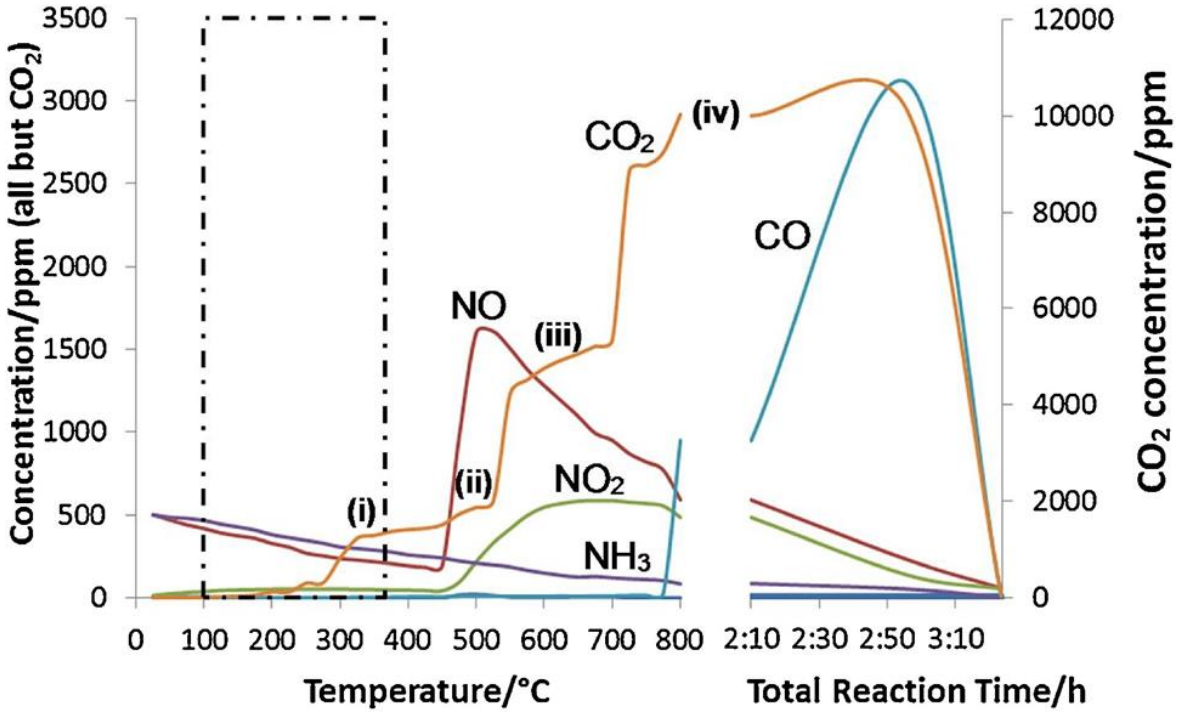

Figure 3.13: SCR + CB reaction data for Ag/CZA from 'Simultaneous removal of NOx and soot particulate from diesel exhaust by *in situ* catalytic generation and utilisation of N_2O'. The simulated exhaust gas consisted of 500 ppm NO, 500 ppm NH_3, 8% O_2, with a balance of N_2. The total flow rate was 200 $mlmin^{-1}$. The temperature was increased in 25°C intervals from 125 to 800°C, the gas concentrations were allowed to stabilise before readings were taken at each temperature. 0.25g of catalyst was used. [1]

Firstly, both catalysts show a stepwise oxidation of PM into CO_2 which is explained by different oxidants being dominate at different temperatures. However, a key difference between the two CO_2 traces is that for Ag-K/CZA a significantly greater quantity of CO_2 is produced at lower temperatures compared to Ag/CZA hence showing the soot oxidation enhancement ability of K. Both catalysts have the ability to utilise *in situ* generated N_2O (formed *via* the non-selective SCR reaction) to oxidise soot at low temperatures. A second crucial difference between the catalysts is that Ag/CZA undergoes the selective SCR reaction between 100 – 400°C (*i.e.* selectively catalytically reduces NO using NH_3) in the presence of soot whilst Ag-K/CZA does not have the ability to reduce NO in the presence of soot. This strongly suggests that the K_2CO_3 is preventing the SCR reaction from taking place. In the absence of soot Ag-K/CZA is a good SCR catalyst however in the presence of soot is a poor SCR catalyst.

3.4.3 Characterisation Data

Characterisation was carried out on each catalyst to determine surface area and surface and bulk properties. Raman Spectroscopy, XRD, BET surface area, XPS and SEM-EDX were carried out on the samples.

Figure 3.14 shows the XRD data for the CZA support and for the catalysts prepared *via* wet impregnation and incipient wetness and Table 3.4 shows data obtained from XRD, Raman and BET for the two catalysts.

Table 3.4: Crystallite size calculated from XRD data, CeO_2 defect ratio calculated from Raman data and surface area from BET analysis for the catalysts prepared *via* incipient wetness and wet impregnation

Sample	Ag Crystallite Size [Å]	CeO_2 Crystallite Size [Å]	CeO_2 Defect Ratio	Catalyst Surface Area [$m^2 g^{-1}$]
IW	>1000	182	0.0037	12.5
IMP	322	202	-	26.4

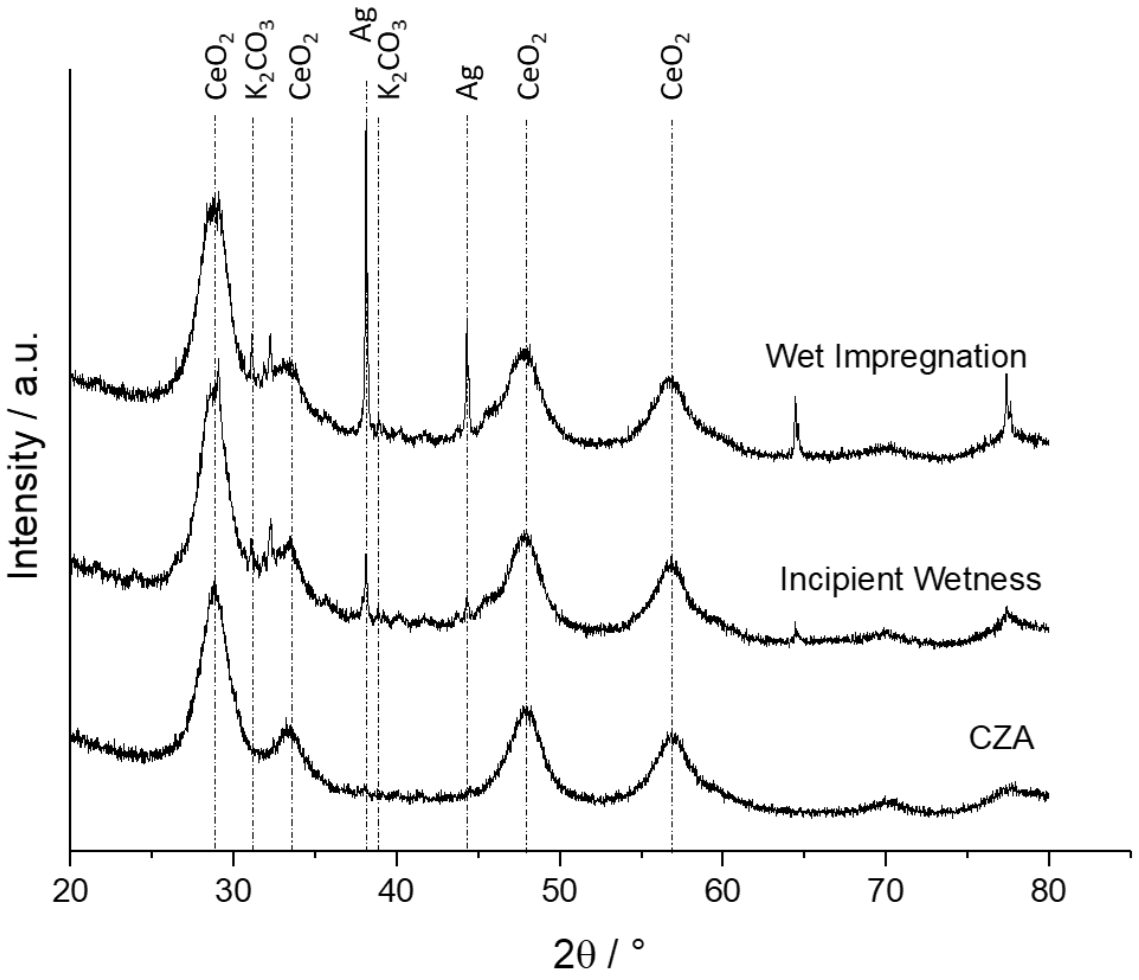

Figure 3.14: XRD patterns for the CZA support and for the catalysts prepared *via* wet impregnation and incipient wetness.

Figure 3.14 shows the XRD data for the CZA support and for the catalysts prepared via wet impregnation and incipient wetness. Like in section 3.3.2, there is a shift in the ceria peaks due to

incorporation of Al_2O_3 and ZrO_2 into the ceria lattice. Similarly, the same bands are present indicating the presence of K_2CO_3, CeO_2 and Ag. Using the Scherrer equation, it was calculated that IW and IMP had Ag crystallite sizes of > 1000 Å and 322 Å respectively (Table 3.4).

The Raman analysis (Figure 3.15) showed that the IW and IMP catalysts had a peak between 141 – 158 cm^{-1}, which is due to silver lattice vibrational modes (*i.e.* phonons) [17,18]. CZA showed bands due to ceria with the peak between 451 – 469 cm^{-1} being due to ceria's F_{2g} Raman mode and peaks between 500 – 600 cm^{-1} are defect-induced modes of the fluorite phase[16].The F_{2g} peak distortion ratio was calculated for IW however it was not possible to calculate the ratio for IMP as it did not have a ceria distortion peak. A band was observed for both catalysts between 1052 – 1064 cm^{-1} which is indicative of carbonate which is from the Na_2CO_3 used as a precipitate in the preparation of the support.

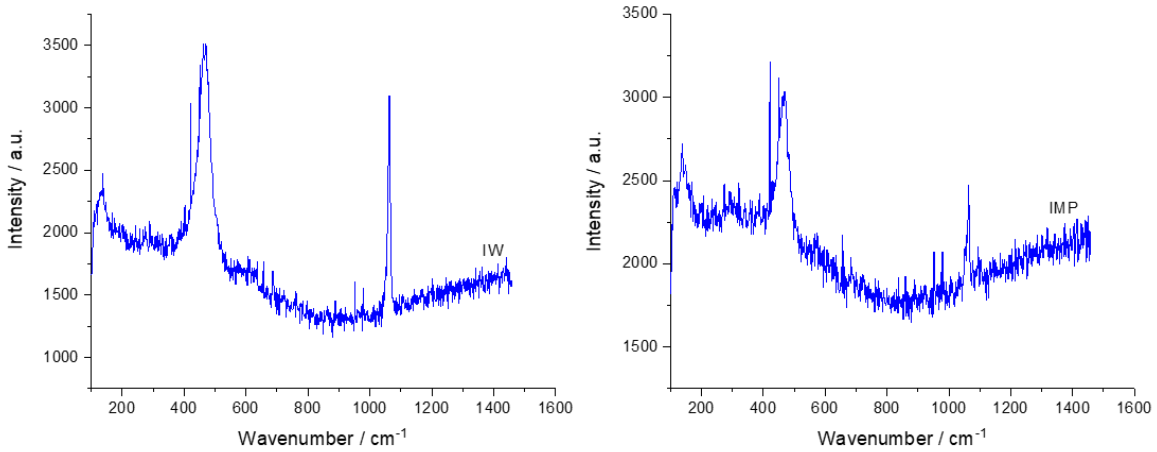

Figure 3.15: Raman spectra for the catalysts prepared *via* incipient wetness (left) and wet impregnation (right).

The XPS analysis also shows that Na is present in the catalysts (Table 3.5). The XPS data also confirmed the presence of high amounts of carbonate in the catalysts, as shown by a C(1s) peak at *ca.* 289.5 eV in the spectra. The catalysts show a low Ag concentration and extremely weak Auger, hence indicating that the Ag is present in large particles. The XRD analysis for the IW catalyst also shows that the Ag is present as large crystallites.

Table 3.5: The elemental ratio of the catalysts prepared via wet impregnation and incipient wetness from XPS analysis

Catalyst	Na	Ce	O	Ag	K	C	Zr	Al
Incipient Wetness	1.3	2.3	53.6	0.1	11.6	21.7	0.6	8.9
Wet Impregnation	0.9	1.7	45.9	0.1	10.5	33.1	0.4	7.6

3.4.4 Conclusions

Both IW and IMP had the ability to utilise in situ generated N_2O to oxidise soot at low temperatures however IMP was shown to be a far superior catalyst. In the presence of soot, IW demonstrated no ability to reduce NOx and was shown to be a poor soot oxidation catalyst. Whilst IMP showed potential as a catalyst for the simultaneous removal of Nox and soot. In the presence of soot, IMP showed exceptional soot oxidation over a wide range of temperatures. The soot was oxidised in four clear steps (catalytic oxidation by N_2O, non-catalytic oxidation by NO_2, catalytic oxidation by O_2 and non-catalytic oxidation by O_2). However, its ability to reduce Nox was significantly reduced in the presence of soot. When the catalyst was compared to a Ag/CZA catalyst from literature[1] it was shown that the presence of K heightens soot oxidation but appears to hinder the reduction of Nox.

From characterisation it was shown that Na was present in both catalysts, the Na was supposed to be removed *via* washing with 2 L hot de-ionised water as a part of the preparation of the CZA support. From XRD data the Ag crystallite size was calculated for each catalyst. For IW the Ag crystallite size was greater than 1000 Å whilst for IMP the crystallite size was 322 Å. This suggests that the smaller the Ag crystallite size the better for the desired reaction.

3.5 Discussion

All six catalysts were prepared to be the same weight loading (2 wt.% Ag-20 wt.% K/CZA) *via* different preparation techniques. Firstly, of the four CVI catalysts prepared only CVI80 showed real potential for use as a catalyst for the simultaneous removal of NOx and soot. It had the ability to utilise *in situ* generated N_2O to oxidise soot at low temperatures as well as being an active combustion catalyst and some NOx reduction took place in the presence of soot. The three other CVI catalysts being unsuited for this reaction. IW despite being able to utilise *in situ* generated

N_2O to oxidise soot was a poor overall soot oxidation catalyst and an extremely poor NOx reduction catalyst. However, IMP showed good soot oxidation over a wide range of temperatures but poor NOx reduction. When IMP was compared to Ag/CZA it was found that the presence of K greatly enhanced soot oxidation but it appears to hinder NOx reduction. This can be extrapolated to explain CVI80's poor NOx reduction in the presence of soot.

The BET analysis carried out on each catalyst showed that IMP had the largest surface area (26.4 $m^2 g^{-1}$) and calculations from the XRD data showed that IMP had the smallest Ag crystallite size, 322 Å. Both of these features may be key in IMP's success as a simultaneous catalyst.

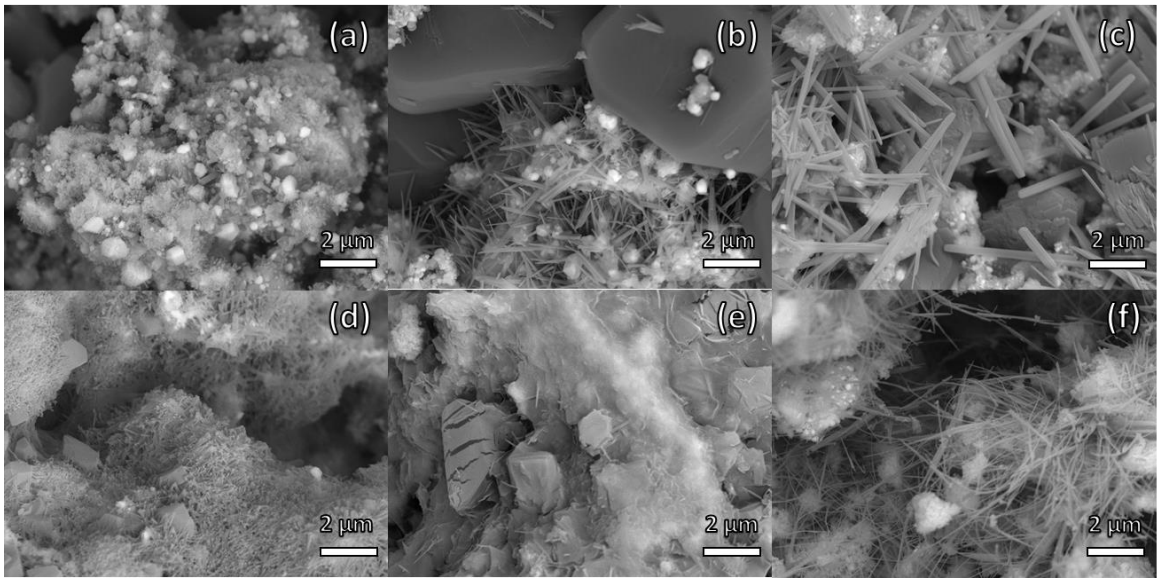

Figure 3.17: SEM Image of (a) CZA and (b) K/CZA at 20 Kx magnification SEM images at 5 Kx magnification where (a) CVI60, (b) CVI70, (c) CVI80, (d) CVI90, (e) incipient wetness and (f) wet impregnation.

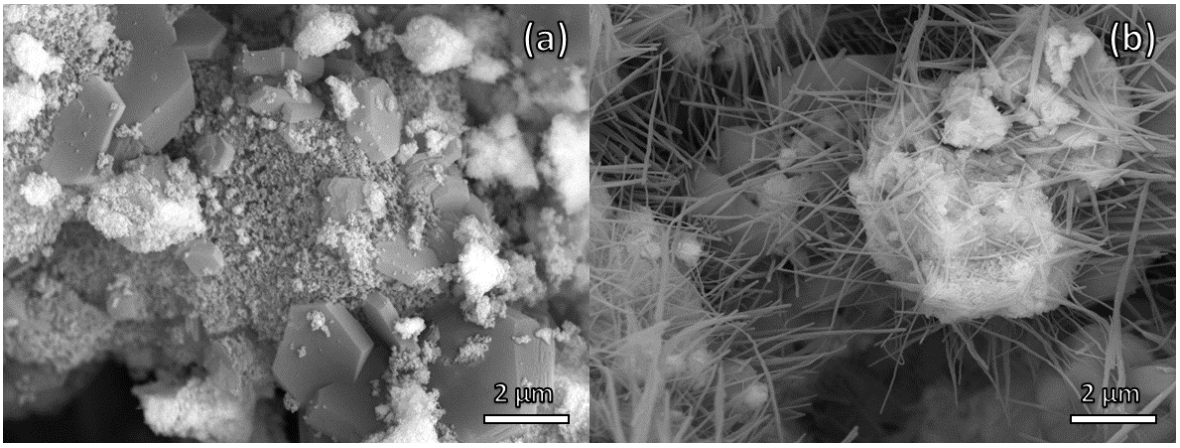

Figure 3.16: SEM Image of (a) CZA and (b) K/CZA at 20 Kx magnification.

Figure 3.16 shows SEM images of all six catalysts, it is clear that the catalysts have different morphologies as a result of the preparation method used. The figure shows that each catalyst, to varying degrees, have 'needle-like' structures on the surface of the catalyst. To help determine

what the needles were comprised of images of CZA and K/CZA were studied (Figure 3.17). Figure 3.17a shows CZA and there are no needles whilst Figure 3.17b shows K/CZA and there are obvious 'needle-like' structures present. Analysis from SEM-EDX (Figure 3.18 and Figure 3.19) shows that the key elemental difference between the two samples is that there is no K present on CZA but there is on K/CZA, from this is can be extrapolated that the 'needles' contain high concentrations of K. The preparation method and temperature used during catalyst preparation has an impact on the morphology of the K needles.

From the images it can be observe that there is phase separation of the CZA (Figure 3.17 and Figure 3.16). As this separation is observed on the pure support as well as for the catalysts it can be determined that the preparation method does not cause the phase separation of the support. From SEM-EDX it was found that Na was present on all of the catalysts, this was confirmed by XPS analysis.

The presence of Na and K carbonates on the surface of the catalysts may impact the visibility of components that form the support such as CeO_2. From XPS and EDX analysis significantly less CeO_2 is observed that what was expected. The presence of Na_2CO_3 is also supported by the Raman data.

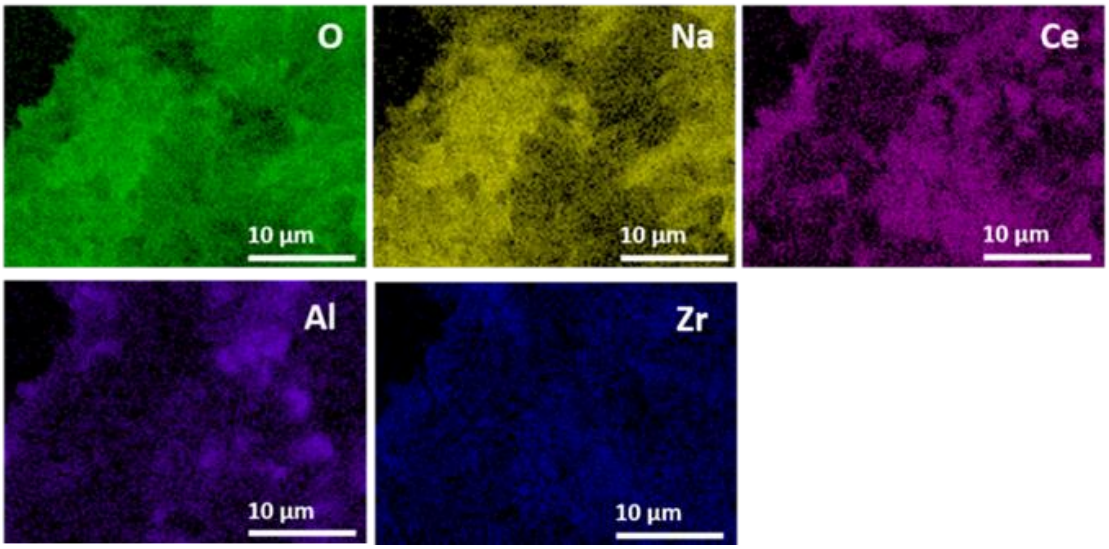

Figure 3.18: SEM-EDX map of elements present in K/CZA SEM-EDX map of elements present in CZA

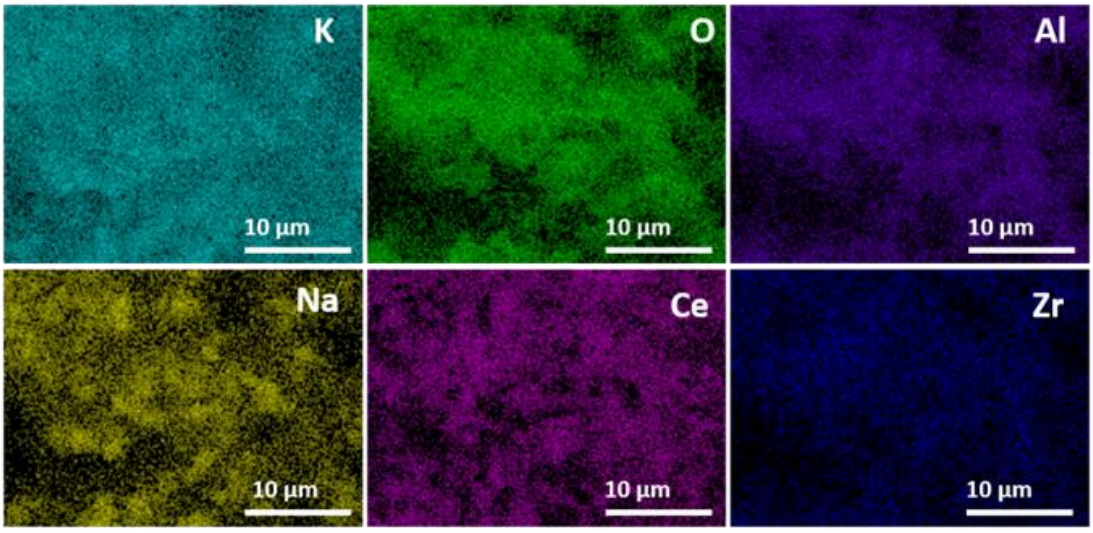

Figure 3.19: SEM-EDX map of elements present in K/CZA

3.6 Conclusions and Future Work

It is clear that CVI is a preparation method which could have potential in the automotive industry however further research is needed. The reason for the effect of preparation temperature on the catalysts is still not clear. The presence of F could hinder the reaction from taking place hence a system to remove the F from the sample should be investigated. Further characterisation including *in situ* techniques should be carried out to help determine the reason why the preparation temperature has such a large effect on the catalyst.

Both the CVI80 and wet impregnation catalyst showed potential for the simultaneous removal of NOx and soot. However, the reactions took place in different temperature windows. This is not ideal, for a simultaneous catalyst to be used in *real-life* the reactions need to take place within the same low temperature window.

The mechanism in which K aids soot oxidation but appears to hinder NOx reduction is unknown. The ability to simultaneously catalyse both reactions (soot oxidation and NOx reduction) is believed to be due to the size and dispersion of the Ag as well as the mobility and dispersion of the K. Consequently, dispersion experiments should be carried out as well as *in situ* studies (such as TEM, XRD, Raman, etc.) to help ascertain the components of the catalyst which enable the reaction to take place. Further weight loadings of K on 2 wt.% Ag/CZA should be studied in order to determine whether there is an ideal weight loading of K which would allow simultaneous removal of NOx and soot to take place over the catalyst.

The presence of CO_2 in the systems in which soot was absenct also requires more explanation. The CO_2 could be due to adsorbed hydrogencarbonate/carbonate species desorbing from the catalyst as it is heated or it may due to incomplete decomposition of cerium carbonate

from preparation of the CZA support. Hence, TGA-MS could be carried out on the catalysts to see the species (if any) that evolve when the catalyst is heated. A pre-treatment, in which the catalyst will be heated in the furnace with flowing air to demine whether after a period of time the CO_2 will no longer be observed. If this is the case, it would suggest that the CO_2 observed is due to carbonate species adsorbing on to the catalyst's surface after calcination. Also, a calcination study will be carried out to determine ideal conditions for ensuring full decomposition of carbonate precursors. As the catalysts were calcined under conditions widely used for preparation of CZA supported metal nanoparticles (5 h, flowing air, 500°C), these conditions may not have been efficient at completely decomposing the CZA-carbonate species.

Na was found to be present in all of the catalysts as a consequence of Na_2CO_3 being used in the co-precipitation method to produce CZA. The presence of Na does not seem to effect the catalysts' reactivity however; its presence is not required. Hence, new washing methods should be researched into and/or a different precipitant could be used during the support preparation.

3.7 References

1 C. Davies, K. Thompson, A. Cooper, S. Golunski, S. H. Taylor, M. Bogarra Macias, O. Doustdar and A. Tsolakis, *Appl. Catal. B Environ.*, 2018, **239**, 10–15.

2 R. Ramdas, E. Nowicka, R. Jenkins, D. Sellick, C. Davies and S. Golunski, *Appl. Catal. B Environ.*, 2015, **176**–**177**, 436–443.

3 A. Rinkenburger, T. Toriyama, K. Yasuda and R. Niessner, *ChemCatChem*, 2017, **9**, 3513–3525.

4 M. M. Forde, L. Kesavan, M. I. Bin Saiman, Q. He, N. Dimitratos, J. A. Lopez-Sanchez, R. L. Jenkins, S. H. Taylor, C. J. Kiely and G. J. Hutchings, *ACS Nano*, 2014, **8**, 957–969.

5 J. Xu, R. D. Armstrong, G. Shaw, N. F. Dummer, S. J. Freakley, S. H. Taylor and G. J. Hutchings, *Catal. Today*, 2016, **270**, 93–100.

6 R. Su, M. M. Forde, Q. He, Y. Shen, X. Wang, N. Dimitratos, S. Wendt, Y. Huang, B. B. Iversen, C. J. Kiely, F. Besenbacher and G. J. Hutchings, *J. Chem. Soc. Dalt. Trans.*, 2014, **43**, 14976–14982.

7 H. Bahruji, M. Bowker, W. Jones, J. Hayward, J. Ruiz Esquius, D. J. Morgan and G. J. Hutchings, *Faraday Discuss.*, 2017, **197**, 309–324.

8 M. S. Rill, C. Plet, M. Thiel, I. Staude, G. von Freymann, S. Linden and M. Wegener, *Nat. Mater. 2008 77*, 2008, **7**, 543–546.

9 F. Q. and S. Y. S. Xiong, Y. Liao, H. Dang, *RSC Adv.*, 2015, **5**, 27785–27793.

10 G. Chandra Dhal, S. Dey, D. Mohan and R. Prasad, , DOI:10.1080/01614940.2018.1457831.

11 E. Aneggi, J. Llorca, C. de Leitenburg, G. Dolcetti and A. Trovarelli, *Appl. Catal. B Environ.*, 2009, **91**, 489–498.

12 Y. Gao, A. Duan, S. Liu, X. Wu, W. Liu, M. Li, S. Chen, X. Wang and D. Weng, *Appl. Catal. B Environ.*, 2017, **203**, 116–126.

13 S. Liu, X. Wu, W. Liu, W. Chen, R. Ran, M. Li and D. Weng, *J. Catal.*, 2016, **337**, 188–198.

14 M. V. Grabchenko, G. V. Mamontov, V. I. Zaikovskii, V. La Parola, L. F. Liotta and O. V. Vodyankina, *Catal. Today*, 2019, **333**, 2–9.

15 A. B.-L. C. Bueno-Ferrer, S. Parres-Esclapez, D. Lozano-Castelló, *J. Rare Earths*, 2010, **28**, 647–653.

16 S. Chang, M. Li, Q. Hua, L. Zhang, Y. Ma, B. Ye and W. Huang, *J. Catal.*, 2012, **293**, 195–204.

17 I. Martina, R. Wiesinger, D. Jembrih-Simbürger and M. Schreiner, *e-PRESERVATIONScience MICRO-RAMAN CHARACTERISATION OF SILVER CORROSION PRODUCTS: INSTRUMENTAL SET UP AND REFERENCE DATABASE 1*, .

18 K. A. Bosnick, *RAMAN STUDIES OF MASS-SELECTED METAL CLUSTERS*, 2000.

19 P. Shah, Cardiff University, 2019.

4 Investigation into the Ideal Weight Loading of Potassium in Ag-K/CeO_2-ZrO_2-Al_2O_3 Catalysts for the Simultaneous Removal of NOx and Soot from Diesel Exhausts

4.1 Introduction

Chapter 3 discussed the potential of 2%Ag-20%K/CZA for catalysing the simultaneous removal of NOx and soot from a simulated diesel exhaust. Several preparation methods were investigated, with wet impregnation and chemical vapour impregnation at 80 °C proving to be most effective techniques. In light of this, this chapter focusses on preparing catalysts *via* wet impregnation as described in Section 2.3.2. Despite, 2%Ag-20%K/CZA showing potential for the simultaneous reaction, the presence of potassium was shown to greatly enhance soot oxidation[1] but hinder the reduction of NOx. The high weight loading of potassium is thought to block NOx reduction active sites, hence a weight loading investigation was carried out to determine whether there is an ideal weight loading of potassium which permits the enhancement of soot oxidation but does not hinder NOx reduction.

Five catalysts were studied in this chapter: 2%Ag-2%K/CZA, 2%Ag-5%K/CZA, 2%Ag-10%K/CZA, 2%Ag-15%K/CZA and 2Ag%-20%K/CZA. For this set of catalysts, a single batch of CZA was prepared by making the support *via* co-precipitation as discussed in Section 2.3.1., as this method only produces 3 g of support at a time, many batches were made and then ground together to form one large batch. This was done to prevent any variability that could arise from making catalysts from separate batches of support.

As in the previous chapter, the catalysts were tested for both their ability to selectively catalytically reduce NOx and their ability to simultaneously remove NOx and soot from a simulated diesel exhaust. The same reactor was used, utilising the same reaction conditions.

4.2 Results

4.2.1 Catalyst Performance Data

The catalyst performance data for each catalyst is reviewed in the following section. Each catalyst was tested for its ability to selectively catalytically reduce NO using NH_3 and its ability to simultaneously reduce NOx and oxidise soot. Every catalyst when tested in the absence of soot showed a trace of CO_2. CO_2 was present in these reactions for two reasons: decomposition of residual $Ce(CO_3)_2$ as a result of calcination not fully converting the CZA-carbonate to CZA-oxide[2], and, as a consequence of carbonate and hydrogencarbonate species adsorbing onto the surface of the catalyst. This explanation is further discussed in section 4.2.2.1.

4.2.1.1 2%Ag-20%K/CZA

When 2%Ag-20%K/CZA was tested for the reduction of NO by NH_3 in the absence of soot, the NO concentration showed a decrease between 175 and 250°C, before increasing in concentration until 300 °C (Figure 4.1a). The inverse peak of NO was mirrored by a peak in N_2O. N_2O was observed in small quantities between 325 and 550°C. The formation of N_2O was due to the non-selective SCR reaction (Equation 4.1). The NH_3 concentration reached 0 ppm by 400 °C and NO reached 0 ppm at 500 °C.

$$\boldsymbol{2NH_3 + 2NO + 1\,{}^{1}\!/_{2}\,O_2 \rightarrow 2N_2O + 3H_2O}$$

Equation 4.1: The Non-Selective SCR Reaction Equation

These results show that 2%Ag-20%K/CZA is active for NOx reduction between 325 and 500°C. This is an improvement on the Ag/CZA catalyst which was not suitable for the reduction of NOx in the absence of soot.[3] In *real life* conditions, the temperature range of the exhaust gas in diesel passenger cars is typically 100–360 °C. Therefore, for this to be a potential SCR catalyst the reduction of NO needs to take place within this temperature range. Furthermore, for the catalyst to be suitable for the simultaneous removal of NO and soot without the need of a fuel injection at high temperatures, soot oxidation also needs to occur within this temperature range.

In the presence of carbon black (Figure 4.1b), N_2O was observed in low quantities (< 35 ppm) at temperatures < 300°C, and a peak between 325 °C and 550 °C was observed. In the presence of soot very little NO reduction takes place, with a small inverted peak at 350 °C, which coincided with the peak of N_2O. As discussed in Chapter 3, a small amount of low temperature oxidation of soot by N_2O may occur over this catalyst. With the levels of N_2O observed in the presence of soot being less than that in the absence of soot. Furthermore, approximately 100 ppm more of CO_2 was observed at low temperatures in the presence of soot, suggesting that the *in situ* formed N_2O is oxidising soot at low temperatures. However, over the Ag/CZA no N_2O is observed at low temperatures and a greater amount of CO_2 is observed, 1290 ppm at 350°C compared to 2%Ag-20%K/CZA's 237 ppm at 350°C. At higher temperatures, N_2O is observed over the 2%Ag-20%K/CZA catalyst whilst over Ag/CZA the concentration of N_2O remains at 0 ppm throughout the reaction.[3] Therefore, Ag/CZA is by far the superior catalyst for low temperature soot oxidation.

However, high levels of CO_2 were observed at temperatures > 300 °C. The presence of K in the catalyst greatly enhanced the soot oxidation ability of the catalyst. The amount of CO_2 formed over 2%Ag-20%K/CZA (29828 ppm) is over 7 times greater than that observed over Ag/CZA (4227 ppm).[3]

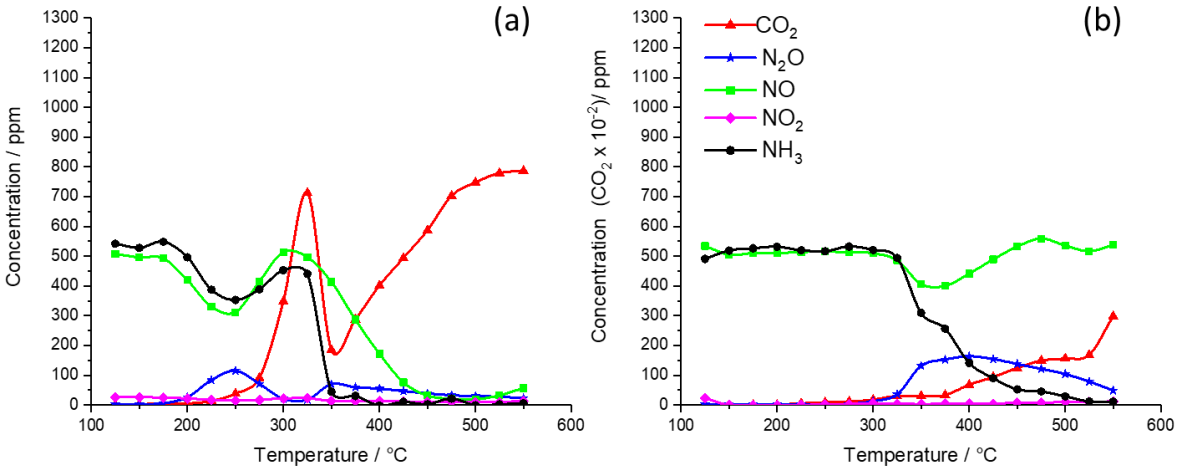

Figure 4.1: Reaction data for 2%Ag-20%K/CZA where (a) is the absence of soot and (b) is in the presence of soot. The simulated exhaust gas consisted of 500 ppm NO, 500 ppm NH_3, 8% O_2, with a balance of N_2. The total flow rate was 200 mlmin^{-1}. The temperature was increased in 25 °C intervals from 125 to 550 °C, the gas concentrations were allowed to stabilise before readings were taken at each temperature. For (a) 0.25 g of catalyst was used and (b) 0.25 g catalyst was mixed in a 10:1 ratio by mass with soot.

4.2.1.2 2%Ag-15%K/CZA

2%Ag-15%K/CZA in the absence of soot (Figure 4.2a) was a poor SCR catalyst, with no NOx reduction to N_2 being observed throughout the reaction. Low levels of NO_2 were observed over the entire temperature range, which is a result of oxidation of NO by O_2, this reaction dominates over the formation of N_2O. The NH_3 concentration remained between 450 – 600 ppm until 350 °C where it decreased in concentration, reaching 0 ppm by 550 °C.

In the presence of soot (Figure 4.2b) there was no reduction of NO to N_2 and there was a constant presence of NO_2 in low concentrations. At 375 °C CO_2 was observed as a result of oxidation of the soot by O_2. Less CO_2 is observed compared to the 2%Ag-20%K/CZA catalyst, but still significantly more is formed compared to the Ag/CZA catalyst, showing that the presence of potassium enhances soot oxidation at high temperatures.

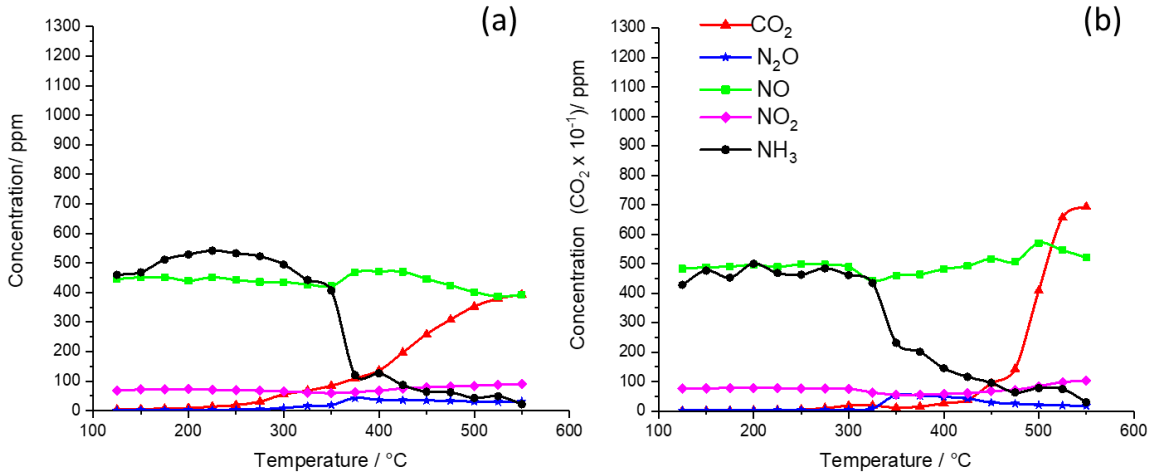

Figure 4.2: Reaction data for 2%Ag-15%K/CZA where (a) is the absence of soot and (b) is in the presence of soot. The simulated exhaust gas consisted of 500 ppm NO, 500 ppm NH_3, 8% O_2, with a balance of N_2. The total flow rate was 200 mlmin^{-1}. The temperature was increased in 25 °C intervals from 125 to 550 °C, the gas concentrations were allowed to stabilise before readings were taken at each temperature. For (a) 0.25 g of catalyst was used and (b) 0.25 g catalyst was mixed in a 10:1 ratio by mass with soot.

4.2.1.3 2%Ag-10%K/CZA

2%Ag-10%K/CZA, also shows poor selectivity towards catalytic reduction (Figure 4.3a), with the NO concentration decreasing slightly at 300 °C until it began to increase again at 475 °C. At 475 °C the rise in NO coincided with a rise in NO_2, which is due to the oxidation of NH_3 and NO by O_2. Low levels of NO_2 were observed for the duration of the experiment.

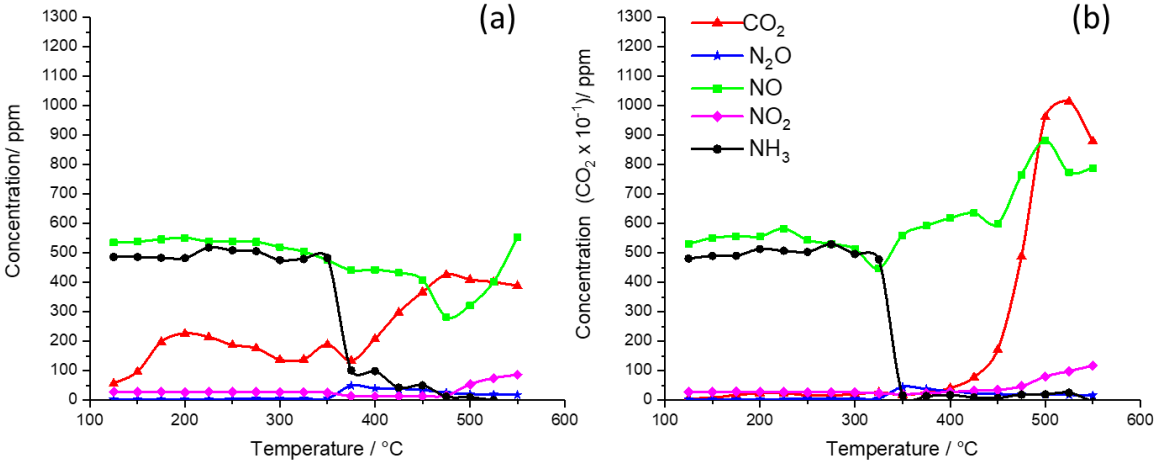

Figure 4.3: Reaction data for 2%Ag-10%K/CZA where (a) is the absence of soot and (b) is in the presence of soot. The simulated exhaust gas consisted of 500 ppm NO, 500 ppm NH_3, 8% O_2, with a balance of N_2. The total flow rate was 200 mlmin^{-1}. The temperature was increased in 25 °C intervals from 125 to 550 °C, the gas concentrations were allowed to stabilise before readings were taken at each temperature. For (a) 0.25 g of catalyst was used and (b) 0.25 g catalyst was mixed in a 10:1 ratio by mass with soot.

In the presence of soot (Figure 4.3b), a small inverted peak in NO is mirrored by a peak of N_2O between 325 °C and 375 °C. At temperatures above 350 °C the NO concentration increased and the NH_3 concentration was 0 ppm. In the presence of soot, high temperature concentrations of NO_2 and NO are higher than when soot is absent from the reaction. At temperatures above 375 °C CO_2 was observed due to oxidation of soot. Unexpectedly, a greater concentration of CO_2 is observed over 2%Ag-10%K/CZA than over 2%Ag-15%K/CZA. One explanation for this, is that there was better potassium-soot contact between 2%Ag-10%K/CZA and the soot than over the 2%Ag-15%K/CZA catalyst.

4.2.1.4 2%Ag-5%K/CZA

As with the previous catalysts, 2%Ag-5%K/CZA was a poor catalyst for selective reduction of NO. The catalyst showed a small decrease in NO until 350 °C, after which it increased in concentration (Figure 4.4a). 350 °C was also when NO_2 was first observed. The increase in concentration of NO and NO_2 at high temperatures is due to oxidation of NO and NH_3 by O_2. N_2O was observed from 250 °C to 500 °C with the maximum at 300 °C.

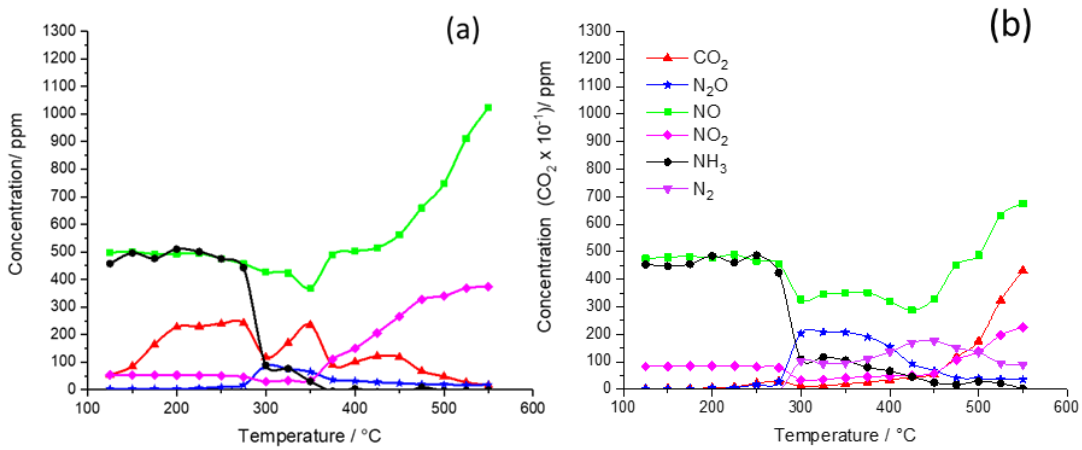

Figure 4.4: Reaction data for 2%Ag-5%K/CZA where (a) is the absence of soot and (b) is in the presence of soot. The simulated exhaust gas consisted of 500 ppm NO, 500 ppm NH_3, 8% O_2, with a balance of N_2. The total flow rate was 200 mlmin^{-1}. The temperature was increased in 25 °C intervals from 125 to 550 °C, the gas concentrations were allowed to stabilise before readings were taken at each temperature. For (a) 0.25 g of catalyst was used and (b) 0.25 g catalyst was mixed in a 10:1 ratio by mass with soot.

In the presence of soot (Figure 4.4b), 2%Ag-5%K/CZA remained poor at reducing NO to N_2. A large peak of N_2O was observed between 275 °C and 500 °C, the peak is mirrored by an inverted peak of NO. Figure 4.4b includes a calculated N_2 balance which took into account all nitrogen containing species. It was calculated that there was sufficient decrease in NO and NH_3 concentrations to confirm that the non-selective reaction was taking place. However, there was a greater than expected reduction in NH_3 which correlates to the formation of N_2. Therefore, the oxidation of NH_3 to N_2 is also taking place at the same time as the non-selective reaction. The

concentration of NO started to increase at 425 °C and NO_2 was observed in higher concentrations at this temperature. Oxidation of soot began at 350 °C and over this catalyst a similar quantity of CO_2 was formed at 550 °C as over Ag/CZA.

4.2.1.5 2%Ag-2%K/CZA

The lowest weight loading investigated in this study was 2%Ag-2%K/CZA, reaction data may be observed in Figure 4.5. In the absence of soot, 2%Ag-2%K/CZA was a poor SCR catalyst (Figure 4.5a). The NO concentration decreased over the range 150 – 300 °C before beginning to increase. At 550 °C the NO concentration reached 1250 ppm as a consequence of high temperature oxidation by O_2. The inverted peak of NO was mirrored by a peak of N_2O ranging from 200 °C – 400 °C. NO_2 begins to form at 325 °C due to oxidation of NH_3 by O_2. At low temperatures (< 300 °C) the formation of N_2O was dominant, but at higher temperatures the oxidation of NO and NH_3 by O_2 dominated. The NH_3 concentration reached 0 ppm by 300 °C, which is the lowest temperature observed for any catalyst in this chapter.

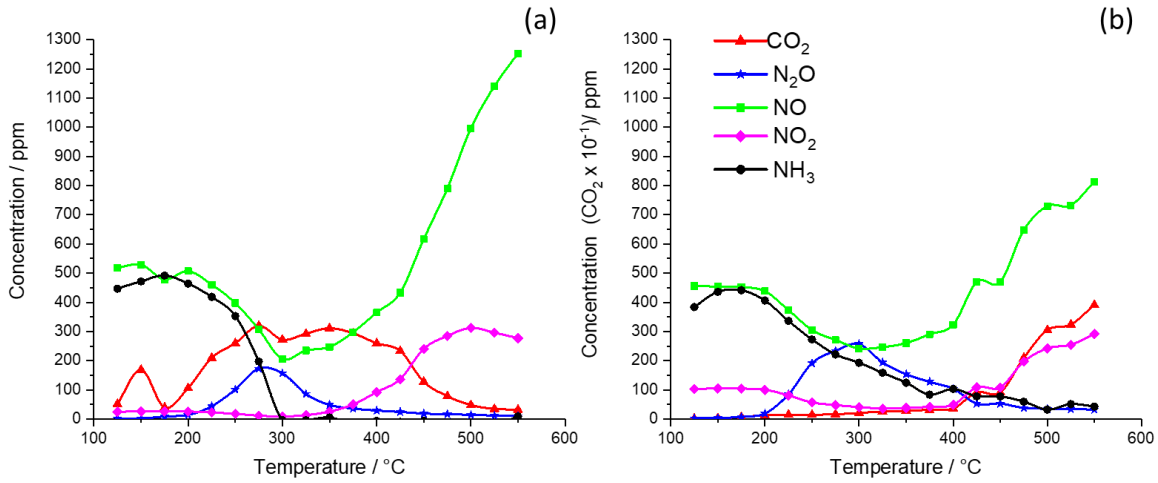

Figure 4.5: Reaction data for 2%Ag-2%K/CZA where (a) is the absence of soot and (b) is in the presence of soot. The simulated exhaust gas consisted of 500 ppm NO, 500 ppm NH_3, 8% O_2, with a balance of N_2. The total flow rate was 200 mlmin^{-1}. The temperature was increased in 25 °C intervals from 125 to 550 °C, the gas concentrations were allowed to stabilise before readings were taken at each temperature. For (a) 0.25 g of catalyst was used and (b) 0.25 g catalyst was mixed in a 10:1 ratio by mass with soot.

In the presence of soot, the catalyst remained a poor SCR catalyst (Figure 4.5b). NO concentration decreased over the temperature range of 200 °C to 300 °C, which, as in the absence of soot, is mirrored by a peak of N_2O. The peak of N_2O ranged from 200 °C to 550 °C, with a maximum at 300 °C. A greater quantity of N_2O was observed in the presence of soot compared to the absence of soot over this catalyst. The N_2O peak remained in the same temperature range as

in the absence of soot. At temperatures above 300 °C the NO concentration increased and NO_2 was observed as a result of the oxidation of NO and NH_3 by O_2 becoming the dominant reaction.

Above 400 °C CO_2 was produced due to oxidation of the soot by O_2 and NO_2. It is of note that the amount of CO_2 formed was significantly less than that compared to the 2%Ag-20%K/CA catalyst. This is due to the K content, as it is known to increase the rate of soot oxidation.

4.2.1.6 Discussion

By preparing different potassium weight loadings on the standard 2%Ag/CZA catalyst the effect of potassium weight loading has been studied. From Chapter 3, it was known that the addition of a 20 w.t.% K to Ag/CZA resulted in enhanced high temperature soot oxidation but hindered the catalyst's ability to reduce NOx. Hence, lower potassium weight loadings were investigated to determine the ideal weight loading which would allow enhancement of both reactions.

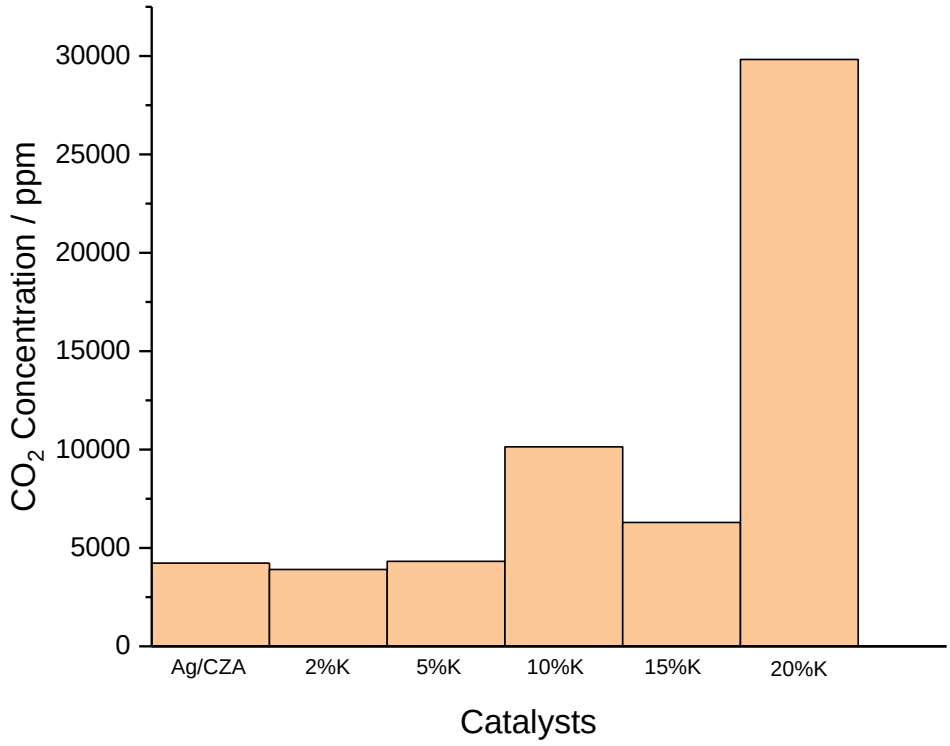

Figure 4.6: Maximum formation of CO_2 over the potassium catalysts and Ag/CZA

From the catalytic performance data it is clear that a higher weight loading of potassium results in higher levels of soot oxidation, however, a low weight loading does not show enhancement when compared to Ag/CZA. This is clearly shown in Figure 4.6, where the maximum concentration of CO_2 formed over each catalyst and Ag/CZA is shown. From the figure, 2%Ag-

2%K/CZA and 2%Ag-5%K/CZA are shown to form similar quantities of CO_2 (3905 and 4320 ppm respectively) compared to that of Ag/CZA (4227 ppm). However, at higher weight loadings of potassium a clear enhancement of soot oxidation is observed, with 2%Ag-10%K/CZA (10140 ppm), 2%Ag-15%K/CZA (6297 ppm) and 2%Ag-20%K/CZA (29829 ppm) producing significantly larger quantities of CO_2 at high temperatures.

Lowering the weight loading of potassium was with the aim of improving NO reduction over the catalysts, this was not observed. Over the majority of the catalysts, both in the presence and absence of soot, the catalysts were poor at reducing NOx. In the absence of soot, only over 2%Ag-20%K/CZA was NO selectively catalytically reduced. This reduction of NO took place between 325 – 500 °C. The temperature window for abatement to take place in diesel passenger vehicles is 100 – 360°C. Therefore, despite 2%Ag-20%K/CZA showing the ability to reduce NO at high temperatures it is not suitable for *real world* application. Over the remaining catalysts in the absence of soot, reduction in NO concentration was the result of the non-selective reaction resulting in the formation of undesirable N_2O.

In the presence of soot, none of the catalysts tested had the ability to catalyse the reduction of NO by NH_3. Altering the potassium weight loading had very little effect on the catalysts' ability to reduce NO. Over 2%Ag-20%K/CZA and 2%Ag-15%K/CZA, there was little change in NO concentration throughout the experiment, with only small inverse peaks of NO being observed corresponding to the formation of N_2O. 2%Ag-10%K/CZA also only showed a small dip in NO concentration mirroring formation of N_2O, but at higher temperatures (> 350°C) the NO concentration rose. 2%Ag-5%K/CZA and 2%Ag-2%K/CZA formed greater amounts of N_2O compared to the other catalysts, which was mirrored by inverse peaks in NO concentration. Analogously to the 10%K catalyst at high temperatures, the concentration of NO rose.

N_2O was observed over all catalysts, however, over 2%Ag-10%K/CZA and 2%Ag-15%K/CZA it was observed in lower concentrations than the other catalysts as a result of low level NO_2 being present throughout the reactions over these two catalysts. Davies *et al.* found that over Ag/CZA in the presence of soot, *in situ* formed N_2O was utilised to oxidise soot at low temperatures[4] this effect was only observed over the 2%Ag-20%K/CZA. However, the degree of soot oxidation by N_2O was considerably less over 2%Ag-20%K/CZA compared to Ag/CZA.

4.2.2 Characterisation Data

The following section focuses on the analysis of the catalysts in order to determine a deeper understanding of their catalytic properties.

4.2.2.1 CO_2 Trace Investigation

Throughout this project, for reactions which take place in the absence of soot a CO_2 trace is observed. In Chapter 3, the CO_2 trace was theorised to be due to adsorbed hydrogencarbonates and carbonates desorbing from the catalytic surface. In order to determine whether this was the case a heat treatment study was carried out on 2%Ag-20%K/CZA. The catalyst was placed in the reactor and heated to 300 °C and N_2 (200 ml min^{-1}) was flowed over the catalyst. Using the connected FTIR, the quantity of CO_2 formed was observed (Figure 4.8). The temperature was maintained at 300 °C with the gas flow until the CO_2 reading reached 0 ppm. After which, the reactor was cooled to 125 °C and an SCR reaction was carried out as described in Section 2.4.1.Figure 4.8: Heat treatment data at 300 °C for 2%Ag-20%K/CZA under the flow of 200 mlmin-1 N2 showing CO2 concentration against time.

Figure 4.7 shows the SCR reaction data for 2%Ag-20%K/CZA without heat treatment and after the heat treatment. Before the heat treatment The CO_2 trace is observed from 125 – 550 °C, whilst after the heat treatment CO_2 is not observed until 250 °C. This suggests that some of the CO_2 trace is from adsorbed hydrogencarbonates and carbonates desorbing from the catalytic surface. However, there is still a CO_2 trace therefore a 500 °C heat treatment (Figure 4.9).

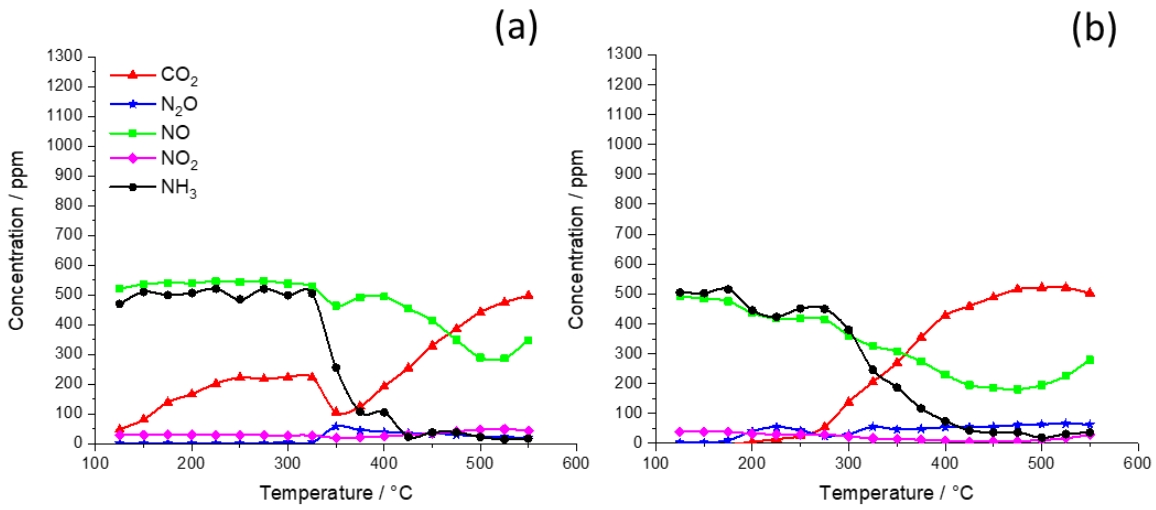

Figure 4.7: SCR data for 2%Ag-20%K/CZA where a is the original SCR data and b is the SCR data for 2%Ag-20%K/CZA after heat treatment at 300 °C. The simulated exhaust gas consisted of 500 ppm NO, 500 ppm NH_3, 8% O_2, with a balance of N_2. The total flow rate was 200 $mlmin^{-1}$. The temperature was increased in 25 °C intervals from 125 to 550 °C, the gas concentrations were allowed to stabilise before readings were taken at each temperature. 0.25 g of catalysts was used.

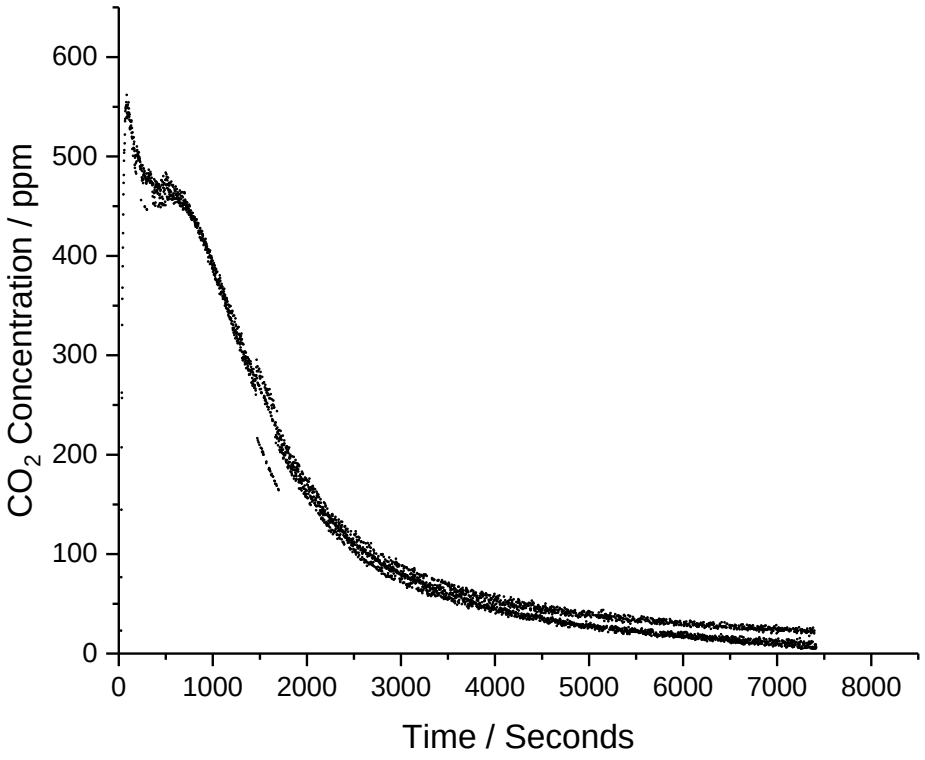

Figure 4.8: Heat treatment data at 300 °C for 2%Ag-20%K/CZA under the flow of 200 mlmin^{-1} N_2 showing CO_2 concentration against time.

Figure 4.10 shows the original SCR data for 2%Ag-20%K/CZA and the data for the SCR reaction after heat treatment at 500 °C. Post heat treatment, CO_2 is not observed until 300 °C. At temperatures above 300 °C CO_2 is observed however at lower concentrations than compared to the original SCR reaction.

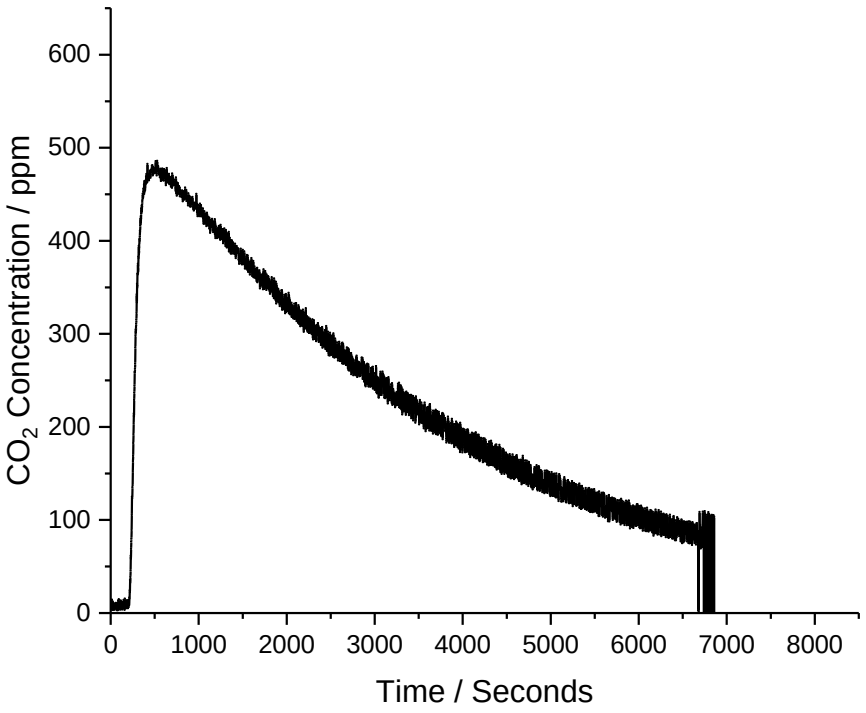

Figure 4.9: Heat treatment data at 500 °C for 2%Ag-20%K/CZA under the flow of 200 mlmin^{-1} N_2 showing CO_2 concentration against time.

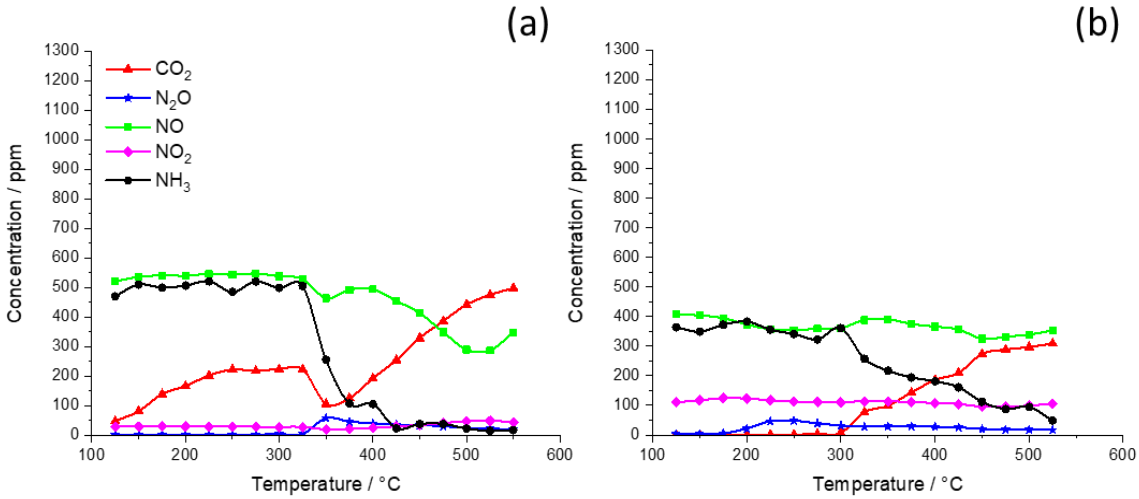

Figure 4.10: SCR data for 2%Ag-20%K/CZA where a is the original SCR data and b is the SCR data for 2%Ag-20%K/CZA after heat treatment at 500 °C. The simulated exhaust gas consisted of 500 ppm NO, 500 ppm NH_3, 8% O_2, with a balance of N_2. The total flow rate was 200 mlmin^{-1}. The temperature was increased in 25 °C intervals from 125 to 550 °C, the gas concentrations were allowed to stabilise before readings were taken at each temperature. 0.25 g of catalyst was used.

The conclusion from the heat treatment experiments is that some of the CO_2 trace observed in the absence of soot is due to adsorbed hydrogencarbonates and carbonates desorbing from the catalytic surface, however, it is not responsible for the full CO_2 trace. The remainder of the CO_2 trace is either due to the decomposition of residual $Ce(CO_3)_2$ as a result of calcination not fully converting the CZA-carbonate to CZA-oxide[2] or a result of the catalyst adsorbing CO_2 from the atmosphere post calcination before being loaded into the reactor.

4.2.2.2 X-ray Diffraction

The catalysts show the four distinct cubic fluorite peaks of CeO_2[5] in the XRD patterns as shown in Figure 4.11. All of the catalysts, excluding the CZA support, show peaks at 37° and 44°, which is due to the presence of crystalline Ag.[6] The CeO_2 and Ag crystallite sizes were calculated using the Scherer equation (Table 4.1).

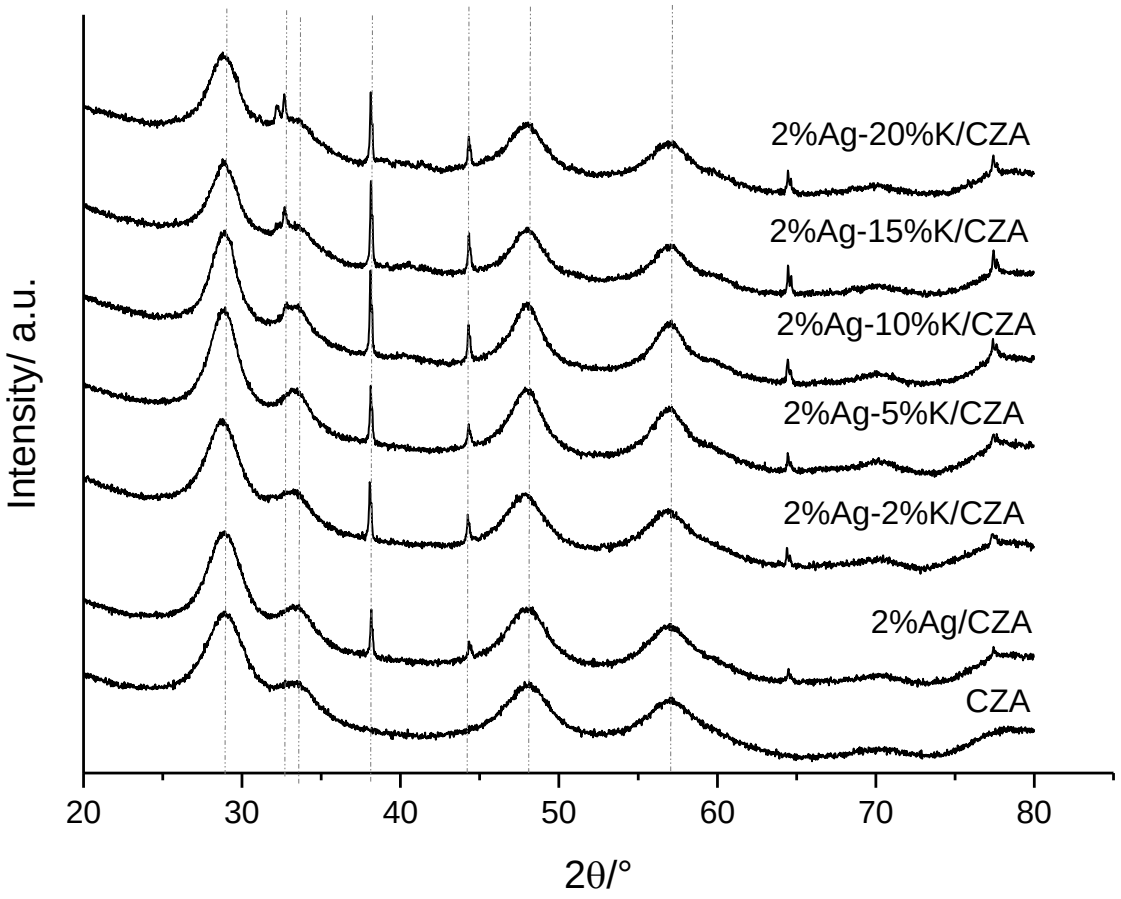

Figure 4.11: XRD patterns for the catalysts

The CZA support had the smallest crystallite size of 27 Å and the remaining catalysts had crystallite sizes ranging from 36 – 50 Å. The Ag/CZA catalyst had a silver crystallite size of 52 Å whilst the potassium containing catalysts had much larger silver crystallite sizes, all of which are above 936 Å. This large difference in silver crystallite size may account for the differences in reactivity between the Ag/CZA catalyst and potassium containing catalysts. Smaller crystallite sizes tend to enhance reactivity. Small silver crystallites could have the ability to reduce NO, whilst larger crystallites are not as effective due to fewer active sites being exposed on the catalytic surface.[7]

Table 4.1: Silver and CeO_2 crystallite sizes calculated from XRD, FWHM and CeO_2 defect ratios calculated from Raman spectroscopy and surface areas from B.E.T. analysis for the catalysts

Sample	Ag Crystallite Size (Å)	CeO_2 Crystallite Size (Å)	FWHM (cm^{-1})	CeO_2 Defect Ratio	Surface Area [$m^2\ g^{-1}$]
CZA	-	27	45.52	0.032	105
2%Ag/CZA	52	42	38.07	0.014	33
2%Ag-2%K/CZA	936	36	55.64	0.055	48
2%Ag-5%K/CZA	959	43	47.58	0.067	42
2%Ag-10%K/CZA	968	50	43.39	0.017	20
2%Ag-15%K/CZA	997	45	52.32	0.034	13
2%Ag-20%K/CZA	1025	37	49.85	0.050	14

4.2.2.3 Raman Spectroscopy

Figure 4.12 shows the Raman spectra for the potassium catalysts as well as Ag/CZA and CZA for comparison. Each sample shows a clear peak centred around 480 cm^{-1}, which is due to the cubic fluorite phase of ceria. Pure ceria typically exhibits a peak centred at 465 cm^{-1}, the shift in the peak position is due to incorporation of different elements into the ceria lattice.[8] Next to this peak, a small broad peak centred around 610 cm^{-1} is observed this is the ceria defect peak. Using these two peaks the ceria defect ratio was calculated for the catalysts (Table 4.1). All but CZA show a peak centred around 1060 cm^{-1},[9] this peak is a result of the symmetric stretching of the C-O carbonate bond present in the catalysts. As the peak is present in Ag/CZA the source of the carbonate is due to Na_2CO_3 which was a precursor used in the preparation of the CZA support. However, the peak is observed in greater intensity over the 10%K, 15%K and 20%K catalysts, which indicates that K_2CO_3 is also contributing to the Raman carbonate peak.

Table 4.1 shows the calculated CeO_2 defect ratios and the FWHM values for the CeO_2 peak for each catalyst. All of the potassium containing catalysts have a greater FWHM value than the CZA support, this is a result of increased oxygen vacancies in the CeO_2 lattice.[10]

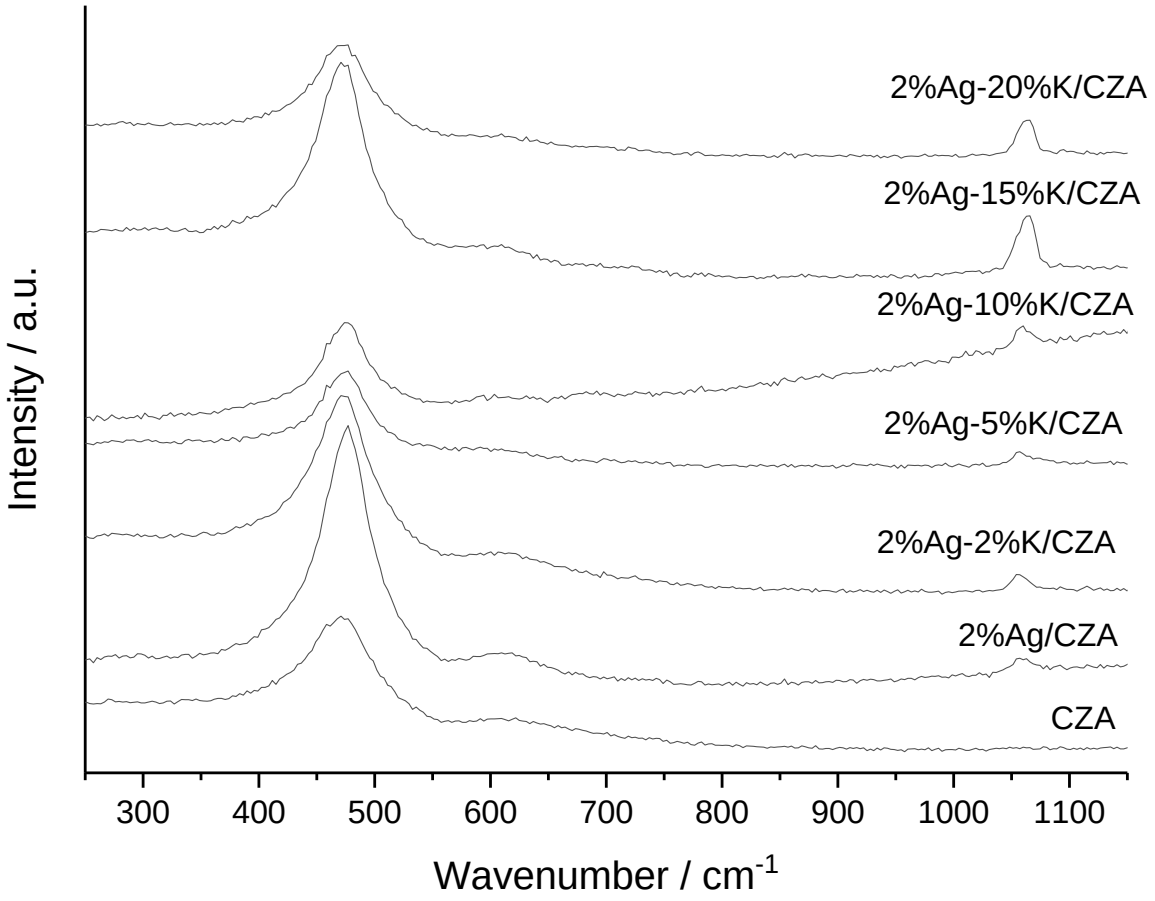

Figure 4.12: Raman spectra for the catalysts studied in this chapter and for Ag/CZA and CZA

4.2.2.4 BET Analysis

BET analysis was used to obtain the surface areas of the catalysts (Table 4.1). The CZA support had the highest surface area (105 $m^2 g^{-1}$), which correlates to it also having the smallest CeO_2 crystallite size (27 Å). The catalysts have lower surface areas than CZA and the potassium containing catalysts show a decrease in surface area with increase in potassium weight loading. The 2%Ag-15%K/CZA and 2%Ag-20%K/CZA catalysts have very similar low surface areas of 13.9 and 14.2 $m^2 g^{-1}$, respectively.

4.2.2.5 XPS Analysis

The surface weight percent of the elements in the catalysts was calculated from the XPS data, Table 4.2. In addition to the catalysts, the table shows the weight percentage for the CZA support and 2%Ag-10%K/CZA post reaction. XPS was carried out on the same sample of 2%Ag-10%K/CZA before and after the SCR reaction to help identify changes to the catalyst during the reaction.

Table 4.2: Weight Percent of Elements Calculated from XPS Analysis

Catalyst	Ag	C (carbonate)	K	Ce	Al	Na	O	Zr
CZA	-	2.68	-	50.74	11.52	1.466	27.23	5.40
2%Ag/CZA	1.06	1.99	-	53.55	10.38	6.221	22.23	3.94
2%Ag-2%K/CZA	1.37	3.37	3.54	30.88	14.74	8.709	29.65	6.78
2%Ag-5%K/CZA	1.43	3.94	8.96	23.15	13.40	7.130	35.37	5.65
2%Ag-10%K/CZA	0.95	5.62	18.62	12.91	16.48	3.803	37.56	3.28
2%Ag-15%K/CZA	1.55	6.41	32.17	2.90	15.72	2.543	36.12	0.86
2%Ag-20%K/CZA	0.56	5.97	32.59	6.23	14.02	1.764	35.90	1.51
Post Reaction 2%Ag-10%K/CZA	0.61	3.69	12.32	24.14	12.96	7.209	32.08	5.58

Figure 4.13 shows the K2p peaks for the potassium containing catalysts. The XPS analysis clearly shows that as the potassium loading is increased the K2p peaks increased in intensity, as expected. This is also reflected in the K weight percentages (Table 4.2), however, 2%Ag-15%K/CZA shows a similar weight percentage of K (32.17 %) as 2%Ag-20%K/CZA (32.59 %). The weight percentages for K for these two catalysts is also higher than expected this is likely to be a result of uneven distribution of potassium across the catalyst. Using the CZA surface area from the BET

analysis it was calculated that for a monolayer of K to cover the CZA surface 6.02 $x10^{-8}$ mol g^{-1} of K would be required. The theoretical number of K moles in the 2w.t.% loading of K is 4.99 $x10^{-4}$ moles. Hence, the lowest weight loading of K in this study has a substantially greater number of K moles than required to form a monolayer on the surface of the support, so therefore, there will be areas which have multiple layers of K on the CZA surface. Higher concentrations of K would be expected with greater weight loading explaining the high atomic percentages of K observed from XPS analysis.

The XPS analysis also shows varying Ag weight percents across the catalysts despite all of the catalysts being prepared as 2w.t.% Ag. As with the K, this is due to uneven distribution of Ag across the catalytic surface. 2%Ag-20%K/CZA was reported as having a Ag weight percent of 0.56% which is the lowest observed over the catalysts. As well as the uneven distribution, the varying Ag weight percentages is also due to the high levels of surface K present. The same is true for the Ce and Zr weight percentages observed through XPS analysis.

The XPS analysis also shows that there is a high amount of carbonate present in the catalysts as shown by the C(1s) peak at *ca.* 289.5 eV in all spectra, however, the quantity varies between the catalysts. The weight percentage for this C(1s) carbonate peak is shown in Table 4.2. Carbonate is present in the CZA support (2.68 %) and Ag/CZA (1.99 %), which is due to the presence of residual carbonate counter ions which were used for during the preparation of the CZA support. Upon the addition of potassium, the carbonate weight loading increases compared to Ag/CZA and the CZA support due to the presence of potassium carbonate. The carbonate weight loading increases with increase in potassium weight loading. As with the potassium weight loadings, the carbonate weight loadings for 2%Ag-15%K/CZA (6.41 %) and 2%Ag-20%K/CZA (5.97 %) are similar.

Na is observed over all of the catalysts and the CZA support from the Na_2CO_3 precursor used in the support preparation. However, the quantity of Na varies from 1.466 – 8.709 w.t.% despite the same batch of CZA being used for all of the catalysts. Again, this may be due to uneven distribution of the element across the support.

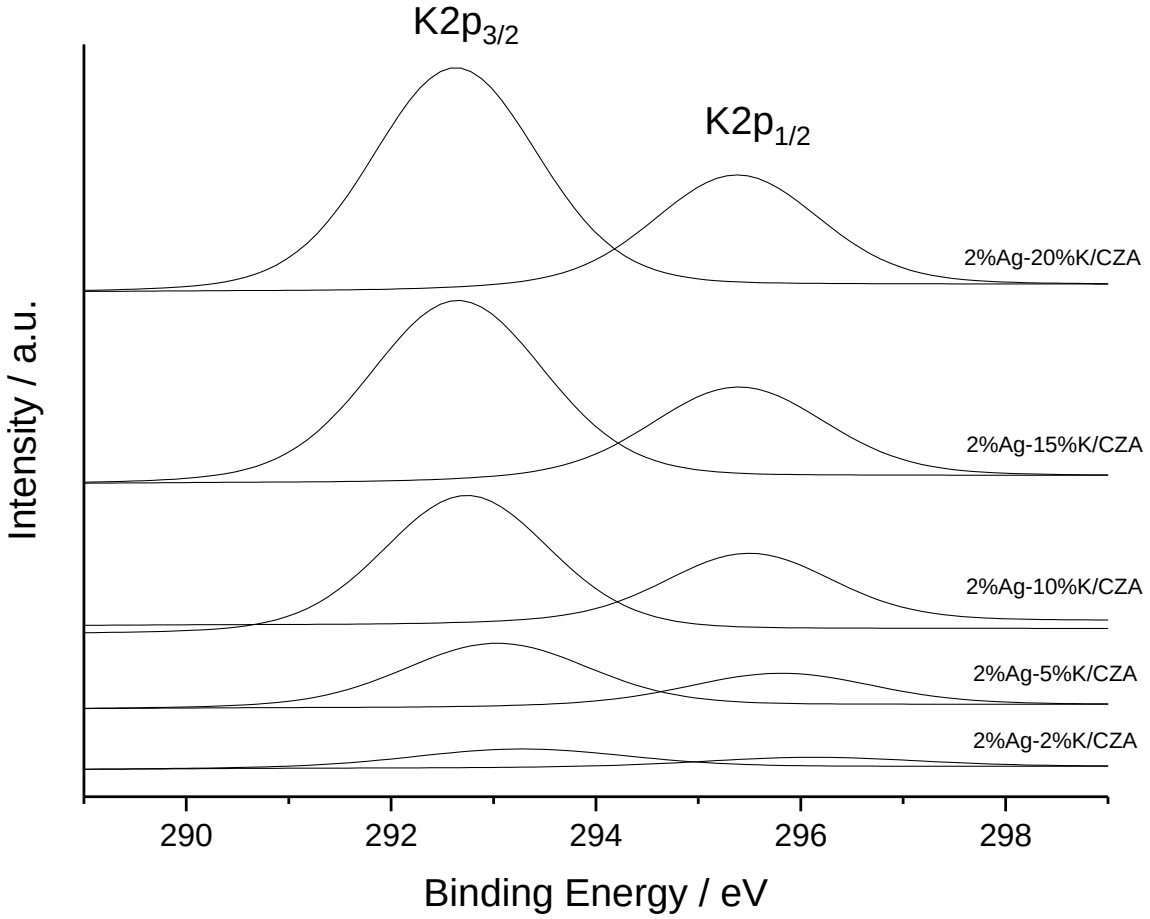

Figure 4.13: K2p bands for the potassium containing catalysts from XPS analysis

XPS analysis was carried out on 2%Ag-10%K/CZA pre and post reaction, Figure 4.14 shows the K2p peaks for both samples. The weight percent of the elements in the samples are shown in Table 4.2. From the figure, it is clear that the pre-reaction K2p peaks are higher in intensity than the post-reaction K2p peaks. This is confirmed by the weight loadings, with the pre-reaction having 18.622 w.t.% and post reaction having 12.320 w.t.%. The post reaction sample also shows a decrease in carbonate weight loading compared to the pre-reaction sample. The post reaction sample shows a shift to higher binding energies for the K2p peaks (Figure 4.14). Shifts in binding energies is either due to change in oxidation states or due to a change in local chemical and physical environment.[11] As potassium in a compound is always the 1+ oxidation state this suggests that there has been a change in the environment. As the amount of carbonate has decreased post reaction, it is likely that during the reaction the K_2CO_3 changed state or/and reacted to form a new compound. The most likely candidate being the formation of K_2O. This is supported by the decrease in O weight percent loading.

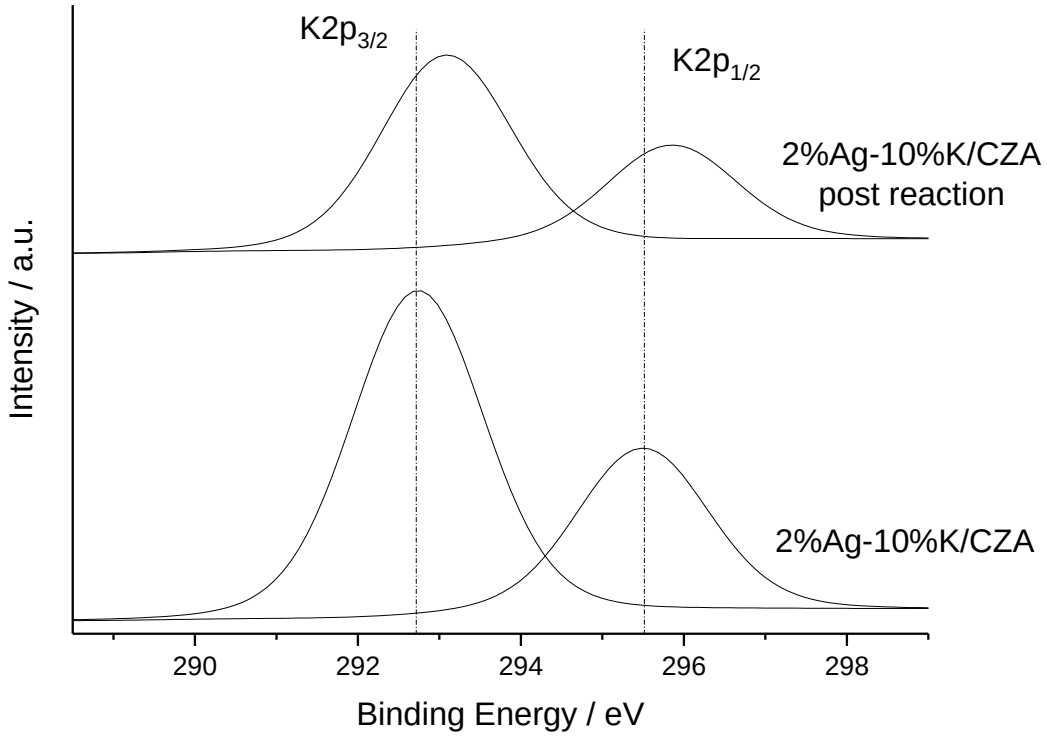

Figure 4.14: K2p bands for 2%Ag-10%K/CZA pre and post reaction from XPS analysis

4.2.2.6 Microscopy

Figure 4.15 shows the SEM images for the catalysts, from the images the complex morphology of the catalysts is clear. In all of the catalysts, the images show phase separation of the CZA support. The bright spots in the images are due to Ag. The silver is observed as relatively large spots which correlates to the large Ag crystallite sizes calculated from the XRD data. From SEM images the 2%Ag-20%K/CZA catalyst has Ag crystallite sizes of approximately 1 µm. From EDX analysis of the samples, K is evenly distributed across the catalyst. Unlike, discussed in Chapter 3 where the K appeared to be localised to 'needle-like' structures in the catalysts.[12]

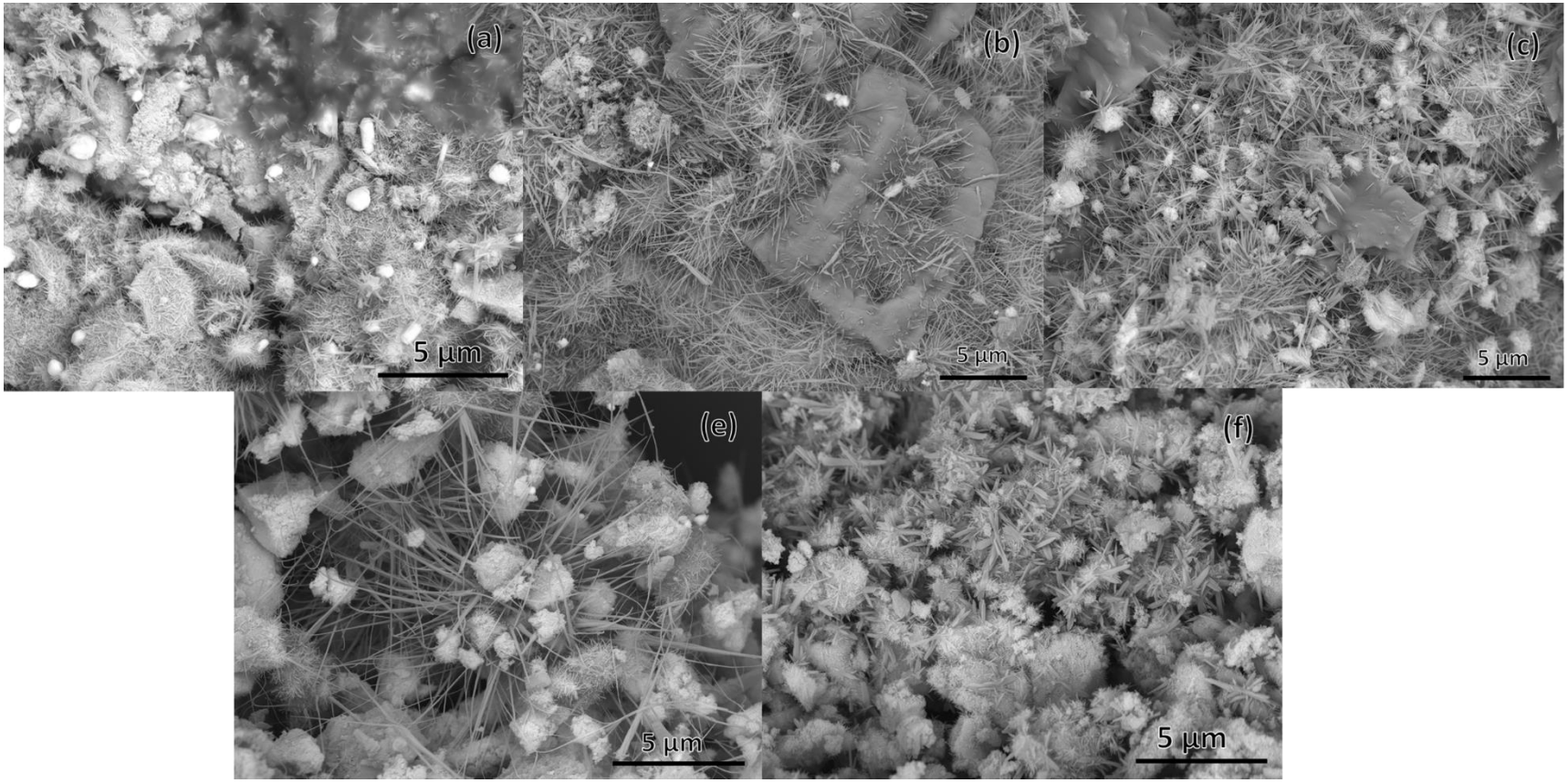

Figure 4.15: SEM images for the catalysts where (a) 2%Ag-2%K/CZA, (b) 2%Ag-5%K/CZA, (c) 2%-10%K/CZA, (d) 2%Ag-15%K/CZA and (e) 2%Ag-20%K/CZA

Across sections of the catalysts large areas containing Na have been identified by SEM-EDX analysis. Figure 4.16 shows an example of this on the 2%Ag-15%K/CZA catalyst. Na is concentrated in the large orthorhombic structure observed in the image and 'needle-like' structures surround the Na. The presence of Na is due to the precursor used to prepare the CZA support. The presence of Na in the samples is confirmed by the XPS analysis.

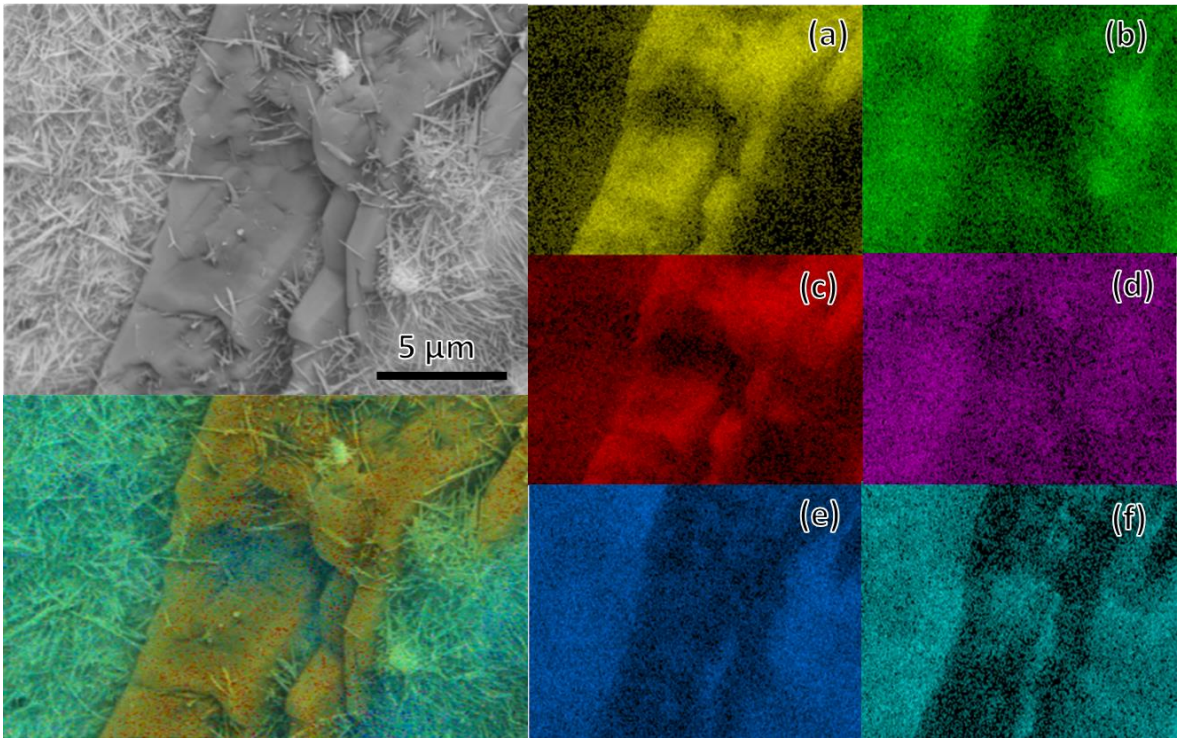

Figure 4.16: SEM-EDX analysis of 2%Ag-15%K/CZA where (a) Na, (b) Al, (c) O, (d) Zr, (e) K, (f) Ce

Altering the potassium weight loading does not appear to significantly change the morphologies of the catalysts. Each catalyst shows phase separation of the CZA support and a wide distribution of K across the catalyst surface. The catalysts show a variety of morphologies; needle-like structures, orthorhombic structures and bright circular spots indicating Ag. The large orthorhombic structures which have been identified as Na are not present in every image in Figure 4.15. This is due to the Na being widely distributed across the surfaces of the catalysts. Over the catalysts with lower weight loadings of potassium, silver is more readily observed as shown in Figure 4.15.

There is no literature containing miscopy for the CZA support however, there is literature on CeO_2-ZrO_2 supports. This literature shows the support to be present in a 'cauliflower' shape with no phase separation. This differs from what is observed over the catalysts studied in this project where there is clear phase separation of the different support components.[13–15] Over the CeO_2-ZrO_2 catalysts in literature there is no observations of 'needle-like' structures suggesting that this is due to either the presence of Al_2O_3 or potassium in this project's catalysts.

4.2.2.7 *In situ* XRD

In situ XRD was carried out to determine how the catalyst changed under reaction conditions. The *in situ* XRD was carried out under flowing air as the reaction gases could not be used due to instrumental limitations. The gas mixture used in the reactor was oxidising, as it contained of 8 % O_2 therefore using flowing air was a suitable alternative. The sample was heated in 50°C intervals between 50 - 600°C and held for 1 h before a measurement was taken. Figure 4.17 - Figure 4.19 show the *in situ* XRD patterns for CZA, 2%Ag-20%K/CZA and 2%Ag-20%K/CZA + soot, respectively.

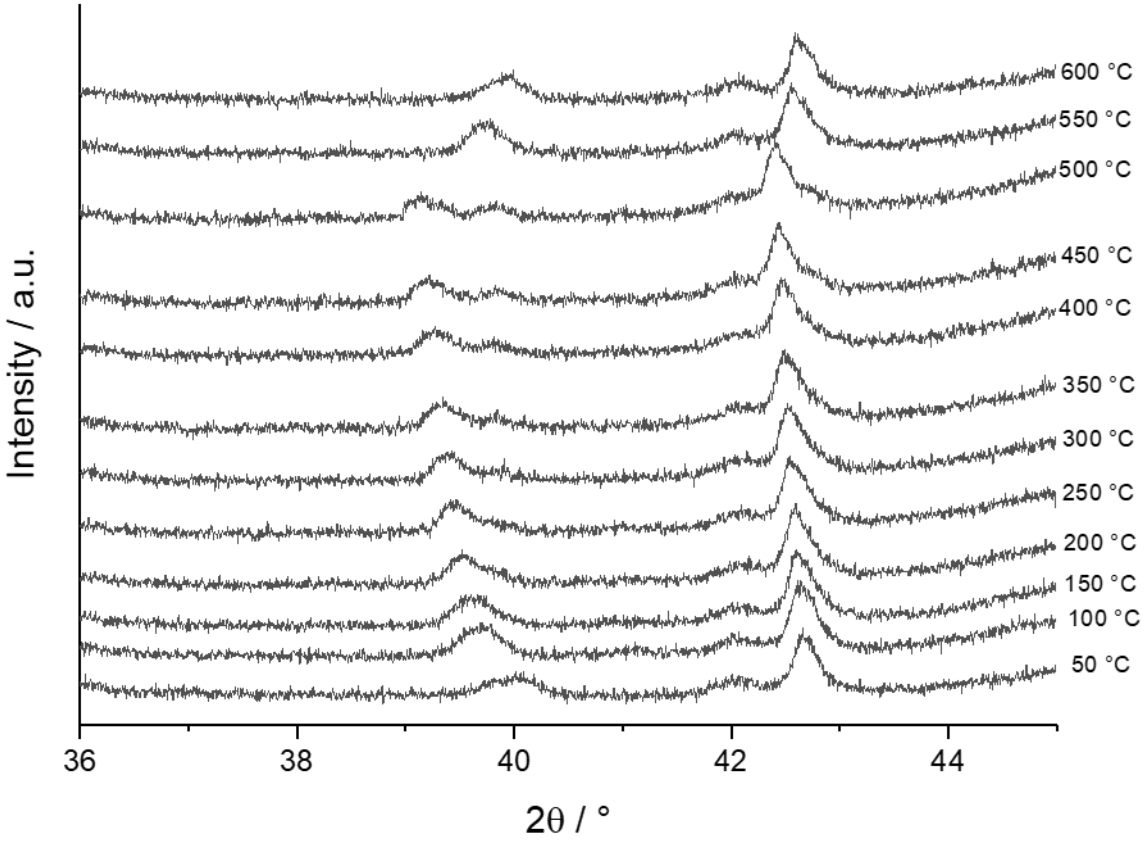

Figure 4.17: *In situ* XRD pattern for CZA

The patterns are focussed on the region 36 – 45°. The *in situ* XRD patterns for the remaining catalysts may be found in Appendix 2. The *in situ* XRD showed very similar results for all of the potassium containing catalysts. The 20% loading of potassium was chosen to be discussed as the higher weight loading showed the highest intensities allowing the patterns to be clearer. The in situ XRD spectra for the remaining catalysts may be found in Appendix 2.

The figures show that two peaks centred around 39 – 40 ° merge to form one more intense peak as the temperature is increased, with a single peak being observed at 550 and 600°C. This is observed for the CZA support and the catalysts hence the peaks must be due to a component of

the support. When the samples are cooled back down, the separate peaks are observed again. From literature the peaks have been assigned to Al_2O_3,[16] the merging of the peaks at high temperature is due to thermal expansion of the lattice parameters.[17]

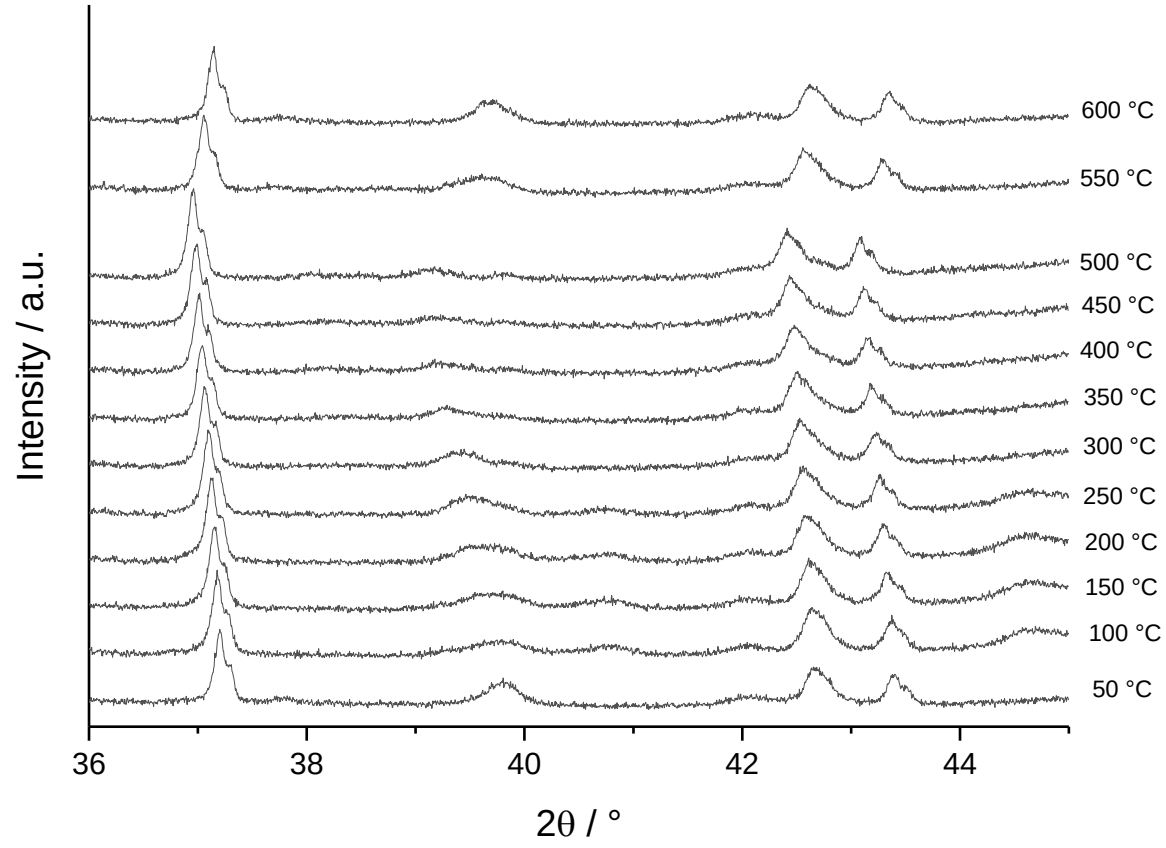

Figure 4.18: *In situ* XRD pattern for 2%Ag-20%K/CZA

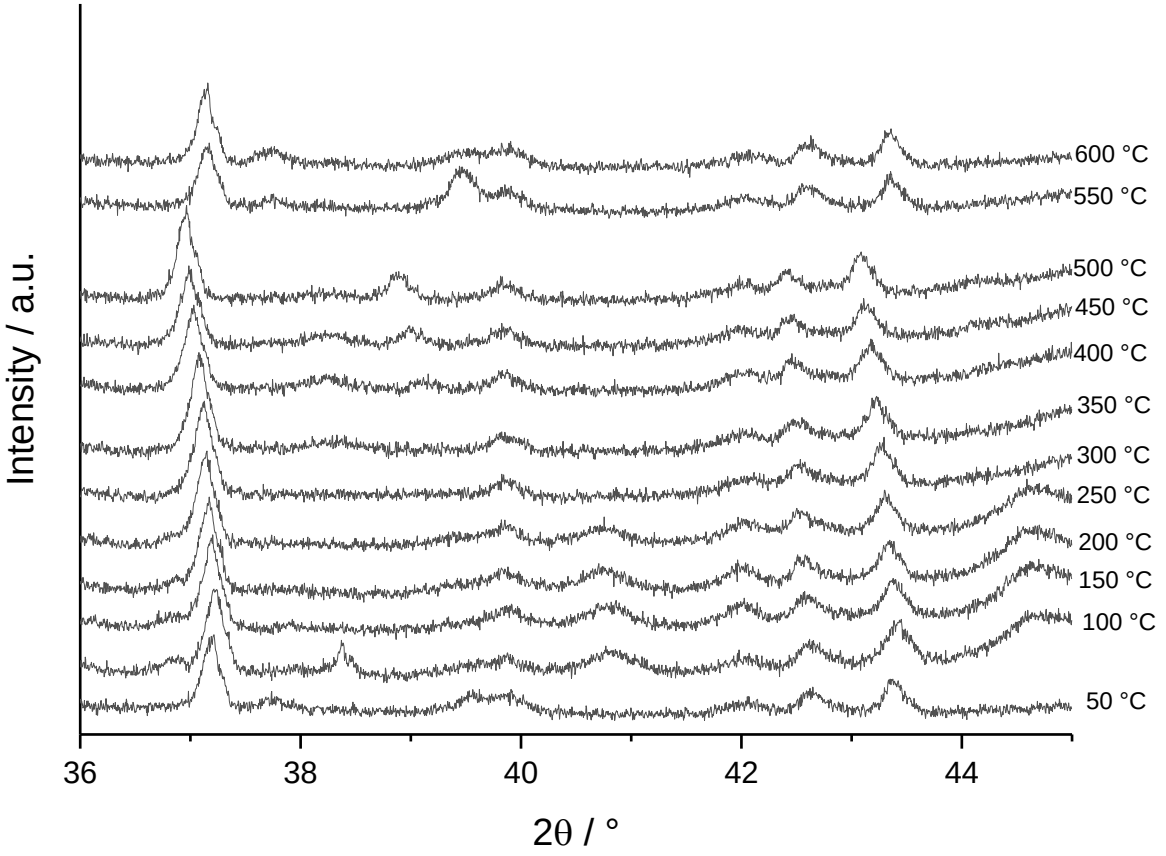

Figure 4.19: *In situ* XRD pattern for 2%Ag-20%K/CZA + CB

All catalysts exhibited similar diffraction patterns, with the initial and final scans showing the typical CeO_2 peaks (28 °, 33 °, 47 °, 56 °),[18] and a peak at 37° indicating the presence of Ag. The silver peak has a shoulder due to the presence of K_2CO_3. A peak at 43.5° is indicative of the presence of potassium.[19] The peaks for K_2CO_3 were more intense for the 2%-Ag-20%K/CZA catalyst, which is to be expected due to its higher weight loading. As temperature is increased the silver and potassium peak (37°) shifts. These shifts are due to the thermal expansion of the Ag lattice parameters.[20]

Davies *et al.* found that operando potassium K-edge X-ray absorption spectroscopy on K_2CO_3/Al_2O_3 showed that the potassium was mobile in a temperature range of 200 – 600 °C .[21] This finding suggests that the K species in the Ag-K/CZA catalysts may also be becoming mobile under reaction conditions. Davies *et al.* also found that when K_2CO_3/Al_2O_3 was in contact with soot that the potassium became increasingly mobile. The presence of soot enhancing potassium's mobility helps to explain why there are changes in reactivity over the catalysts in the absence and presence of soot. Figure 4.19 shows the *in situ* XRD pattern for 2%Ag-20%K/CZA + soot. This figure shows slight shifts in the silver and potassium peak which coincides with Davies *et al.'s* findings on the presence of soot enhancing potassium mobility. The differences in the Ag peak position in absence and in the presence of soot is shown in Table 4.3.

Table 4.3: Ag peak positions from *in situ* XRD analysis for 2%Ag-20%K/CZA in the absence and in the presence of soot

Temperature/ °C	Ag Peak Position Absence of Soot / °	Ag Peak position in the Presence of Soot / °
50	37.22	37.17
100	37.18	37.11
150	37.15	37.22
200	37.13	37.17
250	37.09	37.14
300	37.07	37.13
350	37.03	37.10
400	37.01	37.02
450	36.99	37.01
500	36.95	36.96
550	37.05	37.15
600	37.14	37.16

4.2.2.8 Discussion

The characterisation analysis has provided insight into the catalysts studied in this chapter. From the XRD analysis it was calculated that the silver-potassium catalysts had much greater silver crystallite sizes compared to Ag/CZA. The large difference in crystallite size is likely to be one of the reasons why the silver-potassium catalysts are less effective at reducing NO than Ag/CZA. For the silver-potassium catalysts the total catalyst surface area tended to decrease with potassium weight loading.

The post reaction XPS and *in situ* XRD analysis found that the catalysts experienced changes in state during the reaction. From the post reaction XPS it was determined that the K_2CO_3 loading decreased after the reaction and that K_2O was present after the reaction due to the decomposition of K_2CO_3. The *in situ* XRD showed that thermal expansion of Al_2O_3 and Ag resulted in shifts in the XRD patterns. It is also possible that the shifts in the K peaks is due to and K_2CO_3 becoming mobile under reaction conditions.

4.3 Conclusions and Future Work

From the reaction data it was clear that a higher weight loading of potassium resulted in greater soot oxidation at high temperatures. However, altering the potassium weight loading had very little effect on the catalysts' ability to reduce NO. Suggesting that even a low weight loading of potassium hindered the reduction of NO. Furthermore, only the 2%Ag-20%K/CZA catalyst had the ability to utilise the *in situ* formed N_2O to oxidise soot at low temperatures. The amount of low temperature soot oxidation over 2%Ag-20%K/CZA (237 ppm at 350°C) was significantly less than Ag/CZA (1290 ppm at 350°C). Hence, the presence of potassium also hinders this reaction. As even a low weight loading of potassium hindered the reduction of NO and the utilisation of N_2O to oxidise soot at low temperatures it was theorised that the potassium became mobile under reaction conditions. It was found that some of the catalyst could undergo the SCR reaction and the oxidation of soot but not within the same temperature window. For a catalyst to be successful at the simultaneous removal of NOx and soot these reactions must take place within the same temperature window.

Work by Davies *et al.* found that potassium carbonate becomes mobile between 200 – 600°C and that the mobility of potassium is enhanced in the presence of soot.[21] *In situ* XRD of 2%Ag-20%K/CZA and 2%Ag-20%K/CZA + soot was found to support these findings. The peak of potassium carbonate was observed to shift as the temperature was increased suggesting a change of phase.

XPS analysis of 2%Ag-10%K/CZA before and post reaction showed that after the reaction the sample showed a decrease in K_2CO_3 and showed the presence of K_2O. This is due to the decomposition of K_2CO_3 to form K_2O and CO_2.

The XRD analysis of the catalysts showed that the silver-potassium catalysts had a much larger silver crystallite size than Ag/CZA, this also contributes to the explanation of the catalysts inability to reduce NO. Smaller crystallites are superior at catalysing reactions than larger crystallites.

Both the Raman and XPS analysis shows higher K_2CO_3 intensities for the higher weight loadings, as expected. The techniques also show the presence of Na_2CO_3, due to its use as the precipitate in the formation of the CZA support.

The CO_2 trace which is observed over all catalysts in the absence of soot was found to be a result of two things. Firstly, from adsorbed hydrogencarbonates and carbonates desorbing from the catalytic surface when heated. Secondly, due to the decomposition of residual $Ce(CO_3)_2$ as a result of calcination not fully converting the CZA-carbonate to CZA-oxide.[2]

In order for gaining a deeper understanding on the effect of potassium on the Ag/CZA catalyst further *in situ* studies (e.g. XANES) should be carried out. These tests should be done both in the presence and absence of soot to investigate the effect of soot on potassium mobility. An *in situ* TEM study of the catalysts would also be beneficial. This study would potentially be able to observe the K becoming mobile and its interaction with soot.

Unfortunately, as the presence of potassium hinders the ability to reduce NO and to utilise *in situ* generated N_2O to oxidise soot at low temperatures it is not a suitable component for a simultaneous catalyst. However, the presence of potassium did greatly enhance the oxidation of soot at high temperatures under reaction conditions therefore the catalyst could be considered for use as a soot oxidation catalyst. As the addition of potassium to the Ag/CZA catalyst is not suitable for the simultaneous removal of NO and soot other elements should be investigated. Elements which have been previously found to be able to reduce NO or oxidise soot should be incorporated into the Ag/CZA catalyst and tested for their ability to simultaneously reduce NOx and oxidise soot. Such elements include Pt, Pd and Rh as they are routinely used in automotive aftertreatment systems as well as elements with good redox properties such as Mn and Co.

4.4 References

1 A. Rinkenburger, T. Toriyama, K. Yasuda and R. Niessner, *ChemCatChem*, 2017, **9**, 3513–3525.

2 P. Janoš, T. Hladík, M. Kormunda, J. Ederer and M. Šťastný, *Adv. Mater. Sci. Eng.*, , DOI:10.1155/2014/706041.

3 C. Davies, K. Thompson, A. Cooper, S. Golunski, S. H. Taylor, M. Bogarra Macias, O. Doustdar and A. Tsolakis, *Appl. Catal. B Environ.*, 2018, **239**, 10–15.

4 C. Davies, K. Thompson, A. Cooper, S. Golunski, S. H. Taylor, M. Bogarra Macias, O. Doustdar and A. Tsolakis, *Appl. Catal. B Environ.*, 2018, **239**, 10–15.

5 B. Choudhury, P. Chetri and A. Choudhury, *J. Exp. Nanosci.*, **10**, 103–114.

6 J. D. Grunwaldt, F. Atamny, U. Göbel and A. Baiker, *Appl. Surf. Sci.*, 1996, **99**, 353–359.

7 A. Alshammari, V. N. Kalevaru and A. Martin, *Metal Nanoparticles as Emerging Green Catalysts*, IntechOpen, 2016.

8 R. Schmitt, A. Nenning, O. Kraynis, R. Korobko, A. I. Frenkel, I. Lubomirsky, S. M. Haile and J. L. M. Rupp, *Chem. Soc. Rev.*, 2020, 49, 554–592.

9 Y. Ma, W. Yan, Q. Sun and X. Liu, *Geosci. Front.*, 2021, **12**, 1018–1030.

10 N. Kainbayev, M. Sriubas, D. Virbukas, Z. Rutkuniene, K. Bockute, S. Bolegenova and G. Laukaitis, *Coatings 2020, Vol. 10, Page 432*, 2020, **10**, 432.

11 K. Norrman, S. Cros, R. de Bettignies, M. Firon and F. C. Krebs, *Lifetime and Stability Studies*, International Society for Optics and Photonics, 2008.

12 A. Cooper, T. E. Davies, D. J. Morgan, S. Golunski and S. H. Taylor, *Catalysts*, 2020, **10**, 294.

13 X. Zhang, X. Cheng, C. Ma, X. Wang and Z. Wang, *Catal. Sci. Technol.*, 2018, **8**, 5623–5631.

14 S. N. Maddila, S. Maddila, W. E. van Zyl and S. B. Jonnalagadda, *Res. Chem. Intermed.*, 2017, **43**, 4313–4325.

15 X. Zhang, Q. Wang, J. Zhang, J. Wang, M. Guo, S. Chen, C. Li, C. Hu and Y. Xie, *RSC Adv.*, 2015, **5**, 89976–89984.

16 M. S. Ghamsari, Z. A. S. Mahzar, S. Radiman, A. M. A. Hamid and S. R. Khalilabad, *Mater. Lett.*, 2012, **72**, 32–35.

17 M. Halvarsson, V. Langer and S. Vuorinen, *Determination of the thermal expansion of K-AI 2 0 3 by high temperature XRD*, 1995.

18 G. Jayakumar, A. Irudayaraj, A. D. Raj and A. A. Irudayaraj, , DOI:10.2412/mmse.3.4.481ï.

19 X. Zhang, B. Xu, Y. Xu, S. Shang and Y. Yin, *Int. J. Chem. Eng.*, , DOI:10.1155/2013/870384.

20 P. Guha, R. R. Juluri, A. Bhukta, A. Ghosh, S. Maiti, A. Bhattacharyya, V. Srihari and P. V. Satyam, *CrystEngComm*, 2017, **19**, 6811–6820.

21 C. J. Davies, A. Mayer, J. Gabb, J. M. Walls, V. Degirmenci, P. B. J. Thompson, G. Cibin, S. Golunski and S. A. Kondrat, *Phys. Chem. Chem. Phys.*, 2020, **22**, 18976–18988.

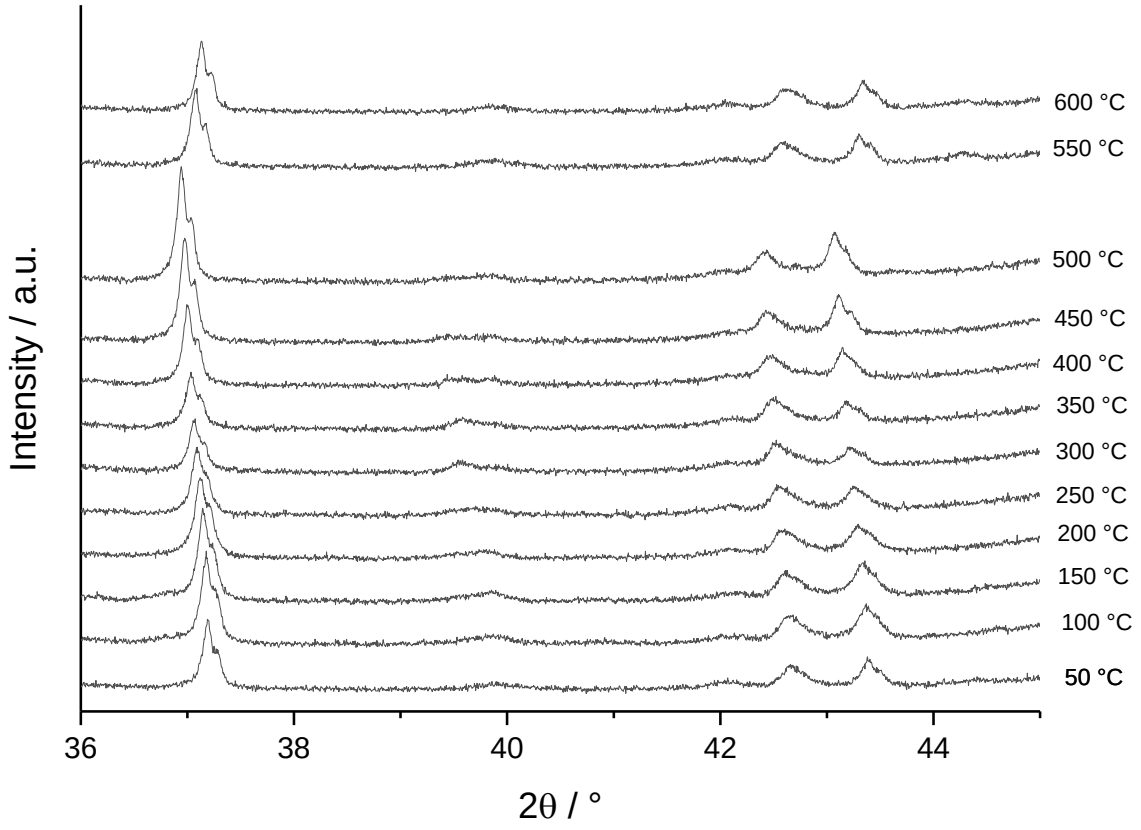

Figure A2.2: *In situ* XRD pattern for 2%Ag/CZA

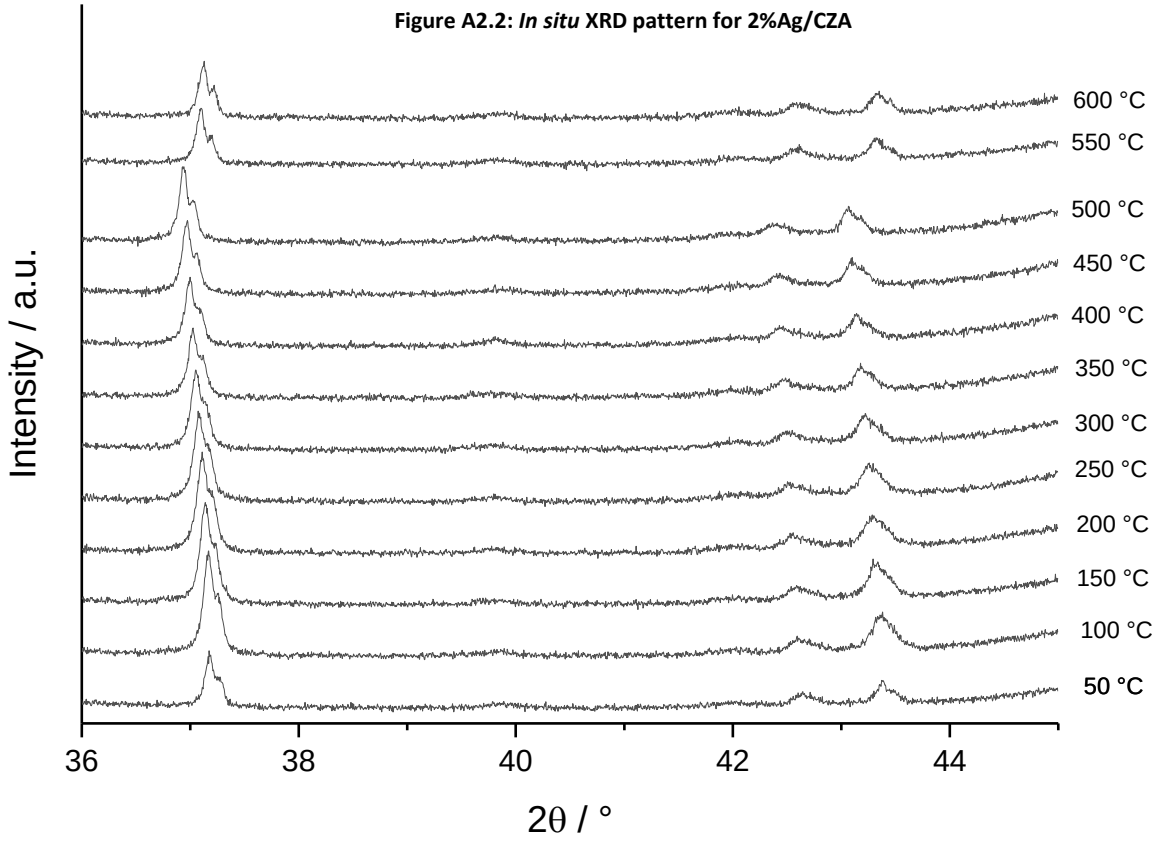

Figure A2.1: *In situ* XRD pattern for 2%Ag-2%K/CZA

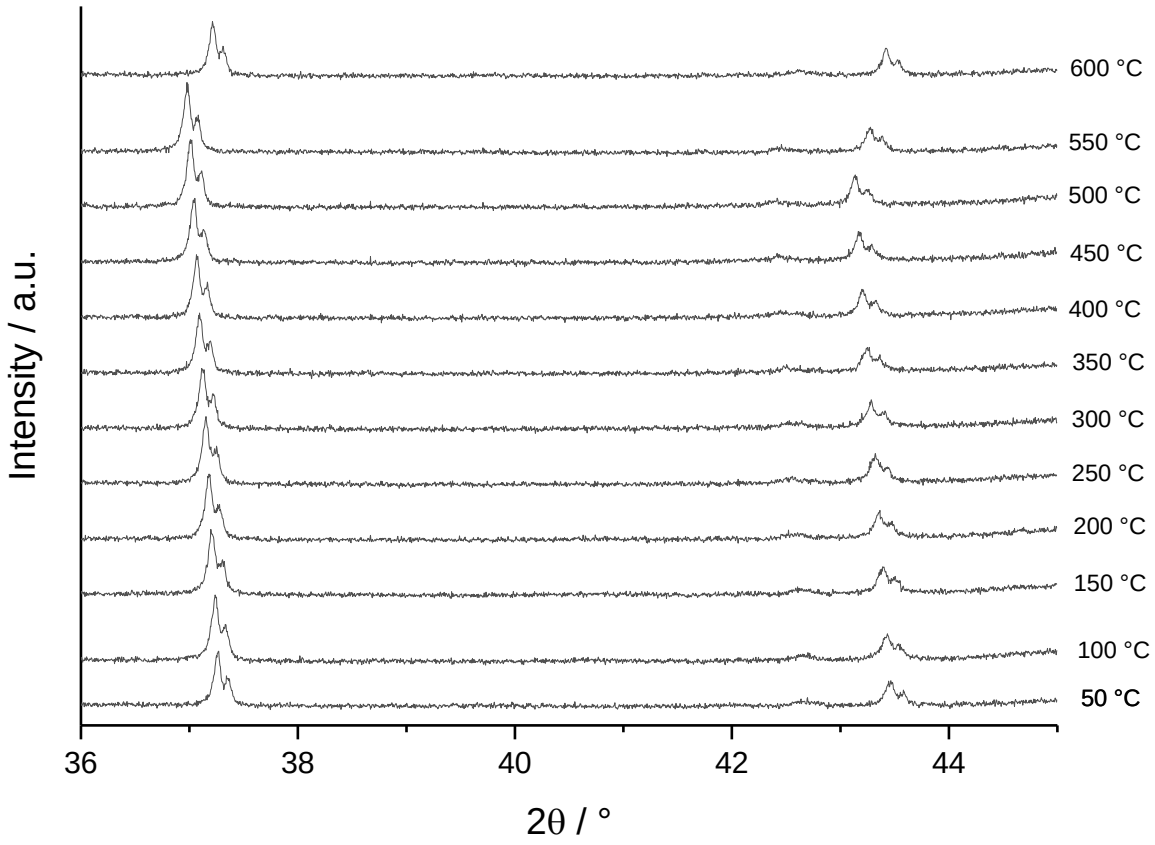

Figure A2.3: *In situ* XRD pattern for 2%Ag-5%K/CZA

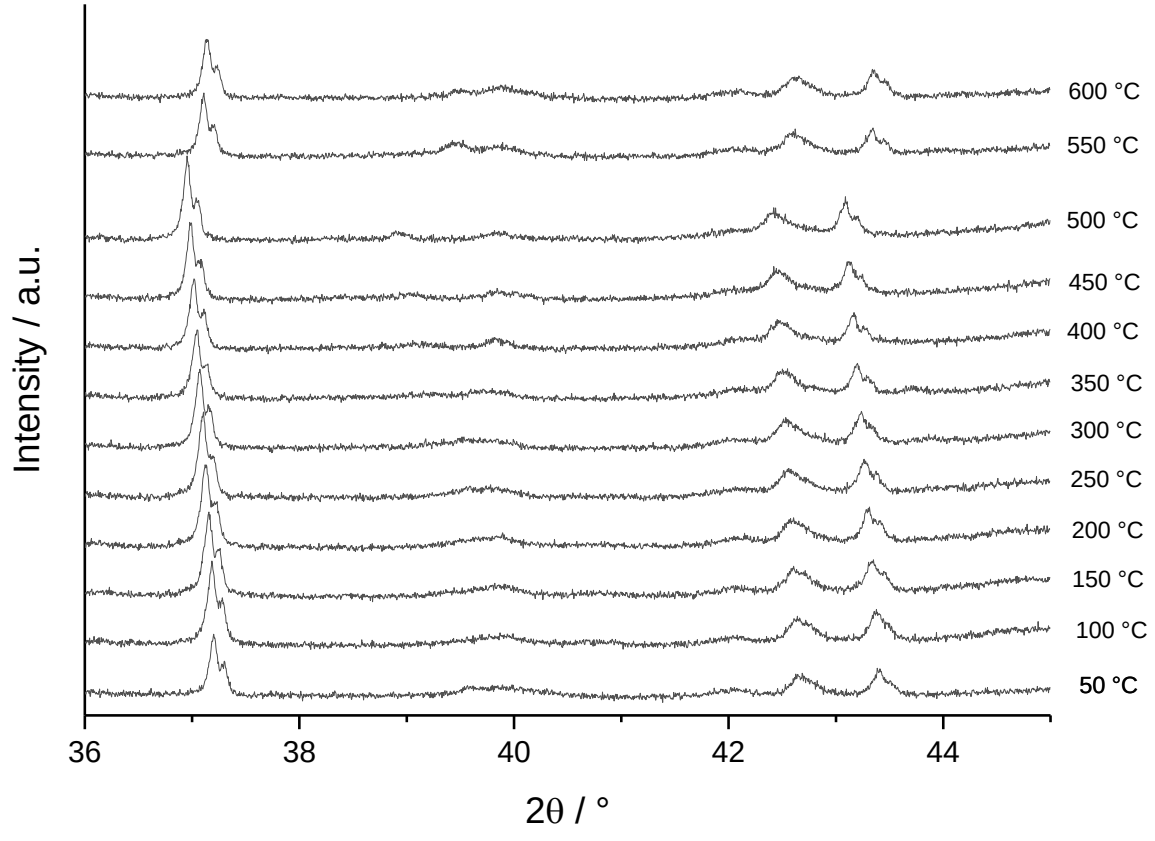

Figure A2.4 *In situ* XRD pattern for 2%Ag-10%K/CZA

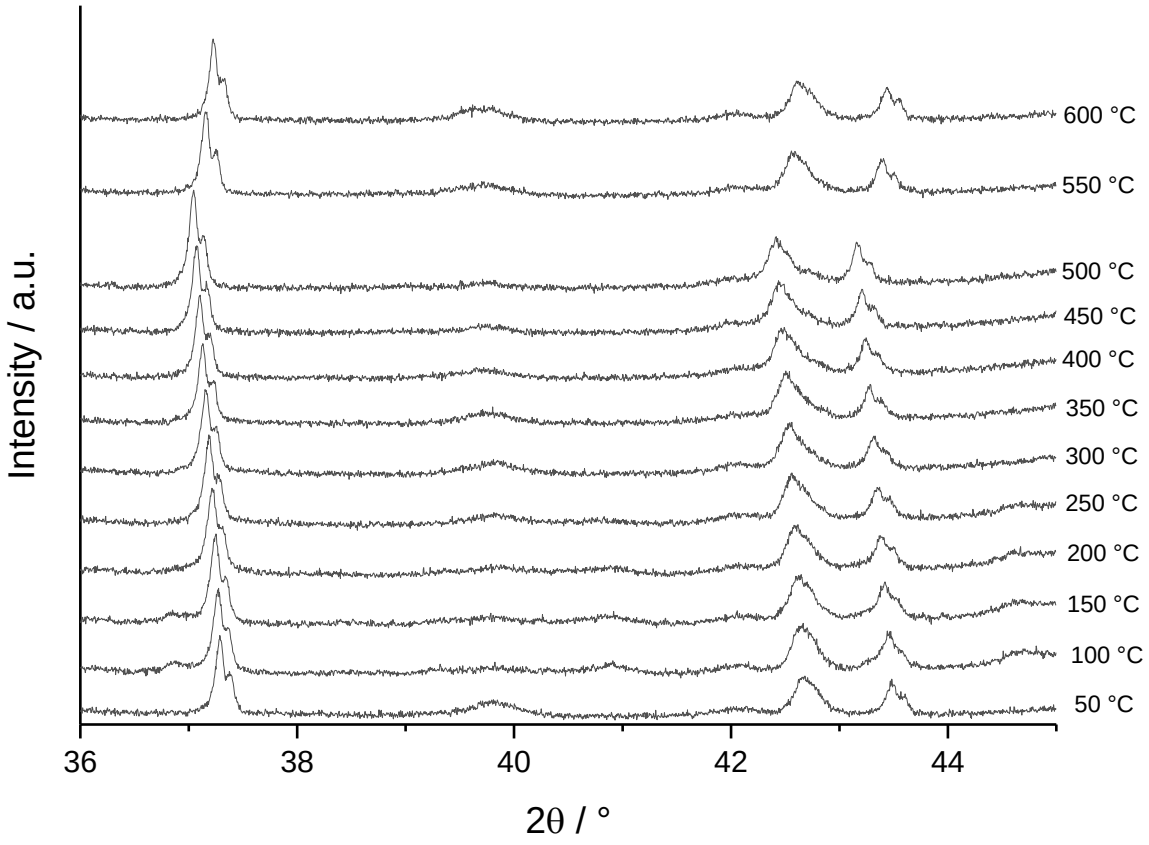

Figure A2.5: *In situ* XRD pattern for 2%Ag-15%K/CZA

5 Copper-Silver Catalysts for the Simultaneous Removal of NOx and Soot

5.1 Introduction

Copper based catalysts are widely used commercially for SCR, most commonly in the form of the metal within a zeolite.[1–7]Copper zeolites have been demonstrated to be active over a wide temperature window as well as being thermally stable and being resistant to sulphur poisoning.[8–15] The copper zeolites used are significantly cheaper than other catalysts, which use expensive metals such as platinum and palladium as the active metal.

The most researched copper zeolites for SCR are Cu/ZSM-5, Cu/SSZ-13 and Cu/SAPO-34. Cu/SSZ-13 and Cu-SAPO-34 have been shown to be active for the reduction of NOx at low temperatures whilst maintaining good hydrothermal stability.[16,17] Gases pass through the pores of zeolites easily allowing NH_3 and NO to adsorb to the zeolite. A key reaction step is the adsorption of ammonia as NH_4^+ onto the acid sites. The preparation method of these zeolites is important as it determines the amount of CuO formed on the catalytic surface at high temperatures. CuO has a negative impact on SCR performance, as it oxidises ammonia rather than reducing it.[5] The two main functions of a Cu-zeolite are:

- Providing an acid site for the adsorption of ammonia
- Providing an exchange redox site which holds the Cu ion which consequently reacts with ammonia, catalytically reducing it to N_2

It is essential to have the correct balance between these two key functions as a high percentage of Cu sites would prevent the adsorption of NH_3 and hence the SCR reaction would no longer be able to proceed. However, if there are insufficient Cu sites present the SCR reaction would not occur due to the lack of redox sites. Currently, a copper weight loading of 3.5 – 4 % is thought to be the ideal percentage for Cu zeolites.[18]

Cu zeolites can achieve up to a 90 % conversion of NO but are not known for their ability to oxidise soot. As the aim was to simultaneously reduce NOx and oxidise soot an extra functionality was required.[7,19] In Chapters 3 and 4 it was found that the Ag-K/CZA based catalysts were unable to convert a high percentage of NOx. Isolated copper species have been found to be active catalysts for the SCR reaction, therefore, various Ag-Cu/CZA catalysts were prepared. With the aim that the presence of Cu in the catalysts would enhance the reduction of NOx as the result of the synergistic effect of two active sites with redox properties. A variety of catalysts were prepared with different weight loadings and using different preparation methods (wet impregnation, sol immobilisation and chemical vapour impregnation) as well as different

calcination temperatures. The catalysts were tested for their ability to simultaneously reduce NOx and oxidise soot using the same equipment and parameters as used in the previous chapters.

5.2 Results

Ten catalysts were prepared *via* a combination of wet impregnation, chemical vapour impregnation and sol immobilisation (section 2.3.2) methods. Each catalyst was tested for its ability to catalyse SCR and the simultaneous removal of NOx and soot as detailed in section 2.4.1. Characterisation was carried out on each catalyst including XRD, BET and Raman, with four catalysts also undergoing SEM-EDX and XPS analysis.

5.2.1 Catalyst performance

The performance data for each catalyst are shown and discussed below. As with the previous chapters the aim of these reactions was to find a catalyst which could simultaneously remove NOx and soot ideally by utilising the *in situ* generated N_2O to oxidise soot at low temperatures.

5.2.1.1 The Effect of Potassium Addition to Copper

2%Cu/CZA was tested for its ability to catalyse the SCR reaction and for its ability to simultaneously reduce NOx and soot. A 2% weight loading of potassium was incorporated into the catalyst (2%Cu-2%K/CZA) to investigate the effect of adding potassium into the system.

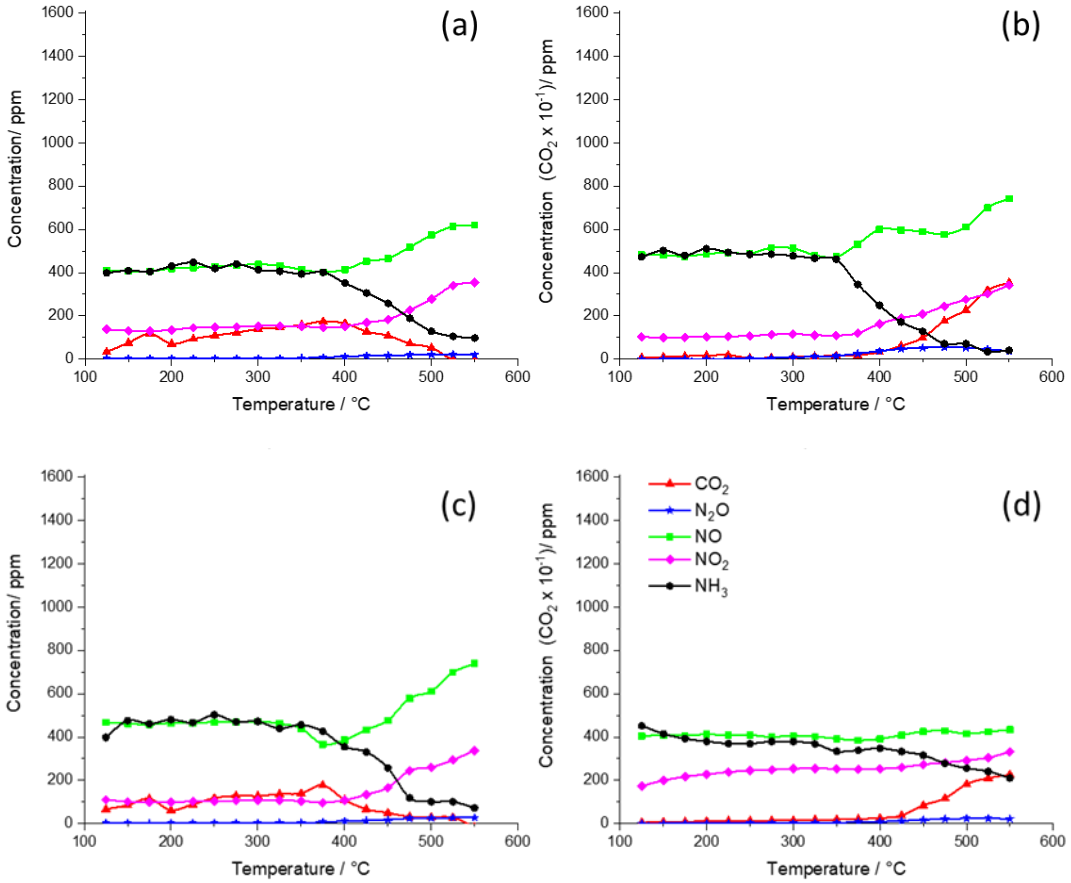

Figure 5.1: Reaction data for copper based catalysts for SCR and the simultaneous removal of soot and NOx. Where (a) 2%Cu/CZA (b) 2%Cu/CZA + soot (c) 2%Cu-2%K/CZA (d) 2%Cu-2%K/CZA + soot. The simulated exhaust gas consisted of 500 ppm NO, 500 ppm NH_3, 8% O_2, with a balance of N_2. The total flow rate was 200 $mlmin^{-1}$. The temperature was increased in 25°C intervals from 125 to 550°C, the gas concentrations were allowed to stabilise before readings were taken at each temperature. For the SCR reaction 0.25 g of catalyst was used and for the simultaneous reaction 0.25 g catalyst was mixed in a 10:1 ratio by mass with soot.

2%Cu/CZA and 2%Cu-2%K/CZA (Figure 5.3a-d) display small quantities of N_2O however these catalysts show > 100 ppm of NO_2 in the temperature window where N_2O is typically observed. The presence of NO_2 at low temperatures is unusual and undesired, it is due to oxidation of NO at low temperatures. For both catalysts, the amount of NO_2 observed at low temperatures is increased when in the presence of soot. Both catalysts show poor selectivity towards the SCR reaction and there was no reduction of NO throughout the reaction temperature range. At temperatures > 400 °C the NO and NO_2 concentrations begin to rise as a result of high temperature oxidation of NH_3. When the catalysts are in the presence of soot, soot oxidation only begins to take place at 400 °C due to oxidation by O_2 and NO_2.

The addition of K to the 2%Cu/CZA catalyst resulted in slightly higher concentrations of low temperature (300°C) CO_2 being observed in the presence of soot. However, less high temperature soot oxidation was observed, Figure 5.3. K is well known for its ability to enhance soot oxidation hence it is unusual that its presence resulted in a lower CO_2 concentration at high temperatures. Figure 5.2 shows that the presence of potassium has lowered the maximum amount of N_2O formed. Furthermore, for 2%Cu-2%K/CZA in the presence of soot the NH_3 concentration did not reach as lower concentration compared to the 2%Cu/CZA catalyst *i.e.*, the conversion of NH_3 was lower over the potassium containing catalyst.

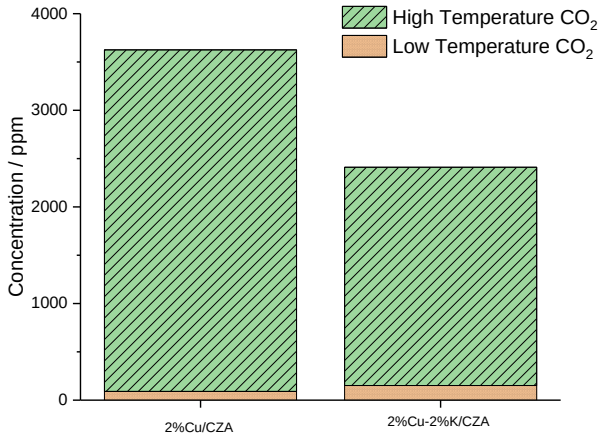

Figure 5.3: The low temperature (300°C) and high temperature (550°C) CO_2 concentrations for 2%Cu/CZA and 2%Cu-2%K/CZA

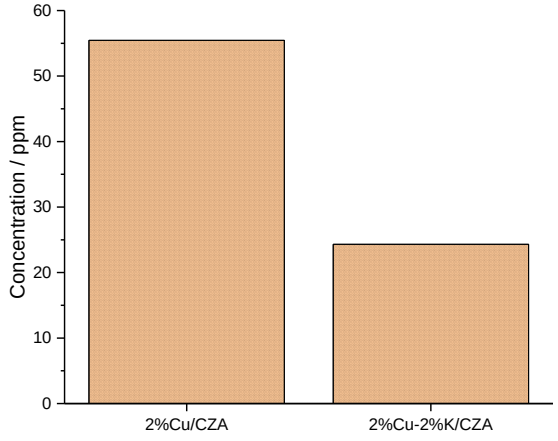

Figure 5.2: The highest concentration of N_2O observed over 2%Cu/CZA and 2%Cu-2%K/CZA

5.2.1.2 The Effect of Changing Calcination Temperature

This next section focuses on comparing the effects of calcining 2%Cu-2%K/CZA at three different temperatures (400, 450 and 500°C) on the catalyst's ability to reduce NOx and oxidise soot.

Figure 5.4a – f shows the reaction data for the 2%Cu-2%Ag/CZA catalysts which were prepared *via* wet impregnation and calcined at 400, 450 and 500°C, respectively, under flowing air. Each catalyst demonstrated that the non-selective SCR reaction took place at low temperatures, as shown by the peak in N_2O, which is mirrored by an inverse peak of NO. In the presence of soot, at temperatures > 350°C the concentrations of NO, NO_2 and CO_2 began to rise. The increase in NO and NO_2 being a result of oxidation of NH_3 and the increase in CO_2 is due to high temperature soot oxidation by NO_2 and O_2. All three catalysts showed high levels of soot oxidation at temperatures above 400°C. The catalyst calcined at 400°C showed the greatest level of soot oxidation, however, it also showed the greatest rise in concentration of NO.

Figure 5.6 and Figure 5.7 help to illustrate the differences between these three catalysts. Figure 5.6 shows that the three catalysts produce relatively the same concentrations of CO_2 at 300°C, however, at high temperatures (550°C) there are clear distinctions between the catalysts.

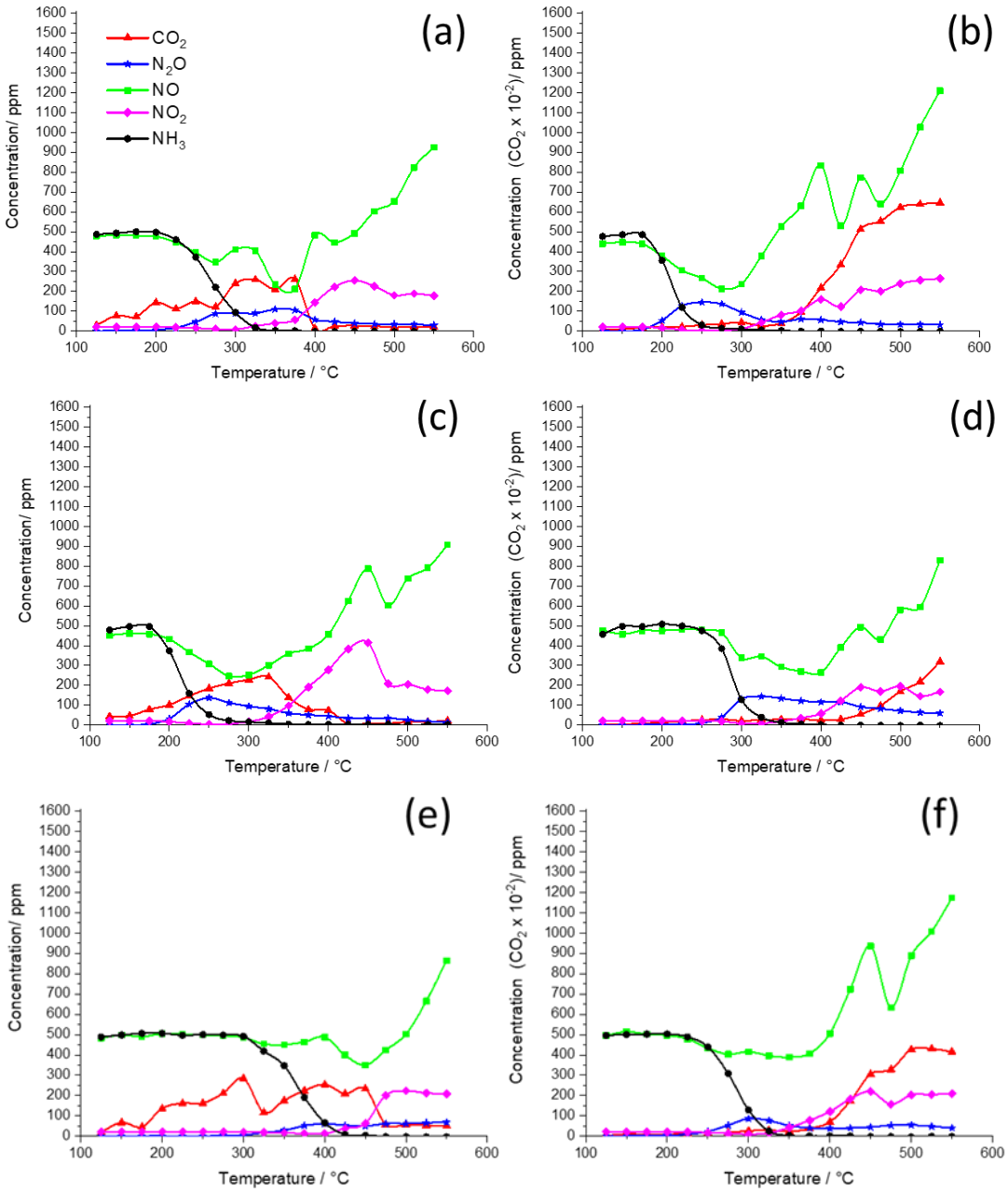

Figure 5.4: Reaction data for copper based catalysts for SCR and the simultaneous removal of soot and NOx. Where (a) 2%Cu-2%Ag/CZA 400°C (b) 2%Cu-2%Ag/CZA 400°C + soot (c) 2%Cu-2%Ag/CZA 450°C (d) 2%Cu-2%Ag/CZA 450°C + soot (e) 2%Cu-2%Ag/CZA 500°C (f) 2%Cu-2%Ag/CZA 500°C + soot.. The simulated exhaust gas consisted of 500 ppm NO, 500 ppm NH_3, 8% O_2, with a balance of N_2. The total flow rate was 200 $mlmin^{-1}$. The temperature was increased in 25°C intervals from 125 to 550°C, the gas concentrations were allowed to stabilise before readings were taken at each temperature. For the SCR reaction 0.25 g of catalyst was used and for the simultaneous reaction 0.25 g catalyst was mixed in a 10:1 ratio by mass with soot.

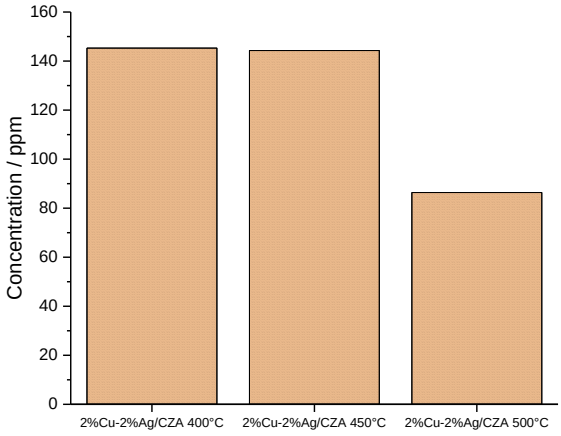

Figure 5.7: The highest concentration of N_2O observed over 2%Cu-2%Ag/CZA 400°C, 2%Cu-2%Ag/CZA 450°C and 2%Cu-2%Ag/CZA 500°C

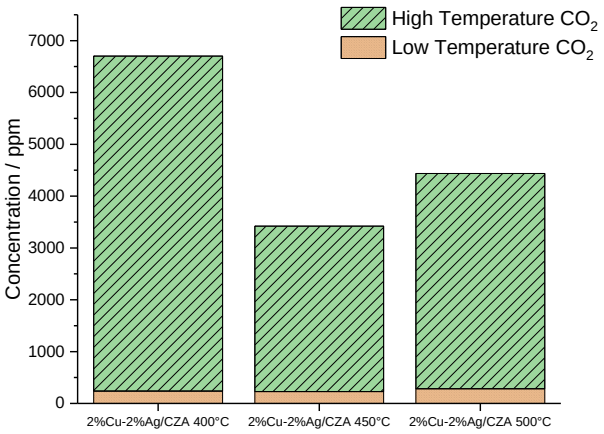

Figure 5.6: The low temperature (300°C) and high temperature (500°C) CO_2 concentrations for 2%Cu-2%Ag/CZA 400°C, 2%Cu-2%Ag/CZA 450°C and 2%Cu-2%Ag/CZA 500°C

2%Cu-2%Ag/CZA 400°C shows the greatest formation of CO_2 out of the three catalysts (6463 ppm), followed by 2%Cu-2%Ag/CZA 500°C (4153 ppm) with 2%Cu-2%Ag/CZA 450°C forming the least (3193 ppm). This shows that over double the amount of CO_2 is formed over the 2%Cu-2%Ag/CZA 400°C when compared to the 2%Cu-2%Ag/CZA 450°C catalyst. Figure 5.7 shows the highest concentration of N_2O formed over the three catalysts. Over 2%Cu-2%Ag/CZA 400°C and 2%Cu-2%Ag/CZA 450°C similar concentrations of N_2O were formed (145 and 144 ppm respectively) whilst over 2%Cu-2%Ag/CZA 500°C only 86 ppm of N_2O was formed.

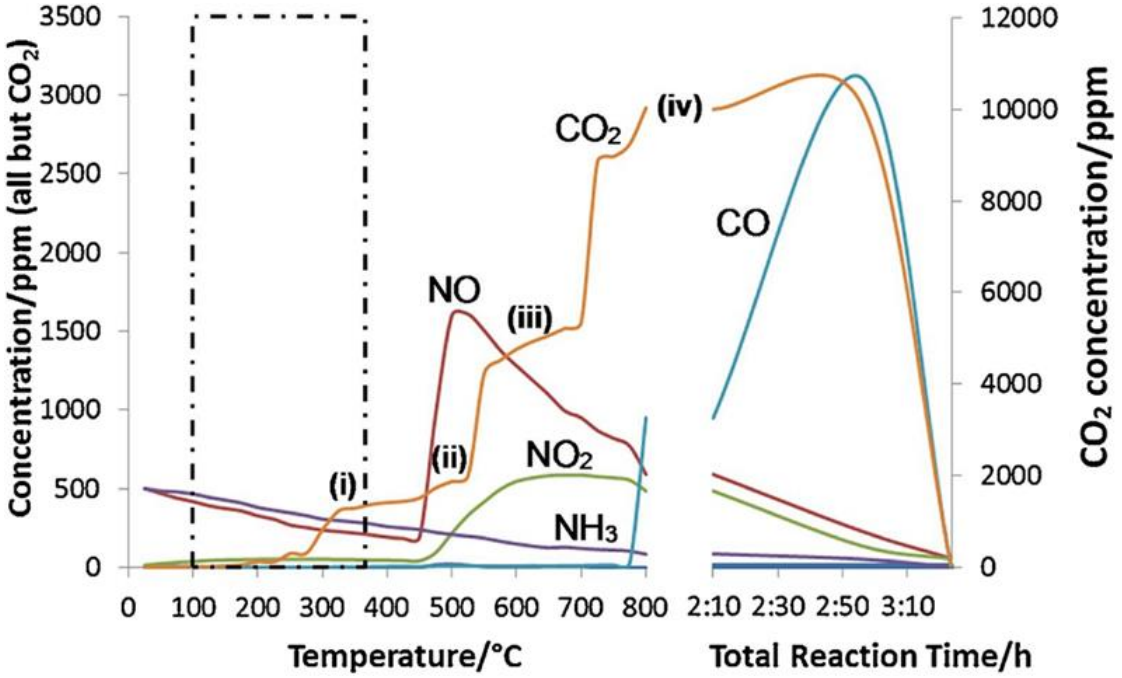

Figure 5.5: The simultaneous removal of NOx and soot over Ag/CZA[20]The simulated exhaust gas consisted of 500 ppm NO, 500 ppm NH_3, 8% O_2, with a balance of N_2. The total flow rate was 200 mlmin^{-1}. The temperature was increased in 25°C intervals from 125 to 800°C, the gas concentrations were allowed to stabilise before readings were taken at each temperature. 0.25 g of catalyst was used.

When compared to the original Ag/CZA data,[20] Figure 5.5 shows that these catalysts are poor at catalysing the simultaneous removal of NOx and soot, as the Ag/CZA catalyst shows no N_2O in the presence of soot and greater levels of low temperature CO_2 is observed. Furthermore, selective catalytic reduction of NO by NH_3 takes place between 100 – 450°C, which is not the case for the copper catalysts. However, at high temperatures (550°C) the 2%Cu-2%Ag/CZA 400°C formed greater concentrations of CO_2 than the Ag/CZA catalyst, with the 500°C catalyst forming similar amounts to the Ag/CZA catalyst and 450°C forming less.

5.2.1.3 Sol immobilisation

2%Cu-2%Ag/CZA catalyst was prepared *via* sol immobilisation and studied for its ability to selectively catalytically reduce NOx and its ability to simultaneously reduce NOx and soot. The reaction data for this catalyst is shown in Figure 5.8.

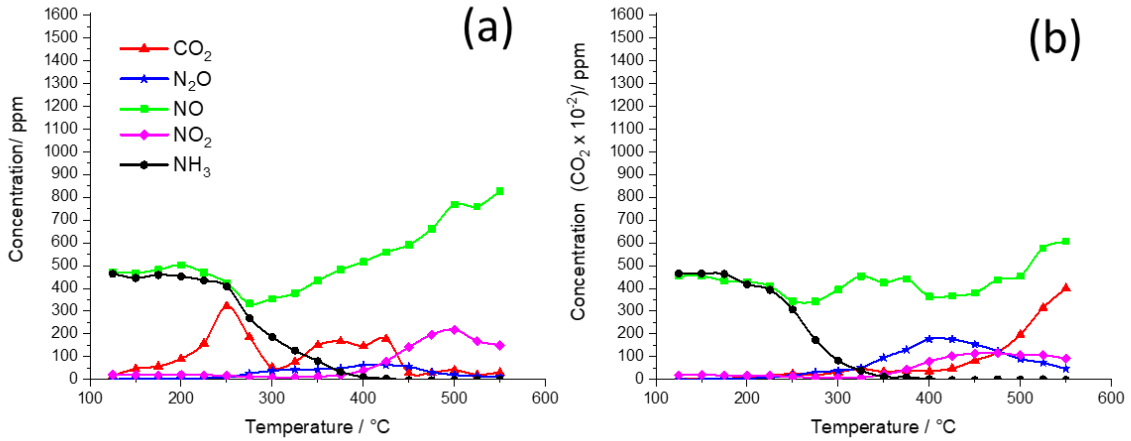

Figure 5.8: Reaction data for copper based catalysts for SCR and the simultaneous removal of soot and NOx. Where (a) 2%Cu-2%K/CZA sol immobilisation (b) 2%Cu-2%K/CZA sol immobilisation + soot. The simulated exhaust gas consisted of 500 ppm NO, 500 ppm NH_3, 8% O_2, with a balance of N_2. The total flow rate was 200 mlmin^{-1}. The temperature was increased in 25°C intervals from 125 to 550°C, the gas concentrations were allowed to stabilise before readings were taken at each temperature. For the SCR reaction 0.25 g of catalyst was used and for the simultaneous reaction 0.25 g catalyst was mixed in a 10:1 ratio by mass with soot.

Figure 5.8b shows a peak of N_2O between 300 – 550°C, this peak is shifted to a higher temperature compared to some of the other catalysts. This is due to the carbon black storing the produced N_2O and then releasing the N_2O at higher temperatures when the carbon black is oxidised.[21] As with the other Cu based catalysts, the catalyst is poor at reducing NOx. Indeed, no NOx reduction was observed over this catalyst. High temperature oxidation of soot by O_2 and NOx reduction was observed over this catalyst. High temperature oxidation of soot by O_2 and NO_2 was observed at temperatures above 400°C.

Compared to the Ag/CZA catalyst in the presence of soot, this sol immobilisation catalyst shows poor NOx reduction, as well as the formation of low levels of N_2O. Furthermore, greater

concentrations of NO and NO_2 are observed at high temperatures over the Cu catalyst. However, at high temperatures the Cu catalyst is superior to Ag/CZA in regards to soot oxidation.

5.2.1.4 Effect of Order of Catalyst Precursors

This sub-section focuses on the differences in catalytic activity over two 2%Cu-2%Ag/CZA catalysts both prepared *via* wet impregnation but with slight differences in the methodology. Catalyst (a) was prepared by the Cu and Ag precursors being added to the CZA support in a step-wise fashion whilst catalyst (b) was prepared by the Cu and Ag precursors being added to the support at the same time. Figure 5.9 shows the reaction data for the catalysts.

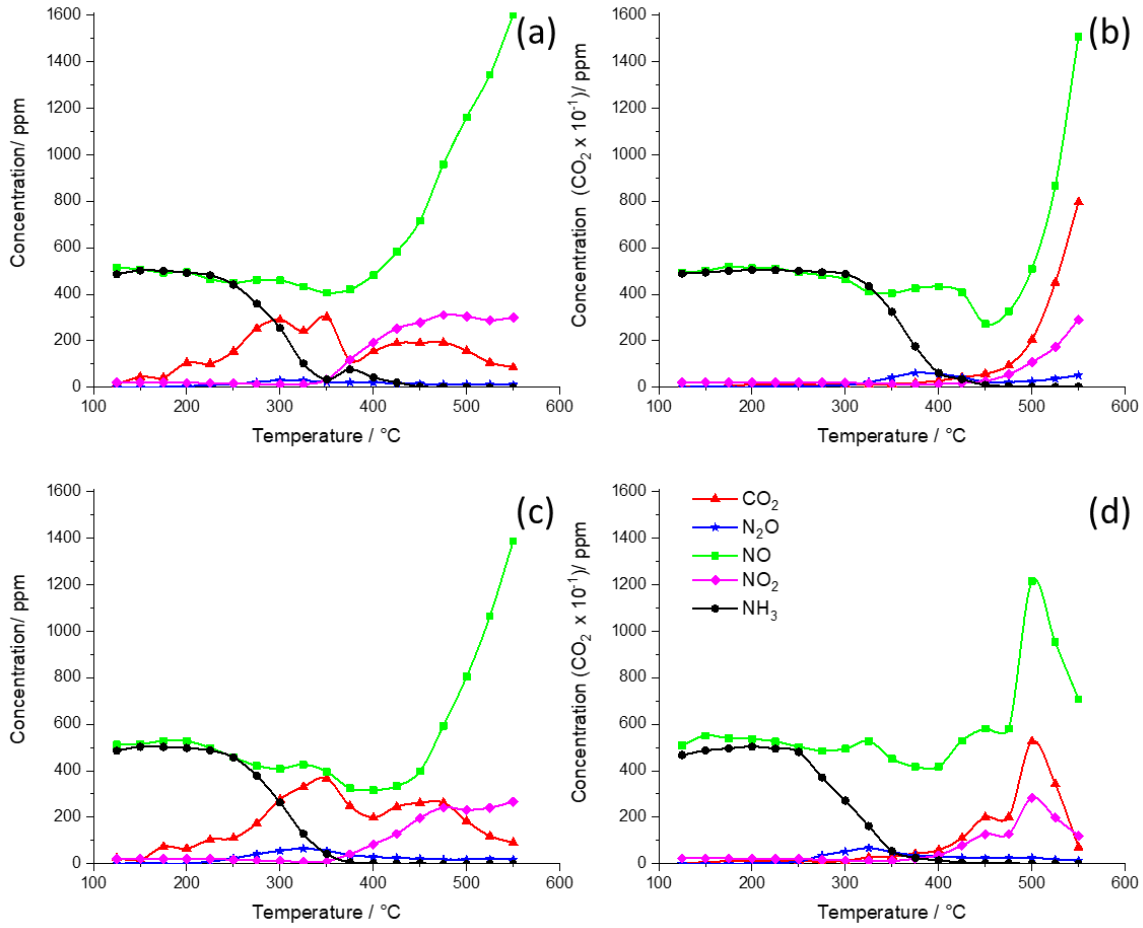

Figure 5.9: Reaction data for copper based catalysts for SCR and the simultaneous removal of soot and NOx. Where (a) 2%Cu-2%Ag/CZA a (b) 2%Cu-2%Ag/CZA a + CB (c) 2%Cu-2%Ag/CZA b (d) 2%Cu-2%Ag/CZA b + soot. The simulated exhaust gas consisted of 500 ppm NO, 500 ppm NH_3, 8% O_2, with a balance of N_2. The total flow rate was 200 mlmin^{-1}. The temperature was increased in 25°C intervals from 125 to 550°C, the gas concentrations were allowed to stabilise before readings were taken at each temperature. For the SCR reaction 0.25 g of catalyst was used and for the simultaneous reaction 0.25 g catalyst was mixed in a 10:1 ratio by mass with soot.

From the reaction data for the catalysts in the presence of soot, there is a high amount of NH_3 oxidation to NO at high temperatures. With catalyst (a) reaching 1600 ppm of NO at 550°C and (b) reaching 1214 at 500°C. Both catalysts show a dramatic increase in NO concentration at

high temperatures, both in the presence and in the absence of soot. Catalyst (a), in the presence of soot shows a small peak of N_2O between 350 and 450°C and catalyst (b) in the presence of soot shows a small peak between 250 and 350°C. Similar quantities of N_2O were observed over the catalysts in the absence of soot. In both cases high levels of soot oxidation are observed at high temperatures, due to oxidation by NO_2 and O_2.

Figure 5.11 compares the low (300°C) and high temperature (550°C) CO_2 formation over the catalysts. The low temperature formation is very similar over both catalysts, however, at 550°C there is a dramatic difference between the two catalysts with catalyst (a) forming 7961 ppm and catalyst (b) 713 ppm. Nonetheless, catalyst (b) was still found to be active for high temperature soot oxidation forming 5259 ppm of CO_2 at 500 °C before beginning to decrease in concentration at higher temperatures. Figure 5.10 demonstrates that the two catalysts formed similar quantities of N_2O at its peak in the presence of soot for both reactions.

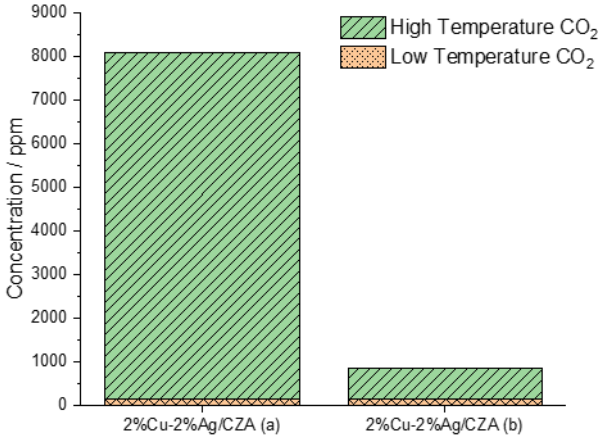

Figure 5.11: The low temperature (300°C) and high temperature (500°C) CO_2 concentrations for 2%Cu-2%Ag/CZA (a) and 2%Cu-2%Ag/CZA (b)

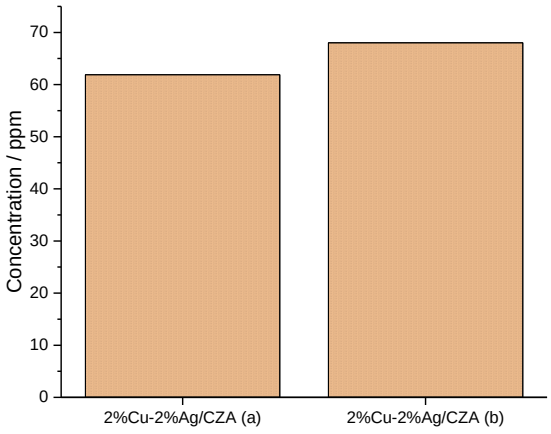

Figure 5.10: The highest concentration of N_2O observed over 2%Cu-2%Ag/CZA 400°C, 2(a) and 2%Cu-2%Ag/CZA (b)

5.2.1.5 Catalysts Prepared *via* CVI

A 2%Cu-Ag/CZA and a 1%Cu-1%Ag/CZA catalyst were prepared *via* CVI, this section investigates the differences in catalytic activity between these two catalysts. Figure 5.12 shows the reaction data for the catalysts.

In the absence of soot, both catalysts show maxima of N_2O at 250°C. In the presence of soot, the temperature window in which N_2O is observed increases, with higher concentrations also being observed. More N_2O is observed over the 1%Cu-1%Ag/CZA catalyst than the 2%Cu-2%Ag/CZA catalyst, as shown in Figure 5.13. Both catalysts, in the absence and presence of soot, are poor SCR catalysts as at low temperatures the non-selective SCR reaction is dominant, and at

higher temperatures the oxidation of NH_3 to NO is prevalent. As with the previous catalysts discussed, soot oxidation is observed at temperatures above 400°C.

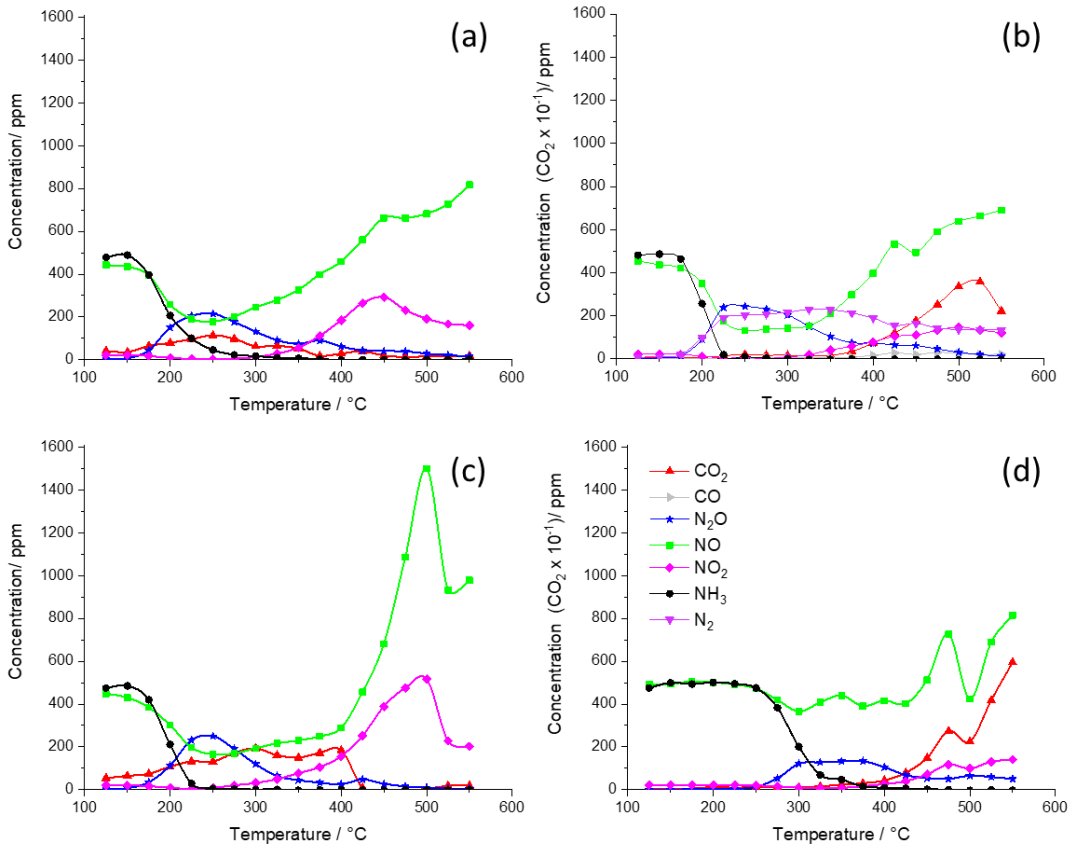

Figure 5.12: Reaction data for copper based catalysts for SCR and the simultaneous removal of soot and NOx. Where (a) 2%Cu-2%Ag/CZA CVI (b) 2%Cu-2%Ag/CZA CVI CB (c) 1%Cu-1%Ag/CZA CVI (d) 1%Cu-1%Ag/CZA CVI + soot. The simulated exhaust gas consisted of 500 ppm NO, 500 ppm NH_3, 8% O_2, with a balance of N_2. The total flow rate was 200 mlmin^{-1}. The temperature was increased in 25°C intervals from 125 to 550°C, the gas concentrations were allowed to stabilise before readings were taken at each temperature. For the SCR reaction 0.25 g of catalyst was used and for the simultaneous reaction 0.25 g catalyst was mixed in a 10:1 ratio by mass with soot.

A nitrogen balance has been calculated for 2%Cu-2%Ag/CZA CVI + soot. From the calculated balance it was determined that the non-selective SCR reaction dominate between 175 – 325°C but that the oxidation of NH_3 to N_2 was also taking place in this temperature range.

Figure 5.14 clearly shows that the low temperature oxidation of soot is very similar between the two catalysts, but at 550°C 1%Cu-1%Ag/CZA is significantly superior at oxidising soot. This may come across as misleading, as despite 2%Cu-2%Ag/CZA being the poorer soot oxidation catalyst at 550°C, at 500°C 3360 ppm is observed over the catalyst compared to the 2054 ppm over 1%Cu-

1%Ag/CZA. Comparing these two catalysts to the Ag/CZA data (Figure 5.5) it can be seen that 2%Cu-2%Ag/CZA (a) forms similar amounts of CO_2 at high temperatures, whilst 2%Cu-2%Ag/CZA (b) forms higher concentrations of CO_2 at high temperatures.

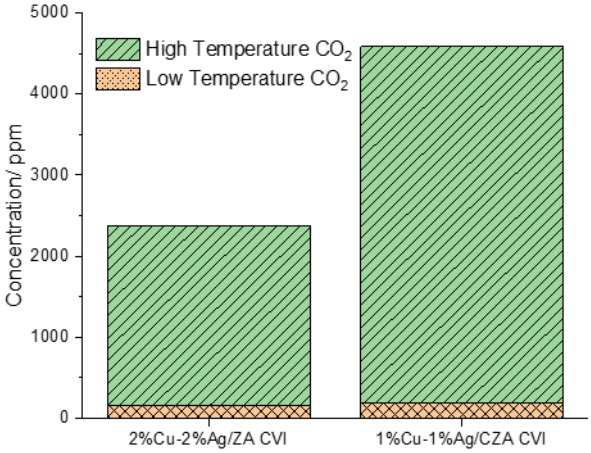

Figure 5.14: The low temperature (300°C) and high temperature (500°C) CO_2 concentrations for 2%Cu-2%Ag/CZA CVI and 1%Cu-1%Ag/CZA CVI

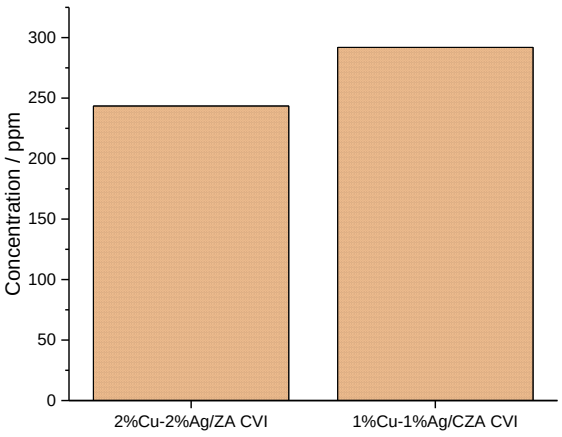

Figure 5.13: The highest concentration of N_2O observed over 2%Cu-2%Ag/CZA CVI and 1%Cu-1%Ag/CZA CVI

5.2.1.6 Silver vs Palladium

The final two catalysts investigated in this chapter are 1%Cu-1%Ag/CZA and 1%Cu-1%Pd/CZA, the two catalysts' reactivities are compared to explore the consequences of using Pd as the secondary metal over Ag. Figure 5.15 shows the reaction data for the catalysts.

1%Cu-1%Ag/CZA (Figure 5.15a and b) is a poor SCR catalyst with very little NO oxidation observed throughout the reaction. A peak of N_2O (maxima 300°C) is observed with and without soot. Following the trend of the previous catalyst, soot oxidation is observed at temperatures above 400°C.

Over 1%Cu-1%Pd/CZA (Figure 5.15c and d), the NH_3 takes up until 450°C to reach 0 ppm, which is a higher temperature than most of the other catalysts discussed. Apart from this the catalyst behaves in a similar manner to the Cu-Ag catalysts. With high temperature soot oxidation being observed as well as peaks of N_2O in the presence and absence of soot.

When comparing the two catalysts, the low temperature oxidation of soot is similar over both catalysts however at high temperatures (550°C) 1%Cu-1%Ag/CZA is superior to 1%Cu-1%Pd/CZA with regards to soot oxidation as seen in Figure 5.17. This observation suggests that the presence of Ag aids soot oxidation in the simultaneous removal of NOx and soot. Figure 5.16

shows that 1%Cu-1%Ag/CZA produces a higher concentration of undesirable N_2O than 1%Cu-1%Pd/CZA.

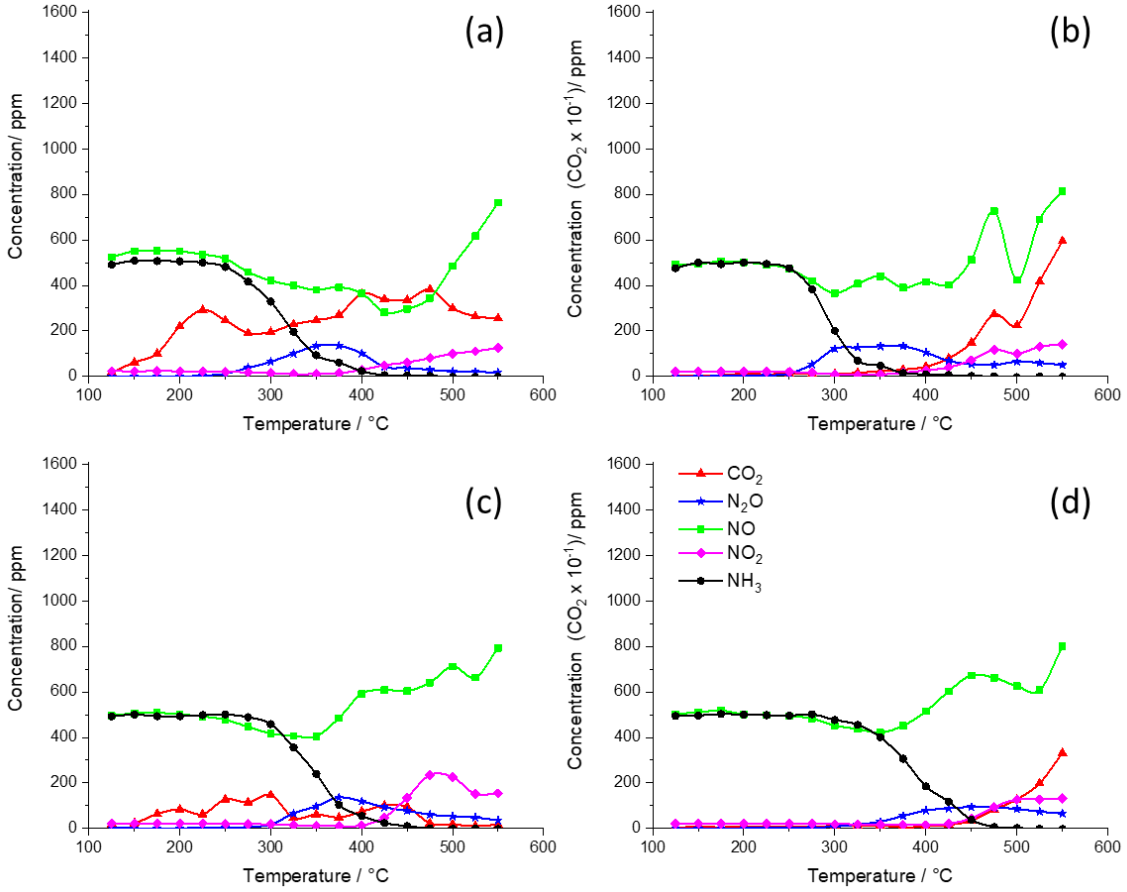

Figure 5.15: Reaction data for copper based catalysts for SCR and the simultaneous removal of soot and NOx. Where (a) 1%Cu-1%Ag/CZA (b) 1%Cu-1%Ag/CZA soot (c) 1%Cu-1%Pd/CZA (d) 1%Cu-1%Pd/CZA + soot. The simulated exhaust gas consisted of 500 ppm NO, 500 ppm NH_3, 8% O_2, with a balance of N_2. The total flow rate was 200 mlmin^{-1}. The temperature was increased in 25°C intervals from 125 to 550°C, the gas concentrations were allowed to stabilise before readings were taken at each temperature. For the SCR reaction 0.25 g of catalyst was used and for the simultaneous reaction 0.25 g catalyst was mixed in a 10:1 ratio by mass with soot.

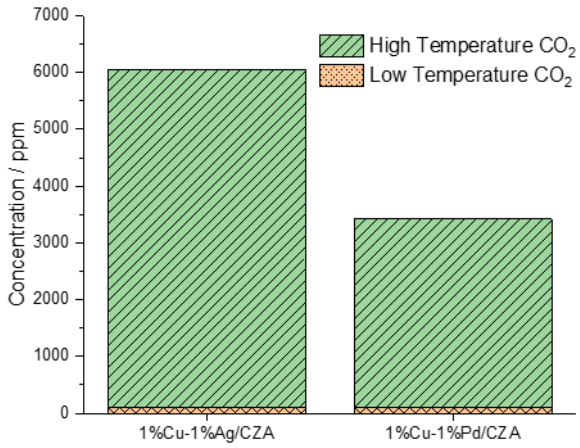

Figure 5.17: The low temperature (300°C) and high temperature (500°C) CO_2 concentrations for 1%Cu-1%Ag/CZA and 1%Cu-1%Pd/CZA

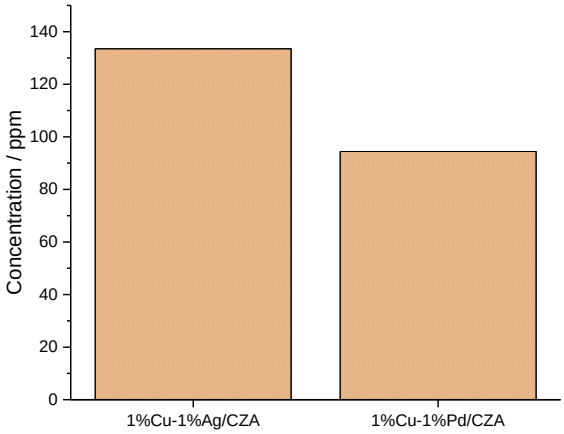

Figure 5.16: The highest concentration of N_2O observed over 21%Cu-1%Ag/CZA and 1%Cu-1%Pd/CZA

5.2.1.7 Comparison of the Catalysts

Over the course of the catalyst performance data discussion, it is clear that the incorporation of Cu into Ag/CZA does not improve the catalyst's ability to simultaneously remove NOx and soot.

With the overall observation from the Cu based catalysts being that they are not suited for the simultaneous removal of NOx and soot.

However, there are distinct differences between the catalysts ranging from their ability to oxidise soot at different temperatures to the amount of N_2O formed. One finding was that a 1w.t.% loading of Ag and Cu is superior to that of a 2w.t.% loading for high temperature soot oxidation. 1%Cu-1%Ag/CZA formed 5947 ppm of CO_2 at 550°C compared to the 4153 ppm formed over 2%Cu-2%Ag/CZA 500°C, a difference of 1794 ppm. However, 2%Cu-2%Ag/CZA 500°C formed less N_2O than 1%Cu-1%Ag/CZA. The catalysts prepared *via* CVI formed the most N_2O of all the catalysts tested.

Despite the Cu catalysts not being suitable for the simultaneous removal of NOx and soot, many of the catalysts investigated in this study showed similar or greater levels of high temperature soot oxidation compared to the Ag/CZA catalyst as shown in Figure 5.18. The figure clearly shows that 2%Cu-2%Ag/CZA (a) was the superior catalyst for high temperature soot oxidation.

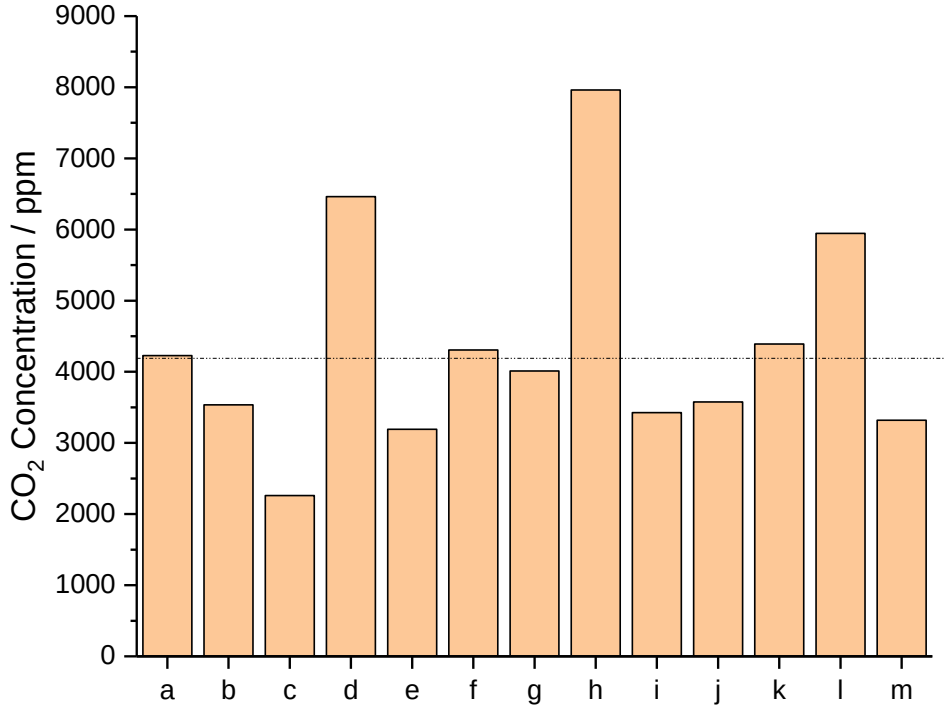

Figure 5.18: Maximum concentration of CO_2 formed where a is Ag/CZA[20], b is 2%Cu/CZA, c is 2%Cu-2%K/CZA, d is 2%Cu-2%Ag/CZA 400°C, e is 2%Cu-2%Ag/CZA 450°C, f is 2%Cu-2%Ag/CZA 500°C, g is 2%Cu-2%Ag/CZA sol immobilisation, h is 2%Cu-2%Ag/CZA (a), i is 2%Cu-2%Ag/CZA (b), j is 2%Cu-2%Ag/CZA CVI, k is 1%Cu-1%Ag/CZA CVI, l is 1%Cu-1%Ag/CZA and m is 1%Cu-1%Pd/CZA

5.2.2 Characterisation

Various characterisation techniques were carried out to provide information about the catalysts' properties.

5.2.2.1 X-ray Diffraction Data

For the purpose of comparison, CZA and 2%Ag/CZA have been included in the XRD analysis. The XRD analysis, Figure 5.19, shows that the catalysts display the clear characteristic diffraction peaks associated with the cubic fluoride phase of ceria. The CZA support shows slight shifts in the CeO_2 peaks compared to pure CeO_2 (28.5°, 33.1°, 47.5° and 56.3° which correspond the to (111), (200), (220) and (311) planes, respectively) [22,23] due to the incorporation of Al_2O_3 and ZrO_2 into the lattice. The CeO_2 peaks are further shifted to a higher Bragg angle when Cu is present in the catalyst, showing that the Cu has been incorporated into the ceria lattice.[24] The typical CeO_2 peaks are observed at 28.4°, 33.0°, 47.3° and 56.0° for the pure CZA support with the Cu catalysts showing a shift to higher angles.

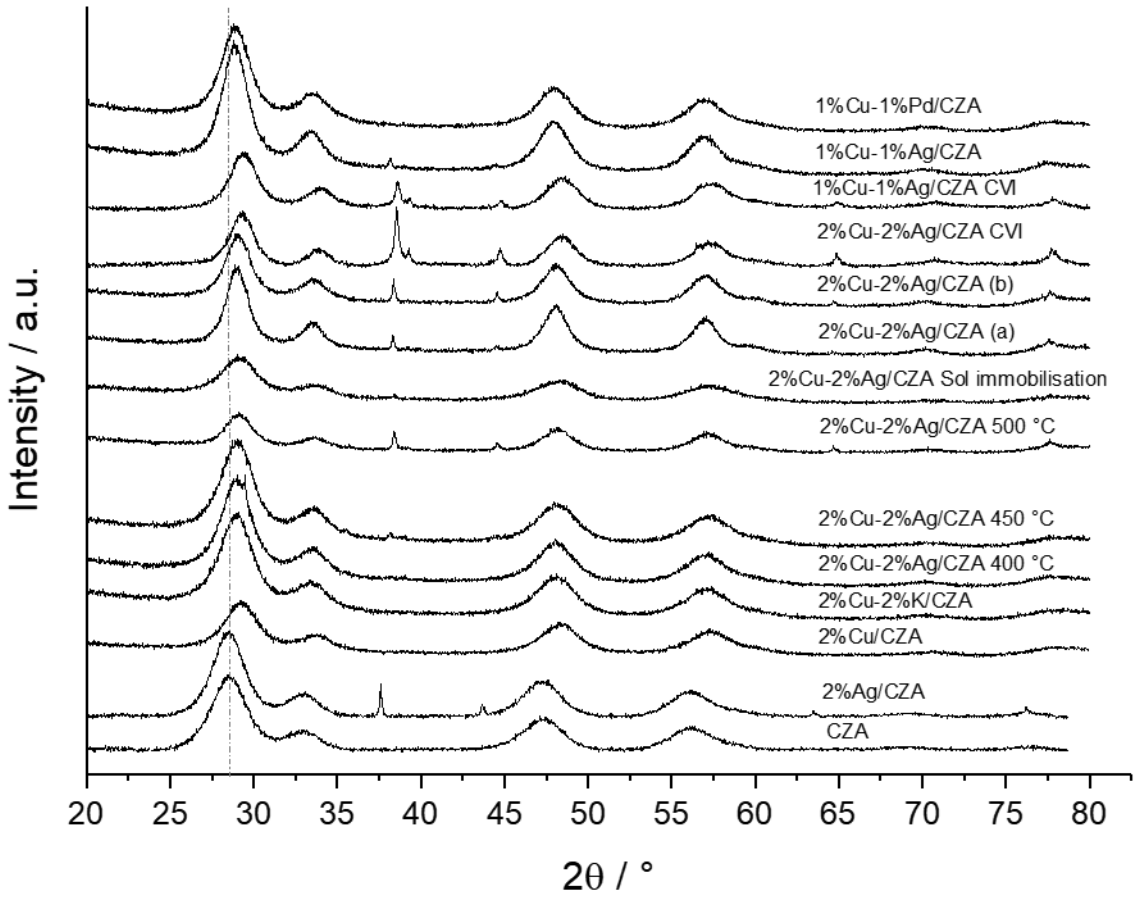

Figure 5.19: X-ray diffraction pattern for Cu based catalysts

Table 5.1 shows the calculated unit cell volumes, using the (111) CeO_2 peak, of CeO_2 for each catalyst. The calculated value for pure CZA was 152.69 $Å^3$, the unit cell volume changes depending on the catalyst. The 2%Cu/CZA, 2%Cu-2%Ag/CZA 450 °C, 2%Cu-2%Ag/CZA 500 °C, 2%Cu-2%Ag/CZA sol immobilisation and 2%Cu-2%Ag/CZA CVI catalysts have a calculated unit cell volume which is less than that of the CZA support. Copper has a lower ionic radius than Ce and O and it is predicted by Vegard's law that substitution of a smaller element into the lattice will result in lattice shrinkage,[25] which is observed over these catalysts. 2%Cu-2%Ag/CZA (b) had a similar unit cell volume (152.03 $Å^3$) to that of CZA suggesting that little/no substitution of Cu into the CeO_2 lattice has taken place. The remaining catalysts showed an increase in unit cell volume which may be a result of Cu entering vacant sites in the lattice and hence increasing the lattice strain. As the same batch of CZA was used for each catalyst the changes in the lattice is not due to differing amounts of ZrO_2 and Al_2O_3 being incorporated into the CeO_2 lattice.

Table 5.1 CeO_2 Information Calculated from XRD analysis

Catalyst	d Spacing [Å]	Peak Position [°]	FWHM	Lattice Parameter, a [Å]	Unit Cell Volume [Å^3]
CZA	3.090	28.91	2.69	5.34	152.69
Ag/CZA	3.090	28.86	2.40	5.35	153.40
2%Cu/CZA	3.044	29.32	0.09	5.27	146.52
2%Cu-2%K/CZA	3.117	28.64	0.47	5.40	157.28
2%Cu-2%Ag/CZA 400 °C	3.094	28.86	0.54	5.36	153.85
2%Cu-2%Ag/CZA 450 °C	3.044	29.34	0.54	5.27	146.55
2%Cu-2%Ag/CZA 500 °C	3.058	29.18	0.09	5.30	148.56
2%Cu-2%Ag/CZA sol immobilisation	3.044	29.32	0.09	5.27	146.52
2%Cu-2%Ag/CZA (a)	3.108	28.73	0.27	5.38	155.96
2%Cu-2%Ag/CZA (b)	3.081	28.98	0.60	5.34	152.03
2%Cu-2%Ag/CZA CVI	3.060	29.18	0.87	5.30	148.94
1%Cu-1%Ag/CZA CVI	3.089	29.31	0.33	5.35	153.13
1%Cu-1%Ag/CZA	3.105	28.76	0.60	5.38	155.49
1%Cu-1%Pd/CZA	3.105	28.75	0.27	5.38	155.59

Some of the catalysts (2%Ag/CZA, 2%Cu-2%Ag/CZA 450 °C, 2%Cu-2%Ag/CZA 500 °C, 2%Cu-2%Ag/CZA (a), 2%Cu-2%Ag/CZA (b) and 1%Cu-1%Ag/CZA) show a peak or peaks at 34 ° and 44 ° due to the presence of crystalline Ag.[26] Table 5.2 shows the calculated crystallite sizes for Ag, Cu and CeO_2 which were calculated from the XRD data using the Scherrer equation. The crystallite sizes vary considerably from catalyst to catalyst. The CeO_2 crystallite size typically fell within the range of 33 – 55 Å with the exception of 2%Cu-2%K/CZA (12 Å) and 2%Cu-2%Ag/CZA 400 °C (122 Å). For the catalysts which the Ag and Cu crystallite sizes could be calculated saw a large range in crystallite sizes. With 2%Cu-2%Ag/CZA 450 °C having a Ag crystallite size of 77 Å and 2%Cu-2%Ag/CZA (a) and (b) having Ag crystallite sizes of > 1000 Å. The Cu crystallite sizes ranged from 117 - >1000 Å.

Table 5.2: Cu, Ag and CeO_2 crystalline sizes calculated from XRD analysis, CeO_2 defect ratio and CeO_2 FWHM calculated from Raman Spectroscopy and the catalytic surface area from B.E.T analysis for each catalyst

Catalyst	Cu Crystallite size [Å]	Ag Crystallite size [Å]	CeO_2 Crystallite size [Å]	CeO_2 Defect Ratio	CeO_2 FWHM	Catalyst Surface Area [m^2g^{-1}]
CZA	-	-	27	0.032	45.52	105
2%Cu/CZA	-	-	47	0.064	52.91	71
2%Cu-2%K/CZA	-	-	12	0.23	45.50	67
2%Cu-2%Ag/CZA 400 °C	-	-	222	0.14	48.50	61
2%Cu-2%Ag/CZA 450 °C	-	77	36	0.12	54.0	79
2%Cu-2%Ag/CZA 500 °C	117	948	46	0.19	40.12	44
2%Cu-2%Ag/CZA sol immobilisation	-	506	33	0.031	41.07	91
2%Cu-2%Ag/CZA (a)	-	1222	55	0.30	36.22	27
2%Cu-2%Ag/CZA (b)	1655	3673	48	0.42	39.23	35
2%Cu-2%Ag/CZA CVI	651	501	49	-	-	52
1%Cu-1%Ag/CZA CVI	214	306	55	-	-	55
1%Cu-1%Ag/CZA	-	971	51	0.17	44.14	40
1%Cu-1%Pd/CZA	-	-	45	0.12	45.57	58

5.2.2.2 BET Analysis

Table 5.2 shows the surface areas for the Cu catalysts. The surface areas, from BET analysis also have a wide range across the catalysts without a discernible pattern. Ranging from 22 $m^2\ g^{-1}$ (2%Cu-2%Ag/CZA (a)) – 91 $m^2\ g^{-1}$ (2%Cu-2%Ag/CZA sol immobilisation). There is also little correlation between the catalysts' surface area and crystallite size. It would be expected to see a pattern where the smaller the crystallite size the greater the surface area as shown by the high surface area and low CeO_2 crystalline size of the CZA support.

5.2.2.3 Raman Spectroscopy

Table 5.2, shows the CeO_2 defect ratios calculated from the Raman data. Excluding the sol immobilisation catalyst, all the catalysts show clear CeO_2 peaks in the Raman spectra[27] (Figure 5.20). There is no Raman data available for catalysts prepared *via* CVI as the catalysts were too dark in colour for analysis.[28] Table 5.2 also shows the FWHM values for the CeO_2 peak for each

catalyst. The FWHM value for CZA is 45.52 higher FWHM values were observed for 2%Cu/CZA, 2%Cu-2%Ag/CZA 400°C and 2%Cu-2%Ag/CZA 450 °C. Whilst, 2%Cu-2%K/CZA, 1%Cu-1%Ag/CZA and 1%Cu-1%Pd/CZA had similar FWHM values to CZA. An increase in the CeO_2 FWHM value can correlate to smaller crystallite sizes.[29]However, from the XRD analysis this is not the case for these catalysts with all of them having greater calculated CeO_2 crystallite sizes than CZA. The increase in FWHM values therefore suggests increased defects in the catalysts.[30] With the remaining catalysts having lower values which would suggest that these catalysts have larger crystallite sizes than the CZA support. This supported by the crystallite sizes calculated from the XRD data with the catalysts with lower Raman FWHMs having larger crystallite sizes.

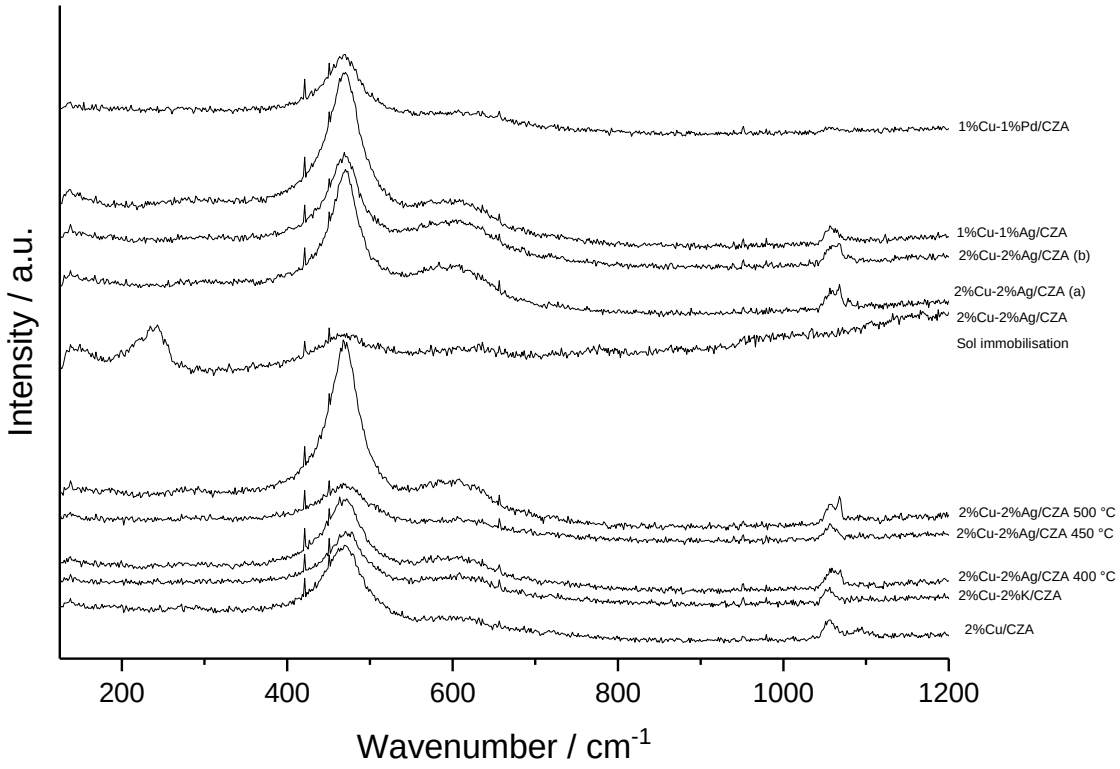

Figure 5.20: Raman data for the Cu based catalysts. There is no Raman spectra for the catalysts prepared *via* CVI as the samples were too dark for analysis

The sol immobilisation catalyst shows less intense CeO_2 peaks, as well as an additional peak at 243 cm^{-1} which indicates the presence of CuO.[31] The presence of CuO in the sol immobilisation catalyst is also detected by XPS analysis, Section 5.2.2.4. The presence of CuO in the catalyst is of particular note as CuO catalyses the oxidation of NH_3 opposed to the desired SCR reaction. This helps to explain why the catalyst is poor at reducing NO.

5.2.2.4 XPS Analysis

XPS analysis confirms the presence of CuO due to the satellite peaks observed at 943 eV and 962 eV in addition to the Cu^0 peaks at 934 eV and 954 eV[32,33] (Figure 5.21). From the XPS analysis it can be determined that the majority of Cu present in the sol immobilisation catalyst is in the form of CuO with remainder as Cu^0. The XPS analysis shows that the $Cu2p_{1/2}$ peak at 954 eV and Cu^{2+} satellite peak at 962 eV are present for the 2%Cu-2%Ag/CZA 400 °C, 450 °C and 500 °C catalysts. This suggests that for these catalysts the majority of the Cu is in the form of Cu^0 with the rest being CuO (Cu^{2+}). XPS analysis does not show clear Ag peaks for the sol immobilisation catalyst but distinct Ag peaks may be observed for the 2%Cu-2%Ag/CZA 400 °C, 450 °C and 500 °C catalysts at 368 and 374 eV[34], Figure 5.22. The full elemental percentage breakdown for these four catalysts is shown in Table 5.3. The atomic percentage of Ag for the sol immobilisation catalyst is very low (0.07 %) explaining why the Ag cannot be easily observed in the XPS spectra, XRD pattern or Raman spectra.

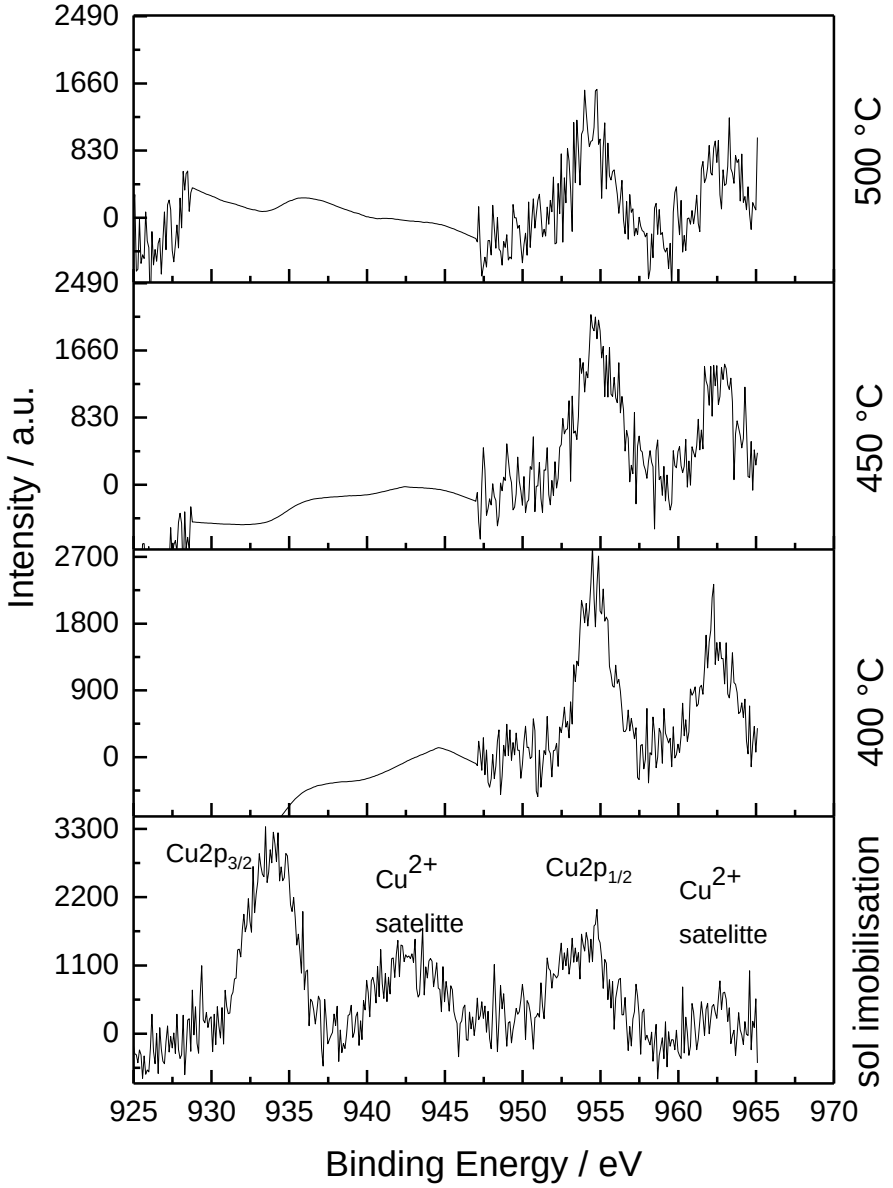

Figure 5.21: XPS spectra for Cu regions for 2%Cu-2%Ag/CZA 500 °C, 450 °C, 400 °C and sol immobilisation

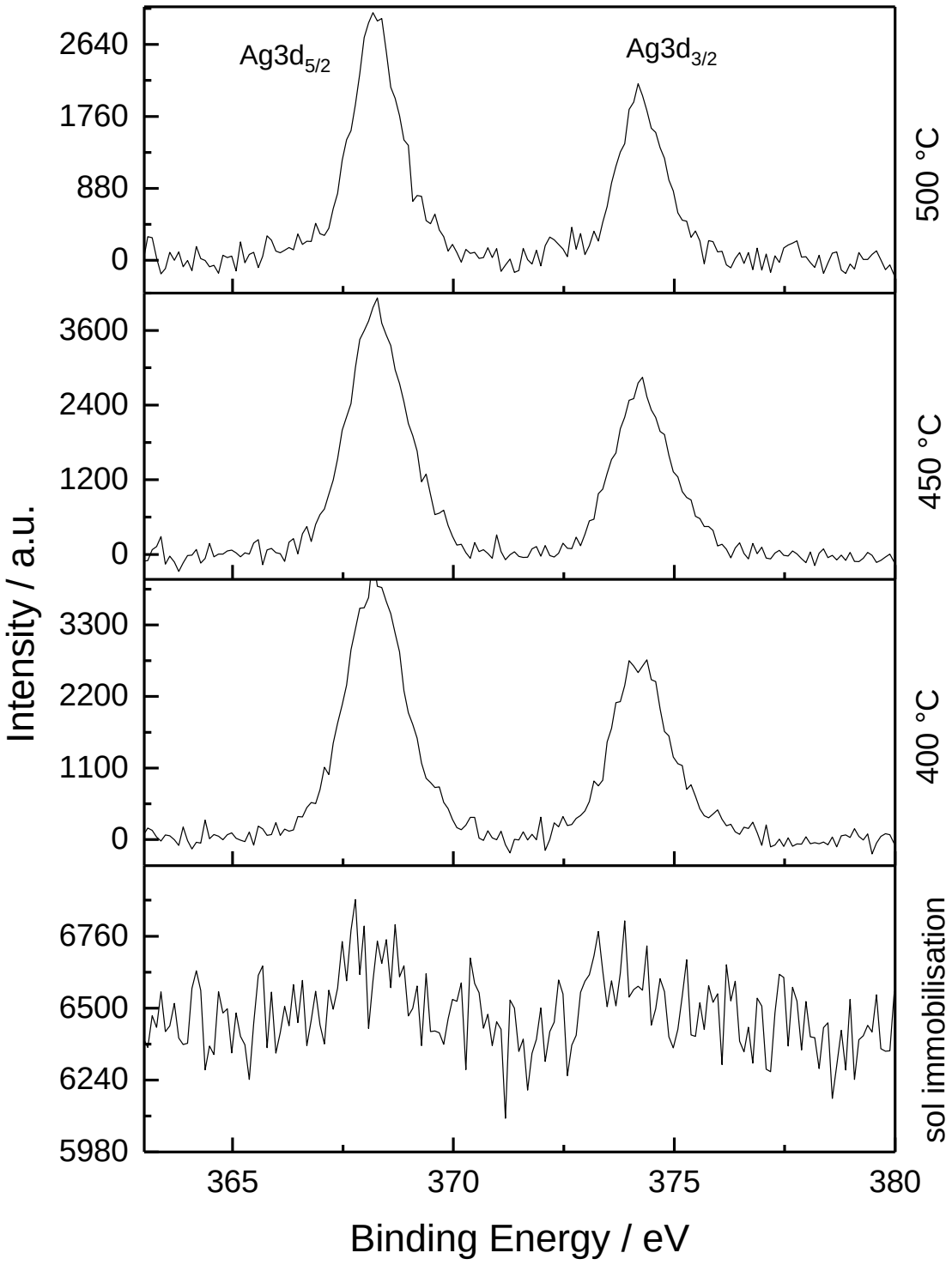

Figure 5.22: XPS spectra for Ag regions for 2%Cu-2%Ag/CZA 500 °C, 450 °C, 400 °C and sol immobilisation

Table 5.3: Atomic percentage of elements present in catalysts calculated from XPS data

Catalyst	Ag	C	Ce	Cu	Al	N	Na	O	Zr
400°C	0.73	5.22	4.80	3.67	17.86	1.22	8.40	55.83	2.26
450°C	0.61	4.48	3.63	2.77	22.29	0.65	9.00	55.83	1.73
500°C	0.35	4.77	4.56	1.45	16.87	1.46	14.16	55.03	1.35
Sol Immobilisation	0.07	7.6	6.71	2.96	17.17	-	1.92	61.04	2.53

The XPS analysis determined that CuO was present in the 2%Cu-2%Ag/CZA 400 °C, 450 °C, 500 °C and sol immobilisation catalysts. It is known that CuO catalyses the oxidation of NH_3 rather than Cu^0, which facilitates the SCR reaction. This helps to explain why the catalysts were poor catalysts for both the SCR reaction and for the simultaneous removal of NOx and soot. In the preparation of the sol immobilisation catalyst, it proved difficult to reduce the Cu precursor resulting in the high levels of CuO present in the catalyst, which consequently resulted in poor catalytic activity.

5.2.2.5 SEM-EDX Analysis

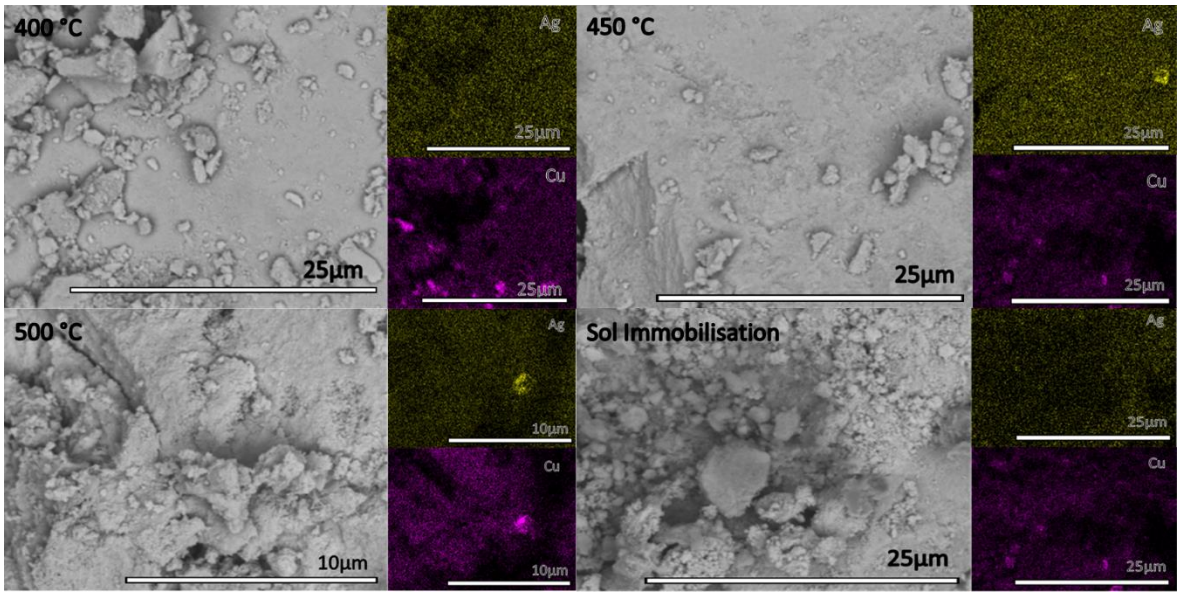

Figure 5.23: SEM-EDX images for 2%Cu-2%Ag/CZA 400 °C, 450 °C, 500 °C and sol immobilisation catalysts

SEM-EDX analysis was carried out on the 2%Cu-2%Ag/CZA 400 °C, 450 °C, 500 °C and sol immobilisation catalysts (Figure 5.23). The only catalyst to display Cu nanoparticles was 2%Cu-

2%Ag/CZA 400 °C. Across all four samples larger particles of Cu were identified with some areas of the 450 and 500 °C catalysts containing large particles of Ag mixed with the Cu.

Ag particles were significantly harder to find than the Cu particles with the 400 °C and sol immobilisation catalysts not displaying any Ag particles. The 450 °C and 500 °C showed some Ag particles however these particles were rare across the surface of the sample. The lack of Ag particles from the sol immobilisation catalyst supports the findings from the XPS analysis however from the XRD analysis it was possible to calculate that the catalyst had a Ag crystallite size of 506 Å. These inconsistencies over the catalyst is due to only a small section of the surface being imaged, therefore the images do not show the full story of the catalyst. From the XRD analysis it is known that large particles of Ag are present in the catalyst hence it is likely that these large particles are dispersed over the catalytic surface.

From the SEM-EDX analysis it appears that Ag and Cu did not form an alloy for these four catalysts. For an alloy to form higher calcination temperatures or stronger reducing agents would be required during the catalyst preparation.

5.3 Conclusions

Despite various preparation methods and calcination conditions, not one of the tested catalysts showed potential for catalysing the simultaneous removal of NOx and soot from a diesel exhaust. The majority of the catalysts only showed soot oxidation at high temperatures and showed a peak of the undesirable N_2O. Furthermore, no catalyst selectively catalytically reduced NO using NH_3 instead the undesirable nonselective SCR reaction dominated at low temperatures and at higher temperatures the oxidation of NH_3 to NO and NO_2 became predominant.

One explanation for the poor affinity of the catalysts towards the SCR reaction is that CuO was present in the catalysts (2%Cu-2%Ag/CZA 400°C, 450°C, 500°C and sol immobilisation) and CuO is known to catalyse the oxidation of NH_3 to NO. The desired Cu^0 was either present in too little quantity, or not at all, which resulted in poor SCR across the catalysts tested. Therefore, to improve catalytic activity the Cu needs to be reduced from the precursor to Cu^0 this could be achieved by using higher calcination temperatures[35] or by using stronger reducing agents during the catalyst preparation. Teichert *et al.* found that when using $CuNO_3$ as a precursor Cu_2O and CuO were formed unless a high temperature were used which resulted in the formation of Cu^0.[35]

Despite being poor SCR catalysts the presence of Cu in the catalysts improved the ability of the Ag/CZA catalyst to oxidise soot especially at high temperatures. The Ag/CZA catalyst formed 4250 ppm at 550°C whilst some of the catalysts investigated in this chapter formed considerably

higher quantities of CO_2, with 2%Cu-2%Ag/CZA (a) (7961 ppm of CO_2 at 550°C) being the superior catalyst for high temperature soot oxidation.

The effect of calcination temperature was investigated for 2%Cu-2%Ag/CZA catalysts. It was found that the lower temperature investigated (400°C) was superior to the higher calcination temperatures for high temperature soot oxidation, but that calcination temperature did not affect the catalyst's ability to undergo low temperature soot oxidation. However, the catalyst calcined at 500°C formed the least amount of undesired N_2O.

It was found that using a weight loading of 1%Cu-1%Ag/CZA opposed to 2%Cu-2%Ag/CZA resulted in greater formation of high temperature CO_2, but did form slightly more N_2O. When the catalysts were prepared *via* CVI it was also found that 1%w.t. was better for catalysing soot oxidation. Replacing Ag with Pd, was shown to be less effective as a soot oxidation catalyst, but neither hindered nor improved the catalyst's ability to reduce NOx.

In this chapter, it was found that 2%Cu/CZA was superior to 2%Cu-2%K/CZA for the oxidation of soot – this was a surprising result as K is a well-known soot oxidation enhancer. Throughout the chapter the presence of Cu, in addition to the Ag, enhanced the soot oxidation considerably.

In conclusion, the Cu-Ag catalysts prepared in this chapter show interesting properties with regards to soot oxidation, however, they have no potential for catalysing the simultaneous removal of NOx and soot from a diesel exhaust gas.

5.4 Future Work

Characterisation of the catalysts was limited due to equipment limitations as a result of COVID-19, however, in the future XPS analysis of all the catalysts could prove interesting. Especially, with regards to the oxidation state of Cu in the catalysts. If the currently uncharacterised catalysts show high percentages of CuO over Cu^0 it would help to rationalise why the catalysts were poor at reducing NO. TPR (Temperature Programmed Reduction) could also be used to determine whether the Cu species are in the correct oxidation state. Furthermore, as discussed in the previous section, if the catalysts were prepared at higher calcination temperatures or using stronger reducing agents then the Cu would be in the Cu^0 form. It would be interesting to see if when the copper is in the form of Cu^0 where the catalysts have the ability to reduce NOx. Using higher calcination temperatures could also result in the Ag and Cu forming an alloy.

Another avenue which could be explored is incorporating the Ag onto a zeolite support. Ag zeolites have been found to be capable of catalysing the SCR reaction[36–38] but have not been

tested for the combustion of soot. Zeolites provide a high surface area support with pores which facilitates gas flow to the active sites. A Ag catalyst supported on a zeolite could enhance the reduction of NOx compared to Ag on the CZA support. However, in the presence of soot the zeolite pores could become blocked and hence deactivate the catalyst.[39]

The combination of Cu and Ag did not result in an active catalyst for the desired reaction however that does not rule out a different secondary metal being able to enhance the reaction. Therefore, Chapter 6 continues the investigation into the use of a secondary metal to enhance the Ag/CZA catalyst for the simultaneous removal of NOx and soot by researching different metals for the reaction.

5.5 References

1 R. Daya, C. J. Keturakis, D. Trandal, A. Kumar, S. Y. Joshi and A. Yezerets, *React. Chem. Eng.*, , DOI:10.1039/D1RE00041A.

2 K. Hirata, N. Masaki, H. Ueno and H. Akagawa, in *SAE Technical Papers*, SAE International, 2005.

3 Milestone to Clean Diesel Engines, https://www.basf.com/gb/en/who-we-are/innovation/our-innovations/copper-chabazite.html, (accessed 24 May 2021).

4 Y. Shan, J. Du, Y. Zhang, W. Shan, X. Shi, Y. Yu, R. Zhang, X. Meng, F.-S. Xiao and H. He, *Natl. Sci. Rev.*, 2021, **8**, 2021.

5 L. Ma, Y. Cheng, G. Cavataio, R. W. McCabe, L. Fu and J. Li, *Chem. Eng. J.*, 2013, **225**, 323–330.

6 J. H. Kwak, R. G. Tonkyn, D. H. Kim, J. Szanyi and C. H. F. Peden, *J. Catal.*, 2010, **275**, 187–190.

7 S. S. R. Putluru, L. Schill, A. D. Jensen and R. S. N. Fehrmann, *J. Chem.*, , DOI:10.1155/2018/8614747.

8 J. H. Kwak, D. Tran, S. D. Burton, J. Szanyi, J. H. Lee and C. H. F. Peden, *J. Catal.*, 2012, **287**, 203–209.

9 Y. Shan, W. Shan, X. Shi, J. Du, Y. Yu and H. He, *Appl. Catal. B Environ.*, 2020, **264**, 118511.

10 T. Usui, Z. Liu, S. Ibe, J. Zhu, C. Anand, H. Igarashi, N. Onaya, Y. Sasaki, Y. Shiramata, T. Kusamoto and T. Wakihara, *ACS Catal.*, 2018, **8**, 9165–9173.

11 M. Valdez Lancinha Pereira, A. Nicolle and D. Berthout, *Catal. Today*, 2015, **258**, 424–431.

12 Y. Cheng, C. Lambert, D. H. Kim, J. H. Kwak, S. J. Cho and C. H. F. Peden, in *Catalysis Today*, Elsevier, 2010, vol. 151, pp. 266–270.

13 J. Luo, D. Wang, A. Kumar, J. Li, K. Kamasamudram, N. Currier and A. Yezerets, *Catal. Today*, 2016, **267**, 3–9.

14 H. Jiang, B. Guan, X. Peng, Y. Wei, R. Zhan, H. Lin and Z. Huang, *Chem. Eng. Sci.*, 2020, **226**, 115855.

15 L. Olsson, K. Wijayanti, K. Leistner, A. Kumar, S. Y. Joshi, K. Kamasamudram, N. W. Currier and A. Yezerets, *Appl. Catal. B Environ.*, 2016, **183**, 394–406.

16 S. Mohan, P. Dinesha and S. Kumar, *Chem. Eng. J.*, 2020, 384.

17 D. W. Fickel, E. D'Addio, J. A. Lauterbach and R. F. Lobo, *Appl. Catal. B Environ.*, 2011, **102**, 441–448.

18 J. Tang, M. Xu, T. Yu, H. Ma, M. Shen and J. Wang, *Chem. Eng. Sci.*, 2017, **168**, 414–422.

19 I. Song, H. Lee, S. W. Jeon, I. A. M. Ibrahim, J. Kim, Y. Byun, D. J. Koh, J. W. Han and D. H. Kim, *Nat. Commun.*, 2021, **12**, 1–9.

20 C. Davies, K. Thompson, A. Cooper, S. Golunski, S. H. Taylor, M. Bogarra Macias, O. Doustdar and A. Tsolakis, *Appl. Catal. B Environ.*, 2018, **239**, 10–15.

21 A. Cooper, T. E. Davies, D. J. Morgan, S. Golunski and S. H. Taylor, *Catalysts*, 2020, **10**, 294.

22 D. Parimi, V. Sundararajan, O. Sadak, S. Gunasekaran, ⊥ Sahabudeen, S. Mohideen and A. Sundaramurthy, , DOI:10.1021/acsomega.8b02747.

23 A. A. Aboud, H. Al-Kelesh, W. M. A. E. Rouby, A. A. Farghali, A. Hamdedein and M. H. Khedr, *J. Mater. Res. Technol.*, 2018, **7**, 14–20.

24 H. Zhu, Y. Chen, Z. Wang, W. Liu and L. Wang, *RSC Adv.*, 2018, **8**, 14888–14897.

25 A. R. Denton and N. W. Ashcroft, *Phys. Rev. A*, 1991, **43**, 3161.

26 J. D. Grunwaldt, F. Atamny, U. Göbel and A. Baiker, *Appl. Surf. Sci.*, 1996, **99**, 353–359.

27 X. M. Lin, L. P. Li, G. S. Li and W. H. Su, *Mater. Chem. Phys.*, 2001, **69**, 236–240.

28 Y. Wang, T. Mu, Y. Li, W. Qi and S. Chen, *Anal. Lett.*, 2021, **54**, 2423–2430.

29 J. E. Spanier, R. D. Robinson, F. Zhang, S.-W. Chan and I. P. Herman, *Phys. Rev. B*, 2001, **64**, 245407.

30 I. Kosacki, T. Suzuki, H. U. Anderson and P. Colomban, *Solid State Ionics*, 2002, **149**, 99–105.

31 X. Q. Xu, J. F. , Ji, W., Shen, Z. X. , Li, W. S., Tang, S. H., Ye, X. R. Jia, D. Z., Xin, *J. Raman Spectrosc.*, 1999, **30**, 413–415.

32 T. Ghodselahi, M. A. Vesaghi, A. Shafiekhani, A. Baghizadeh and M. Lameii, *Appl. Surf. Sci.*, 2008, **255**, 2730–2734.

33 T. M. Ivanova, K. I. Maslakov, A. A. Sidorov, M. A. Kiskin, R. V. Linko, S. V. Savilov, V. V. Lunin and I. L. Eremenko, *J. Electron Spectros. Relat. Phenomena*, 2020, **238**, 146878.

34 U. Kiran John, R. J. Peechat and S. Mathew, in *Materials Today: Proceedings*, Elsevier Ltd, 2019, vol. 33, pp. 1263–1267.

35 Johannes Teichert, Thomas Doert and Michael Ruck, *Dalt. Trans.*, 2018, **47**, 14085–14093.

36 J. Shibata, Y. Takada, A. Shichi, S. Satokawa, A. Satsuma and T. Hattori, *Appl. Catal. B Environ.*, 2004, **54**, 137–144.

37 K. Rahkamaa-Tolonen, T. Maunula, M. Lomma, M. Huuhtanen and R. L. Keiski, *Catal. Today*, 2005, **100**, 217–222.

38 K. Góra-Marek, K. A. Tarach, Z. Piwowarska, M. Łaniecki and L. Chmielarz, *Catal. Sci. Technol.*, 2016, **6**, 1651–1660.

39 E. Tronconi, I. Nova, F. Marchitti, G. Koltsakis, D. Karamitros, B. Maletic, N. Markert, D. Chatterjee and M. Hehle, *Emiss. Control Sci. Technol.*, 2015, **1**, 134–151.

6. A Study into Silver Bimetallic Catalysts for the Simultaneous Removal of NOx and Soot from a Diesel Exhaust

6.1 Introduction

The focus of this thesis has been to improve upon a Ag/CZA catalyst for the simultaneous removal of NOx and soot,[1] whilst also reducing the amount of N_2O formed as a by-product of the SCR reaction. Chapter 3 investigated the effect of preparation method on the catalyst as well as introducing K into the catalyst, Chapter 4 the effect of K weight loading and Chapter 5 the effect of incorporating Cu into the system. This final chapter continues the investigation by incorporating a range of elements into the Ag/CZA and Ag-K/CZA catalysts, in an attempt to enhance NOx reduction and soot oxidation. The M-Ag and M-Ag-K catalysts (where M represents a secondary metal) will be compared against the Ag/CZA catalyst (Figure 6.1).[1]

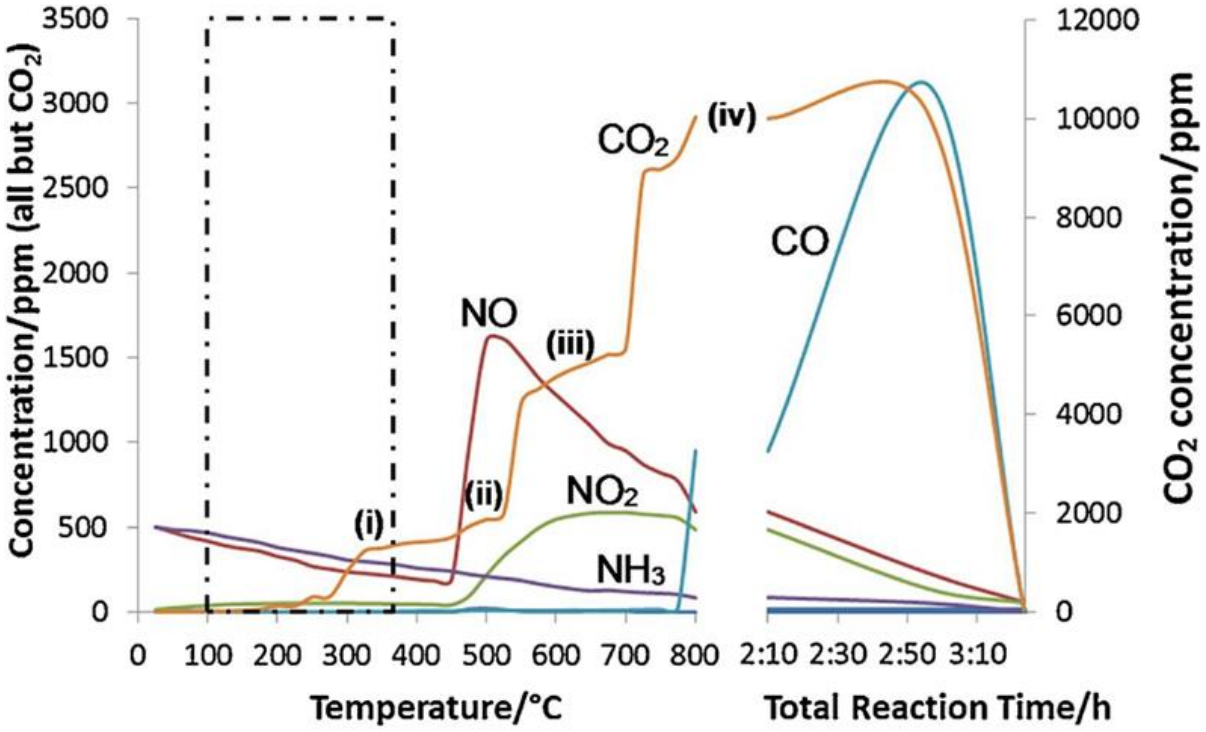

Figure 6.1: The simultaneous removal of NOx and soot over Ag/CZA[1]. The simulated exhaust gas consisted of 500 ppm NO, 500 ppm NH_3, 8% O_2, with a balance of N_2. The total flow rate was 200 $mlmin^{-1}$. The temperature was increased in 25°C intervals from 125 to 900°C, the gas concentrations were allowed to stabilise before readings were taken at each temperature. 0.25 g catalyst was mixed in a 10:1 ratio by mass with soot.

The platinum group metals (PGMs) which were added were Pt, Pd and Rh, all three metals are commonly used in aftertreatment systems,[2] however, as they are expensive metals the industry is trying to find cheaper alternatives. Lietti *et al.* found that Pt-Ba/Al_2O_3 showed the ability to simultaneously remove NOx and soot, whilst Pt/Al_2O_3 was able to oxidise soot but was poor at reducing NOx[3]. Lietti also found that for the same reaction, Pt-K/Al_2O_3 showed a decrease in NOx storage in the presence of soot, a consequence of competition between K and soot sites.[4] Rh/CeO_2 and Rh/La_2O_3 catalysts have been shown to be active for soot oxidation[5,6] and Rh based catalysts have been shown to be effective for the decomposition of N_2O.[7,8]

The non-PGMs which were investigated were Co, Mn, Ba, La, Sr, Ni and Fe. These 7 metals have been previously researched for their ability to facilitate either soot oxidation, NOx reduction and/or the simultaneous removal of NOx and soot.

NOx traps are a type of NOx aftertreatment system, which are typically comprised of Pt or Rh and BaO supported on Al_2O_3.[9–11] NOx traps work by the precious metal oxidising NO to NO_2, which is then stored as nitrates or nitrites by the BaO. The stored NOx is later released and reduced to N_2.

Co, Ni and Fe have been shown to be active for NO decomposition, with Co being the most active catalyst.[12,13] Co doped with Ag or Na results in increased catalytic activity,[14] as a result of increasing the surface electron density.[15] Perovskite-type catalysts have also been researched for NO decomposition, where the catalysts have an ABO_3 chemical composition. The A cation is a rare earth metal or belongs to group 2, *i.e.*, La, Sr, Ba etc. and B is a transition metal.[16]

Zeolite based catalysts containing La, Mn, Co and Fe have been researched for the simultaneous removal of NOx and soot.[17,18] Nanostructured perovskite-type lanthanum ferrites have shown affinity for the simultaneous reaction within the temperature range of 350 – 450 °C.[19]

6.2 Results

The results are split into two sections, 6.2.1 and 6.2.3, which discuss the catalytic performance data and the characterisation of the catalysts, respectively.

6.2.1 Catalyst Performance Data

The reaction data for the simultaneous removal of NOx and soot over each catalyst are presented below.

6.2.1.1 Co based Catalysts

Figure 6.2a and b shows the reaction data for the simultaneous removal of NOx and soot over Ag-Co/CZA and Ag-Co-K/CZA, respectively. Ag-Co/CZA is shown to be a poor SCR catalyst with poor reduction of NO throughout the reaction temperature range. This catalyst is also poor at oxidising soot, it forms the least amount of CO_2 (339 ppm) of all the catalysts in this chapter. N_2O is observed from 300°C onwards and NO_2 from 400°C.

The formation of CO_2 over Co-Ag-K/CZA is a complete contrast to Co-Ag/CZA. CO_2 is first observed at 375°C and rises dramatically with increase in temperature reaching 6990 ppm at 550°C, which is several thousand ppm higher than over the standard Ag/CZA catalyst. However, undesirable N_2O is observed between 275 - 550°C. NO and NO_2 concentrations begin to rise from 375°C and continue to rise with temperature. The high levels of NO at high temperature is considerably higher than levels over Co-Ag/CZA (346 ppm higher at 550°C).

The presence of K in the Co-Ag/CZA catalyst has been found to enhance the high temperature soot oxidation, but it did not improve the catalyst's ability to reduce NOx.

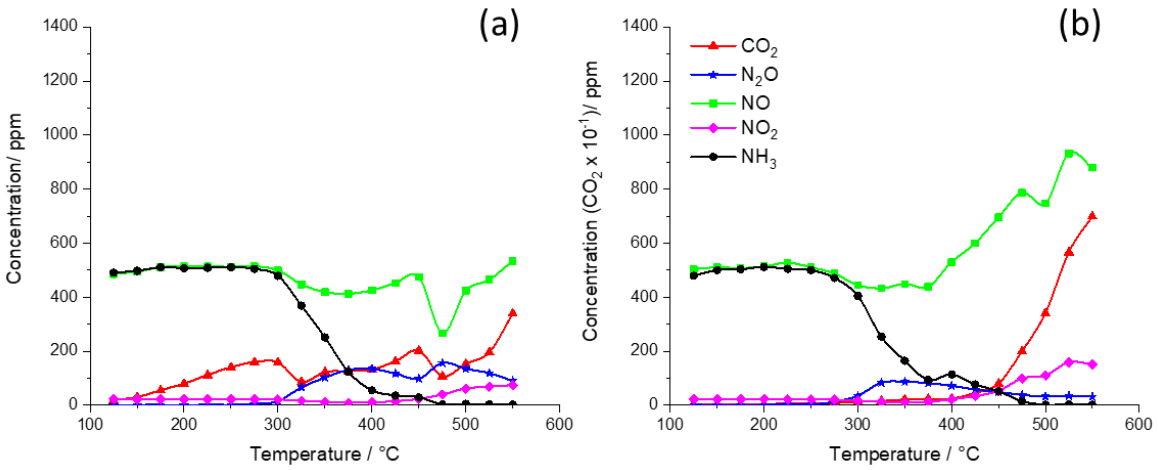

Figure 6.2: Performance data for the simultaneous removal of NOx and soot over (a) Co-Ag/CZA and (b) Co-Ag-K/CZA. The simulated exhaust gas consisted of 500 ppm NO, 500 ppm NH_3, 8% O_2, with a balance of N_2. The total flow rate was 200 mlmin^{-1}. The temperature was increased in 25°C intervals from 125 to 550°C, the gas concentrations were allowed to stabilise before readings were taken at each temperature 0.25 g catalyst was mixed in a 10:1 ratio by mass with soot.

6.2.1.2 Mn based Catalysts

Figure 6.3 shows the catalyst performance data for the simultaneous removal of NOx and soot over Mn-Ag/CZA and Mn-Ag-K/CZA. Mn-Ag/CZA is active for SCR between 175 °C – 300 °C, as shown by simultaneous decrease in NO and NH_3. After 300°C, the NH_3 concentration continues to

decrease until reaching 0 ppm at 475 °C, whilst the concentration of NO fluctuates, ultimately reaching 700 ppm at 550°C. N_2O is observed between 275 °C - 550 °C. At 450 °C NO_2 is observed and increases in concentration with temperature. CO_2 is first observed at 375 °C and continues to increase in concentration with temperature reaching 2120 ppm at 550°C, this is half the amount of CO_2 formed over Ag/CZA.

Mn-Ag-K/CZA is active for the selective catalytic reduction of NO by NH_3 between 125 – 350°C with NO reaching 291 ppm at 350°C. This is a very similar concentration as observed over Ag/CZA (250 ppm at 350°C). The NO concentration rises at temperatures > 350°C, whilst over the Ag/CZA catalyst the increase in NO concentration does not start until 450°C. The NH_3 concentration reached 0 ppm at 425°C, which is lower than both Mn-Ag/CZA and Ag/CZA. There is a small peak of N_2O (32 ppm) at 325°C, at 375°C the concentration begins to rise but only to a maximum of 82 ppm (475°C). NO_2 is first detected at 325°C and rises with temperature. The concentration of NO_2 is higher over Mn-Ag-K/CZA compared to Mn-Ag/CZA. Soot oxidation is more prevalent at higher temperatures (> 350°C) reaching its peak at 525°C (3993 ppm) this value is similar to that of Ag/CZA (4228 ppm). A small quantity of CO is observed from 275°C, the formation of CO is highly undesirable especially for automotive catalysts.

Mn-Ag-K/CZA is a superior catalyst to Mn-Ag/CZA for the simultaneous removal of NOx and soot, as it reduces NO over a larger temperature window and oxidises more soot. Mn-Ag-K/CZA performs comparably to Ag/CZA with regards to the reduction of NO and the oxidation of soot at high temperatures. However, Mn-Ag-K/CZA forms N_2O and CO, which is not the case over Ag/CZA. Furthermore, Ag/CZA oxidises soot at low temperatures (< 300°C) to a much higher degree than Mn-Ag-K/CZA.

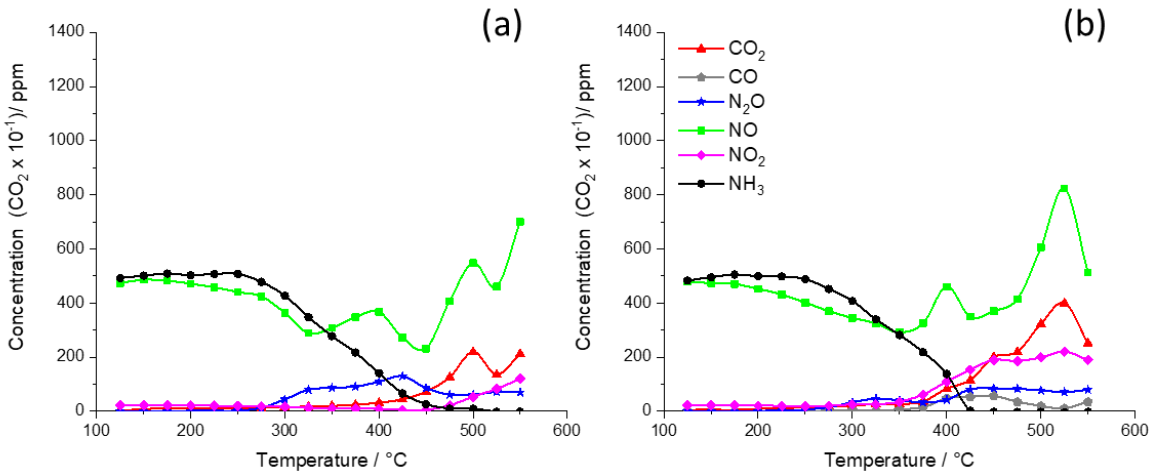

Figure 6.3: Performance data for the simultaneous removal of NOx and soot over (a) Mn-Ag/CZA and (b) Mn-Ag-K/CZA. The simulated exhaust gas consisted of 500 ppm NO, 500 ppm NH_3, 8% O_2, with a balance of N_2. The total flow rate was 200 mlmin^{-1}. The temperature was increased in 25°C intervals from 125 to 550°C, the gas concentrations were allowed to stabilise before readings were taken at each temperature 0.25 g catalyst was mixed in a 10:1 ratio by mass with soot.

6.2.1.3 Ba based Catalysts

The reaction data for Ba-Ag/CZA and Ba-Ag-K/CZA are shown in Figure 6.4.

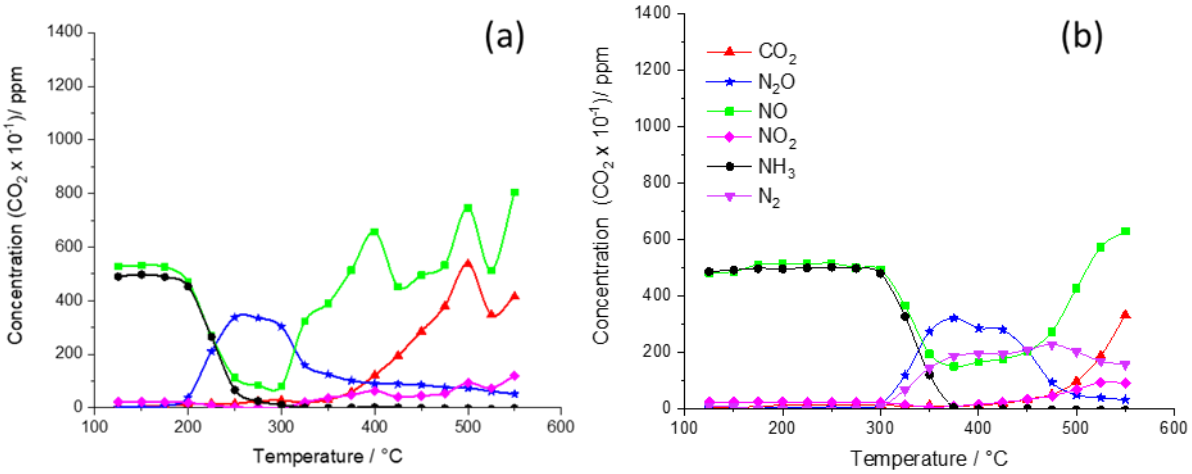

Figure 6.4: Performance data for the simultaneous removal of NOx and soot over (a) Ba-Ag/CZA and (b) Ba-Ag-K/CZA. The simulated exhaust gas consisted of 500 ppm NO, 500 ppm NH_3, 8% O_2, with a balance of N_2. The total flow rate was 200 mlmin^{-1}. The temperature was increased in 25°C intervals from 125 to 550°C, the gas concentrations were allowed to stabilise before readings were taken at each temperature 0.25 g catalyst was mixed in a 10:1 ratio by mass with soot.

Over Ba-Ag/CZA, the concentrations of NO and NH_3 remain close to their starting concentrations until 200°C, at which point they decrease in concentration. NH_3 reaches 0 ppm by 300°C. Despite NO and NH_3 decreasing in concentration at the same rate the selective catalytic

reduction of NO by NH_3 is not observed over this catalyst. The inverse peak of NO is mirrored by a peak in N_2O between 200 – 375°C. The N_2O peak reaches its maximum concentration (335 ppm) at 275°C, after which it begins to decrease in concentration, at temperatures > 375°C N_2O is present but in low concentrations. At temperatures above 300°C the NO concentration rises with temperature but fluctuates between 375 – 550°C. At 550°C the NO concentration was 803 ppm. CO_2 concentrations increase with temperature, reaching 5366 ppm at 500°C, at temperatures above this the concentration decreases. This level of soot oxidation is superior to that seen over the Ag/CZA catalyst.

Over Ba-Ag-K/CZA, NO and NH_3 remained at 500 ppm until 300°C at which point the NH_3 concentration decreases rapidly reaching 0 ppm at 375°C. The concentration of NO also appears to decrease rapidly, and this is due to the non-selective SCR reaction taking place. Between 300 – 550°C there is a large peak of N_2O which is mirrored by an inverse peak of NO. CO_2 and NO_2 begin to increase in concentration with temperature from 400 °C with CO_2 reaching a concentration of 3306 ppm at 550°C. This is less than the amount of CO_2 formed over Ag/CZA.

The introduction of K into Ba-Ag/CZA appears to have shifted reactions to higher temperatures with no reactions taking place until 300°C. Both catalysts show large peaks of undesirable N_2O. A nitrogen balance has been calculated for Ba-Ag-K/CZA which shows that in addition to the non-selective SCR reaction that the oxidation of NH_3 to N_2 is prevalent in 300 - 500°C temperature range. Over the temperature range investigated, more soot is oxidised over Ba-Ag/CZA than Ba-Ag-K/CZA. This is unusual as K is known to enhance soot oxidation. At 500°C Ba-Ag/CZA forms more CO_2 than Ag/CZA, however, Ba-Ag-K/CZA forms considerably less. Both catalysts are poor at reducing NOx and both favour the non-selective reaction resulting in the formation of N_2O. Furthermore, over Ag/CZA there is low temperature oxidation of soot, this is not observed over the Ba catalysts.

6.2.1.4 La based Catalysts

Figure 6.5a shows that over La-Ag/CZA, the concentrations of NO and NH_3 remain at approximately 500 ppm until 300°C. Above 300°C the concentration of NH_3 begins to decrease and reaches 0 ppm by 400°C. NO slightly decreases in concentration, mirroring the peak in N_2O between 300 – 500°C. This is due to the non-selective SCR reaction being dominant. At temperatures above 400°C, the concentrations of CO_2 and NO_2 begin to rise, with CO_2 reaching 4216 ppm at 550°C this is similar to the CO_2 concentration observed over Ag/CZA.

Figure 6.5b shows that over La-Ag-K/CZA, the concentrations of NO and NH_3 remain relatively stable at 500 ppm until 275°C, where the concentrations begin to decrease, with NH_3 reaching 0

ppm at 350°C. An inverse peak of NO mirrors the peak of N_2O between 275 – 425°C. From 325°C, increasing concentrations of CO_2 and NO_2 are observed. The soot oxidation reaches its maximum at 525°C (4316 ppm), which is similar to that observed over Ag/CZA.

Both La catalysts show large peaks of N_2O which are mirrored by inverse peaks of NO as a result of the non-selective SCR reaction. Both catalysts are poor at selectively catalytically reducing NO to N_2 as the non-selective SCR reaction is favoured. Over the La-Ag-K/CZA catalyst, reactions begin at slightly lower temperatures than over La-Ag/CZA. Both catalysts form similar amounts of CO_2 as the Ag/CZA catalyst at high temperatures, but do not show the ability to oxidise soot at low temperatures.

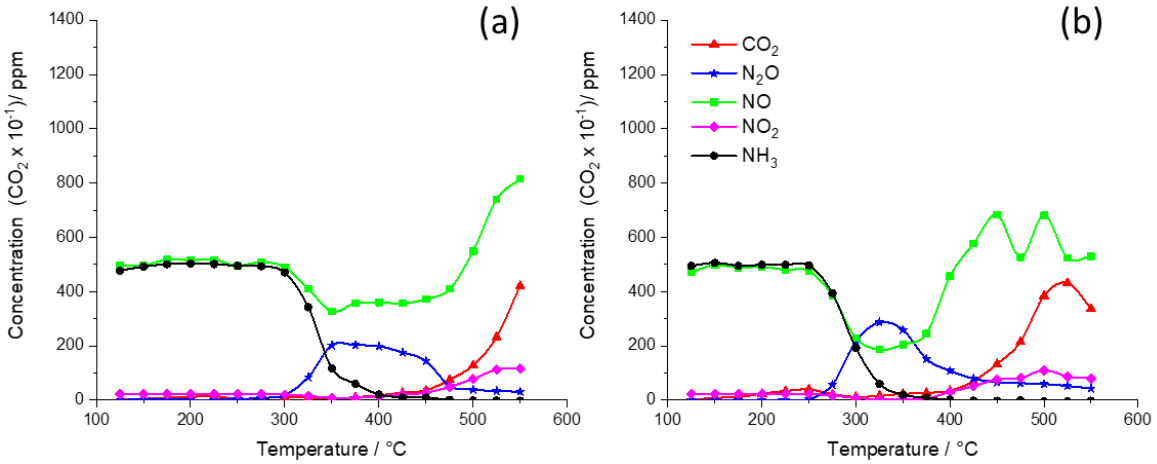

Figure 6.5: Performance data for the simultaneous removal of NOx and soot over (a) La-Ag/CZA and (b) La-Ag-K/CZA. The simulated exhaust gas consisted of 500 ppm NO, 500 ppm NH_3, 8% O_2, with a balance of N_2. The total flow rate was 200 $mlmin^{-1}$. The temperature was increased in 25°C intervals from 125 to 550°C, the gas concentrations were allowed to stabilise before readings were taken at each temperature 0.25 g catalyst was mixed in a 10:1 ratio by mass with soot.

6.2.1.5 Sr based Catalysts

Figure 6.6 shows the catalytic performance data for Sr-Ag/CZA and Sr-Ag-K/CZA. Over Sr-Ag/CZA the NO and NH_3 concentrations remain at 500 ppm until 225°C, where the concentration begins to decrease. As with some of the previous catalysts, the decrease in NO concentration is mirrored by a peak in N_2O. This peak is observed between 225 – 400°C, after which N_2O is still observed but in low concentrations. At temperatures > 400°C the NO concentration increases with temperature with a fluctuation at 500°C. CO_2 is observed from 275°C and increases with temperature, as with the NO, there is a fluctuation at 500°C resulting in a dip in CO_2 concentration.

The concentrations of NO and NH_3 also stay constant at 500 ppm until 225°C over Sr-Ag-K/CZA with NH_3 reaching 0 ppm at 325°C. Between 200 – 350°C a peak in N_2O is observed with a mirrored inverse peak of NO. At temperatures above 350°C, the concentration of NO rises due to high temperature oxidation of NH_3. The concentration of NO_2 increases at temperatures above 400°C due to the high temperature oxidation of NO. CO_2 is observed from 275°C, increasing in concentration until 500°C, where it reaches its maximum of 3354 ppm.

Over both catalysts, the reactions did not begin until 225°C and both catalysts favour the non-selective SCR reaction, resulting in the formation of N_2O. Sr-Ag/CZA reaches a CO_2 concentration of 4073 ppm at 475°C, whilst Sr-Ag-K/CZA's highest measured concentration of CO_2 was 3354 ppm at 500°C. Sr-Ag/CZA forms similar concentrations of CO_2 as Ag/CZA at high temperatures. However, neither catalyst forms low temperature CO_2.

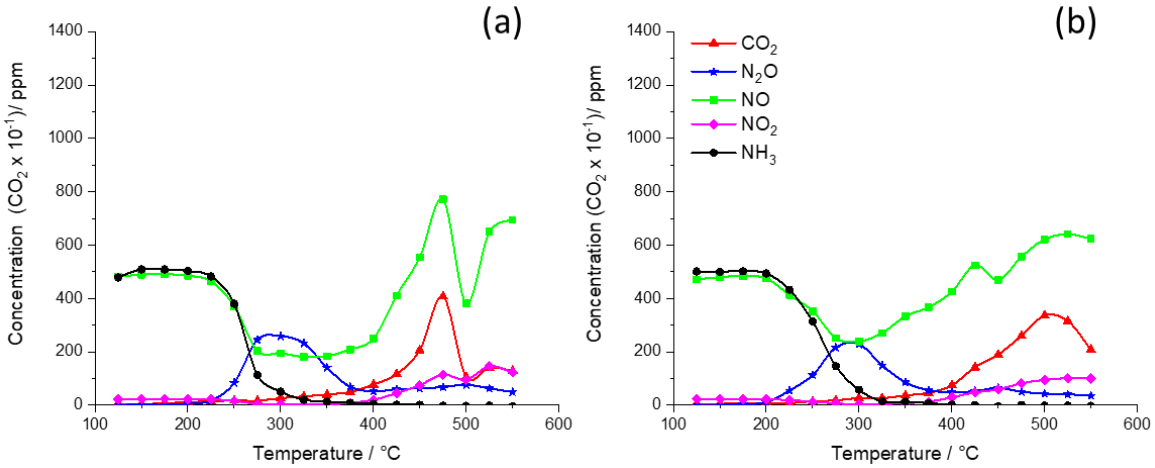

Figure 6.6: Performance data for the simultaneous removal of NOx and soot over (a) Sr-Ag/CZA and (b) Sr-Ag-K/CZA. The simulated exhaust gas consisted of 500 ppm NO, 500 ppm NH_3, 8% O_2, with a balance of N_2. The total flow rate was 200 $mlmin^{-1}$. The temperature was increased in 25°C intervals from 125 to 550°C, the gas concentrations were allowed to stabilise before readings were taken at each temperature 0.25 g catalyst was mixed in a 10:1 ratio by mass with soot.

6.2.1.6 Ni based Catalysts

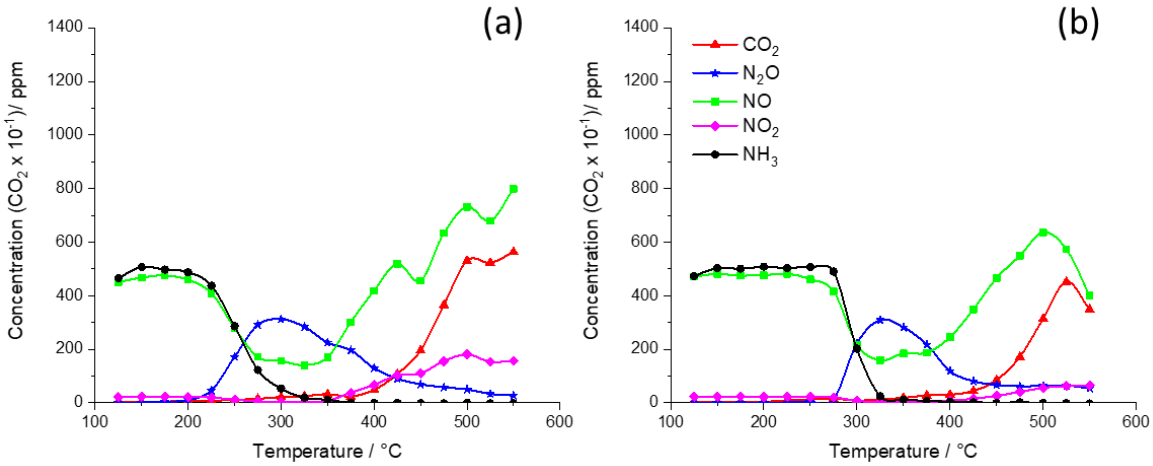

Figure 6.7: Performance data for the simultaneous removal of NOx and soot over (a) Ni-Ag/CZA and (b) Ni-Ag-K/CZA. The simulated exhaust gas consisted of 500 ppm NO, 500 ppm NH_3, 8% O_2, with a balance of N_2. The total flow rate was 200 mlmin^{-1}. The temperature was increased in 25°C intervals from 125 to 550°C, the gas concentrations were allowed to stabilise before readings were taken at each temperature 0.25 g catalyst was mixed in a 10:1 ratio by mass with soot.

The Ni based catalysts showed similar reactivities to the Ba, La and Sr catalysts as shown in Figure 6.7. Over Ni-Ag/CZA, the NO and NH_3 concentrations remained around their starting value of 500 ppm, before starting to decrease at 225°C. A peak in N_2O is observed between 225 – 425°C, which is mirrored by an inverse peak of NO. At temperatures above 400°C the NO concentration continues to rise whilst the N_2O concentration decreases. NO_2 is first observed at 300°C and continues to rise with temperature. CO_2 is first observed at 300°C and continues to rise with increase in temperature reaching 5627 ppm at 550°C, which is superior to the Ag/CZA catalyst at the same temperature.

The reactivity over Ni-Ag-K/CZA is very similar to that of Ni-Ag/CZA. The concentrations of NO and NH_3 remain at approximately 500 ppm until 275°C, at which point both decrease in concentration. The NH_3 concentration reaches 0 ppm by 325°C. A peak of N_2O is observed between 275 – 450°C, which is mirrored by NO. At temperatures > 400°C, the NO concentration continues to rise until 500°C, after which it begins to decrease. Small concentrations of NO_2 are observed at temperatures > 400°C. CO_2 increases with temperature from 350°C reaching its maximum concentration (4519 ppm) at 525°C, before beginning to decrease.

The activity over both catalysts was very similar with the addition of K not enhancing this catalyst. The Ni-Ag/CZA formed a higher concentration of CO_2 (5226 ppm at 525°C) compared to Ni-Ag-K/CZA (4519 ppm at 525°C). This is unexpected as K is a known enhancer of soot oxidation. The main difference between the catalysts is that over Ni-Ag-K/CZA the reactions are shifted to slightly higher temperatures than over Ni-Ag/CZA. Both catalysts favour the non-selective SCR

reaction, resulting in the formation of N_2O rather than reducing NO to N_2. Also, both catalysts do not show an affinity for low temperature soot oxidation

6.2.1.7 Fe based Catalysts

The catalytic performance data for Fe-Ag/CZA and Fe-Ag-K/CZA are shown in Figure 6.8. Over Fe-Ag/CZA the concentrations of NO and NH_3 begin to decrease at 225°C, with NH_3 continuing to decrease with temperature until reaching 0 ppm at 375°C. Between 250 – 425°C a peak of N_2O is observed, which is mirrored by an inverse peak of NO. At temperatures above 425°C N_2O remains, but at low concentrations, whilst NO increases in concentration until reaching 788 ppm at 500°C. Both NO_2 and CO_2 concentrations begin to increase with temperature from 325°C with CO_2 reaching 4043 ppm at 500°C, before starting to decrease in concentration.

The reactivity over Fe-Ag-K/CZA is very similar to that of Fe-Ag/CZA with a peak of N_2O being observed between 250 – 425°C, which is mirrored by an inverse peak of NO. NO_2 and CO_2 increases in concentration from 350°C, with the CO_2 concentration reaching 5682 ppm at 525°C.

Both catalysts have very similar activity, favouring the non-selective reaction resulting in the formation of undesirable N_2O. The N_2O peak is observed over the same temperature window (250 – 425°C) over both catalysts. The CO_2 formed over Fe-Ag/CZA is slightly less than that observed over Ag/CZA, whilst Fe-Ag-K/CZA forms more CO_2. In the case of the Fe catalysts the presence of K does enhance high temperature soot oxidation. However, neither catalyst demonstrates the ability to oxidise soot at low temperatures.

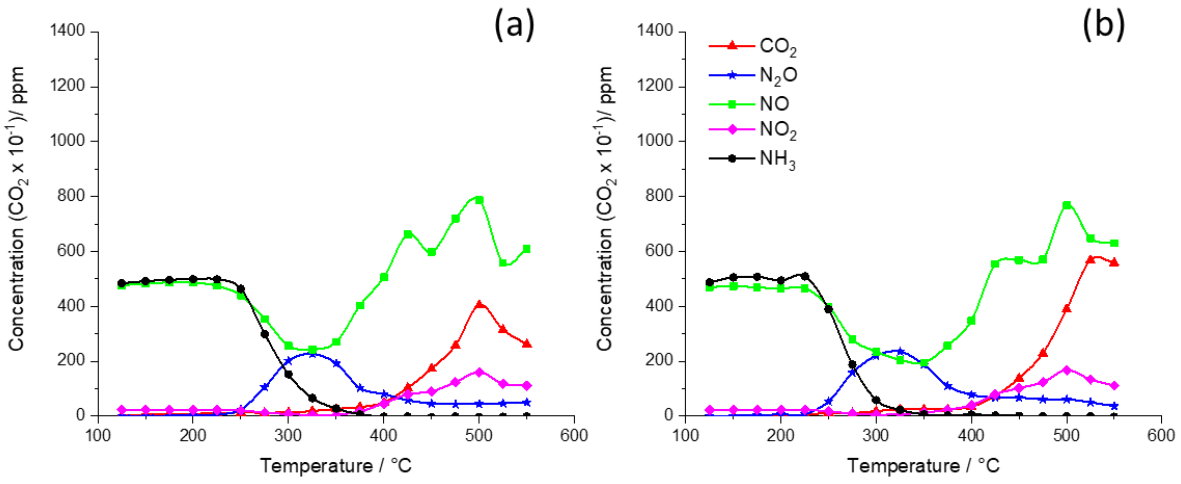

Figure 6.8: Performance data for the simultaneous removal of NOx and soot over (a) Fe-Ag/CZA and (b) Fe-Ag-K/CZA. The simulated exhaust gas consisted of 500 ppm NO, 500 ppm NH_3, 8% O_2, with a balance of N_2. The total flow rate was 200 mlmin^{-1}. The temperature was increased in 25°C intervals from 125 to 550°C, the gas concentrations were allowed to stabilise before readings were taken at each temperature 0.25 g catalyst was mixed in a 10:1 ratio by mass with soot.

6.2.1.8 Pt based Catalysts

Figure 6.9 shows the reaction data for the Pt-Ag/CZA and Pt-Ag-K/CZA catalysts. Over Pt-Ag/CZA the concentrations of NO and NH_3 remain stable around 500 ppm until 275°C. At temperatures above 275°C the concentration of NH_3 begins to gradually decrease with temperature until reaching 0 ppm at 500°C. A small peak of N_2O is observed between 300 – 400°C, after which it remains and is only observed in low concentrations. The NO concentration decreases slightly when mirroring the N_2O peak, at temperatures above 400°C the concentration rises with temperature, reaching 932 ppm at 525°C. The concentration of NO_2 begins to rise at temperatures > 400°C. The CO_2 concentration rises slowly between 350 – 450°C, before increasing at a much more rapid rate until 550°C where it reaches 6990 ppm.

Figure 6.9b shows the catalytic performance data for Pt-Ag-K/CZA. Over this catalyst the peak in N_2O is shifted to the slightly higher temperature range of 350 – 450°C, this peak is mirrored by the inverse peak in NO. At temperatures above 450°C, the NO concentration continues to rise until starting to plateau at 475 °C. NO_2 begins to rise with temperature from 400°C. At temperatures above 400°C CO_2 concentration increases with temperature, reaching 4767 ppm at 550°C.

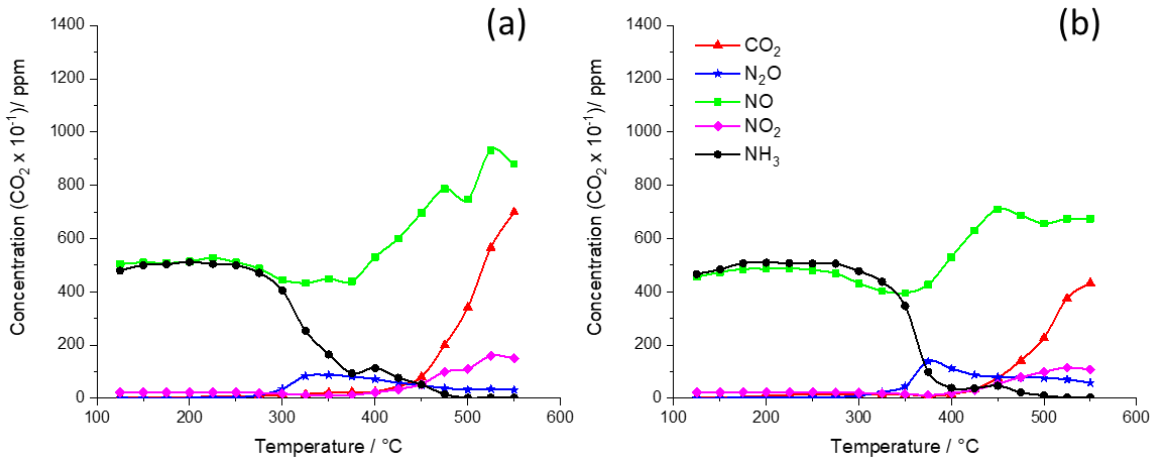

Figure 6.9: Performance data for the simultaneous removal of NOx and soot over (a) Pt-Ag/CZA and (b) Pt-Ag-K/CZA. The simulated exhaust gas consisted of 500 ppm NO, 500 ppm NH_3, 8% O_2, with a balance of N_2. The total flow rate was 200 mlmin^{-1}. The temperature was increased in 25°C intervals from 125 to 550°C, the gas concentrations were allowed to stabilise before readings were taken at each temperature 0.25 g catalyst was mixed in a 10:1 ratio by mass with soot.

Both these catalysts form less N_2O compared to the previous catalysts in this chapter, however, they are still poor at reducing NO to N_2. The addition of K to Pt-Ag/CZA results in the shifting of the N_2O peak to higher temperatures and unusually results in less CO_2 being formed at high temperatures. Over Ag-Pt/CZA, 6990 ppm is formed at 550°C, whilst only 4767 ppm is formed over Pt-Ag-K/CZA at the same temperature. However, both catalysts form more high temperature CO_2 than Ag/CZA. Unfortunately, neither of the Pt catalysts show the ability to

oxidise soot at low temperatures. Over both catalysts the NH_3 concentration reaches 0 ppm at higher temperatures than most catalysts in this chapter. The Pt-Ag/CZA catalyst is the superior of the two catalysts, but is still only active for soot oxidation at high temperatures in the tested reaction conditions.

6.2.1.9 Pd based Catalysts

Figure 6.10 shows the reaction data for the simultaneous removal of NOx and soot over Pd-Ag/CZA and Pd-Ag-K/CZA. The concentrations of the reactant gases remained stable around their input concentrations until 250°C, above which the concentration of NH_3 began to decrease. This decrease continued with increase in temperature until the NH_3 reached 0 ppm at 500°C. Between 250 - 350°C, NO shows a small inverted peak that mirrors the small peak in N_2O observed over this temperature range. At temperatures > 350°C the NO concentration fluctuates around 500 ppm until 500°C, after which the NO concentration rises dramatically with temperature. The NO concentration at 550°C was 1356 ppm, 856 ppm higher than the starting concentration. From 300°C the concentrations of NO_2 and CO_2 begin to increase with temperature and N_2O is also observed in small concentrations at higher temperatures. The catalyst is capable of oxidising soot at high temperatures, with 4054 ppm of CO_2 being observed at 550°C.

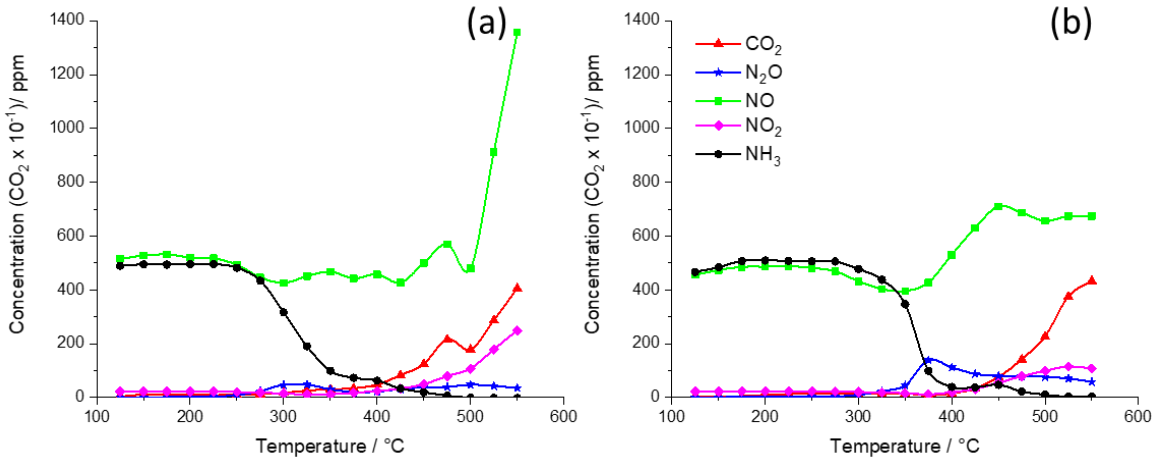

Figure 6.10: Performance data for the simultaneous removal of NOx and soot over (a) Pd-Ag/CZA and (b) Pd-Ag-K/CZA. The simulated exhaust gas consisted of 500 ppm NO, 500 ppm NH_3, 8% O_2, with a balance of N_2. The total flow rate was 200 mlmin^{-1}. The temperature was increased in 25°C intervals from 125 to 550°C, the gas concentrations were allowed to stabilise before readings were taken at each temperature 0.25 g catalyst was mixed in a 10:1 ratio by mass with soot.

Over Pd-Ag-K/CZA, the NH_3 concentration remains around 500 ppm until 300°C where it begins to decrease, which continues with temperature until 525°C where it reaches 0 ppm. Between 300 – 400°C, NO shows a small inverse peak which mirrors the peak in N_2O. At temperatures above 400°C the NO concentration rises until 450°C, after which the concentration plateaus around 670 ppm. At temperatures > 375°C the concentrations of NO_2 and CO_2 begin to increase with temperature, with CO_2 reaching 4335 ppm at 550°C.

Both Pd catalysts form small amounts of N_2O and do not reduce NO to N_2. The presence of K shifts the reactions to higher temperatures, as shown by the shift in temperature window where N_2O is observed, and by how NO and NH_3 start to decrease in concentration at higher temperatures than over Pd-Ag/CZA. Both catalysts show similar soot oxidation properties, with both being poor soot oxidation catalysts at low temperatures and forming 4054 ppm (Pd-Ag/CZA) and 4335 ppm (Pd-Ag-K/CZA) at 550°C. These levels of CO_2 are similar to those observed over Ag/CZA. The addition of Pd and K to the Ag/CZA catalyst does not enhance the catalysts properties, with the Pd catalysts being poor NOx reduction catalysts and oxidising the same amount of soot at high temperatures as Ag/CZA.

6.2.1.10 Rh based Catalysts

The Rh based catalysts, shown in Figure 6.11, show interesting catalytic properties. Over Rh-Ag/CZA, the NH_3 concentration remains around 500 ppm until 325°C, it then begins to decrease. It continues to decrease in concentration with increase in temperature until 525°C where it reaches 0 ppm. The NO concentration remains at approximately 500 ppm for the majority of the experiment, there is a slight dip in concentration between 300 – 450°C, which coincides with the rising concentration of N_2O. The NO concentration increases with temperature from 475°C. CO_2 increases with temperature from 400°C, before ultimately reaching 3493 ppm at 550°C. The formation of N_2O is unusual over this catalyst as it does not begin to form until 325°C and is observed to steadily increase with temperature.

Over Rh-Ag-K/CZA, the NH_3 remains at 500 ppm until 275°C, where it starts to decrease in concentration, this continues with increasing temperature until reaching 0 ppm at 475°C. NO decreases slightly in concentration between 225 – 350°C, before steadily increasing in concentration with increase in temperature, eventually reaching 1016 ppm at 550°C. N_2O formation begins at 300°C, and a broad peak of N_2O is observed between 300 – 550°C. NO_2 is observed from 375°C and increases in concentration with increase in temperature. A large amount of CO_2 is observed over this catalyst. CO_2 concentration increases with temperature from 300°C reaching 9753 ppm at 525°C.

The Rh based catalysts show very interesting properties for the simultaneous removal of NOx and soot. No selective catalytic reduction of NO by NH_3 is observed over these catalysts. Over Rh-Ag/CZA, N_2O begins to form at 300°C and continues to increase in concentration with temperature. This is unusual as typically in this reaction, N_2O is observed as a peak with the maxima being around 300°C. At higher temperatures N_2O is usually only present in small concentrations. High temperature soot oxidation is observed over this catalyst (3493 ppm at 550°C), which is less than observed over Ag/CZA. When K is introduced into the catalyst, the reactions are shifted to lower temperatures. Over, Rh-Ag-K/CZA a broad peak of N_2O is observed between 300 – 550°C, this is again unusual behaviour. One clear difference between the catalysts, is the large formation of NO over the Rh-Ag-K/CZA catalyst. Secondly, the amount of soot oxidation observed over Rh-Ag-K/CZA (9753 ppm of CO_2 at 525°C), which is over double the amount formed over Ag/CZA.

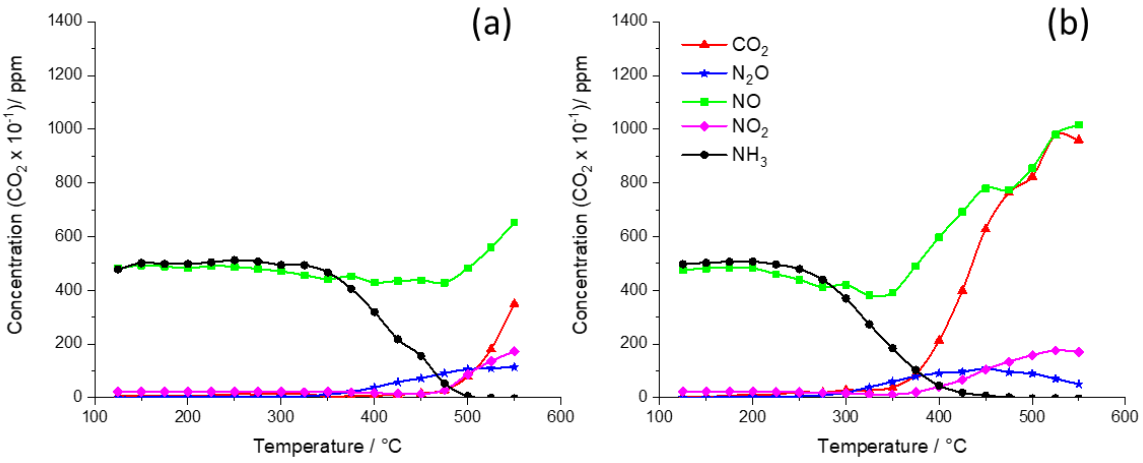

Figure 6.11: Performance data for the simultaneous removal of NOx and soot over (a) Rh-Ag/CZA and (b) Rh-Ag-K/CZA. The simulated exhaust gas consisted of 500 ppm NO, 500 ppm NH_3, 8% O_2, with a balance of N_2. The total flow rate was 200 mlmin^{-1}. The temperature was increased in 25°C intervals from 125 to 550°C, the gas concentrations were allowed to stabilise before readings were taken at each temperature 0.25 g catalyst was mixed in a 10:1 ratio by mass with soot.

6.2.2 Discussion

The catalysts studied in this chapter show a wide range of catalytic properties, however, none of the catalysts show the ability to simultaneously reduce NOx and oxidise soot.

The Ba, La, Sr, Ni and Fe based catalysts show similar reactivities, with a clear peak of N_2O present across each catalyst in the temperature window of 250 – 450°C. These catalysts favour the non-selective SCR reaction, resulting in the formation of N_2O rather than the reduction of NO to N_2.

The PGM catalysts showed some interesting activities, especially with regards to N_2O formation. The Pt and Pd catalysts formed considerably less N_2O compared to any of the other catalysts investigated in this study. Over Rh-Ag/CZA, N_2O was not observed until 375°C, after which its concentration increased with increase in temperature. When K was included in the catalyst (Rh-Ag-K/CZA) a broad peak of N_2O was observed between 275 – 550°C. It was unexpected to observe N_2O over the Rh based catalysts, as Rh/CeO_2 catalysts are routinely used to decompose N_2O.[20–23] Wang *et al.* found that a Rh/CLZ (Zr stabilized La doped ceria) catalyst fully converted N_2O to N_2 using a fixed bed reactor where temperature was maintained at 450°C throughout the experiment.[24] A review by Li *et al.* discusses various supported Rh catalysts which achieve 100 % conversion of N_2O to N_2, however, it is also stated that in the presence of 5% O_2 the conversion drops dramatically, with the best catalysts (Rh/Al_2O_3, $Rh/BaO/Al_2O_3$) showing only 20% conversion of N_2O.[20] Throughout this thesis 8% O_2 has been used in the gas feed to simulate a realistic diesel exhaust gas stream. Therefore, the presence of 8% O_2 in the reaction gas mix explains why the Rh-Ag/CZA catalytic data shows N_2O formation.

K is known to enhance soot oxidation, however, this is not the case over every catalyst in this chapter. The Ba-, Sr-, Ni- and Pt-Ag/CZA all showed superior soot oxidation compared to their corresponding K containing catalyst. Whilst La-Ag/CZA and La-Ag-K/CZA showed very similar levels of high temperature soot oxidation with and without K.

The aim of this chapter was to enhance the Ag/CZA catalyst by adding metals which aid the simultaneous removal of NOx and soot. From the reaction data in sections 6.2.1.1 – 6.2.1.10 it is clear that none of the catalysts studied showed the ability to selectively catalytically reduce NO to N_2. However, some of the catalysts did show superior levels of high temperature soot oxidation than that shown by Ag/CZA. Figure 6.12 shows a bar chart comparing the maximum concentration of CO_2 observed over each catalyst, the maximum amount of CO_2 formed over Ag/CZA (4228 ppm) is also included in the graph.

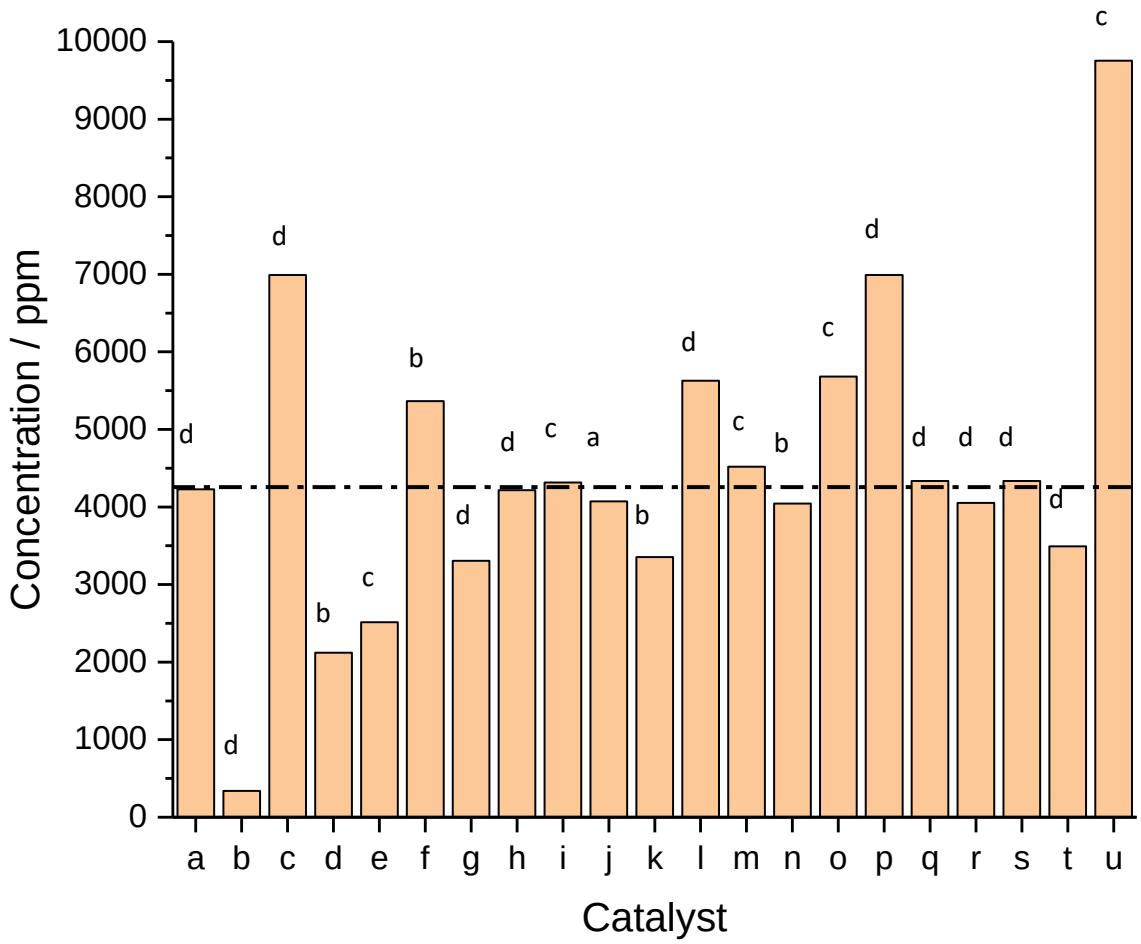

Figure 6.12: Bar chart comparing the highest concentration of CO_2 observed over each catalyst. The data for Ag/CZA is included for comparison and the dashed line indicates the maximum concentration of CO_2 formed over Ag/CZA. Where: (a) Ag/CZA (b) Co-Ag/CZA (c) Co-Ag-K/CZA (d) Mn-Ag/CZA (e) Mn-Ag-K/CZA (f) Ba-Ag/CZA (g) Ba-Ag-K/CZA (h) La-Ag/CZA (i) La-Ag-K/CZA (j) Sr-Ag/CZA (k) Sr-Ag-K/CZA (l) Ni-Ag/CZA (m) Ni-Ag-K/CZA (n) Fe-Ag/CZA (o) Fe-Ag-K/CZA (p) Pt-Ag/CZA (q) Pt-Ag-K/CZA (r) Pd-Ag/CZA (s) Pd-Ag-K/CZA (t) Rh-Ag/CZA and (u) Rh-Ag-K/CZA. The letters above the bars indicates the temperature, where: a is 475°C, b is 500°C, c is 525°C and d is 550°C.

From the graph it is clear that Rh-Ag-K/CZA is the superior catalyst for high temperature soot oxidation under these reaction conditions. Over double the amount of CO_2 is formed over Rh-Ag-K/CZA than over Ag/CZA. Co-Ag-K/CZA and Pt-Ag/CZA also showed the ability to oxidise considerably more soot at high temperatures than Ag/CZA, with Ba-Ag/CZA, Ni-Ag/CZA and Fe-Ag-K/CZA also forming larger quantities of CO_2 than Ag/CZA. The majority of the remaining catalysts showed similar oxidation abilities to Ag/CZA. However, the graph highlights how poor Co-Ag/CZA was as a soot oxidation catalyst. As well as showing that both Mn catalysts were poor soot oxidation catalysts when compared to the other catalysts in this chapter.

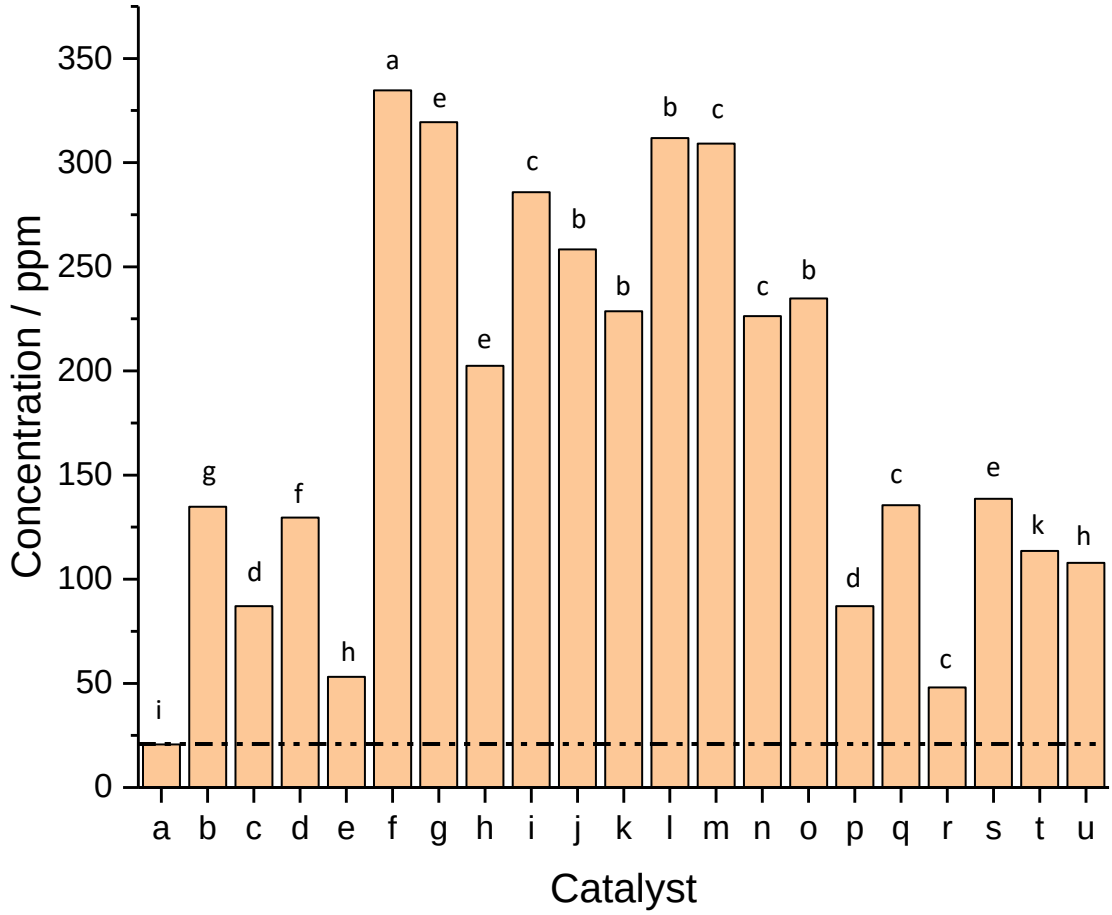

Figure 6.13: Bar chart comparing the highest concentration of N_2O observed over each catalyst. The data for Ag/CZA is included for comparison and the dashed line indicates the maximum concentration of N_2O formed over Ag/CZA. Where: (a) Ag/CZA (b) Co-Ag/CZA (c) Co-Ag-K/CZA (d) Mn-Ag/CZA (e) Mn-Ag-K/CZA (f) Ba-Ag/CZA (g) Ba-Ag-K/CZA (h) La-Ag/CZA (i) La-Ag-K/CZA (j) Sr-Ag/CZA (k) Sr-Ag-K/CZA (l) Ni-Ag/CZA (m) Ni-Ag-K/CZA (n) Fe-Ag/CZA (o) Fe-Ag-K/CZA (p) Pt-Ag/CZA (q) Pt-Ag-K/CZA (r) Pd-Ag/CZA (s) Pd-Ag-K/CZA (t) Rh-Ag/CZA and (u) Rh-Ag-K/CZA. The letters above the bars show the temperature, where: a is 250°C, b is 300°C, c is 325°C, d is 350°C, e is 375°C, f is 425°C, g is 450°C, h is 475°C, i is 500°C and k is 550°C.

A key attribute of the Ag/CZA catalyst is its ability to utilise *in situ* formed N_2O to oxidise soot at low temperatures effectively solving two problems at once: low temperature soot oxidation and preventing the release of N_2O. Over the Ag/CZA catalyst at 300°C 821 ppm of CO_2 and 0 ppm of N_2O was observed, with N_2O only being observed in small concentrations at high temperatures. Low temperature soot oxidation is not observed to the same level over any of the catalysts investigated in this chapter, with soot oxidation ranging from 79 – 272 ppm at 300°C. The levels of N_2O observed over these catalysts are also much greater than that observed over Ag/CZA as shown in Figure 6.13. The Ba based catalysts are shown to form the most amount of N_2O and Pd-Ag/CZA forms the least. None of the catalysts studied showed the ability to utilise the N_2O formed to oxidise soot at low temperatures.

6.2.3 Characterisation Data

The characterisation data are discussed in the following sections. The catalysts underwent XRD, Raman and BET analysis with XPS and TEM-EDX analysis being carried out on Ba-Ag/CZA, Ba-Ag-K/CZA and Co-Ag-K/CZA. The characterisation of the catalysts investigated in this chapter was limited due to restricted laboratory access for the past 18 months as a consequence of COVID-19.

6.2.3.1 X-ray Diffraction

Figure 6.14 shows the XRD patterns for the M-Ag/CZA catalysts and Figure 6.15 shows the XRD patterns for the M-Ag-K/CZA catalysts studied in this chapter.

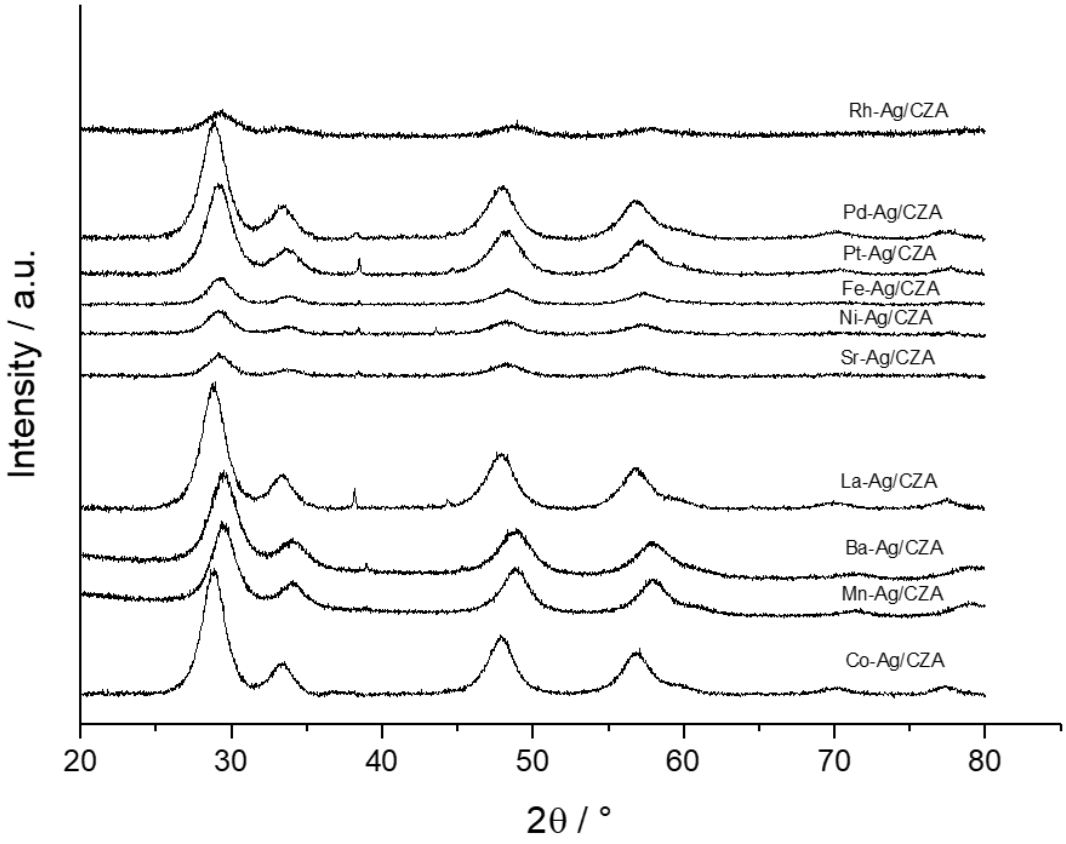

Figure 6.14: XRD Patterns for the M-Ag/CZA catalysts

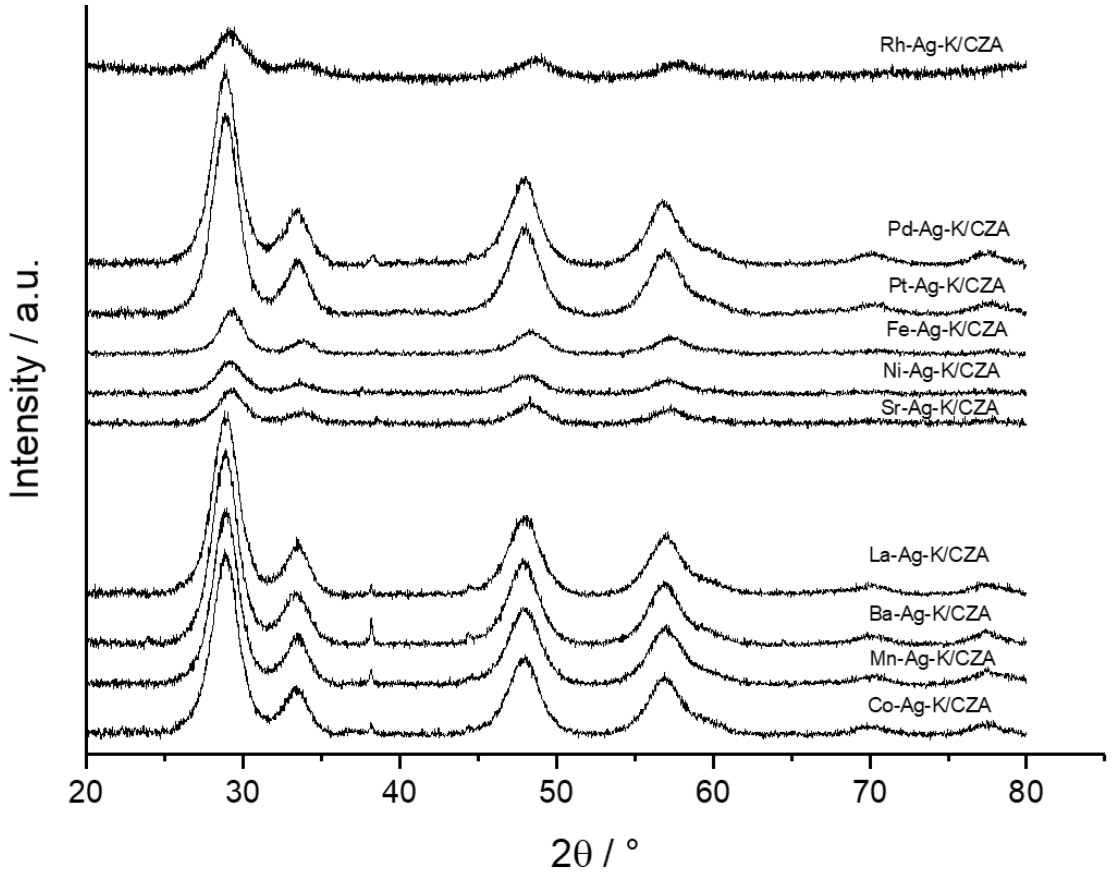

Figure 6.15: XRD patterns for the M-Ag-K/CZA Catalysts

The XRD patterns show four distinct peaks (centred around 28.5°, 33.1°, 47.5° and 56.3° corresponding to the (111), (200), (220) and (311) planes, respectively) which are characteristic of the cubic fluorite phase of CeO_2. The catalysts show shifts in the diffraction peaks from the standard CeO_2 peak (data for the (111) peak is shown in Table 6.1). This is due to the modification of the ceria lattice as a result of incorporation of other species into the lattice.[25,26] Table 6.1 includes literature values for pure CeO_2[27] and values for CZA. A shift in the CeO_2 peak position for CZA is observed, when compared to pure CeO_2, as a consequence of the incorporation of zirconium and aluminium ions into the ceria lattice.

Table 6.1: Calculated data from XRD analysis where the pure CeO_2 values are from literature[28]

Catalyst	Peak Position [°]	Lattice Parameter, a [Å]	Unit Cell Volume [Å^3]
Pure CeO_2	28.5	5.4500	161.88
CZA	28.9	5.3449	152.69
Co-Ag/CZA	28.8	5.3671	154.60
Mn-Ag/CZA	29.0	5.3221	150.75
Ba-Ag/CZA	29.0	5.3216	150.70
La-Ag/CZA	29.2	5.3015	149.00
Sr-Ag/CZA	29.2	5.2960	148.54
Ni-Ag/CZA	29.1	5.3032	149.15
Fe-Ag/CZA	29.2	5.2913	148.14
Pt-Ag/CZA	29.2	5.2977	148.68
Pd-Ag/CZA	28.8	5.3625	154.20
Rh-Ag/CZA	28.8	5.3645	154.38
Co-Ag-K/CZA	28.9	5.3554	153.59
Mn-Ag-K/CZA	28.8	5.3691	154.78
Ba-Ag-K/CZA	28.8	5.3650	154.42
La-Ag-K/CZA	28.6	5.4061	158.00
Sr-Ag-K/CZA	28.9	5.3500	153.13
Ni-Ag-K/CZA	29.1	5.3082	149.57
Fe-Ag-K/CZA	29.2	5.2848	147.60
Pt-Ag-K/CZA	28.9	5.3554	153.59
Pd-Ag-K/CZA	28.8	5.3735	155.16
Rh-Ag-K/CZA	28.8	5.3718	155.01

Table 6.1 also shows the measured values for the lattice parameter (a) and the unit cell volume, using the (111) CeO_2 peak for each of the catalysts. The CZA lattice parameter and unit cell volume is less than that of the pure CeO_2 due to zirconium and alumina having smaller ionic radii than cerium.[29] The contraction of the lattice parameter upon incorporation of zirconium and aluminium into the cubic fluorite ceria lattice is well documented. The incorporation of zirconium and alumina into the lattice results in the formation of defect sites consequently forming oxygen vacancies which causes displacement of cerium, zirconium and alumina.[30] Consequently, the unit

cell size contracts, resulting in the decrease in the unit cell volume.[25,32] This contraction is also seen over several of the catalysts in this chapter. The unit cell volumes are less than that of CZA due to substitution of smaller radii into the CeO_2 lattice.

For the non-potassium containing catalysts, there are a few catalysts which show an increase in unit cell volume (Co-Ag/CZA, Pd-Ag/CZA and Rh-Ag/CZA). If the ionic radii is greater than cerium then an increase in unit cell volume is expected.[33] An increase in unit cell volume has been observed when the incorporated ionic radii is smaller than cerium this may be a result of the metals causing structural distortion. Literature has found that substituting Pd into CeO_2 results in lattice expansion. This is due to the Pd^{2+} ion being located at the centre of one of the ceria faces as a square planar complex. This expansion has also been observed for other square planar oxides. If the lattice did not expand it would result in a Pd-O bond length of 1.91 Å, which is a shorter bond length than observed in typical square planar Pd oxides. Therefore, an expansion of the lattice is expected in order for Pd-O to have its expected bond length (2.01-2.7 Å).[34] The three catalysts which show lattice expansion can exist in square-planar forms hence the above explanation can be extrapolated to understand why a lattice expansion is observed over these catalysts.

The addition of potassium into the catalysts generally resulted in an increase of the unit cell volume of the ceria lattice when compared to the corresponding M-Ag/CZA catalyst. The exceptions being the Co, Ba and Fe catalysts. Potassium has an ionic radius of 280 pm, which is larger than all the other elements present in the catalysts. Therefore, it is not unexpected for the incorporation of potassium into the ceria lattice to result in an increase in the unit cell volume. However, the exact extent of potassium incorporation into the ceria lattice is unknown and is likely to vary between the catalysts. The differing proportions of elemental incorporation into the lattice offers an explanation to why three of the catalysts show a decrease in unit cell volume upon the addition of potassium.

The majority of the catalysts, (excluding Ag-Sr/CZA, Ag-Fe/CZA, Ag-Rh/CZA, Rh-Ag-K/CZA and Pt-Ag-K/CZA) show peaks at 37° and 44°, which is due to the presence of crystalline Ag.[35] Using the XRD data, the crystallite sizes of Ag and CeO_2 were calculated *via* the Scherer equation, Table 6.2,due to small/absence of Ag peaks in some of the samples the Ag crystallite size could not be calculated for all of the samples . For the M-Ag/CZA catalysts, the CeO_2 crystallite sizes range from 36 – 50 Å whilst the Ag crystallite sizes have a considerably larger range of 58 - 3790 Å. With Co-Ag/CZA having the smallest Ag crystallite size and Ag-Pt/CZA the largest. The M-Ag-K/CZA catalyst show a CeO_2 crystallite size range of 39 – 57 Å and Ag crystallite size range of 1504 – 4355 Å. With

Mn-Ag-K/CZA having the smallest Ag crystallite size (1504 Å) and Co-Ag-K/CZA the largest (4355 Å). Upon addition of potassium to the catalysts, the CeO_2 crystallite size is seen to increase slightly but by no more than 10 Å whilst there is a significantly larger change in the Ag crystallite sizes. Demonstrated by, Co-Ag/CZA having a Ag crystallite size of 58 Å and Co-Ag-K/CZA having a much larger crystallite size of 4355 Å.

Table 6.2: Ag and CeO_2 crystallite sizes measured from XRD analysis, FWHM and CeO_2 defect ratios calculated from Raman spectroscopy and surface area of the catalysts obtained from B.E.T. analysis

Sample	Ag Crystallite Size (Å)	CeO_2 Crystallite Size (Å)	FWHM (cm^{-1})	CeO_2 Defect Ratio	Surface Area ($m^2\ g^{-1}$)
CZA	-	27	45.52	0.032	105
2%Ag/CZA	52	42	38.07	0.014	63
Co-Ag/CZA	58	45	39.01	0.014	33
Mn-Ag/CZA	233	46	40.36	0.49	41
Ba-Ag/CZA	394	39	49.48	0.007	51
La-Ag/CZA	1272	50	37.55	0.025	36
Sr-Ag/CZA	-	46	49.48	0.006	59
Ni-Ag/CZA	2911	46	49.04	< 0.001	70
Fe-Ag/CZA	-	46	53.56	0.048	58
Pt-Ag/CZA	3790	45	43.51	0.041	39
Pd-Ag/CZA	448	49	43.95	0.044	33
Rh-Ag/CZA	-	36	1.59	0.007	65
Co-Ag-K/CZA	4355	44	55.52	0.044	45
Mn-Ag-K/CZA	1504	46	52.67	0.085	56
Ba-Ag-K/CZA	2563	44	42.84	0.008	41
La-Ag-K/CZA	2532	46	48.72	0.016	56
Sr-Ag-K/CZA	2152	40	50.39	0.037	52
Ni-Ag-K/CZA	3867	39	45.67	0.023	50
Fe-Ag-K/CZA	-	57	53.43	0.048	70
Pt-Ag-K/CZA	-	50	49.81	0.050	58
Pd-Ag-K/CZA	-	45	53.36	0.070	59
Rh-Ag-K/CZA	-	37	43.63	0.005	53

A small silver crystallite size has been previously discussed as being an important factor in a catalysts ability to reduce NOx. Hence the large Ag crystallite sizes, especially for the potassium containing catalysts, offer an explanation to why the catalysts are poor at reducing NOx. The catalysts having large Ag crystallite sizes also suggest poor dispersion across the catalytic surface and offers less active sites compared to smaller crystallites.

6.2.3.2 Raman Spectroscopy

The Raman data shows clear CeO_2 peaks for all of the catalysts, centred at approximately 480 cm^{-1}. Pure ceria shows a Raman peak at 465 cm^{-1}, which is characteristic of ceria's cubic fluorite phase (F_{2g}).[36,37] The shift of the ceria peak observed over the catalysts is due to the incorporation of additional elements into the ceria lattice. The frequency shift is a consequence of two factors: an increase in the number of oxygen vacancies and the size factor *i.e.* a change in the lattice constant, a.[38]

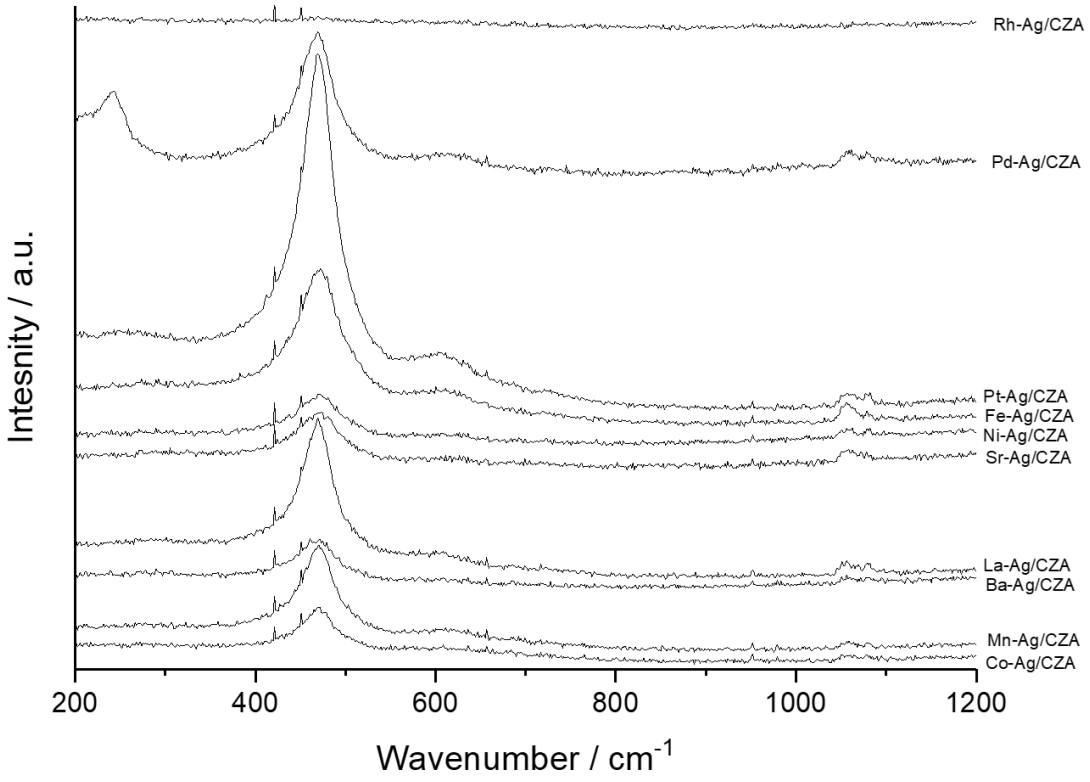

Figure 6.16: Raman Spectroscopy for M-Ag/CZA catalysts

The CeO_2 defect ratio has been calculated and is shown in Table 6.2.The CeO_2 peak is shown at approx. 480 cm^{-1} and the shoulder adjacent to the peak was used to calculate the defect ratio. Ag-Pd/CZA shows a peak at 250 cm^{-1}, which indicates the presence of nanocrystalline CeO_2.[39,40] Table 6.2 also shows the values for the FWHM of the CeO_2 peak for each catalyst. A larger value of FWHM than for the CZA support (45.52 cm^{-1}) could be due to various reasons, including reduction in crystallite size and increased oxygen vacancies.[41,42] The M-Ag/CZA catalysts which have a greater FWHM value than CZA are Ba-Ag/CZA, Sr-Ag/CZA, Ni-Ag/CZA and Fe-Ag/CZA.

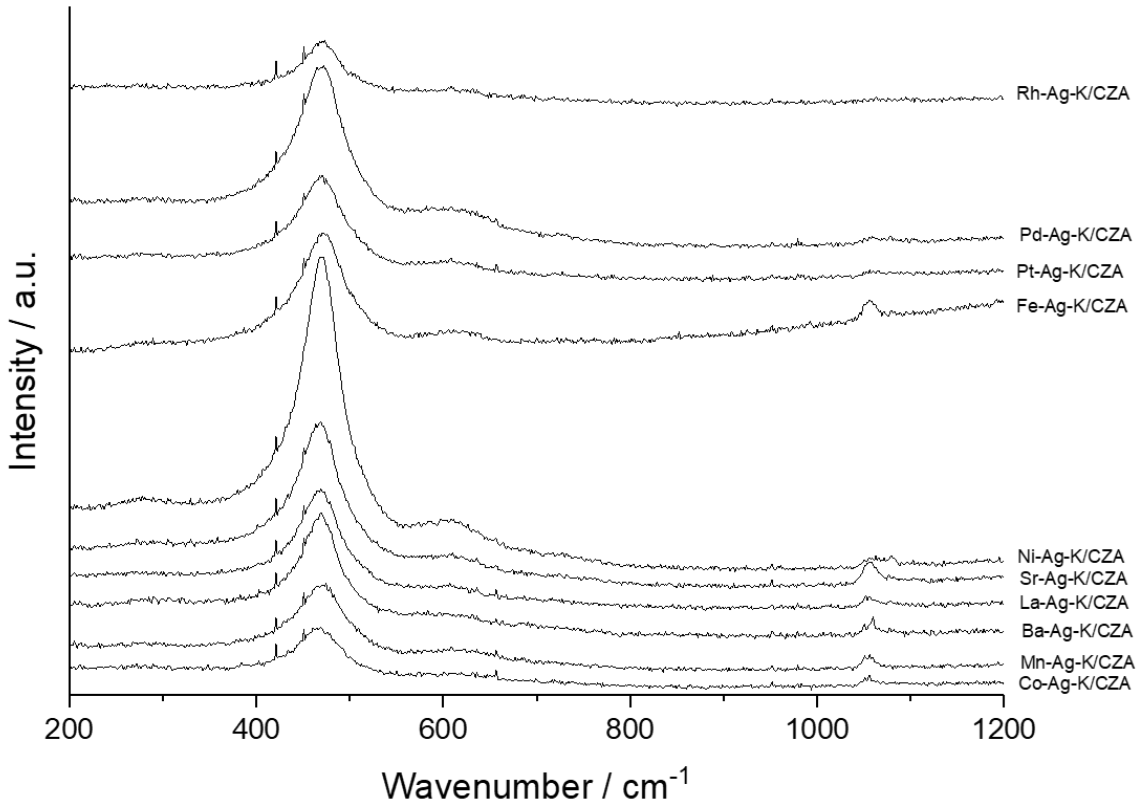

Figure 6.17: Raman Spectroscopy for M-Ag-K/CZA catalysts

The remaining M-Ag/CZA catalysts have a FWHM that is less than that of CZA, which indicates that these catalysts have larger crystallite sizes or fewer defects in the ceria phase than the CZA support. The catalysts having larger ceria crystallite sizes is supported by the XRD analysis (section 6.2.3.1). From the XRD analysis, the CZA had a CeO_2 crystallite size of 27 Å and the catalysts have a CeO_2 crystallite size larger than 27 Å.

The obvious outlier in the Raman analysis is the Rh-Ag/CZA catalyst, which shows considerably less intense peaks compared to the other catalysts. This is due to the sample being very dark in colour making it difficult to analyse using Raman spectroscopy. Therefore, the data obtained for Rh-Ag/CZA is not fully representative of the sample. Derevyannikova *et. al.* found that for Rh/CeO_2 based catalysts calcined at 450°C and 600°C, a main Raman band at 463 cm^{-1} was

present, which corresponds to the F_{2g} vibrational mode of oxygen ions in the CeO_2 lattice. Another band was observed between 550-600 cm^{-1}, which was assigned as the CeO_2 defect peak. When the Rh/CeO_2 based catalysts were calcined at higher temperatures (800°C) peaks were observed at 273, 427, 568 and 658 cm^{-1}, which were assigned to the vibrations of rhodium oxide.[43] However, Rh-Ag-K/CZA was easier to analyse compared to its non-potassium containing counterpart. With the addition of potassium resulting in a lighter coloured sample allowing Raman analysis to be completed.

The majority of the M-Ag-K/CZA catalysts have greater FWHM values than their non-potassium containing counterparts. Of these catalysts, La-Ag-K/CZA, Sr-Ag-K/CZA and Pd-Ag-K/CZA have smaller CeO_2 crystallite sizes (from XRD analysis) than their corresponding non-potassium containing catalysts. The remaining catalysts which display larger FWHM values (Co-Ag-K/CZA, Mn-Ag-K/CZA, Fe-Ag-K/CZA and Rh-Ag-K/CZA) have larger CeO_2 crystallite sizes than their corresponding catalysts suggesting that the explanation for the increased FWHM value is due to increased oxygen vacancies in the ceria lattice.

The M-Ag-K/CZA catalysts which have a lower FWHM value than their corresponding catalysts are Ba-Ag/CZA, Ni-Ag-K/CZA and Pt-Ag-K/CZA. From the XRD data, the Ba-Ag-K/CZA and Pt-Ag-K/CZA catalysts have larger CeO_2 crystallite sizes than the catalysts without potassium. Whilst, Ni-Ag-K/CZA has a smaller CeO_2 crystallite size suggesting that the reason for its lower FWHM value is due to fewer defects in the ceria.

The Raman analysis for all of the catalysts show small peaks centred around 1060 cm^{-1}. This peak indicates the presence of carbonate species in the samples. The carbonate source for the M-Ag/CZA catalysts is Na_2CO_3, which was used as a precursor in the preparation of the CZA support. In addition to Na_2CO_3, the peak is also a result of the presence of K_2CO_3 in the M-Ag-K/CZA catalysts. The 1060 cm^{-1} peak is more defined for the M-Ag-K/CZA catalysts when compared to the M-Ag/CZA catalysts, and this is a consequence of the higher concentrations of carbonate in the catalysts.

6.2.3.3 BET Analysis

Table 6.2 shows the surface areas of the catalysts that were obtained through BET analysis. The surface areas of the M-Ag/CZA catalysts range from 33 – 70 m^2g^{-1}, the typical surface area of the CZA support is 105 m^2g^{-1}. The catalysts have lower surface areas than the CZA support due to the addition of other elements to the support. Another reason for this, is a result of the catalysts having undergone a double calcination procedure, *i.e.* the support was calcined and then calcined again after impregnation of the active metals. Higher calcination temperatures and prolonged

calcinations can result in sintering, which consequently results in larger crystallite sizes.[44–47] Typically, the higher the surface area of a catalyst the smaller the crystallite size. With regards to CeO_2 crystallite size, half of the catalysts have a crystallite size of 46 Å. Rh-Ag/CZA has the smallest crystallite size (36 Å) and the second highest surface area (65 m^2g^{-1}). Ni-Ag/CZA has the highest surface area (70 m^2g^{-1}) and had a CeO_2 crystallite size of 46 Å. Co-Ag/CZA and Pd-Ag/CZA both had the smallest surface area of 33 m^2g^{-1}.

The M-Ag-K/CZA catalysts also have smaller surface areas than CZA, ranging between 41 – 70 $m^2\ g^{-1}$. When compared to the catalysts without potassium there is a fluctuation of no more than +/- 20 m^2g^{-1}.

6.2.3.4 TEM and XPS Analysis

Three of the catalysts (Ba-Ag/CZA, Ba-Ag-K/CZA and Co-Ag-K/CZA) were analysed using TEM and XPS. Ba-Ag and Ba-Ag-K were chosen to highlight the differences in the catalyst after the addition of potassium. Co-Ag-K was shown to be superior to Ba-Ag-K with regards to high temperature soot oxidation and was studied to understand the differences between the catalysts. Furthermore, the size of the Ag crystallites is believed to be instrumental in the catalysts' ability to reduce NOx. Co-Ag-K showed the largest Ag crystallite size, therefore further analysis of the catalyst could offer additional explanations.

Table 6.3 shows the measured elemental weight percentages of the three catalysts obtained from the XPS analysis, as well as the data for CZA, 2%Ag/CZA and 2%Ag-2%K/CZA extracted from Chapter 4, which has been included to allow for comparison. Over the Ba catalysts the silver content is less than the expected bulk content. As XPS is a surface technique this is not unexpected, however, over the Co catalyst the measured silver surface weight loading was 1.72 % which is higher than the expected bulk content. The differences in the measured surface weight loadings of silver is due to dispersion across the catalytic surface. From the XRD analysis, it is known that Co-Ag-K/CZA has the largest Ag crystallite size in this chapter (4355 Å) whilst Ba-Ag-K has a silver crystallite size of almost half the size (2563 Å) and Ba-Ag has an even smaller Ag crystallite size (394 Å). The differences in Ag crystallite size could also have an impact on the measured surface weight loadings in addition to the effects of dispersion.

Table 6.3: The calculated atomic weight percentages from XPS analysis where M represents Ba or Co depending on the catalyst. Data from Chapter 4 has been included for comparison

Catalyst	Ag	M	C	K	Ce	Al	Na	O	Zr
CZA	-	-	2.68	-	50.74	11.52	1.47	27.23	5.40
2%Ag/CZA	1.06	-	1.99	-	53.55	10.38	6.22	22.23	3.94
2%Ag-2%K/CZA	1.37	-	3.37	3.54	30.88	14.74	8.71	29.65	6.78
Ba-Ag/CZA	0.66	1.93	2.70	-	40.31	11.41	8.21	29.16	5.63
Ba-Ag-K/CZA	0.65	1.69	3.60	1.96	36.47	10.05	9.82	29.18	6.58
Co-Ag-K/CZA	1.72	0.62	3.23	2.41	30.12	13.14	10.55	32.60	5.62

Co-Ag-K and Ba-Ag-K showed higher surface weight loadings of C (carbonate) than Ba-Ag. In the absence of potassium, the carbonate present is due to Na_2CO_3, which was a precursor used in the preparation of the CZA support. In the potassium containing catalysts, additional carbonate is observed due to potassium being present in the carbonate form. Sodium is observed in all of the catalysts and the CZA support. The preparation method of the support involved a washing procedure which aids the removal of sodium, however, some still remained.

The measured weight loadings from TEM-EDX (Table 6.4) show different values than the weight loading measured from the XPS data. The EDX analysis shows that Ba-Ag had a Ag weight loading of 0.30%, Ba-Ag-K 0.62% and Co-Ag-K 0%. The weight loadings from TEM-EDX are not fully representative of the sample as the analysis only takes place on a small section of the sample. Therefore, Ag was not present in the sample section under analysis but is dispersed across the surface of the catalyst. Furthermore, XPS and XRD confirms that Ag is present in the Co-Ag-K/CZA sample. From the XRD analysis it is known that Co-Ag-K has large silver crystallites. Potassium is shown to be present in Ba-Ag-K in a higher than expected weight loading, 1.96%, whilst over Co-Ag-K it is only present in a 0.20 % weight loading. Again, this is due to dispersion of the element across the catalytic surface. Both Ba-Ag and Co-Ag-K have higher weight loadings of Ce measured from XPS analysis. Again, this is from only a small section of the sample being analysed by the TEM-EDX.

Table 6.4: Calculated atomic weight percentages from TEM-EDX analysis where M represents Ba or Co depending on the catalyst

Catalyst	Ag	M	K	Ce	Al	Na	O	Zr
Ba-Ag/CZA	0.30	0.66	-	62.59	7.58	2.53	22.54	3.79
Ba-Ag-K/CZA	0.62	1.02	1.96	32.98	26.65	4.28	30.15	2.34
Co-Ag-K/CZA	-	0.43	0.20	61.65	9.17	-	23.50	5.06

Figure 6.18 shows the TEM images obtained for Ba-Ag/CZA, Ba-Ag-K/CZA and Co-Ag-K/CZA, which show the morphology of the samples. The morphology across the three samples is similar. The darker regions of the images are due to the presence of the heavier elements such as Ce, Ag and Ba and the lighter regions due to the lighter elements such as K, Co, Al and Zr. The Ba-Ag/CZA image shows a larger dark region compared to the other catalysts, this is due to the high atomic percentage of Ce. The Ba catalysts also have more darker areas due to the larger atomic mass of Ba whilst Co is a lighter element and appears brighter than Ba in the TEM images.

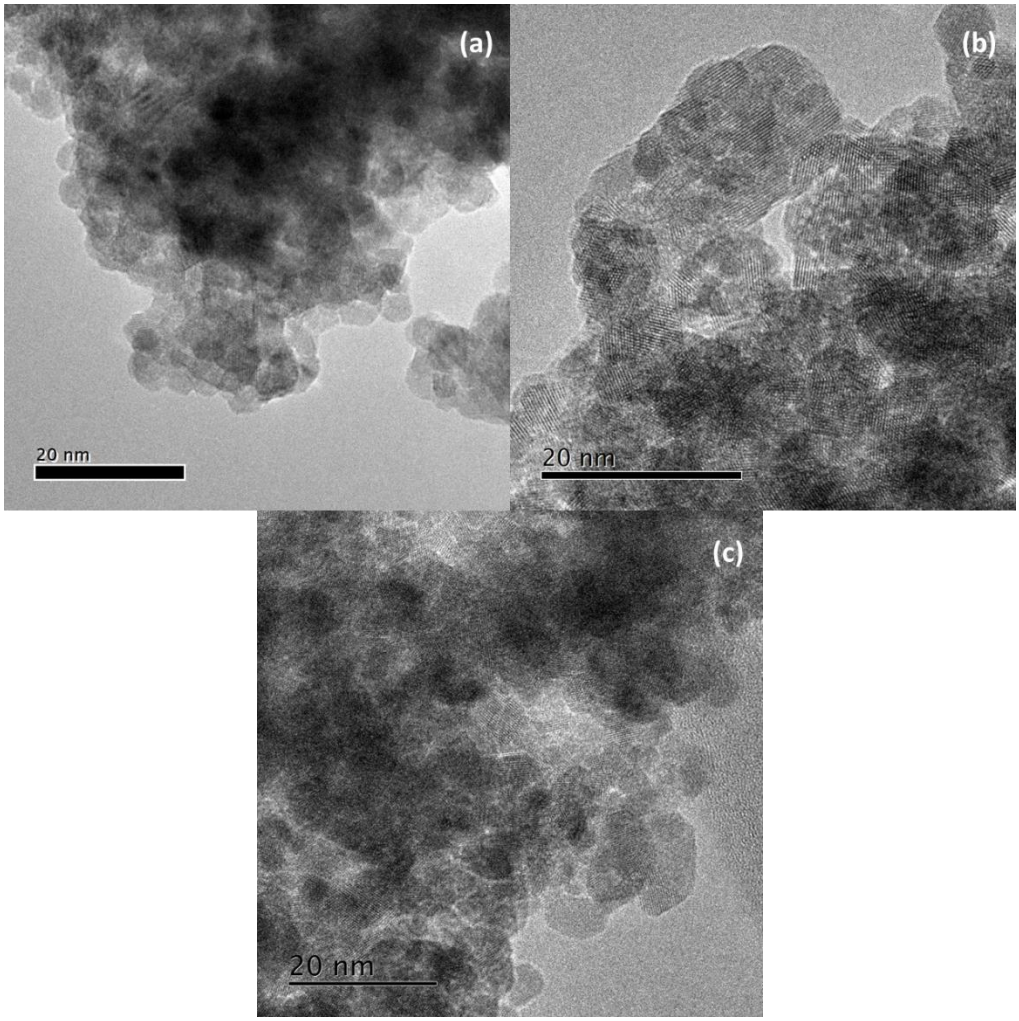

Figure 6.18: TEM images where (a) Ba-Ag/CZA (b) Ba-Ag-K/CZA and (c) Co-Ag-K/CZA

6.3 Discussion

The aim of the chapter was to improve upon Ag/CZA's ability to simultaneously remove NOx and soot from a simulated diesel exhaust by introducing a secondary metal which would enhance the reactions through synergistic effects. The secondary metals were chosen based on their ability to oxidise soot or reduce NOx. Overall, the addition of a secondary metal has not been shown to improve on Ag/CZA's ability to simultaneously oxidise soot and reduce NOx. Possible explanations for this are discussed below.

From previous work, it is known that a small silver crystallite size favours the reduction of NOx. From the XRD analysis, none of the catalysts studied in this chapter have a silver crystallite size less than that observed for the original Ag/CZA catalyst. The addition of potassium to the M-Ag/CZA catalysts has also been shown to result in an increase in Ag crystallite size. The Ag crystallite size appears to be key for the simultaneous removal of NOx.

Suggestions for the inability of the secondary metals to enhance NOx reduction, soot oxidation or both is discussed in further detail below using literature to explore possible explanations. However, it is key to remember that the catalysts in this chapter were tested under simultaneous reaction conditions (*i.e.* in the presence of NOx and soot) whilst the majority of their comparisons from literature are not. Therefore, it is not reasonable to expect direct comparisons as the reaction conditions differ.

6.3.1 Co Catalysts

Both Co-Ag and Co-Ag-K were proven to be poor NOx reduction catalysts with Co-Ag also being poor at oxidising soot. In fact, it was the worst catalyst investigated in this chapter for the oxidation of soot. Co was chosen as a secondary metal as it has variable oxidation states making it ideal for redox reactions and it has been found to be a good catalyst for HC-SCR. Gao *et al.* found that doping Co into a $MnCr_2O_4$ catalyst enhanced the catalyst's ability to reduce NOx. The enhancement was found to be due to four factors: an increase in the specific surface area, enhanced redox ability due to the presence of Co^{3+}, increase in oxygen vacancies and a greater number of acid sites.[48] However, the addition of Co did not enhance the SCR ability of the Ag/CZA catalyst and did not increase the surface area, as known from the BET analysis.

6.3.2 Mn Catalysts

Mn-Ag and Mn-Ag-K were found to be poor at reducing NOx and poor at oxidising soot. Figure 6.12 clearly shows that the Mn catalysts formed significantly lower concentrations of CO_2 compared to the Ag/CZA catalyst. Mn based perovskite-type catalysts have been previously found to catalyse the simultaneous removal of NOx and soot from a diesel exhaust.[49–53] Catalysts

containing Mn oxide have been shown to have high activity and selectivity for the reduction of NOx due to the redox properties of manganese oxides.[54] However, Mn catalysts are known to be easily poisoned by sulphur and water.[55] Doping the Mn catalyst with transition metals has been shown to improve the catalyst's adsorption capacity and oxidation ability.[54] Due to ceria's high oxygen storage capacity using it alongside Mn oxide results in the enhancement of the oxidation of Mn^{3+} to Mn^{4+}.[56] Based on the literature, introducing Mn into the Ag/CZA should have resulted in enhancement of NOx reduction. There are a couple of possible explanations for why this did not occur: firstly, H_2O formed as the result of the SCR reaction is deactivating the Mn catalyst; secondly, the Mn is not present in the Mn^{3+}/Mn^{4+} oxide state.

6.3.3 Ba Catalysts

Ba is used to store NOx in NOx traps. When the system is fuel-lean, NOx is stored as nitrates on Ba, and when the system becomes fuel-rich, hydrocarbons, hydrogen and CO react with the trapped nitrates forming N_2, CO_2 and H_2O.[57] NOx trap catalysts require two different active sites: a site for NOx adsorption (alkaline or alkaline-earth compounds) and sites for NOx oxidation and/or reduction (noble metals). Due to Ba's storage capabilities it is frequently used in conjunction with a second metal for the simultaneous removal of NOx and soot.[58–61] When alternating between fuel-lean and fuel-rich stages, a Pt-Ba/Al_2O_3 catalyst has shown the ability to simultaneously remove NOx and soot, whilst a Pt/Al_2O_3 catalyst was only active for the oxidation of soot.[60] Pisarello *et al.* found that Ba/CeO_2 and Ba-K/CeO_2 were effective at storing NOx in form of nitrates, however, the nitrates were found in inhibit soot oxidation.[61] Castoldi *et al.* found that under cyclic conditions that Ag-Ba/CeO_2 was superior to Pt-Ba/Al_2O_3 for NOx reduction in the absence of soot. However, in the presence of soot the NOx storage capacity of the catalyst is affected. The Ag based catalyst was found to be superior, in regards to soot oxidation, to Pt-Ba/Al_2O_3 due to active oxygen species from the CeO_2 and/or Ag.[59] The reaction conditions used in this thesis are non-cyclic and remain constant throughout the experiment, hence it is likely that Ba based catalysts work more effectively under cyclic conditions as the nitrates can be adsorbed and desorbed during the cycle. The addition of Ba to Ag/CZA resulted in an enhancement in soot oxidation, whilst the addition of Ba-K resulted in a decrease in soot oxidation. This was an unusual finding as Ba is not known for its soot oxidation abilities, whilst K is. From the characterisation data, Ba-Ag had a higher surface area (50.6 m^2g^{-1}) than Ba-Ag-K (40.7 m^2g^{-1}), it is well established that a larger surface area favours catalysis. Furthermore, as mentioned above, the Ag crystallite size is believed to be a key factor in the catalyst reactivity. Ba-Ag has a significantly smaller Ag crystallite size (394 Å) compared to Ba-Ag-K (2563 Å). These two factors offer explanations to why Ba-Ag was a superior soot oxidation catalyst than Ba-Ag-K.

6.3.4 La Catalysts

As with Mn, La has been investigated as a component in perovskite-type catalysts for the simultaneous removal of NOx and soot.[62–67] Perovskite-type catalysts are popular for the simultaneous removal of NOx and soot, due to their excellent redox properties, thermal stability and low cost. La_2O_3 is a basic oxide with the ability to store NOx.[67] Both La-Ag and La-Ag-K show similar reactivity, showing poor selectivity towards the SCR reaction as well as displaying similar levels of soot oxidation compared to Ag/CZA. As with the Ba catalysts the K containing catalyst doesn't display the expected soot oxidation enhancement. This is due to La-Ag having a significantly smaller crystallite size (1272 Å) than La-Ag-K (2532 Å). La has been used to dope Mn based perovskite catalysts for the SCR reaction. The doping of La has been found to promote the presence of Mn^{4+} and surface adsorbed oxygen.[68] However, there is no evidence of La promoting surface oxygen for Ag based catalysts. There is little evidence in the literature, or in this work, that Sr promotes SCR over Ag based catalysts.

6.3.5 Sr Catalysts

The incorporation of Sr and Sr-K into the Ag/CZA catalyst had a detrimental effect on both soot oxidation and the reduction of NOx. As with Ba, Sr has been previously incorporated into perovskite type catalysts to enhance NOx reduction. It has been proposed that small quantities of Sr doping doesn't have a significant effect on catalysis, whilst larger levels of doping can increase the weakly bonded oxygen to the catalytic support.[69] Sr-Co catalysts have been shown to lower soot oxidation temperatures and reduce the importance of soot-catalyst contact.[70] The substitution of Sr into perovskite type catalysts has also been shown to enhance soot oxidation through improving the redox properties of the catalyst.[71] However, the introduction of Sr was shown to reduce the soot oxidation observed over Ag/CZA. It is likely that Sr wasn't able to enhance soot oxidation or NOx reduction due to Sr not having a synergistic interaction with Ag indeed it had a detrimental interaction with Ag resulting in blocking active sites and thus hindering reactivity. It is also of note that the Sr-Ag-K catalyst had a significantly higher Ag crystallite size (2152 Å) compared to Ag/CZA (52 Å).

6.3.6 Ni Catalysts

The addition of Ni into SCR catalysts has been shown to improve NOx reduction by increasing the number of acid sites, as well as improving the catalysts' sulphur poisoning resistance.[72–77] Gao *et al.* found that the addition of Ni toa $MnOx/CeO_2$ catalyst enhanced NOx reduction due to an increase in surface area and an increase in chemisorbed oxygen.[77] The addition of Ni to the Ag/CZA catalyst results in a slight increase in surface area (69.7 m^2g^{-1}) compared to Ag/CZA (62.6

m^2g^{-1}). The introduction of Ni also causes contraction of the ceria lattice and formation of oxygen vacancies which aids redox reactions. Wan *et al.* suggested that a redox-cycle synergistic effect between Ni and Mn enabled low temperature SCR to take place over a Ni-MnOx catalyst as a result of electron transfer between Mn and Ni.[76] Ni has also been found to promote the active species of Mn hence aiding catalysis.[74] The Ni-Ag and Ni-Ag-K catalysts were shown to be poor SCR catalysts in the presence of soot, suggesting that a synergistic effect between Ni and Ag did not take place. There is some literature that suggests that doping ceria with NiO results in enhancement of soot oxidation as the NiO is involved in the catalytic oxygen of NO to NO_2 as well as the formation of active oxygen.[78] From the reaction data the addition of Ni to Ag/CZA showed increased soot oxidation compared to Ag/CZA, which could be due to NiO enhancing the reaction. Ni-Ag-K did show an increase in high temperature soot oxidation compared to Ag/CZA, but formed less CO_2 than over the Ni-Ag catalyst. This is unusual as K is known to enhance soot oxidation.

6.3.7 Fe Catalysts

Fe also has redox properties, which have been previously exploited for soot oxidation. In particular, Fe doped ceria catalysts have been investigated.[79–82] Fe^{3+} uses its bonded oxygen to oxidise soot whilst being reduced to Fe^{2+}. Fe^{2+} is consequently re-oxidised to Fe^{3+} from it's interaction with ceria. Fe doping distorts the ceria lattice and creates oxygen vacancies to varying degrees depending on the level of incorporation.[82] From the XRD analysis it has been concluded that the incorporation of Fe into Ag/CZA resulted in a contraction in the ceria lattice, resulting in the formation of oxygen vacancies. Therefore, it would be expected to see an improvement in soot oxidation over both Fe catalysts, however, this was only observed over the Fe-Ag-K catalyst. As catalytic soot oxidation is a surface sensitive reaction, the contact between the soot and catalyst is an important factor for the activity. The Fe crystallite sizes were not able to be measured from the XRD as the Fe peaks were not present in the XRD patterns, suggesting that they are dispersed as small crystallites across the catalytic surface. Knowing the Fe crystallite size could help understand why the Fe-Ag/CZA catalyst was not superior to Ag/CZA with regards to soot oxidation. Whilst Fe-Ag-K did show an enhancement in high temperature oxidation, which is thought to be due to the incorporation of Fe and the addition of K which is well established for its ability to enhance soot oxidation. Both Fe-Ag and Fe-Ag-K were shown to be poor at selectively catalytically reducing NO. There is limited literature based on Fe catalysts for NH_3-SCR with the research being focused on Fe zeolite catalysts.[83–85] Fe zeolites have been found to be active for the SCR reaction at temperatures above 400 °C, which is a higher temperature than desired for real world application. Cho *et al.* found that using a Fe-zeolite catalyst for NH_3-SCR resulted in the

formation of large quantities of undesirable N_2O at temperatures above 300°C.[83] The formation of N_2O is also observed over the Fe catalysts in this chapter.

6.3.8 PGM Catalysts

The platinum group metals are well documented for their use in automotive abatement technology.[86–88] Of the ones studied in this chapter, only Pt-Ag and Rh-Ag-K showed an improvement of soot oxidation compared to Ag/CZA. Additionally, none of PGM catalysts displayed the ability to catalyse the SCR reaction. Pt enhances soot oxidation indirectly by catalysing the oxidation of NO into NO_2 which subsequently oxidises the soot into CO_2.[89] Due to this it was expected for Pt-Ag to show high levels of soot oxidation however it was unexpected for Pt-Ag-K not to show further promotion of soot oxidation. The current characterisation data does not highlight any explanation for this observation especially since the Ag crystallite size could not be measured for Pt-Ag-K, Pd-Ag-K and Rh-Ag-K. The inability to calculate the Ag crystallite size suggests that the metals are present in small clusters which are too small to be detected.

Rh-Ag-K was shown to be the best catalyst studied in this chapter for high temperature soot oxidation. Lee *et al.* found that Rh/CeO_2 and Ag/CeO_2 catalysts showed enhanced soot oxidation compared to other noble metal/CeO_2 catalysts, due to their ability to promote vacancy formation and enhance oxygen adsorption.[90] This property combined with K's ability to enhance soot oxidation helps to explain why Rh-Ag-K/CZA was the superior catalyst for soot oxidation. In the same study, Pd/CeO_2 was found to form less vacancies than Ag, Pt and Rh/CeO_2. Rh is known for its ability to catalyse the decomposition of N_2O and the aim of combining it with Ag/CZA was to assist with the abetment of N_2O. However, as discussed earlier, the presence of 8% O_2 in the simulated exhaust gas deactivated the catalyst. Pd and Pt have been investigated for use as catalysts for SCR using H_2,[91,92] and for the noble metal in NOx traps which operate under cyclic conditions.[93–97] This study has operated under constant lean conditions suggesting that these catalysts are better suited under cyclic conditions.

6.4 Conclusions and Future Work

This chapter explored the incorporation of many different secondary elements into the Ag/CZA catalyst for the simultaneous removal of NOx and soot. It has been established than none of the studied catalysts improved upon the Ag/CZA catalyst for the overall reaction. However, the introduction of secondary elements did, on occasions, result in the enhancement of high temperature soot oxidation.

The real challenge is the enhancement of NOx reduction under these reaction conditions. From the current reaction and characterisation data a few key characteristics for a successful

catalyst have been determined; small Ag crystallite sizes; large surface areas; and the formation of oxygen vacancies to enable redox reactions to take place. The formation of the oxygen vacancies can come from the incorporation of external elements into the ceria lattice. Investigation into the dispersion of the active metal across the catalytic surface *via* CO chemisorption would be useful information to obtain. Knowing the dispersion would allow greater insight into the information provided by the surface techniques (*e.g.* XPs and SEM). A high dispersion is also likely to collate to better activity.

Several of the elements investigated had previously been studied as perovskite type catalysts. With the promotion of NOx reduction coming from the element being substituted into the perovskite. Whilst the catalysts in this thesis are based on a mixed oxide support (CeO_2-Al_2O_3-Zr_2O_3), hence differences in reactivity were to be expected. Additionally, as stated previously, the secondary metals were chosen for their ability to either promote NOx reduction or soot oxidation, not many of them having been previously investigated for the simultaneous removal of NOx and soot. A single catalyst for the simultaneous removal of NOx and soot is still a relatively novel concept, due to difficulties of finding a catalyst which can perform both reactions under the lean diesel exhaust conditions. With added complexity of attempting to prevent the formation of N_2O.

The Rh based catalysts showed interesting activities with regards to the formation of N_2O. Rh/CeO_2 based catalysts are used to decompose N_2O, however, Rh-Ag/CZA and Rh-Ag-K/CZA form N_2O especially at high temperatures. When N_2O is present in simultaneous removal of NOx and soot reactions it is typically observed as a peak between 250 - 450°C, whilst over Rh-Ag/CZA the formation of N_2O occurred at 375°C and increased with temperature. Over Rh-Ag-K/CZA a broad peak of N_2O was observed between 275 – 550°C. However, literature states that the presence of O_2 can deactivate Rh for the decomposition of N_2O and 8% O_2 is present in the simulated exhaust gas mix.

Rh-Ag-K/CZA was the best catalyst for high temperature oxidation of soot under the reaction conditions, however, it was poor at reducing NOx. Lower weight loadings of Rh and K (0.5, 0.2 and 0.1 w.t.%) should be investigated to determine whether that would allow the Rh and K to enhance soot oxidation, but still permit Ag/CZA to reduce NOx. Depending on the findings, lower weight percentages of the other catalysts could also be investigated.

Hiley *et. al*. used Extended X-ray absorption fine structure (EXAFS) analysis to discover that when Pd^{2+} with square-planar coordination sits in the square faces of the oxide ions of cubic CeO_2 lattice expansion occurs.[34] It would be useful to carry out EXAFS analysis on Co-Ag/CZA, Pd-

Ag/CZA and Rh-Ag/CZA to confirm whether the same explanation for the expansion of the ceria lattice is true for these catalysts.

A systematic approach to the catalysts studied in this chapter could shine greater light on their properties. The catalysts could be broken down and studied. With reactions on the pure CZA support followed by CZA and K, CZA and the metal of interest and then begin to add the Ag. This way the effect of the different metals could be more easily investigated.

6.5 References

1 C. Davies, K. Thompson, A. Cooper, S. Golunski, S. H. Taylor, M. Bogarra Macias, O. Doustdar and A. Tsolakis, *Appl. Catal. B Environ.*, 2018, **239**, 10–15.

2 A. S. Ayodhya and K. G. Narayanappa, *Environ. Sci. Pollut. Res.*, 2018, 25, 35034–35047.

3 P. F. Lidia Castoldi, Roberto Matarrese, Luca Lietti, *Appl. Catal. B Environ.*, 2006, **64**, 25–34.

4 R. Matarrese, L. Castoldi, N. Artioli, E. Finocchio, G. Busca and L. Lietti, *Appl. Catal. B Environ.*, 2014, **144**, 783–791.

5 B. S. Sánchez, C. A. Querini and E. E. Miró, *Appl. Catal. A Gen.*, 2009, **366**, 166–175.

6 J. H. Lee, D. Y. Jo, J. W. Choung, C. H. Kim, H. C. Ham and K. Y. Lee, *J. Hazard. Mater.*, 2021, **403**, 124085.

7 M. Hussain, D. Fino and N. Russo, *J. Hazard. Mater.*, 2012, **211**–**212**, 255–265.

8 S. Parres-Esclapez, M. J. Illán-Gómez, C. S. M. de Lecea and A. Bueno-López, *Appl. Catal. B Environ.*, 2010, **96**, 370–378.

9 W. S. Epling, L. E. Campbell, A. Yezerets, N. W. Currier and J. E. Parks, *Catal. Rev. - Sci. Eng.*, 2004, 46, 163–245.

10 B. M. Weiss and E. Iglesia, *J. Phys. Chem. C*, 2009, **113**, 13331–13340.

11 V. E. Yaying Ji, CourtneyFisk and K. W. Uschi Graham, Adam Poole, Mark Crocker, Jae-Soon Choi, William Partridge, *Catal. Today*, 2010, **151**, 362–375.

12 M. Piumetti, S. Bensaid, D. Fino and N. Russo, *Catal. Struct. React.*, 2015, 1, 155–173.

13 I. M. and H. H., *Catal. Today*, 1991, **10**, 57–71.

14 Y. T. and M. N. Iwamoto M., Yahiro H., Torikai Y., *Catal. Letters*, 1990, **11**, 1967–1970.

15 H. M. S. and M. G. Roy S., *Appl. Energy*, 2009, **86**, 2283–2297.

16 D. Marrocchelli, N. H. Perry and S. R. Bishop, *Phys. Chem. Chem. Phys.*, 2015, **17**, 10028–10039.

17 D. Fino, S. Bensaid, M. Piumetti and N. Russo, *Appl. Catal. A Gen.*, 2016, 509, 75–96.

18 D. Fino, N. Russo, G. Saracco and V. Specchia, *J. Catal.*, 2006, **242**, 38–47.

19 D. Mescia, J. C. Caroca, N. Russo, N. Labhsetwar, D. Fino, G. Saracco and V. Specchia, *Catal.*

Today, 2008, **137**, 300–305.

20 Y. Li, A. Sundermann, O. Gerlach, K. Bin Low, C. C. Zhang, X. Zheng, H. Zhu and S. Axnanda, *Catal. Today*, 2020, **355**, 608–619.

21 S. Imamura, R. Hamada, Y. Saito, K. Hashimoto and H. Jindai, *J. Mol. Catal. A Chem.*, 1999, **139**, 55–62.

22 S. S. Kim, S. J. Lee and S. C. Hong, *Chem. Eng. J.*, 2011, **169**, 173–179.

23 C. Moreau, Á. Caravaca, P. Vernoux and S. Gil, *ChemCatChem*, 2020, **12**, 3042–3049.

24 Y. Wang, J. P. de Boer and M. Makkee, *Catal. Sci. Technol.*, 2021, **11**, 671–680.

25 P. M. Shah, J. W. H. Burnett, D. J. Morgan, T. E. Davies and S. H. Taylor, *Catal. 2019, Vol. 9, Page 475*, 2019, **9**, 475.

26 S. Damyanova, B. Pawelec, K. Arishtirova, M. V. M. Huerta and J. L. G. Fierro, *Appl. Catal. A Gen.*, 2008, **337**, 86–96.

27 M. Michalska, K. Lema Nski C and A. Sikora, , DOI:10.1016/j.heliyon.2021.e06958.

28 P. M. Shah, J. W. H. Burnett, D. J. Morgan, T. E. Davies and S. H. Taylor, *Catalysts*, , DOI:10.3390/catal9050475.

29 L. Pauling, *J. Am. Chem. Soc.*, 1947, **69**, 542–553.

30 P. M. Shah, J. W. H. Burnett, D. J. Morgan, T. E. Davies and S. H. Taylor, *Catal. 2019, Vol. 9, Page 475*, 2019, **9**, 475.

31 A. Trovarelli and P. Fornasiero, .

32 A. Sarkar and G. G. Khan, *Nanoscale*, 2019, **11**, 3414–3444.

33 Rafael Schmitt, Andreas Nenning, Olga Kraynis, Roman Korobko, A. I. Frenkel, Igor Lubomirsky, S. M. Haile and J. L. M. Rupp, *Chem. Soc. Rev.*, 2020, **49**, 554–592.

34 C. I. Hiley, J. M. Fisher, D. Thompsett, R. J. Kashtiban, J. Sloan and R. I. Walton, , DOI:10.1039/c5ta02007g.

35 J. D. Grunwaldt, F. Atamny, U. Göbel and A. Baiker, *Appl. Surf. Sci.*, 1996, **99**, 353–359.

36 * Benjaram M. Reddy, and Ataullah Khan, P. Lakshmanan, Mimoun Aouine, and Stéphane Loridant and J.-C. Volta, *J. Phys. Chem. B*, 2005, **109**, 3355–3363.

37 N. Kainbayev, M. Sriubas, D. Virbukas, Z. Rutkuniene, K. Bockute, S. Bolegenova and G. Laukaitis, *Coatings 2020, Vol. 10, Page 432*, 2020, **10**, 432.

38 V. V. Sal'nikov and E. Y. Pikalova, *Phys. Solid State*, 2015, **57**, 1944–1952.

39 C. Schilling, A. Hofmann, C. Hess and M. V. Ganduglia-Pirovano, *J. Phys. Chem. C*, 2017, **121**, 20834–20849.

40 S. Loridant, *Raman spectroscopy as a powerful tool to characterize ceria-based catalysts*, .

41 N. Kainbayev, M. Sriubas, D. Virbukas, Z. Rutkuniene, K. Bockute, S. Bolegenova and G. Laukaitis, *Coatings 2020, Vol. 10, Page 432*, 2020, **10**, 432.

42 I. Kosacki, T. Suzuki, H. U. Anderson and P. Colomban, *Solid State Ionics*, 2002, **149**, 99–105.

43 E. A. Derevyannikova, T. Y. Kardash, L. S. Kibis, E. M. Slavinskaya, V. A. Svetlichnyi, O. A. Stonkus, A. S. Ivanova and A. I. Boronin, *Phys. Chem. Chem. Phys.*, 2017, **19**, 31883–31897.

44 M. Kusuma and G. T. Chandrappa, *J. Sci. Adv. Mater. Devices*, 2019, **4**, 150–157.

45 H. Wu, M. Zou, L. Guo, F. Ma, W. Mo, Y. Yu, I. Mian, J. Liu, S. Yin and N. Tsubaki, *RSC Adv.*, 2020, **10**, 4166–4174.

46 A. S. A. Al-Fatesh and A. H. Fakeeha, *J. Saudi Chem. Soc.*, 2012, **16**, 55–61.

47 N. M. Deraz and A. Alarifi, .

48 E. Gao, B. Huang, Z. Zhao, H. Pan, W. Zhang, Y. Li, M. T. Bernards, Y. He and Y. Shi, *Catal. Sci. Technol.*, 2020, **10**, 4752–4765.

49 K. Wang, L. Qian, L. Zhang, H. Liu and Z. Yan, in *Catalysis Today*, 2010, vol. 158, pp. 423–426.

50 X. Peng, H. Lin, W. Shangguan and Z. Huang, *Catal. Commun.*, 2007, **8**, 157–161.

51 G. C. Dhal, S. Dey, D. Mohan and R. Prasad, *Mater. Discov.*, 2017, **10**, 37–42.

52 Y. Teraoka, K. Kanada and S. Kagawa, *Synthesis of La-K-Mn-O perovskite-type oxides and their catalytic property for simultaneous removal of NO x and diesel soot particulates*, 2001, vol. 34.

53 H. Wang, J. Liu, Z. Zhao, Y. Wei and C. Xu, in *Catalysis Today*, 2012, vol. 184, pp. 288–300.

54 S. Zhang, B. Zhang, B. Liu and S. Sun, *RSC Adv.*, 2017, 7, 26226–26242.

55 C. Gao, J. W. Shi, Z. Fan, G. Gao and C. Niu, *Catalysts*, 2018, 8.

56 R. Jin, Y. Liu, Z. Wu, H. Wang and T. Gu, *Chemosphere*, 2010, **78**, 1160–1166.

57 J. R. González-Velasco, R. López-Fonseca and B. Pereda-Ayo, in *RSC Catalysis Series*, Royal Society of Chemistry, 2018, vol. 2018-January, pp. 36–66.

58 R. Matarrese, E. Aneggi, L. Castoldi, J. Llorca, A. Trovarelli and L. Lietti, *Catal. Today*, 2016, **267**, 119–129.

59 L. Castoldi, E. Aneggi, R. Matarrese, R. Bonzi, J. Llorca, A. Trovarelli and L. Lietti, *Catal. Today*, 2015, **258**, 405–415.

60 L. Castoldi, R. Matarrese, L. Lietti and P. Forzatti, *Appl. Catal. B Environ.*, 2006, **64**, 25–34.

61 M. L. Pisarello, V. Milt, M. A. Peralta, C. A. Querini and E. E. Miró, *Simultaneous removal of soot and nitrogen oxides from diesel engine exhausts*, 2002, vol. 75.

62 G. Peron and A. Glisenti, *Top. Catal.*, 2019, **62**, 244–251.

63 J. A. Onrubia-Calvo, B. Pereda-Ayo, U. De-La-Torre and J. R. González-Velasco, *Catal. Today*, 2019, **333**, 208–218.

64 H. Wang, Z. Zhao, P. Liang, C. Xu, A. Duan, G. Jiang, J. Xu and J. Liu, *Catal. Letters*, 2008, **124**, 91–99.

65 J. A. Onrubia, B. Pereda-Ayo, U. De-La-Torre and J. R. González-Velasco, *Appl. Catal. B Environ.*, 2017, **213**, 198–210.

66 D. Fino, N. Russo, G. Saracco and V. Specchia, *J. Catal.*, 2003, **217**, 367–375.

67 X. G. Li, Y. H. Dong, H. Xian, W. Y. Hernández, M. Meng, H. H. Zou, A. J. Ma, T. Y. Zhang, Z. Jiang, N. Tsubaki and P. Vernoux, *Energy Environ. Sci.*, 2011, **4**, 3351–3354.

68 X. Shi, J. Guo, T. Shen, A. Fan, S. Yuan and J. Li, *Chem. Eng. J.*, , DOI:10.1016/j.cej.2021.129995.

69 L. Hackermüller, U. Schneider, M. Moreno-Cardoner, T. Kitagawa, T. Best, S. Will, E. Demler, E. Altman, I. Bloch and B. Paredes, *Science (80-.).*, 2010, **327**, 1621–1624.

70 L. Sui, L. Yu and Y. Zhang, *Energy and Fuels*, 2007, **21**, 1420–1424.

71 P. Doggali, H. Kusaba, S. Rayalu, Y. Teraoka and N. Labhsetwar, in *Topics in Catalysis*, 2013, vol. 56, pp. 457–461.

72 L. Chen, X. Niu, Z. Li, Y. Dong, Z. Zhang, F. Yuan and Y. Zhu, *Catal. Commun.*, 2016, **85**, 48–51.

73 J. Zhu, F. Gao, L. Dong, W. Yu, L. Qi, Z. Wang, L. Dong and Y. Chen, *Appl. Catal. B Environ.*, 2010, **95**, 144–152.

74 B. Thirupathi and P. G. Smirniotis, *J. Catal.*, 2012, **288**, 74–83.

75 Y. Liu, Y. Hou, X. Han, J. Wang, Y. Guo, N. Xiang, Y. Bai and Z. Huang, *ChemCatChem*, 2020, **12**, 953–962.

76 Y. Wan, W. Zhao, Y. Tang, L. Li, H. Wang, Y. Cui, J. Gu, Y. Li and J. Shi, *Appl. Catal. B Environ.*, 2014, 148–149, 114–122.

77 F. Gao, X. Tang, H. Yi, J. Li, S. Zhao, J. Wang, C. Chu and C. Li, *Chem. Eng. J.*, 2017, **317**, 20–31.

78 B. Sellers-Anton, E. Bailon-García, A. Cardenas-Arenas, A. Davo-Quiñonero, D. Lozano-Castello and A. Bueno-Lopez, *Environ. Sci. Technol.*, 2020, **54**, 2439–2447.

79 Z. Zhang, D. Han, S. Wei and Y. Zhang, *J. Catal.*, 2010, **276**, 16–23.

80 Q. Shen, G. Lu, C. Du, Y. Guo, Y. Wang, Y. Guo and X. Gong, *Chem. Eng. J.*, 2013, **218**, 164–172.

81 Y. Gao, S. Teng, Z. Wang, B. Wang, W. Liu, W. Liu and L. Wang, *J. Mater. Sci.*, 2020, **55**, 283–297.

82 B. Li, A. Raj, E. Croiset and J. Z. Wen, *Catalysts*, , DOI:10.3390/catal9100815.

83 C. P. Cho, Y. D. Pyo, J. Y. Jang, G. C. Kim and Y. J. Shin, *Appl. Therm. Eng.*, 2017, **110**, 18–24.

84 P. S. Metkar, M. P. Harold and V. Balakotaiah, *Appl. Catal. B Environ.*, 2012, **111**–**112**, 67–80.

85 K. Krishna, G. B. F. Seijger, C. M. Van Den Bleek, M. Makkee, G. Mul and H. P. A. Calis, *Selective catalytic reduction of NO with NH 3 over Fe-ZSM-5 catalysts prepared by sublimation of FeCl 3 at different temperatures*, .

86 B. A. A. L. Van Setten, M. Makkee and J. A. Moulijn, *Catal. Rev. - Sci. Eng.*, 2001, 43, 489–564.

87 IPA - International Platinum Group Metals Association - Catalytic Converters, https://ipa-news.de/index/pgm-applications/automotive/catalytic-converters/, (accessed 28

September 2021).

88 J. Cooper and J. Beecham, *Platin. Met. Rev.*, 2013, 57, 281–288.

89 J. Oi-Uchisawa, S. Wang, T. Nanba, A. Ohi and A. Obuchi, *Appl. Catal. B Environ.*, 2003, **44**, 207–215.

90 J. H. Lee, D. Y. Jo, J. W. Choung, C. H. Kim, H. C. Ham and K. Y. Lee, *J. Hazard. Mater.*, , DOI:10.1016/j.jhazmat.2020.124085.

91 K. Duan, B. Chen, T. Zhu and Z. Liu, *Appl. Catal. B Environ.*, 2015, **176**–**177**, 618–626.

92 K. Duan, Z. Liu, J. Li, L. Yuan, H. Hu and S. I. Woo, *Catal. Commun.*, 2014, **57**, 19–22.

93 R. D. Clayton, M. P. Harold, V. Balakotaiah and C. Z. Wan, *Appl. Catal. B Environ.*, 2009, **90**, 662–676.

94 B. A. Silletti, R. T. Adams, S. M. Sigmon, A. Nikolopoulos, J. J. Spivey and H. H. Lamb, *Catal. Today*, 2006, **114**, 64–71.

95 F. Basile, G. Fornasari, A. Grimandi, M. Livi and A. Vaccari, *Appl. Catal. B Environ.*, 2006, **69**, 58–64.

96 I. Nova, L. Castoldi, L. Lietti, E. Tronconi and P. Forzatti, *On the dynamic behavior of 'NO x-storage/reduction' Pt-Ba/Al 2 O 3 catalyst*, 2002, vol. 75.

97 L. Lietti, P. Forzatti, I. Nova and E. Tronconi, *J. Catal.*, 2001, **204**, 175–191.

7 Conclusions and Future Work

7.1 Conclusions

This thesis has focused on attempting to improve a Ag/CZA catalyst for the simultaneous removal of NOx and soot from a simulated diesel exhaust. Despite electric vehicles becoming increasingly dominant, it is essential to research and improve the aftertreatment systems of diesel and gasoline vehicles. The development of a single catalyst for simultaneous removal of NOx and soot from diesel exhausts is complex, due to the lean operating conditions of diesel vehicles, however, it is possible. Davies *et al.* showed that a Ag/CZA catalyst was active for the simultaneous reaction, in addition to being able to utilise *in situ* generated N_2O to oxidise soot at low temperatures.[1] This finding was particularly novel, as it offered a potential solution for three key diesel aftertreatment challenges: the simultaneous removal of NOx and soot, low temperature soot oxidation and limiting the release of undesirable N_2O. The Ag/CZA, shows great potential, but there is also room for improvement with regards to soot oxidation and NOX reduction, which was tackled in this thesis.

Initially, potassium was incorporated into the Ag/CZA catalyst in a 20w.t.% loading and different preparation methods were investigated. It was found that wet impregnation and CVI at 80°C showed the most potential for the reaction. It was also found that the introduction of potassium greatly enhanced the catalyst's ability to oxidise soot at high temperatures, but hindered the reduction of NOx. Hence, a potassium weight loading study was carried out to determine whether a lower weight loading of potassium would still allow the enhancement of soot oxidation to take place, but not hinder the reduction of NOx. However, it was discovered that even a 2w.t.% loading of potassium hinders the reduction of NOx. An EXAFs study found that potassium carbonate becomes mobile when heated.[2] *In situ* XRD suggested that this was also the case over the Ag-K/CZA catalysts in this study, but further investigation is required.

The effect of incorporating copper into the Ag/CZA was investigated, as copper zeolite based catalysts are widely used for SCR, and have been shown to be active over a wide temperature window, and to be thermally stable. Several preparation methods and conditions were studied, with none of the prepared catalysts proving suitable for the simultaneous removal of NOx and soot. From XPS analysis on a selection of the catalysts, the majority of the copper was present as CuO which catalyses the undesirable oxidation of NH_3 to NO. The desired Cu^0 species was found to be either not present or present in too lower concentration to be able to successfully catalyse the desired reaction.

The final chapter investigated the incorporation of a wide range of secondary elements into the Ag/CZA catalyst. With the aim, that the secondary element would provide a synergistic effect, which would enhance soot oxidation and/or NOx reduction. None of the studied catalysts resulted in an improvement of NOx reduction, but several did result in an enhancement of high temperature soot oxidation, with Rh-Ag-K/CZA being the superior catalyst for high temperature soot oxidation.

Despite the investigated catalysts not enhancing the overall simultaneous reaction, several key conclusions were found. Firstly, various elements can be utilised to improve the high temperature soot oxidation reaction. Secondly, the silver crystallite size is key to the activity of the catalyst for this reaction, with a small silver crystallite size being an essential component for a simultaneous catalyst. Additionally, large surface areas and the formation of oxygen vacancies to allow redox reactions to take place were important. Formation of oxygen vacancies can be a result of the incorporation of external elements into the ceria lattice in the CZA support.

7.2 Future Work

The nature of potassium under reaction conditions should be further investigated to provide insight on how it aids soot oxidation. It has been suggested that the potassium becomes mobile under reaction conditions, but further studies should be carried out. These include an *in situ* TEM study which would be able to observe how the potassium interacts with soot under reaction conditions and would be able to determine whether the potassium does indeed become mobile. In addition, an EXAFs study could be carried out to also determine whether potassium does become mobile.

The copper-silver catalysts in Chapter 5 were found to be poor catalysts due to the presence of CuO and the absence of active Cu^0. Using stronger reducing agents or higher calcination temperatures would favour the presence of copper in the Cu^0 state.[3] Cu^0 catalyses the selective reduction of NO to N_2 and hence should enhance the Ag/CZA catalytic properties.

Chapter 6 investigated the effect of introducing a variety of secondary metals into the Ag/CZA catalyst. It was found that Rh-Ag-K/CZA was the best catalyst for high temperature soot oxidation, however, the catalyst was poor at reducing NOx. Lower weight loadings of Rh and K (0.5, 0.2 and 0.1 w.t.%) should be studied to determine whether this would permit NOX reduction to take place over the catalyst. If successful, using lower weight loadings could be investigated for the other catalysts in the chapter.

Both Chapter 5 and Chapter 6 were limited with characterisation due to the impacts of COVID-19. In the future, further characterisation on the catalysts could be carried out to help develop a deeper understanding of the catalysts including XPS and microscopy.

To further develop this project, different pre-treatments could be investigated so that the only CO_2 observed is a result of soot oxidation. When comparing the amount of CO_2 formed between different catalysts an integrated quantity could be used instead of comparing the highest concentration for each catalyst.

The catalysts throughout this project have been shown to oxidise soot at high temperatures but not at the desired low temperatures. The catalysts which were capable of reducing NOx and oxidising soot were not able to do so within the same temperature window. Different conditions could be investigated, such as researching the effect of different gas flows. As an FTIR was used to monitor the reactions, O_2 and N_2 could not be monitored directly. Calculating the O_2 and N_2 balances for all the catalysts could highlight the different reaction taking place. Furthermore, as there are several N containing species involved in the reactions, labelling the different N species would also help to determine the reactions taking place.

The development of a single catalyst for the simultaneous removal of NOx and soot from a diesel exhaust is a worthwhile endeavour which require further research. The use of a CZA mixed metal oxide support has been shown to be a good support, however, a zeolite support could also be a promising support for the reaction. Silver zeolites are capable of catalysing the SCR reaction[4–6] but have yet to be tested for the combustion of soot. Zeolites are excellent supports as they provide high surface areas and their pores can facilitate gas flow to active sites. It would be interesting to compare the activity of the Ag/CZA catalyst compared to a silver supported zeolite catalyst for the simultaneous removal of NOx and soot. One potential issue with the use of zeolites for this reaction is that the pores could become blocked with soot.[7]

7.3 References

1 C. Davies, K. Thompson, A. Cooper, S. Golunski, S. H. Taylor, M. Bogarra Macias, O. Doustdar and A. Tsolakis, *Appl. Catal. B Environ.*, 2018, **239**, 10–15.

2 C. J. Davies, A. Mayer, J. Gabb, J. M. Walls, V. Degirmenci, P. B. J. Thompson, G. Cibin, S. Golunski and S. A. Kondrat, *Phys. Chem. Chem. Phys.*, 2020, **22**, 18976–18988.

3 Johannes Teichert, Thomas Doert and Michael Ruck, *Dalt. Trans.*, 2018, **47**, 14085–14093.

4 J. Shibata, Y. Takada, A. Shichi, S. Satokawa, A. Satsuma and T. Hattori, *Appl. Catal. B Environ.*, 2004, **54**, 137–144.

5 K. Rahkamaa-Tolonen, T. Maunula, M. Lomma, M. Huuhtanen and R. L. Keiski, *Catal. Today*, 2005, **100**, 217–222.

6 K. Góra-Marek, K. A. Tarach, Z. Piwowarska, M. Łaniecki and L. Chmielarz, *Catal. Sci. Technol.*, 2016, **6**, 1651–1660.

7 E. Tronconi, I. Nova, F. Marchitti, G. Koltsakis, D. Karamitros, B. Maletic, N. Markert, D. Chatterjee and M. Hehle, *Emiss. Control Sci. Technol.*, 2015, **1**, 134–151.